Highly Developed Coherent Detection OTDR Technology and Its Applications to Optical Fiber Networks Monitoring

高性能化したコヒーレント検波 OTDR 技術と

光ファイバー網監視への応用

December 2008

Hisashi Izumita

Abstract

This thesis, examining coherent-detection optical time-domain reflectometry (C-OTDR) and its applications to optical fiber network monitoring, is based on the author's research and development work at NIPPON TELEGRAPH and TELEPHONE Corporation.

In the 2000s, the number of broadband service users in Japan has increased rapidly and exceeded 28 million by the end of September 2007. This figure includes 10 million fiber to the home (FTTH) service users. In order to deliver high-quality, cost-effective FTTH services throughout Japan, it is important to construct and maintain such huge optical fiber networks effectively. The demand for greater transmission capacity in trunk line networks is growing rapidly, because of the increasing IP traffic of broadband multimedia services via access networks. Optical transmission systems operating at several hundred gigabits per second have been developed through application of wavelength division multiplexing (WDM) technology. Moreover, the span of long-haul fiber optic communication systems has been increased to several hundred or several thousand kilometers. These spans are achieved, respectively, by using a repeaterless optical transmission system with distributed Raman amplifiers (DRAs) which use the installed optical fiber for Raman amplification, or by using a system based on fiber submarine transmission using in-line optical amplifiers (FSA). Ensuring the high quality and reliability of such high-capacity, long-haul fiber optic communication systems require optical fiber monitoring technologies for optical fiber network maintenance. In particular, we require the following measurement techniques: (1) testing fiber loss to confirm the integrity of optical fiber after installation; (2) finding fault locations in optical fiber for maintenance; and (3) evaluating the fiber parameters of installed optical fibers in order to upgrade a transmission system. Fiber-distributed strain measurement techniques are also important for evaluating the reliability of optical fiber cables affected by major accidents, e.g., earthquakes.

Optical time-domain reflectometry (OTDR) is a useful technique for fault location and characterization in optical fiber lines under construction or maintenance. The Rayleigh backscattered light and reflections from the optical fiber are detected as a function of the round-trip time corresponding to the fiber length. This approach can be applied at one end of the optical fiber. Since enhancement of the dynamic range of OTDR increases the measurable fiber length and reduces the measurement time, many studies have sought to extend the dynamic range by using a high-power laser and a

high-sensitivity receiver, e.g., an avalanche photodiode (APD). Since Brillouin scattering in the backscattering from an optical fiber has the characteristics of strain and temperature dependence, the strain and temperature distributions can be measured by using the relative tensile strain and the temperature dependence of the Brillouin frequency shift in Brillouin backscattering. Brillouin optical time-domain reflectometry using a coherent-detection technique (B-OTDR) has been proposed and developed for predicting the reliability of optical fiber. There are two problems, however, with B-OTDR: (1) the complexity of optical frequency control between the probe light and local light; and (2) degradation of the strain measurement accuracy because of environmental temperature changes.

This thesis first proposes high-performance OTDR for trunk line network maintenance. The application of optical fiber amplifier technologies with the characteristics of high gain and high saturation, together with a coherent-detection technique with shot-noise-limited sensitivity, promises to enhance the single-way dynamic range of OTDR. Since the high-power coherent pulsed light from OTDR is confined to a small region in an optical fiber, with a mode field diameter of 10 μm, nonlinear optical phenomena occur in the optical fiber and degrade the OTDR performance. Therefore, the critical pulse powers at which these phenomena occur and the performance limit of coherent detection OTDR (C-OTDR) with optical fiber amplifiers are investigated theoretically and experimentally.

Next, the thesis examines the problem of amplitude fluctuations in C-OTDR traces, which are caused by both fading noise and the heterodyne detection efficiency fluctuation. These fluctuations must be reduced before C-OTDR can be practically applied in optical fiber networks. A stochastic description of the amplitude fluctuation is obtained using the probability density functions of the Rayleigh backscattering light fluctuation and the heterodyne detection efficiency fluctuation, and the calculated amplitude fluctuation is demonstrated. A sophisticated technique for effectively reducing the amplitude fluctuation is also proposed, and its feasibility is confirmed theoretically and experimentally.

Next, for monitoring long-haul optical transmission systems including optical fiber amplifiers, the applications of a highly developed C-OTDR based on the above enhancements are described. An application for measuring the fiber-distributed tensile strain by upgrading C-OTDR to B-OTDR is proposed. A 1.55- / 1.65- μm B-OTDR approach for measuring both the strain and optical fiber loss distributions is also described. Furthermore, a novel fiber-distributed strain measurement technique is proposed. This technique separates temperature fluctuation effects by using the strain

and temperature cross-dependency of the Brillouin frequency shift and the Brillouin scattering power.

Finally, the thesis describes the fundamental requirements and methods for effectively maintaining optical access networks, and an advanced future system for maintaining various types of optical networks is investigated.

Contents

Chapter 1. Introduction

1.1. Background

1.1.1. Progress in OTDR technologies

Optical time-domain reflectometry (OTDR) is a commonly used technique for fault location and characterization in fiber optic communication systems. In 1976, Barnoski and Jensen demonstrated this technique for the first time [1-1]. Personick first formulated the Rayleigh backscattered power together with a variety of experimental data [1-2]. Theoretical analysis of OTDR applied to single-mode fibers was performed by Brinkmeyer [1-3] in terms of wave optics. This technique can be used to evaluate fiber parameter fluctuation and splice loss and to locate faults in an optical transmission line composed of several optical fiber cables. The significant advantage is that the technique can be applied nondestructively at one end face. Hence, this technique has become a practical, helpful tool in manufacturing, testing, and installing optical fiber cables. In the 1980s, many studies were undertaken to extend the dynamic range of OTDR, in order to enlarge the measureable fiber length and reduce the measurement time [1-4]-[1-6].

The required performance of OTDR has evolved drastically with the development of fiber optic communication systems enhanced with various key technologies, as described in the following section. Since the 1990s, erbium-doped fiber amplifier (EDFA) and Raman fiber amplifier (RFA) technologies have expanded the repeater span and capacity of these systems. The OTDR dynamic range must now cover a span of over 100 km from the end of an optical fiber line.

This thesis mainly describes the developments in OTDR performance for monitoring the optical fiber networks of fiber optic communications systems since the 1990s. The related applications of highly developed OTDR are also demonstrated.

1.1.2. Development of key technologies for fiber optic communication systems

Fiber optic communication systems have been developed since the invention of the laser in 1960 [1-7]. The possibility of an optical fiber guiding light in a similar manner to the guiding of electrons in copper wires was suggested in 1966 [1-8]. In 1970, a

20-dB/km optical fiber [1-9] and a GaAs semiconductor laser operating continuously at room temperature were demonstrated [1-10]. Compact optical components based on low-loss optical fiber technologies and semiconductor technologies accelerated the development of fiber optic communication systems [1-11]. Figure 1.1(a) shows the typical structure of a fiber optic communication system for trunk lines. Line-terminating multiplexers (LT) are connected to each other by optical fibers and repeaters. The repeaters, called 3R-repeaters, have three functions: reshaping, retiming, and regenerating communication signals in the optical fibers. Commercially available systems operating near 0.8 μm and using GaAs semiconductor lasers and multimode fibers were deployed in 1980 [1-11]. The bit rate was 45 Mb/s, and the repeater span was about 10 km. This span was ten times larger than that of a conventional coaxial system, so construction and maintenance costs could be reduced. This is one of the major advantages of fiber optic communication systems.

Operation at the 1.3-μm wavelength was a promising way to extend the repeater span, because of the characteristics of an optical fiber with low loss and minimum dispersion in this wavelength region. The development of InGaAsP semiconductor lasers and detectors operating near 1.3 μm and the use of single-mode fiber led to the second generation of fiber-optic communication systems, available in the early 1980s. A 2-Gb/s transmission system operating over 44 km of single-mode fiber was demonstrated [1-12]. By 1985, commercially available systems with a bit rate of 400 Mb/s and a repeater span of 40 km were deployed in NTT trunk lines from Hokkaido to Kyushu over 3400 km [1-13], [1-14].

Operation at the 1.55-μm wavelength using silica fiber had great potential to extend the repeater span, because silica fiber has its minimum loss around this wavelength region [1-15]. The use of dispersion-shifted optical fiber (DSF), which is designed to have minimum dispersion near 1.55 μm, and of distributed-feedback laser diodes (DFB-LDs), which limit the laser spectrum to a single longitudinal mode, overcame the dispersion limit in high-bit-rate transmission systems operating at 1.55 μm. In 1989, commercially available systems operating at 2.4 Gb/s with a 3R-repeater span of about 80 km were deployed [1-13], [1-16]. Such 1.55-μm systems are capable of operating at a bit rate of up to 10 Gb/s [1-16].

The coherent detection technique was a promising way to improve the sensitivity of the receiver in a fiber optic communication system, enabling the repeater span to be increased [1-17]-[1-20]. Such coherent optical transmission systems were investigated in the 1980s [1-21]-[1-23]. Since coherent detection has the major advantage of improving the sensitivity of a receiver with narrow bandwidth, however, the advantage

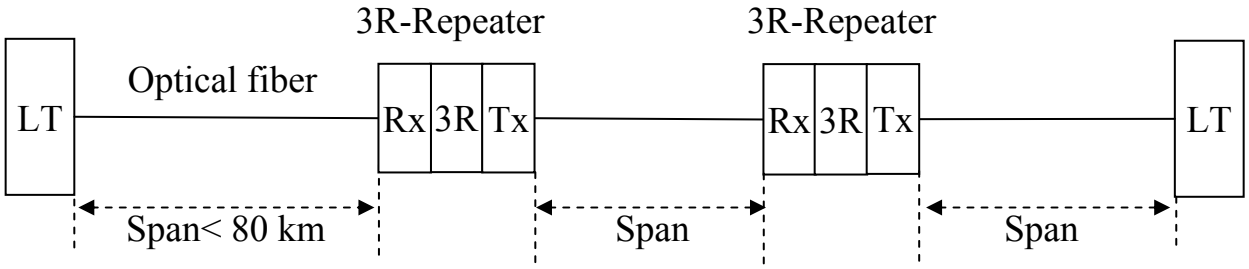

0.8-μm LD: Multi-mode fiber
1.31-μm LD: Single-mode fiber
1.55-μm LD: Dispersion-shifted single-mode fiber

LT: Line-terminating multiplexer
3R: 3R-circuit including functions for reshaping, retiming, regenerating
Rx: Optical receiver
Tx: Optical transmitter

(a) Optical transmission system with repeaters including 3R functions

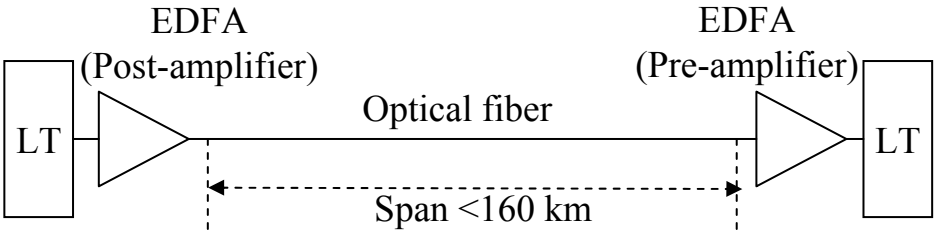

EDFA: Erbium-doped fiber amplifier

(b) Optical transmission system with EDFAs as post-amplifier and/or pre-amplifier

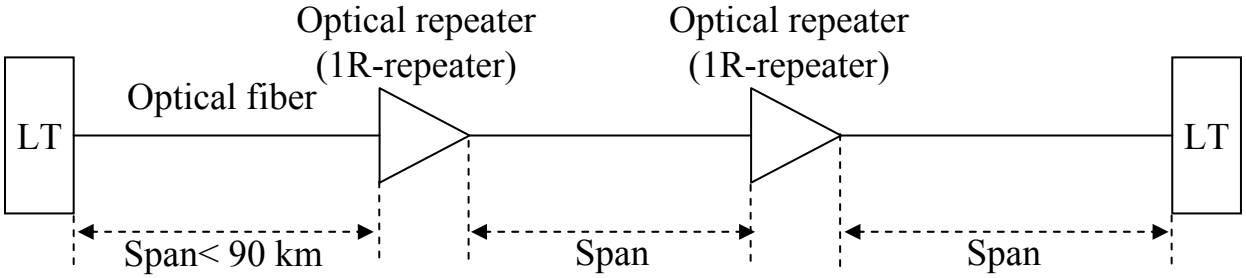

(c) Optical transmission system with optical repeaters including EDFAs

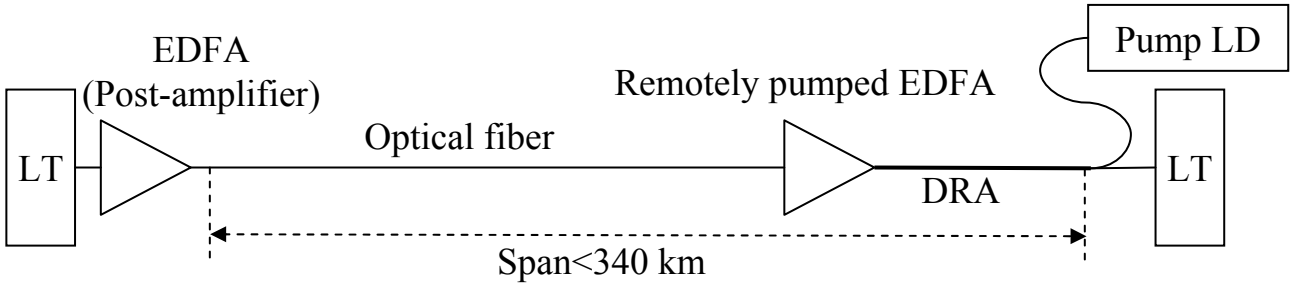

DRA: Distributed Raman amplifier

(d) Optical transmission system with post-amplifier and remotely pumped amplifiers

Figure 1.1 Fiber optic communication systems for trunk lines

is reduced in optical transmission systems with higher bit rates [1-23].

Erbium-doped fiber amplifier (EDFA) has been investigated since the proposal of fiber laser cavities [1-24]. Low-loss fiber fabrication technology and semiconductor laser technology have improved the performance of EDFA [1-25]-[1-29]. In 1989, a high-gain, low-noise EDFA pumped with a laser diode (LD) was demonstrated for practical use [1-29]. The EDFA technology enabled the evolution of fiber optic communication systems operating at 1.55 μm [1-30], [1-31]. In 1994, commercially available systems enhanced with an EDFA as a post-amplifier in the optical transmitter (Tx) of an LT were deployed as trunk line systems in Japan. As shown in Fig. 1.1(b), the span was increased up to 160 km, which was twice the span of previously deployed systems [1-16]. Then, as shown in Fig. 1.1(c), optical repeaters including EDFAs were introduced into terrestrial and submarine optical transmission systems to increase the repeater span and reduce the number of 3R-repeaters. An optical repeater, called a 1R-repeater, has the capability to linearly amplify optical communication signals by using an EDFA. In 1995, a submarine optical transmission system with in-line optical fiber amplifiers as 1R-repeaters and a repeater span of 90 km was deployed on the Kagoshima-Okinawa route, with a total length of 900 km [1-32]. The capacity of this system was upgraded to 40 Gb/s by using the wavelength-division multiplexing (WDM) technique [1-33]. Commercial transpacific cable systems with optical repeaters also became available [1-34]. A large number of transoceanic submarine systems have been deployed worldwide [1-11], [1-35]-[1-38].

In the 2000s, the number of broadband service users in Japan has increased rapidly and exceeded 27 million by the end of September 2007, including over 10 million Fiber To the Home (FTTH) service users [1-39]. The demand for greater transmission capacity of trunk line networks is growing rapidly as a result of the increasing number of broadband multimedia services available in access networks. WDM technology is a promising way to meet this demand. Application of Raman fiber amplifier (RFA) in WDM systems provided one way to extend the WDM channel wavelength range and transmission span [1-40]-[1-45]. Moreover, the signal wavelength band of WDM systems could be extended from the C-band (1530-1565 nm) to triple bands: the S-band (1460-1530 nm), C-band, and L-band (1565-1625 nm), as defined by ITU-T Supplement.39. The system capacity could be increased to 10.92 Tb/s (273 WDM channels, each operating at 40 Gb/s) by using triple bands with WDM in combination with optical fiber amplifiers and dispersion management [1-42]. 1000 channels WDM optical transmission system was demonstrated [1-43], and by the end of 2000, commercial WDM terrestrial systems were available [1-46]. In Japan, a WDM optical

transmission system with remotely pumped EDFAs and distributed Raman amplifiers (DRAs), as shown in Fig. 1.1(d), was deployed on the route between the islands of Okinawa and Miyako-jima, with a total length of 340 km in 2005 [1-47].

Since the 1990s, by using the above key technologies to enhance the repeater span in commercially available fiber optic communication systems, the span was increased from 80 to 160 km by using an EDFA as a post-amplifier, as shown in Fig. 1.1(b). The use of 1R-repeaters enhanced the span to 90 km and reduced the number of 3R-repeaters, as shown in Fig. 1.1(c). Finally, the use of remotely pumped EDFAs and DRAs greatly enlarged the span to 340 km, as shown in Fig. 1.1(d).

Consequently, this thesis focuses on the development of optical fiber monitoring technologies that are applied for such long-haul fiber optic communication systems:

(1) A 160-km repeaterless optical transmission system using EDFAs as post-amplifiers;
(2) A submarine optical transmission system with in-line optical fiber amplifiers as 1R-repeaters, giving a repeater span of 90 km; and
(3) A 340-km optical transmission system using remotely pumped EDFAs and DRAs.

1.1.3. Fundamental required optical fiber monitoring technologies for constructing and upgrading fiber optic communication systems

In constructing the optical fiber networks of fiber optic communication systems, the integrity of the optical fibers before and after installation of optical fiber cables must be confirmed. The required fundamental items for monitoring optical fiber networks are the following:

- Total optical loss of the optical fibers;
- Loss distribution of the optical fibers; and
- Reflection in the optical fiber and at the connection points between optical fiber cables.

The typical methods for measuring the above fundamental items are as follows:

- ✓ Cut-back method using an optical source and an optical power meter to measure the total optical loss; and
- ✓ OTDR to measure the total loss, loss distribution, and reflection in the optical fiber.

OTDR is a useful method for evaluating the above items from one end of an optical

fiber. Therefore, the development of OTDR technologies has been required for monitoring the three types of optical fiber networks described in section 1.1.2. This is one of the main topics of this thesis.

In upgrading the capacity of an optical transmission system to over 10 Gb/s by applying WDM [1-33],[1-45] and fiber dispersion management technologies [1-48], the following additional parameters of the existing optical fibers also require evaluation:

- Chromatic dispersion;
- Polarization mode dispersion; and
- Nonlinear coefficient.

Sophisticated measurement techniques have already been developed and standardized in ITU-T recommendations [1-49], [1-50]. Hence, optical fiber network monitoring for the above additional items is outside the scope of this thesis.

1.1.4. Fundamental required optical fiber monitoring technologies for optical fiber network maintenance

Reliable optical fiber networks are designed and constructed by applying the key technologies of optical fiber fabrication, optical fiber cabling, optical fiber splicing and connection, optical fiber cable installation, and optical fiber cable termination [1-51]-[1-64]. For trunk line networks, submarine optical transmission systems are designed for 25 years of service life, with at most three failures during operation [1-46]. For optical access networks, optical fiber cables are typically designed with a failure rate of less than 0.1 Fit/fiber/km for 20 years of use [1-65]. To ensure the reliability of fiber optic communication systems, optical fiber maintenance technologies are fundamentally important, as are outside plant technologies.

Outside plant technologies for reliable optical fiber networks

Since silica-based single-mode optical fiber is brittle, a few cracks on the surface of such fiber can considerably reduce the optical fiber strength [1-66], through a failure mechanism in accordance with fracture mechanics theory [1-67]. Proof testing assures the mechanical reliability of optical fiber [1-54]-[1-56]. Optical fiber cable is designed to protect the optical fibers from strain or stress during optical fiber installation and operation [1-52],[1-53]. Hydrogen absorption of optical fiber, caused by water penetration into optical fiber cables and joint boxes, leads to increased optical loss and degrades the reliability of the fiber [1-68]. Therefore, water-blocking cables [1-57] and

water sensor systems [1-69] have been developed and deployed. In a joint box or closure, optical fiber cables are connected to each other by using fusion splicing, mechanical splicing, or MT connectors [1-53],[1-58]-[1-61]. The connected optical fibers are accommodated in organizers that are designed by considering the optical loss increase and the reliability of the bent optical fiber [1-62]. Outside optical fiber cables are introduced into network building and terminated at an optical distribution frame (ODF) [1-63],[1-70]. Finally, indoor optical fiber cables are connected between optical transmission systems and the outside optical fiber cables. To manage the huge number of optical fiber cables in a network building, optical fiber distribution and management systems have been developed and deployed [1-70]. These systems optionally include a sub-system for testing and monitoring the outside optical fiber cables, to support optical fiber network maintenance.

Origins of optical fiber faults

Optical fiber faults are categorized with three types [1-71],[1-72]:

- Fiber failure, which is typically caused by tensile strain and bending strain in the cable, bending strain and torsion strain in a joint box or closure, or lateral stress in a crushed cable conduit;
- Fiber loss increase, which is typically caused by a micro-bending loss increase due to fiber axial strain in the cable, a fiber bending loss increase in a cable closure, or a hydrogen absorption loss increase in the cable, a cable closure, or a joint box; and
- Fiber connection abnormality, which is caused by tensile strain and a change in the fiber alignment [1-73].

The residual strain and bending of the optical fiber in the cable and the closure are the major origins of optical fiber faults. Therefore, optical fiber monitoring technologies for strain and bending in optical fiber cables are required for optical fiber network maintenance before faults occur.

Fundamental optical fiber network maintenance

Table 1.1 summarizes the fundamental functions for optical fiber network maintenance [1-72]. The maintenance is categorized into two types: post-fault maintenance, and preventive maintenance. It consists of three activities: surveillance, testing, and control of network elements (NEs).

- Surveillance, which monitors the conditions of NEs, has two functions:

  Inform of NE degradation before trouble occurs, and

Table 1.1 Fundamental functions and suitable test methods

Category	Activity	Functions	Methods
Preventative maintenance	Surveillance (e.g., Periodic testing)	Detection of fiber loss increase Detection of signal power loss increase Detection of water penetration	OTDR/loss testing Power monitoring OTDR/losstesting
	Testing (e.g., Fiber degradation testing)	Measurement of fiber fault location Measurement of fiber strain distribution Measurement of water penetration	OTDR testing B-OTDR testing OTDR/loss testing
	Control (e.g., Network element control)	Fiber identification Fibre transfer	ID light detecting*1 Switching*2
After installation before service, or post-fault maintenance	Surveillance (e.g., Reception of transmission system alarm or customer trouble report)	Refer to alarm from path operation Refer to alarm from customer service operation system	On-line/External medium On-line/External medium
	Testing (e.g., Fiber fault testing)	Confirmation of fiber condition Fault distinction between transmission equipment and fiber network Measurement of fiber fault location	OTDR/loss testing OTDR/loss testing OTDR testing
	Control (e.g., Cable repair/removal)	Fiber identification Fiber transfer Storage of outside plant database Information on cable route	ID light detecting*1 Switching*2 On-line/External medium On-line/External medium

*[1]) ID light means identification light, for example270-Hz, 1-kHz, or 2-kHz modulated light.

*[2]) Switching includes mechanical and manual switching.

Inform of NE abnormality when trouble occurs.

- Testing measures NE characteristics and checks whether they satisfy required levels.
- Control restores NEs to normal status or takes action to maintain service quality.

Requirements of optical fiber monitoring technologies for optical fiber network maintenance

Maintenance of optical fiber networks after a fault occurs, i.e., post-fault maintenance, requires quick repair of optical fibers. Therefore, optical fiber monitoring technologies require the following functions:

- Distinguish fault between transmission equipment and optical fiber networks; and
- Find fault locations in optical fibers.

Maintenance of optical fiber networks before a fault occurs, i.e., preventive maintenance, requires periodic testing and fiber degradation testing by monitoring the following items:

- Optical fiber loss increase;
- Water penetration location; and
- Fiber strain distribution.

Monitoring these items enables diagnosis and prediction of optical fiber cable degradation [1-71], [1-72]. In particular, fiber strain distribution measurement is very important for evaluating the reliability of optical fiber cables affected by a major earthquake.

The typical methods for measuring the above items are the following:

- ✓ OTDR for measuring the loss distribution in an optical fiber;
- ✓ Long-wavelength OTDR for locating the bending loss caused by the water sensor [1-69]; and
- ✓ Brillouin optical time-domain reflectometry (B-OTDR) for measuring the fiber strain distribution by using Brillouin backscattering in single-mode optical fibers, which relies on the relative tensile strain and temperature dependence of the Brillouin frequency shift [1-74],[1-75].

All of the above methods are performed by using OTDR technologies with the following characteristics:

- High dynamic range for measuring long-haul optical fibers or reducing the measurement time;
- Long-wavelength operation, which is sensitive to bending loss; and

- A high-sensitivity receiver for detecting weak Brillouin backscattered light.

Consequently, highly developed monitoring techniques based on OTDR are required for optical fiber network maintenance. This is the major scope of this thesis.

1.1.5. Review of high-performance OTDR technologies up to early 1990s

As mentioned in section 1.1.4, high-performance OTDR technologies are required for optical fiber network maintenance. OTDR yields a high dynamic range with high-power sources, such as Nd:YAG lasers [1-76] or Er^{3+}:glass lasers [1-77]. These power sources, however, are impractical for field use because of the size of the equipment and consideration of the eye safety of network operators.

The coherent detection technique is one of the most promising approaches for extending the dynamic range of OTDR [1-78]. J. P. King et al. developed coherent-detection OTDR (C-OTDR) with a single-way dynamic range (SWDR) of 28 dB with a 5-μs pulse [1-79]. By applying coherent detection and EDFAs, Y. Koyamada et al. constructed a high-performance OTDR with an SWDR of 33 dB with 1-μs launch pulses [1-80]. There have also been a few studies on enhancing direct-detection OTDR (D-OTDR) with EDFAs [1-81]. There is still the possibility of further extending the SWDR, however, by optimizing the application of EDFAs. C-OTDR has the problem of amplitude fluctuation of as much as 0.2 dB in the OTDR trace [1-79], which is caused by the fading phenomenon of the Rayleigh scattering signal [1-82]. Therefore, my colleagues and I began to investigate the development of C-OTDR since 1989 in NTT labs. A highly developed C-OTDR can also be applied with B-OTDR to measure the strain distribution in an optical fiber [1-75].

1.1.6. Requirements of optical fiber maintenance support, monitoring, and testing system

High-speed FTTH services have already become available [1-39]. Several thousands of optical fibers in access networks are accommodated into a central office [1-70]. Cost-effective maintenance of such a huge number of optical fibers requires an optical fiber maintenance support, monitoring, and testing system operating automatically and remotely [1-83],[1-84]. Table 1.1 lists the fundamental functions and suitable methods of such a system. This system can be adapted for a single-star network. Adapting the system to various network structures, such as a passive optical network (PON) or a

ring network [1-85], as well as trunk networks, however, requires modifying the system's functions and methods. The fundamental requirements and advanced optical fiber monitoring technologies for maintaining PON and ring networks, as well as trunk networks carrying high-power signals, such as an optical transmission system employing a remotely pumped EDFA and a DRA as shown in Fig. 1.1(d) must be clarified.

In-service line monitoring is also required for preventive maintenance. The test light wavelength should be allocated in the U-band because it does not interfere with the communication signals from the O-band to the L-band [1-86]. Optical fiber maintenance support, monitoring, and testing systems using the 1650-nm wavelength band have been developed and deployed [1-87]. The criteria for in-service line monitoring must also be clarified. Therefore, this thesis deals with the above considerations.

1.2. Objectives of this thesis

This thesis first proposes enhancement of OTDR by using optical fiber amplifier technologies and a coherent detection technique for maintaining trunk line networks. Coherent-detection OTDR (C-OTDR) with EDFAs is a promising approach for enlarging the SWDR. To maximize the SWDR of C-OTDR, this thesis theoretically and experimentally investigates the following:

(1) The optimum configuration of C-OTDR with EDFAs.

(2) The limit of the incident optical pulse power of C-OTDR because of the effect of optical nonlinear phenomena in a single-mode optical fiber.

Next, the thesis focuses on the problem of amplitude fluctuation in a C-OTDR trace caused by fading noise and the heterodyne detection efficiency fluctuation [1-88]. This fluctuation must be reduced before C-OTDR can be practically applied in optical fiber networks. Effective reduction techniques for amplitude fluctuations are theoretically and experimentally investigated.

The applications of a highly developed C-OTDR are then investigated for long-haul fiber optic communication systems, including the following:

(1) A repeaterless optical transmission system using EDFAs as post-amplifiers.

(2) A submarine optical transmission system with in-line optical fiber amplifiers as 1R-repeaters.

(3) An optical transmission system employing a remotely pumped EDFA and DRA.

The fiber-distributed tensile strain measurement technique is investigated as the next

application of C-OTDR. Measurement of the fiber-distributed strain is very important in terms of preventive maintenance in optical fiber networks. Many approaches have been proposed for measuring the fiber-distributed strain and temperature by using Brillouin scattering in single-mode optical fibers. These approaches rely on the relative tensile strain and temperature dependence of the Brillouin frequency shift. Brillouin optical time-domain reflectometry employing a coherent detection technique (B-OTDR) is a useful method for measuring the fiber-distributed strain and temperature from one end of an optical fiber. Despite this, however, there are two problems with this approach [1-89]:

(1) The complexity of optical frequency control between the probe light and local light.
(2) Degradation of the strain measurement accuracy because of environmental temperature change.

Given these problems, this thesis investigates the upgrade C-OTDR to B-OTDR by using a sideband generation technique and a simultaneous measurement technique for separating the strain and temperature. The U-band wavelength used in B-OTDR for measuring both the strain and the optical fiber loss of an in-service line is also investigated.

Finally, the fundamental requirements and methods for maintaining optical fiber networks for PON and ring networks and trunk networks carrying high-power signals are clarified. An advanced future system for maintaining various types of networks is also discussed.

1.3. Outline of this thesis

Figure 1.2 illustrates the organization of this thesis, which consists of eight chapters.

After this introduction, chapter 2 discusses the enhancement of optical time-domain reflectometry (OTDR) by using optical fiber amplifier technologies and a coherent detection technique, which with compact optical components suited for integration into a robust, portable instrument. First, the basic principles of direct-detection OTDR (D-OTDR) and coherent-detection OTDR (C-OTDR) are reviewed, and the dynamic range enhancement of OTDR with EDFAs is numerically evaluated. Then, the feasibilities of D-OTDR and C-OTDR enhanced with EDFAs are demonstrated [1-90]-[1-92]. The observation of nonlinear phenomena in an optical fiber, which degrades the SWDR of C-OTDR, is also presented [1-93]. This leads to the motivation of chapter 3.

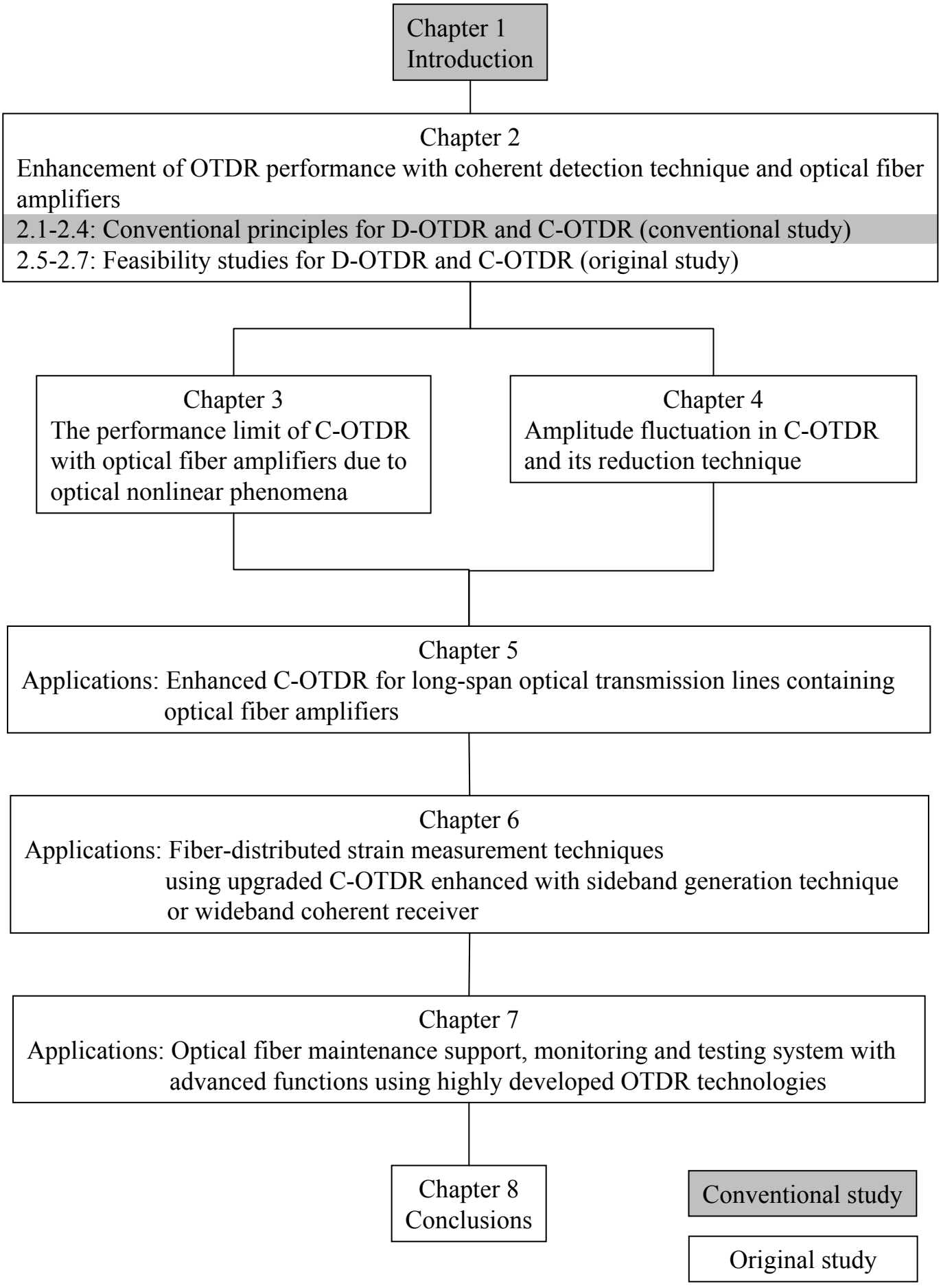

Figure 1.2 Thesis organization

Chapter 3 describes theoretical and experimental studies on clarifying the limit of the incident optical pulse power in C-OTDR enhanced with optical fiber amplifiers. The critical pulse power, at which the performance of C-OTDR is degraded by the effects of optical nonlinear phenomena in a single-mode optical fiber, depends on the amplified optical pulse waveform and the pulse width [1-93]-[1-95]. Under the critical condition of such nonlinear phenomena, the highest C-OTDR performance is demonstrated by using EDFAs as post-amplifiers and inline amplifiers [1-94]-[1-95].

Chapter 4 focuses on the problem of amplitude fluctuation in a C-OTDR trace, which is caused by fading noise and the heterodyne detection efficiency fluctuation [1-88]. This fluctuation must be reduced before C-OTDR can be practically applied in optical fiber networks. This thesis provides a stochastic description of the amplitude fluctuation using probability density functions and the calculated amplitude fluctuation [1-96] and proposes a synchronous optical frequency hopping technique [1-97]. In this technique, an RF current pulse is induced in the drive current of the laser diode (LD) during an LD temperature change. This effectively reduces the amplitude fluctuation.

The above research enables a highly developed C-OTDR with a high dynamic range and low fading noise. The following chapters describe applications of this advanced C-OTDR.

Chapter 5 describes the application of C-OTDR for monitoring long-haul optical transmission lines containing (a) in-line amplifiers as 1R-repeaters and (b) distributed Raman amplifier (DRA) [1-98]-[1-100].

Chapter 6 describes the application of the highly developed C-OTDR to the distributed strain measurement in an optical fiber, in order to evaluate the reliability of the fiber [1-101]-[1-105]. C-OTDR can be upgraded to B-OTDR by using a side-band generation technique with a high-speed $LiNbO_3$ (LN) phase modulator [1-101], [1-102] or a wideband coherent receiver [1-104]. A 1.55- / 1.65- μm B-OTDR for measuring both the strain and optical fiber loss distributions [1-103] is also described, and a simultaneous measurement technique for separating strain and temperature [1-105] is discussed.

Chapter 7 describes the application of an optical fiber maintenance support, monitoring, and testing system using highly developed OTDR technologies. It clarifies the fundamental requirements, methods, and criteria for maintaining various access networks (i.e., PONs, and ring networks) and trunk networks carrying high-power signals [1-106]-[1-111]. The future target technologies for this system are also presented.

The final chapter concludes this thesis. It summarizes the results obtained

throughout the course of this research on enhancing OTDR with a coherent detection technique and optical fiber amplifiers, and the applications of this research in optical fiber network monitoring.

1.4. References

[1-1] M. K. Barnoski and S. M. Jensen, "Fiber waveguides: A novel technique for investigating attenuation characteristics," Appl. Opt., vol. 15, no. 9, pp. 2112-2115, 1976.

[1-2] S. D. Personick, "Photon probe-An optical-fiber time-domain reflectometer," Bell Syst. Tech. J., vol. 56, no. 3, pp. 355-366, 1977.

[1-3] E. Brinkmeyer, "Backscattering in single-mode fibers," Electron. Lett., vol. 16, no. 9, pp. 329-330, 1980.

[1-4] M. D. Rouke, "An overview of optical time-domain reflectometry," in Proc. Amer. Ceramic Soc. Meet. Physics, pp. 252-272, 1980.

[1-5] P. Healey, "Review of long wavelength single-mode optical fiber reflectometry techniques," IEEE J. Lightwave Technol., vol. LT-3, no. 4, pp. 876-886, 1985.

[1-6] M. Tateda and T. Horiguchi, "Advances in optical time-domain reflectometry," IEEE J. Lightwave Technol., vol. LT-7, no. 8, pp. 1217-1224, 1989.

[1-7] T. H. Maiman, "Stimulated optical radiation in ruby masers," Nature, vol. 187, pp. 493-494, 1960.

[1-8] K. C. Kao and G. A. Hockham, "Dielectric-fiber surface waveguide for optical frequency," Proc. Inst. Electr. Eng., vol. 113, no. 7, pp. 1151-1158, 1966.

[1-9] F. P. Kapron, D. B. Keck, and R. D. Maurer, "Radiation losses in glass optical waveguides," Appl. Phys. Lett., vol. 17, pp. 423-425, 1970.

[1-10] I. Hayashi, M. B. Panish, P. W. Foy, and S. Sumski, "Junction lasers which operate continuously at room temperature," Appl. Phys. Lett., vol. 17, pp. 109-111, 1970.

[1-11] For example, G. P. Agrawal, "Fiber optics communication systems," third edition, chapter 1, John Wiley & Sons, Inc., New York 2002.

[1-12] J. Yamada, S. Machida, and T. Kimura, "2 Gbit/s optical transmission experiments at 1.3 μm with 44 km single-mode fibre," Electron. Lett., vol. 17, no. 13, pp. 479-480, 1981.

[1-13] N. Sato ed., "Optical Fiber Technologies toward IT Era," Chapters 1 and 7, IEICE 2001. (in Japanese)

[1-14] H. Shinohara, "Fiber optic communication systems in Japan," in the proc. of IEEE Lasers and Electro-Optics Society 2000 (LEOS 2000) 13th Annual Meeting, vol. 1, pp. 3-4, 2000.

[1-15] T. Miya, Y. Terunuma, T. Hosaka, and T. Miyoshita, "Ultimate low-loss single-mode fibre at 1.55 μm," Electron. Lett., vol. 15, no. 4, pp. 106-108,

1979.

[1-16] K. Nakagawa, "Large capacity optical communication systems," IEICE Trans., J78B-1, no. 12, pp. 713-723, 1995. (in Japanese)

[1-17] T. Okoshi and K. Kikuchi, "Frequency stabilization of semiconductor lasers for heterodyne-type optical communication systems," Electron. Lett., vol. 16, pp. 179-181, 1980.

[1-18] F. Favre and D. Le. Gum, "High frequency stability of laser diode for heterodyne communication systems," Electron. Lett., vol. 16, pp. 709-710, 1980.

[1-19] S. Saito, Y. Yamamoto, and T. Kimura, "Optical heterodyne detection of directly frequency modulated semiconductor laser signals," Electron. Lett., vol. 16, pp. 826-827, 1980.

[1-20] Y. Yamamoto and T. Kimura, "Coherent optical fiber transmission systems," IEEE Journal of Quantum Electronics, vol. 17, no. 6, pp. 919-935, 1981.

[1-21] T. Kimura, "Coherent optical fiber transmission," IEEE J. Lightwave Technol., vol. 5, no. 4, pp. 414-428, 1987.

[1-22] T. Okoshi, "Recent advances in coherent optical fiber communication systems," IEEE J. Lightwave Technol., vol. 5, no. 1, pp. 44-52, 1987.

[1-23] G. P. Agrawal, "Fiber optics communication systems, " third edition, chapter 10, John Wiley & Sons, Inc., New York 2002.

[1-24] E. Snitzer, "Proposed fiber cavities for optical masers," J. Appl. Phys., vol. 32, pp. 36-39, 1961.

[1-25] S. B. Poole, D. N. Payne, R. J. Mears, M. E. Fermann, and R. I. Laming, "Fabrication and characterization of low-loss optical fibers containing rare-earth ions," IEEE J. Lightwave Technol., vol. LT-4, no. 7, pp. 870-876, 1986.

[1-26] R. J. Mears, L. Reekie, I. M. Jauncey, and D. N. Payne, "Low-noise erbium-doped fibre amplifier operating at 1.54 μm," Electron. Lett., vol. 23, no. 19, pp. 1026-1028, 1987.

[1-27] E. Snitzer, H. Po. F. Hakimi, R. Tumminelli, and B. C. McCollum, "Erbium fiber laser amplifiers at 1.55 μm with pump at 1.49 μm and Yb sensitized Er oscillator," in the technical digest of OFC'88, PD-2, 1988.

[1-28] R. I. Laming, L. Reekie, D. N. Payne, P. L. Schrivenver, F. Fontana, and A. Righetti, "Optical pumping of erbium-doped-fiber optical amplifiers," in the proc. of ECOC'88, PD, pp. 25-28, 1988.

[1-29] M. Nakazawa, Y. Kimura, and K. Suzuki, "Efficient Er^{3+}-doped optical fiber

amplifier pumped by a 1.48 μm InGaAsP laser diode," Appl. Phys. Lett., vol. 57, no. 4, pp. 295-297, 1989.

[1-30] K. Hagimoto, K. Iwatsuki, A Takada, M. Nakazawa, M. Saruwatari, K. Aida, K. Nakagawa, and M. Horiguchi, "A 212 km non-repeated transmission experiments at 1.8 Gb/s using LD pumped Er^{3+}-doped fiber amplifiers in an IM/direct-detection repeater system," in the technical digest of OFC'89, PD-15, 1989.

[1-31] Special issue on Optical Amplifiers; IEEE J. Lightwave Technol., vol. LT-9, no. 2, 1991.

[1-32] M. Murakami, T. Takahashi, M. Aoyama, T. Imai, M. Amemiya, M. Sumida, and M. Aiki, "System performance evaluation of the FSA submarine optical amplifier system," IEEE J. Lightwave Technol., vol. 14, no. 12, pp. 2657-2671, 1996.

[1-33] M. Murakami, T. Matsuda, H. Maeda, Y. Tada, and T. Imai, "WDM upgrading of an installed submarine optical amplifier system," IEEE J. Lightwave Technol., vol. 19, no. 11, pp. 1665- 1674, 2001.

[1-34] W. C. Barnett, H. Takahira, J. C. Baroni, and Y. Ogi, "The TPC-5 Cable Network," IEEE Commun. Mag., vol. 34, no. 2, pp. 36-40, 1996.

[1-35] P. R. Trischitta and W. C. Marra, "The TAT-12/13 Cable Network," IEEE Commun. Mag., vol. 34, no. 2, pp. 24-28, 1996.

[1-36] T. Welsh, R. Smith, H. Azami, and R. Chrisner, "The FLAG cable system," IEEE Commun. Mag., vol. 34, no. 2, pp. 30-45, 1996.

[1-37] D. R. Gunderson, A. Lecroart, and K. Tatekura, "The Asia Pacific Cable Network," IEEE Commun. Mag., vol. 34, no. 2, pp. 42-48, 1996.

[1-38] W. C. Marra and J. Schesser, "Africa ONE: the Africa Optical Network," IEEE Commun. Mag., vol. 34, no. 2, pp. 50-57, 1996.

[1-39] "Number of Broadband Service Contracts, Etc. (as of the end of September 2007)," MIC (Ministry International Affairs and Communications, Japan Government) Press release – Telecom, December 18, 2007.

[1-40] K. Aida, S. Nishi, Y. Sato, K. Hagimoto, and K. Nakagawa, "1.8 Gb/s 310 km fiber transmission without outdoor repeater equipment using a remotely pumped in-line Er-doped fiber amplifier in an IM/DIRECT-DETECTION system," in the proc. of ECOC'89, PDA-7, pp. 29-32, 1989.

[1-41] P. B. Hansen, A. Stentz, T. N. Nielsen, R. Espindola, L. E. Nelson, and A. A Abramov, "Dense wavelength-division multiplexed transmission in 'zero-dispersion' DSF by means of hybrid Raman/Erbium-doped fiber

amplifiers," in the proc. of OFC, PD8, 1999.

[1-42] K. Fukuchi, T. Kasamatsu, M. Morie, R. Ohhira, T. Ito, K. Sekiya, D. Ogasahara, and T. Ono, "10.92-Tb/s (273 x 40-Gb/s) triple-band/ultra-dense WDM optical-repeatered transmission experiment," in the proc. of OFC 2001, PD24, 2001.

[1-43] J. Kani, H. Suzuki, M. Teshima, N. Takachio, and K. Iwatsuki, "Triple-wavelength-band WDM transmission technologies," in the proc. of OFC 2002, TuR-5, pp. 122-123, 2002.

[1-44] H. Masuda, H. Kawakami, S. Kuwahara, A. Hirano, K. Sato, and Y. Miyamoto, "1.28 Tbit/s (32 x 43 Gbit/s) field trial over 528 km (6/spl times/88 km) DSF using L-band remotely-pumped EDF/distributed Raman hybrid inline amplifiers," Electron. Lett., vol. 39, no. 23, pp. 1680-1670, 2003.

[1-45] C. Headley and G. P. Agrawal eds., "Raman amplification in fiber optical communication systems," Elsevier Academic Press, Elsevier Inc., London 2005.

[1-46] G. P. Agrawal, "Fiber optics communication systems," third edition, chapter 5, John Wiley & Sons, Inc., New York 2002.

[1-47] NTT WEST News Release 24/Dec./2003, http://www.ntt-west.co.jp/news/0312/031224.html. (in Japanese)

[1-48] G. P. Agrawal, "Fiber optics communication systems, " third edition, chapter 7, John Wiley & Sons, Inc., New York 2002.

[1-49] ITU-T Recommendation of G.650.1, "Definitions and test methods for linear, deterministic attributes of single-mode fibre and cable," (06/2004).

[1-50] ITU-T Recommendation of G.650.2, "Definitions and test methods for statistical and non-linear related attributes of single mode fibre and cable," (07/2007).

[1-51] T. Izawa and S. Sudo, "Optical fiber: Materials and Fabrication," KTK Scientific Publishers, Tokyo 1987.

[1-52] H. Murata, "Handbook of optical fibers and cables," second edition, Marcel Dekker, Inc., New York 1996.

[1-53] M. Kawase, T. Fuchigami, M. Matsumoto, S. Nagasawa, S. Tomita, and S. Takashima, "Subscriber single-mode optical fiber ribbon cable technologies suitable for midspan access," IEEE J. Lightwave Technol., vol. 7, no. 11, pp. 1675-1681, 1989.

[1-54] S. M. Wiederhorn, "Prevention of failure in glass by proof-testing," J. Am. Ceram. Soc., vol. 56, pp. 277-278, 1973.

[1-55] Y. Mitsunaga, Y. Katsuyama, and Y. Ishida, "Reliability assurance for long length optical fiber based on proof testing," Electron. Lett., vol. 17, no. 16, pp. 567-568, 1981.

[1-56] Y. Mitsunaga, Y. Kitayama, H. Kobayashi, and Y. Ishihara, "Failure prediction for long length optical fiber based on proof testing," J. Appl. Phys., vol. 53, no. 7, pp. 4846-4853, 1982.

[1-57] S. Tomita, F. Ashiya, and M. Kawase, "1000-fiber water-blocking cable," IEICE transactions, vol. E73-B, no. 9, pp. 1511-1516, 1990.

[1-58] ITU-T Recommendation of L. 12, "Optical fibre splices," (03/2008).

[1-59] M. Takaya, T. Katagiri, S. Nagasawa, and N. Kashima, “Design and development of optical fiber jointing techniques for efficient construction of aerial distribution cables,” in the proc. of IWCS, pp. 500-505, 1997.

[1-60] T. Katagiri, M. Tachikura, and Y. Murakami, "Basic design for highly stable mechanical optical fiber splice and its development," IEEE J. Lightwave Technol., vol. 17, no. 11, pp. 2297-2306, 1999.

[1-61] T. Satake, S. Nagasawa, and R. Arioka, "A new type of demountable plastic-molded single-mode multifiber connector," IEEE J. Lightwave Technol. vol. 4, no. 8, pp. 1232-1236, 1986.

[1-62] N. Tomita, H. Kobayashi, M. Shimizu, and J. Takagi, "A new high-density fiber organizer for optical fiber cable joints," IEEE J. Lightwave Technol., vol. 4, no. 8, pp. 1223-1227, 1986.

[1-63] ITU-T Recommendation of L. 50, "Requirements for passive optical nodes: Optical distribution frames for central office environments," (11/2003).

[1-64] N. Sato ed., "Optical Fiber Technologies toward IT Era," Chapters 4 and 5, IEICE 2001. (in Japanese)

[1-65] H. Hakozaki, H. Iwata, K. Hogari, and K. Sato, "Reliability of optical fiber cables for access network," in the proc. of Eurocable2000, pp. 87-94, 2000.

[1-66] K. Takayama, N. Susa, M. Hirai, and N. Uchida, "Observation of surface flaws in fused silica optical fibers," Appl. Phys. Lett., vol. 30, no. 3, pp. 155-157, 1977.

[1-67] J. E. Ritter, J. M. Sullivan, and K. Jakus, "Application of fracture-mechanics theory to fatigue failure optical glass fibers," J. Appl. Phys., vol. 49, pp. 4779-4782, 1978.

[1-68] K. Noguchi, N. Shibata, N. Uesugi, K. Ishihara, and Y. Negishi, "Optical fiber loss increase due to hydrogen and long-term loss stability for optical fiber cables," IEICE Trans. Japan, vol. J68-B, no. 7, pp. 795-802, 1985.

[1-69] S. Tomita, H. Tachino, and N. Kasahara, "Water sensor with optical fiber," IEEE J. Lightwave Technol., vol. 8, no. 12, pp. 1829-1832, 1990.

[1-70] M. Tachikura, K. Mine, H. Izumita, S. Uruno, and M. Nakamura, "Newly developed optical fiber distribution system and cable management in central office," in the proc. of 50th IWCS, pp. 98-105, 2001.

[1-71] I. Sankawa, Y. Koyamada, S. Furukawa, T. Horiguchi, N. Tomita, and Y. Wakui, "Optical fiber line surveillance system for preventive maintenance based on fiber strain and loss monitoring," IEICE Transactions on Communications, vol. E76-B, no. 4, pp. 402-409, 1993.

[1-72] ITU-T Recommendation of L. 25, "Optical fibre cable network maintenance," (10/1996).

[1-73] S. Yoshino, M. Takaya, H. Sonoda, M. Uchino, Y. Yuki, R. Nagano, H. Izumita, and N. Kuwaki, "Analysis of mechanical splicing faults in FTTH trial," in the proc. of OFC/NFOEC 2008, NthC-4, 2008.

[1-74] T. Horiguchi, T., Kurashima, and M. Tateda, "Tensile strain dependence of Brillouin frequency shift in silica optical fibers," IEEE Photon. Technol. Lett, vol. 1, no. 5, pp. 107-108, 1989.

[1-75] T. Kurashima, T. Horiguchi, H. Izumita and S. Furukawa, "Brillouin optical-fiber time domain reflectometry", IEICE Trans., vol. E76B, no. 4, pp. 382-390, 1993.

[1-76] M. P. Gold and A. H. Hartog, "Improved-dynamic-range single-mode OTDR at 1.3 μm," Electron. Lett., vol. 20, pp. 285-287, 1984.

[1-77] M. Nakazawa, M. Tokuda, K. Washio, and Y. Asahara, "130-km-long fault location for single-mode optical fiber using 1.55-μm Q-switched Er^{3+}:glass laser," Optics Lett., vol. 9, no. 7, pp. 312-314, 1984.

[1-78] P. Healey and D. J. Malyon, "OTDR in single-mode fiber at 1.5 μm using heterodyne detection," Electron. Lett., vol. 18, no. 12, pp. 862-863, 1982.

[1-79] J. King, D. F. Smith, K. Richards, P. Timson, R. E. Epworth, and S. Wright, "Development of coherent OTDR instrument, " IEEE J. Lightwave Technol., vol. LT-5, no. 4, pp. 616-624, 1987.

[1-80] Y. Koyamada and H. Nakamoto, "High performance single mode OTDR using coherent detection and fibre amplifiers," Electron. Lett., vol. 26, no. 9, pp. 573-574, 1990.

[1-81] L. C. Bank and D. M. Spirit, "OTDR performance enhancement through erbium fibre amplification," Electron. Lett., vol. 25, no. 25, pp. 1693-1694, 1989.

[1-82] P. Healey, "Fading in heterodyne OTDR, "Electron. Lett., vol. 20, no. 1, pp. 30-32, 1984.

[1-83] N. Tomita, H. Takasugi, N. Atobe, I. Nakamura, F. Takaesu, and S. Takashima, "Design and performance of a novel automatic fiber line testing system with OTDR for optical subscriber loops," IEEE J. Lightwave Technol., vol. 12, no. 5, pp. 717-726, 1994.

[1-84] ITU-T Recommendation L.40, "Optical fibre outside plant maintenance support, monitoring and testing system," (10/2000).

[1-85] ITU-T Recommendation L.42, "Extending optical fibre solutions into the access network," (05/2003).

[1-86] ITU-T Recommendation L.41, "Maintenance wavelength on fibers carrying signals," (05/2000).

[1-87] N. Nakao, H. Izumita, T. Inoue, Y. Enomoto, N. Araki, and N. Tomita, "Maintenance method using 1650-nm wavelength band for optical fiber cable networks," IEEE J. Lightwave Technol., vol. 19, no. 10, pp. 1513-1520, 2001.

[1-88] H. Izumita, S. Furukawa, Y. Koyamada, and I. Sankawa, "Fading Noise Reduction in Coherent OTDR," IEEE Photon. Technol. Lett. vol. 4, no. 2, pp. 201-203, 1992.

[1-89] T. Horiguchi, K. Shimizu, T. Kurashima, M. Tateda, and Y. Koyamada, "Development of a distributed sensing technique using Brillouin scattering," IEEE J. Lightwave Technol., vol. 13, no. 7, pp. 1296-1302, 1995.

[1-90] S. Furukawa, Y. Koyamada, I. Sankawa, and H. Izumita, "Enhancement of OTDR performance using optical fiber amplifiers," IEICE Transactions on Communications, vol. J75B-1, no. 5, pp. 304-313, 1992. (in Japanese)

[1-91] S. Furukawa, H. Izumita, I. Sankawa, and Y. Koyamada, "High dynamic range, low fading noise coherent OTDR using erbium fiber amplification and LD temperature changing techniques," in the proc. of ECOC'91/IOOC'91, Mo.C1-3, pp. 81-84, 1991.

[1-92] H. Izumita, Y. Koyamada, I. Sankawa, and S. Furukawa, "A coherent optical time-domain reflectometer with a 40-dB dynamic range enhanced with erbium-doped fiber amplifiers," in the technical digest of OFC'92, WK6, p. 147, 1992.

[1-93] H. Izumita, Y. Koyamada, S. Furukawa, and I Sankawa, "Optical nonlinearities in coherent OTDR enhanced with optical fiber amplifiers," IEICE Trans., J76B-1, no. 2, pp. 171-181, 1993. (in Japanese)

[1-94] H. Izumita, Y. Koyamada, S. Furukawa, and I Sankawa, "The performance

limit of coherent OTDR enhanced with optical fiber amplifiers due to optical nonlinear phenomena," IEEE J. Lightwave Technol., vol. 12, no. 7, pp. 1230-1238, 1994.

[1-95] H. Izumita, Y. Koyamada, S. Furukawa, and I. Sankawa, "Performance limits of coherent OTDR due to optical nonlinear effects," in the proceeding of Symposium on Optical Fiber Measurements (SOFM'94), pp. 39-44, 1994 (Invited).

[1-96] H. Izumita, Y. Koyamada, S. Furukawa, and I. Sankawa, "Stochastic of amplitude fluctuation in coherent OTDR and its reduction technique," IEICE Trans., vol. J76B-1, no. 6, pp. 439-450, 1993. (in Japanese)

[1-97] H. Izumita, Y. Koyamada, S. Furukawa, and I. Sankawa, "Stochastic amplitude fluctuation in coherent OTDR and a new technique for its reduction by stimulating synchronous optical frequency hopping," IEEE J. Lightwave Technol., vol. 15, no. 2, pp. 267-278, 1997.

[1-98] K. Tanaka, H. Izumita, S. Furukawa, Y. Koyamada, M. Sumida, and M. Murakami, "Coherent OTDR enhanced with optical fiber amplifiers for testing optical fiber transmission lines containing in-line Er-doped fiber amplifiers," IEICE Technical Report OCS93-23, pp. 21-26, 1993. (in Japanese)

[1-99] I. Ogushi, H. Izumita, K. Tanaka, and M. Nakamura, "A highly developed coherent detection OTDR for measuring the distributed fiber loss and Raman gain of a 200 km single-mode fiber," in the proc. of OFS-16, We1-2, pp. 262-265, 2003.

[1-100] I. Ogushi, H. Izumita, K. Tanaka, and M. Nakamura, "Measurement of a 340 km optical fiber line with a remotely pumped EDFA and DRA by using a highly developed coherent detection OTDR," in the proc. of ECOC2004, Tu3.6.5, vol. 2, pp. 224-225, 2004.

[1-101] H. Izumita, T. Sato, M. Tateda, and Y. Koyamada, "Brillouin OTDR employing optical frequency shifter using sideband generation technique with high-speed phase modulator," IEEE Photon. Technol. Lett., vol. 8, no. 12, pp. 1674-1676, 1996.

[1-102] H. Izumita, T. Sato, M. Tateda, and Y. Koyamada, "Brillouin OTDR enhanced with an optical frequency shifter using a high-speed phase modulator," in the technical digest of Optoelectronics and Communication Conference (OECC'96), 17C1-3, pp. 138 - 139, 1996.

[1-103] H. Izumita, T. Sato, M. Tateda, T. Horiguchi, and Y. Koyamada, "1.65 μm Brillouin optical time-domain reflectometry employing a Raman fiber amplifier

and lithium-niobate phase modulator," in the technical digest of OFC'97, WJ7, pp. 159-160, 1997.

[1-104]H. Izumita, T. Sato, M. Tateda, Y. Koyamada, and H. Suda, "Brillouin OTDR enhanced with wideband double-balanced receiver," in the proc. of IEICE Communications Society Conference, B-981, p. 466, autumn, 1996. (in Japanese)

[1-105]H. Izumita, T. Horiguchi, and T. Kurashima, "Distributed sensing techniques using Brillouin scattering," in the proc. of the 12th Conference on Optical Fiber Sensors (OFS-12), OWD1, pp. 316-319, 1997 (Invited).

[1-106]H. Izumita, "Recent development in fiber optic monitoring system for access networks," in the proc. of OFS-16, We1-1, pp. 258-261, 2003 (Invited).

[1-107]H. Izumita, "Standardization trend of optical fiber maintenance technologies in optical access networks," IEICE Technical Report OCS2005-85, pp. 55-60, 2005 (Invited). (in Japanese)

[1-108]H. Izumita, "Recent developed monitoring technologies for optical access networks," IEICE Technical Report OFT2003-114, pp. 7-12, 2004. (in Japanese)

[1-109]ITU-T Recommendation of L. 53, "Optical fibre maintenance criteria for access networks," (05/2003).

[1-110]ITU-T Recommendation of L. 66, "Optical fibre cable maintenance criteria for in-service fibre testing in access networks," (05/2007).

[1-111]ITU-T Recommendation of L. 68, "Optical fibre cable maintenance support, monitoring and testing system for optical fibre cable networks carrying high total optical power," (10/2007).

Chapter 2. Enhancement of OTDR performance with coherent detection technique and optical fiber amplifiers

The performance of optical time-domain reflectometry (OTDR) is significantly improved by applying a coherent detection technique and optical fiber amplification. This chapter discusses theoretical and experimental studies of both direct-detection and coherent-detection OTDR enhanced with erbium-doped fiber amplifiers (EDFAs).

2.1. Introduction

The EDFA has attracted much attention in fiber optic communication systems, since it offers the potential of operation with high gain, high saturation output power, and high bandwidth [2-1], [2-2]. Moreover, transmission systems using EDFAs can upgrade their signal bit rates and accommodate wavelength-division multiplexing (WDM) signals through exchanges of terminal equipment [2-3], [2-4]. These advantages have resulted in very rapid development of EDFAs. For example, the commercial systems, with a span of 160 km, enhanced with an EDFA as a post-amplifier and an InGaAsP- avalanche photodiode (APD) are deployed in NTT trunk line network [2-5]. Furthermore, long-haul submarine optical transmission systems with EDFAs as 1R optical repeaters have also been deployed [2-6].

OTDR is an important method for fault location and characterization of optical fiber transmission lines. Many studies have been made into extending the dynamic range of the OTDR [2-7], [2-8] in accordance with the development of advanced optical transmission systems. OTDR yields its highest dynamic range with high-power sources, such as Nd:YAG lasers [2-9] or Er^{3+}:glass lasers [2-10]. These power sources, however, are impractical for field use, because they are not suitable for robust, portable instruments. In addition, the safety of network operator must be considered [2-11], [2-12].

The coherent detection technique is one of the most promising approaches for extending the dynamic range of OTDR. J. P. King et al. developed a coherent -detection OTDR (C-OTDR) with a single-way dynamic range (SWDR) of 28 dB with a 5-μs pulse width (i.e., a 500-m spatial resolution) and 10^6 integrations [2-13]. By applying a coherent detection technique and EDFAs, Y. Koyamada et al. constructed a high-performance OTDR having an SWDR of 33 dB with 1-μs launch pulses (100-m spatial resolution) and 10^4 integrations [2-14]. There have also been a few investigations of enhancing direct-detection OTDR (D-OTDR) with EDFAs [2-15].

There is still the possibility of further extending the SWDR, however, by optimizing the application of EDFAs. In addition, the C-OTDR has the problem of amplitude fluctuation of as much as 0.2 dB in the backscattered trace [2-13], caused by the fading phenomenon of the Rayleigh scattering signal [2-16].

This chapter describes the optimized design of a C-OTDR enhanced with EDFAs. This C-OTDR has the potential of a very high dynamic range, achieved using compact optical components suited for integration into a robust, portable instrument. Sections 2.2 and 2.3 describe the basic principles of OTDR and define key parameters, and describe the basic principles of C-OTDR, respectively. Section 2.4 gives a numerical evaluation of the dynamic range enhancement with EDFAs. Sections 2.5 and 2.6 describe the feasibility of enhancing D-OTDR and C-OTDR, respectively, with EDFAs. Finally, section 2.7 discusses the nonlinear phenomena occurring in an optical fiber, which can degrade the SWDR of C-OTDR.

2.2. Basic principles of OTDR

2.2.1. Basic configuration and typical trace

Figure 2.1 shows the basic OTDR configuration and a typical OTDR trace for a single-mode optical fiber. The main components of a conventional OTDR are a laser diode (LD), an APD an analog-digital (A-D) converter, a digital processor, and a computer [2-18].

The LD launches pulse light with low repetition into the test fiber. Backscattered light is generated by Rayleigh scattering and Fresnel reflection in the test fiber. The backscattered signals are introduced into the APD via a directional fiber coupler and averaged to improve the signal-to-noise ratio (SNR). The backscattered signals as a function of the round-trip time indicate the attenuation of the test fiber, or the reflectance in the test fiber. After logarithmic transformation, the resultant signals are displayed as an OTDR trace on the computer monitor.

When pulse light with peak power p_0 and pulse width τ is launched into a single-mode optical fiber, the Rayleigh backscattered power p_R observed at the input fiber end face at time t is given by [2-8],[2-18],[2-19]

$$p_R = p_0 S \alpha_R \left(\frac{c\tau}{2n} \right) \exp\left[-2\alpha \left(\frac{ct}{2n} \right) \right], \tag{2.1}$$

where S is the recapture ratio of the Rayleigh backscattered power into the fiber, α_R is the attenuation coefficient of Rayleigh scattering, c is the light velocity in vacuum, n is

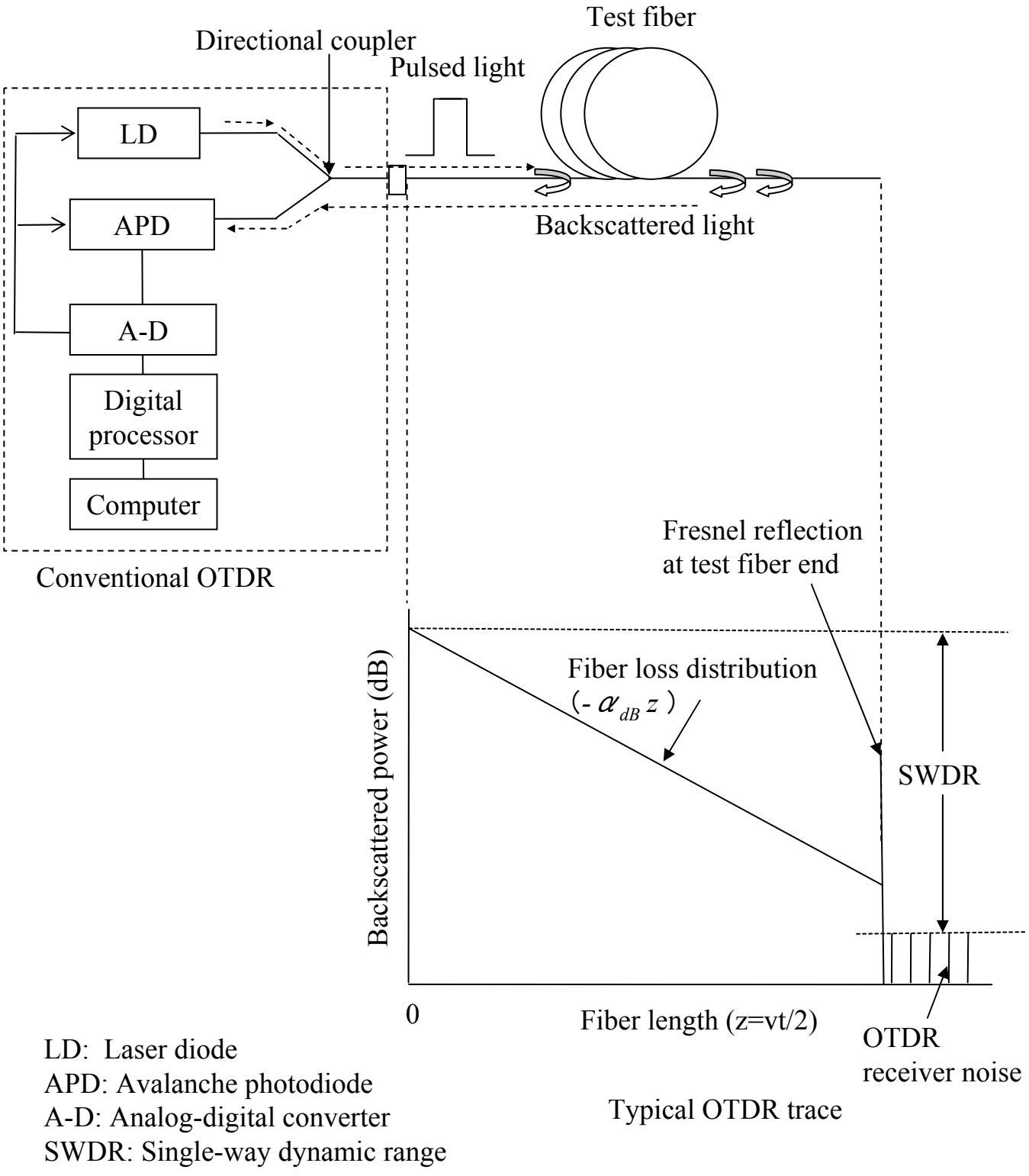

Figure 2.1 Basic OTDR configuration for a single-mode optical fiber, and a typical OTDR trace

the refractive index of the test fiber core, and $\alpha(ct/2n)$ is the cumulative attenuation up to a distance $ct/2n$, in nepers. The time t corresponds to the location z (= $ct/2n$) in the fiber. For simplicity, the detected backscattered signal power given by Eq. (2.1) is logarithmically transformed and multiplexed by a factor of 1/2. Then, the backscattered signal distribution indicates the single-way loss of the test fiber. The backscattered signal power $P(z)$ in the OTDR trace is given by

$$P(z) = \frac{P_0 + R_R}{2} - \alpha_{dB} z \text{ , (dBm)} \tag{2.2}$$

$$R_R = 10 \log\left[\alpha_R S \frac{c\tau}{2n} \right] \text{, (dB)} \tag{2.3}$$

where P_0 is the pulse power of p_0 (in dBm), R_R is the Rayleigh backscattering factor, and α_{dB} (= $10\alpha\log_{10}(e)$) is the attenuation coefficient of the fiber (in dB/km). Therefore, we can see that the fiber loss distribution in the OTDR trace in Fig. 2.1 is a linear function of distance in the fiber, z. In conventional OTDR measurement of a test fiber with a large loss, the pulse power P_0 is changed under certain conditions to avoid electrical and optical saturation of the OTDR receiver. Hence, the vertical axis in the OTDR trace, i.e., the "Backscattered power (dB)," usually represents the relative backscattered signal power. This conventional description is adopted in this thesis.

The OTDR technique, which can be applied nondestructively at one end face, can be used to evaluate fiber parameter fluctuations and splice loss and to locate faults in an optical transmission line composed of several optical fiber cables. Hence, OTDR has become a practical, helpful tool in manufacturing, testing, and installing optical fiber cables.

2.2.2. Dynamic range

The dynamic range of OTDR is an important parameter for evaluating performance. The dynamic range provides information on both the maximum measurement range and the measurement time required for a given fiber loss. An IEC standard gives detailed definitions [2-17]. The SWDR of OTDR, illustrated in Fig. 2.1, is defined as the difference between the initial Rayleigh backscattered signal level, $P(0)$ in Eq. (2.2), and the peak level of the OTDR receiver noise, expressed in decibels for the single-way fiber loss. The SWDR is thus given by

$$SWDR = \frac{\left[P_0 + R_R - L_c - P_{\min} + \frac{SNIR_{AVE}}{2} \right]}{2} - M_P \text{ (dB).} \tag{2.4}$$

P_0: Incident pulse power (dBm).

L_C: Directional coupler loss (dB).

P_{min}: Minimum detectable power of receiver with SNR = 1 (dBm).

$SNIR_{AVE}$: Electrical signal-to-noise improvement ratio by signal averaging (dB).

In addition, M_P is the margin (in dB) for defining the noise level as 99.7% of the peak noise level, not as an SNR of 1. Assuming a Gaussian noise distribution, 99.7% of all noise samples are included within three standard deviations. This corresponds to M_P = 2.4 dB.

Equation (2.4) indicates that increasing the SWDR requires the following:

(1) increasing the incident pulse power,

(2) improving the OTDR receiver sensitivity, and

(3) increasing the amount of averaging to improve the SNR.

The Rayleigh backscattering factor depends on the pulse width. The next subsection discusses the relationship between the pulse width, i.e., the spatial resolution, and dynamic range improvement.

2.2.3. Tradeoff between spatial resolution (bandwidth) and dynamic range

The spatial resolution of OTDR, Δz, with pulse width τ is given by [2-17]

$$\Delta z = \frac{c\tau}{2n} \text{ (m)}. \tag{2.5}$$

Then, the required bandwidth of the OTDR receiver, B, is $1/\tau$ (in Hz). From Eqs. (2.3) and (2.5), the Rayleigh backscattering factor is derived as

$$R_R = 10\log[\alpha_R S\Delta z] = 10\log\left[\alpha_R S\frac{c}{2nB}\right]. \tag{2.6}$$

If the pulse width τ is narrowed by a factor of 1/10, e.g., from 1 μs to 100 ns, the spatial resolution Δz is improved from 100 m to 10 m, but the Rayleigh backscattering factor R_R is decreased by 10 dB, and the required bandwidth B is increased by 10 dB. The minimum detectable power of the OTDR receiver for direct detection is inversely proportional to the square root of the bandwidth B. For coherent detection, the minimum detectable power is inversely proportional to the bandwidth B. Consequently, from Eq. (2.4), the SWDRs for D-OTDR and C-OTDR decrease by 7.5 and 10 dB, respectively. Conversely, if the spatial resolution Δz is changed from 10 to 100 m by increasing the pulse width, the SWDR increases by 7.5 and 10 dB for D-OTDR and C-OTDR, respectively.

2.3. Coherent detection OTDR (C-OTDR)

Coherent detection is an attractive technique for improving the receiver sensitivity up to the quantum limit, which is advantageous for direct detection [2-13], [2-14]. This section describes the basic principle of C-OTDR and the requirements for constructing a compact, high-performance C-OTDR. The advanced performance of C-OTDR is also compared with that of D-OTDR.

2.3.1. Basic principle

Figure 2.2 shows the basic C-OTDR configuration. Continuous wave (CW) light from a narrow-linewidth light source with optical frequency ν is divided by a 3-dB fused-fiber directional coupler (FC1) into two paths: a signal path, and a local oscillator (LO) path. The signal pulse is produced by an acousto-optic (AO) switch (AO-SW1), consisting of an acousto-optic modulator (AOM) made of $PbMoO_4$ and operated in a pulsed mode. The optical frequency of the signal pulse is shifted by the modulation frequency of AO-SW1 and amplified by an EDFA. A second AO switch (AO-SW2) is operated in pulsed mode and synchronized with AO-SW1 to eliminate amplified spontaneous emission (ASE) noise from the EDFA. For a 100-ns or shorter pulse width, an optical waveguide switch made of $LiNbO_3$ (EO-SW) is used instead of AO-SW2 in order to reshape the signal pulse. Finally, the amplified signal pulse is launched into a test fiber.

When a signal pulse with unit pulse power is launched into the test fiber and passes through FC2 at time $t = 0$, the Rayleigh backscattered signal, $E_B(t)\exp(j2\pi(\nu+\nu_A)t)$ at time t, is mixed with the LO light, $E_{LO}\exp(j2\pi\nu t)$, by FC3 and then detected by a double-balanced p-i-n field-effect transistor (FET) receiver. The detected signal current $I_{SC}(t)$ is proportional to the square of the total signal field and is given by

$$I_{SC}(t) = \left(\frac{\eta e}{h\nu}\right)\left[{E_{LO}}^2 + {E_B}^2 + 2E_{LO}\cdot E_B(t)\cdot\cos(j2\pi\nu_A t)\right]. \tag{2.7}$$

The intermediate-frequency- (IF-) band signal of Eq. (2.7) is converted to the baseband signal by a mixer, an electrical LO, and a low-pass filter (LPF). The baseband signals are squared and averaged after analog-digital conversion. The resultant signal is given by

$${I_{SC}}^2(t) = 2\left(\frac{\eta e}{h\nu}\right)^2 {E_{LO}}^2\cdot E_B(t)^2. \tag{2.8}$$

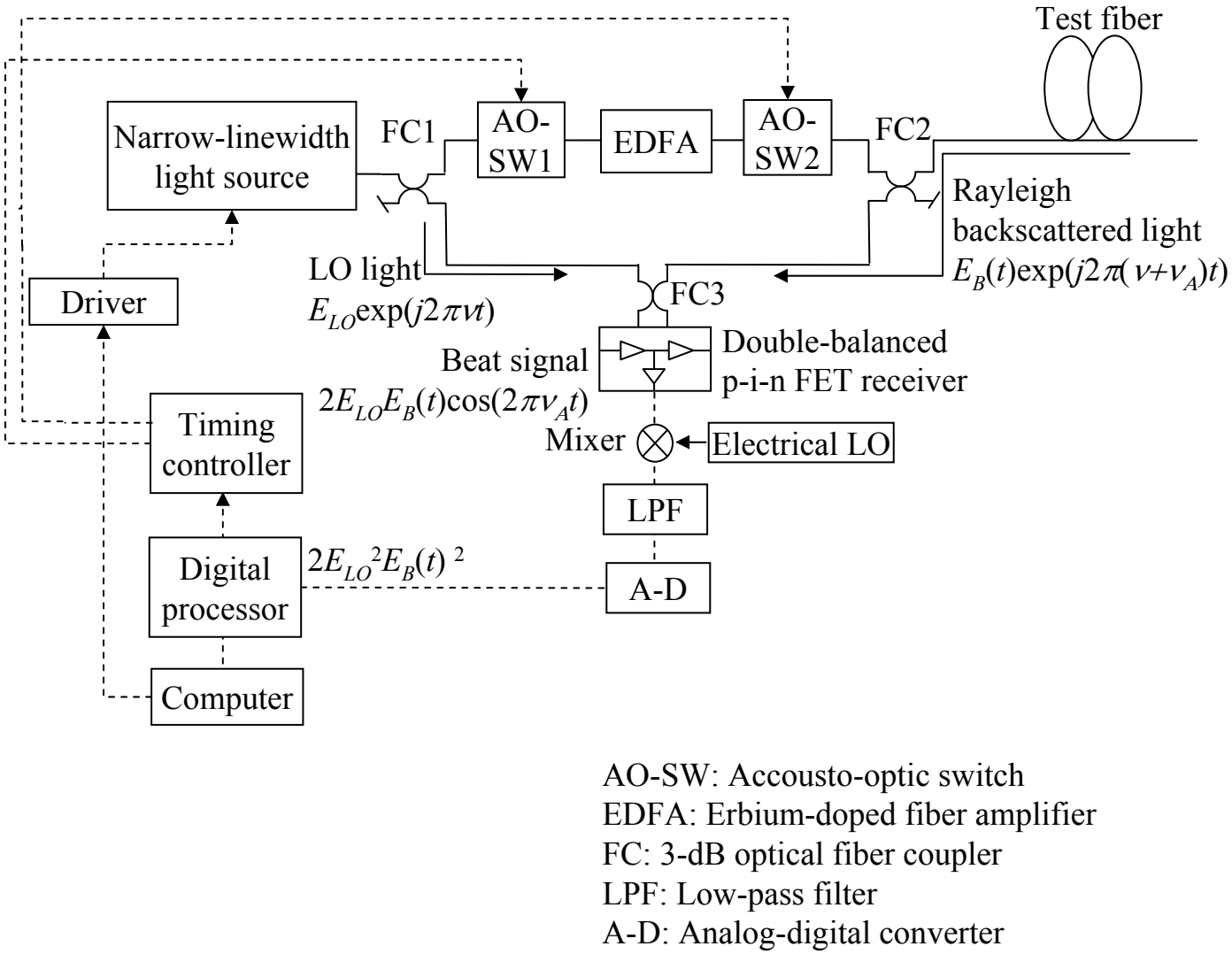

Figure 2.2 Basic C-OTDR configuration

Here, $E_B(t)^2$ corresponds to the backscattered signal power p_R in Eq. (2.1). Consequently, a signal detected by C-OTDR can be displayed as a conventional OTDR trace.

2.3.2. Requirements for optical components

Constructing C-OTDR requires optical components with special characteristics. To achieve coherent detection and improve the sensitivity up to the shot noise limit, the light source should have a narrow linewidth, which is sufficiently narrower than the bandwidth B of the receiver. Since the linewidth of a conventional distributed-feedback laser diode (DFB-LD) is several megahertz, an external cavity is needed. A 1-km single-mode optical fiber with an optical isolator embedded at the far end can be connected to the DFB-LD to reduce the line width [2-20]. For the advanced C-OTDR described in this thesis, the resultant linewidth was less than 10 kHz. Extension of C-OTDR to Brillouin optical time-domain reflectometry (B-OTDR), as described in chapter 6, uses a $LiNbO_3$ phase modulator (LN-PM) whose operation depends on the state of polarization (SOP), thus requiring polarization stability for the CW light used in C-OTDR. Therefore, for the external cavity, a 250-m polarization-maintaining fiber is used in this case, instead of a 1-km single-mode optical fiber. The LO light power from the above-mentioned light source with a narrow linewidth should be sufficiently large. For the C-OTDR described in this thesis, the typical power was about -3 dBm. Recently, a high-power laser can be implemented as an InGaAsP multiple quantum well (MQW) DFB-LD. The output power is over 10 dBm, which is sufficiently large to achieve ideal coherent detection.

For the coherent receiver, a double-balanced p-i-n FET receiver is used to reduce the intensity noise. For the C-OTDR described here, the typical common mode rejection ratio (CMRR) was about 20 dB with a 1-MHz bandwith over the IF band.

2.3.3. Fading noise in C-OTDR trace

The coherent detection technique is a promising approach for improving the receiver sensitivity up to the shot noise limit. This leads to problems, however, with the OTDR trace: (1) measurement accuracy degradation due to fading noise, and (2) fluctuation of the detection efficiency because of SOP mismatch between the backscattered signals and the LO light [2-16].

Figure 2.3 shows typical C-OTDR traces with (a) N=1 integration and (b) N=1000

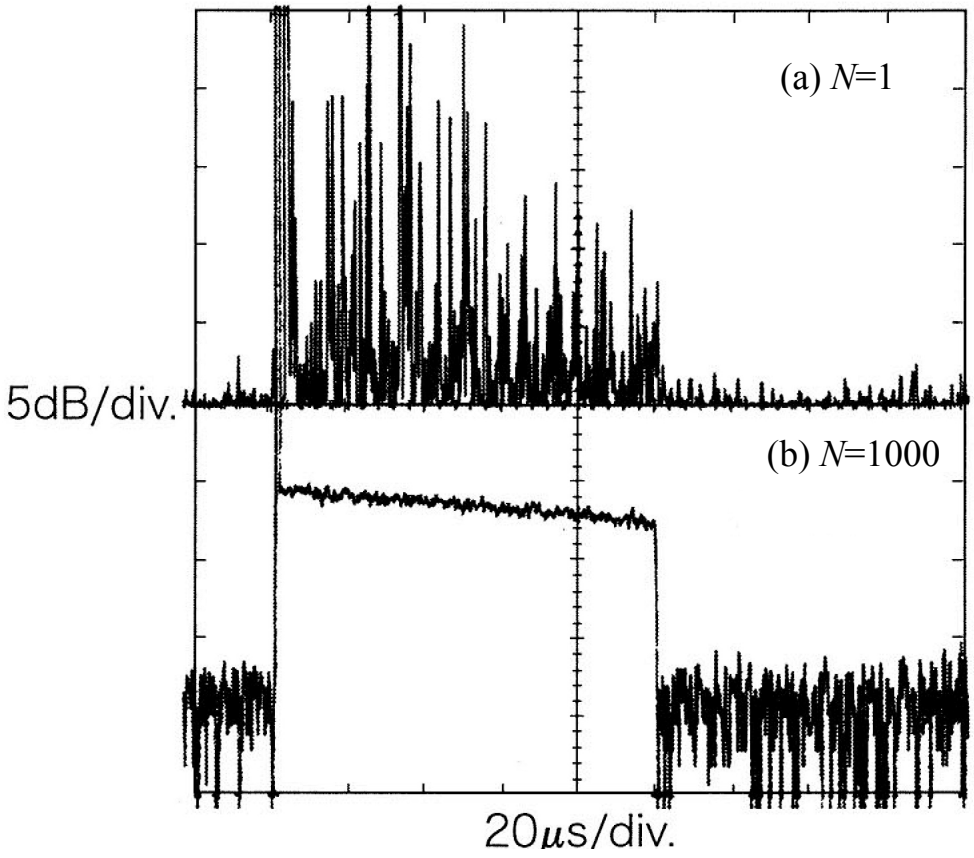

Figure 2.3 C-OTDR traces (a) with N=1 integration and (b) with N=1000 integrations

integrations, measured using the experimental setup shown in Fig. 2.2. For (a), a large amplitude fluctuation appears in the C-OTDR trace. For (b), the SWDR increased by about 7.5 dB, which agrees with the calculated value, since the SNR improvement by averaging is proportional to the square root of the number of integrations, *N*. The large amplitude fluctuation, however, was not reduced. Therefore, a reduction technique for this is still required. The amplitude fluctuation of the OTDR trace decreases in proportion to the square root of the number of integrations of independent backscattered signals [2-13]. Changing the optical frequency of the source produces independent backscattered signals, thus reducing the amplitude fluctuation by integration over the optical frequency range [2-21]. Chapter 4 proposes a powerful reduction technique and discusses its feasibility.

2.4. Numerical evaluation of dynamic range enhancement with EDFAs

An EDFA has the characteristics of high gain and high saturation output power, so the SWDR of OTDR can be increased by incorporating EDFAs [2-14], [2-15]. When an EDFA amplifies the incident pulse or a backscattered signal in OTDR, the ASE from the EDFA increases the noise at the receiver. The effective configuration of OTDR with EDFAs is thus clarified through numerical evaluation of the SNR enhancement achieved by applying EDFAs in both D-OTDR and C-OTDR as (a) a post-amplifier, (b) an inline amplifier, and (c) a pre-amplifier.

2.4.1. SNR improvement of D-OTDR with EDFAs

Figure 2.4 shows three possible arrangements by which EDFAs can be incorporated into D-OTDR: as (a) a post-amplifier, (b) an inline amplifier, and (c) a pre-amplifier.

SNR of conventional D-OTDR

Let P_S be the backscattered signal light power measured at the D-OTDR receiver. The SNR at the output of the receiver is given by

$$SNR_d = \frac{I_{Sd}^{\ 2}}{I_{Nd}^{\ 2}}, \tag{2.9}$$

where I_{Sd}^2 and I_{Nd}^2 are the mean square signal current and noise current, respectively, and are defined as the following:

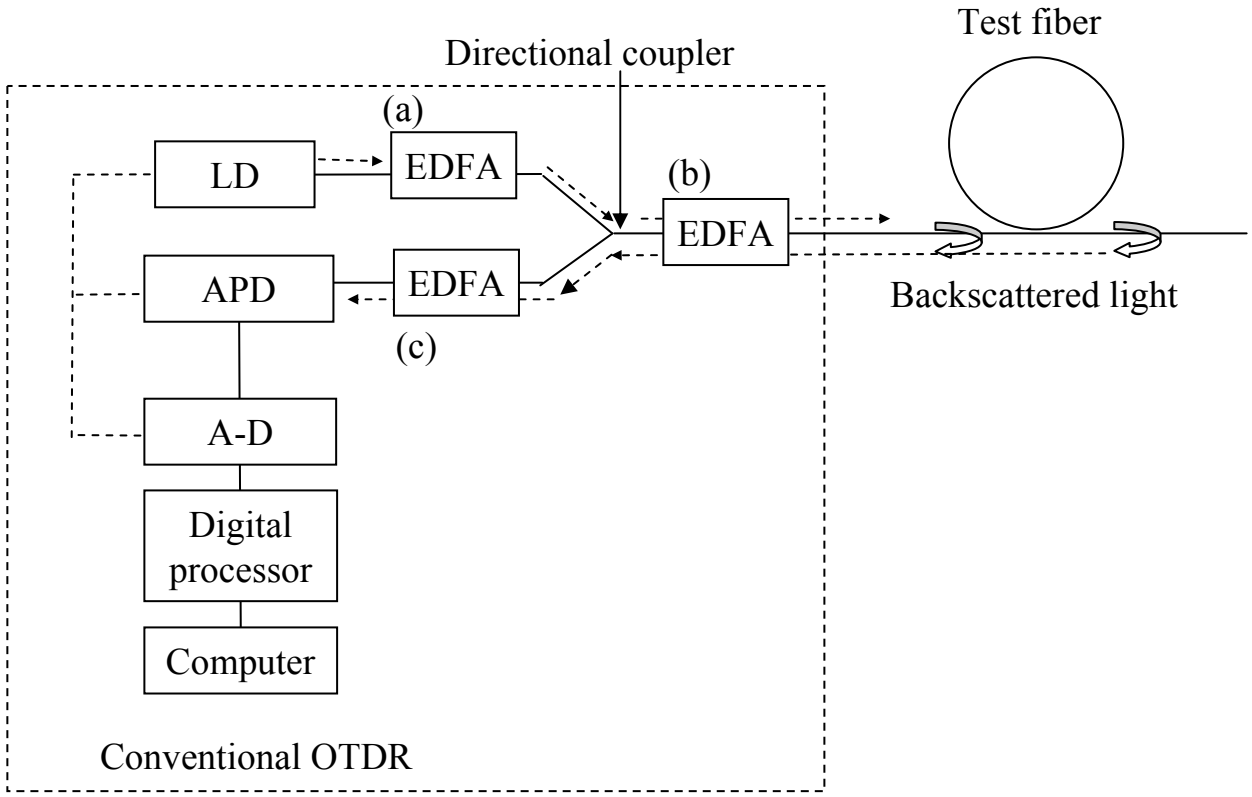

LD: Laser diode
APD: Avalanche photodiode
A-D: Analog-digital converter
EDFA: Erbium-doped fiber amplifier

Figure 2.4 Arrangements for incorporating EDFAs into D-OTDR

$$I_{Sd}{}^2 = \left[P_S \left(\frac{\eta e}{h\nu} \right) M \right]^2 , \tag{2.10}$$

$$I_{Nd}{}^2 = \left[\frac{4Fk_BT}{R_L} + 2eM^{2+y} \left\{ i_d + P_S \left(\frac{\eta e}{h\nu} \right) \right\} \right] B . \tag{2.11}$$

η: Photodiode quantum efficiency.
e: Electron charge.
h: Planck's constant.
v: Optical frequency.
M: Multiplication factor of APD.
F: Receiver noise figure.
k_B: Boltzmann's constant.
T: Temperature.
R_L: Receiver load resistance.
y: Excess noise factor of APD.
i_d: Photodiode dark current.
B: Receiver bandwidth.

The first, second, and last terms of $I_{Nd}{}^2$ represent the thermal noise, the shot noise of the dark current, and the shot noise of the backscattered signal, respectively. Since the mean square noise $I_{Nd}{}^2$ is proportional to the bandwidth B, the minimum detectable power of D-OTDR is derived from Eq. (2.9) by assuming $SNR_d = 1$. If the multiplication factor of APD, M, is sufficiently large and the excess noise factor, y, is negligibly small, then the dark current shot noise dominates the mean square noise. Assuming that the photodiode dark current, receiver bandwidth, optical frequency of the OTDR pulse, and photodiode quantum efficiency are set to typical values of $I_d = 30$ nA, $B = 1$ MHz, $v = 194$ THz (1.55 μm), and $\eta = 0.8$, respectively, the calculated minimum detectable power is about -70 dBm.

SNR of D-OTDR with EDFA as post-amplifier

When an EDFA is used as a post-amplifier, as shown in Fig. 2.4(a), the signal pulse is amplified by a factor of g and sent into the test fiber; the backscattered signal light power at the receiver becomes gP_S. The backscattered ASE originating from the ASE and transmitted into the test fiber is introduced to the receiver via the directional coupler. The ASE power density per unit bandwidth radiated from the EDFA is given by $2(g - 1)\mu hv$ [2-22], where μ is the population inversion factor of the amplifier. The

factor of two is included to account for the two orthogonal polarization modes. The ASE power density per unit bandwidth at the receiver is given by

$$2P_{APO} = 2T_1^2 T_2 (g-1)\mu h\nu , \tag{2.12}$$

where T_1 is the transmission coefficient of the coupler, and T_2 is the reflection coefficient of the test fiber.

The SNR in this case is given by

$$SNR_{\mathrm{d,PO}} = \frac{I_{SPO,d}{}^2}{I_{NPO,d}{}^2}, \tag{2.13}$$

where $I_{SPO,d}{}^2$ and $I_{NPO,d}{}^2$ are the mean square signal current and noise current, respectively, and are defined as the following:

$$I_{SPO,d}{}^2 = g^2 I_{Sd}{}^2, \tag{2.14}$$

$$I_{NPO,d}{}^2 = I_{Nd}{}^2 + \left[M^{2+y} \left\{ 4eP_{APO}\Delta\nu \left(\frac{\eta e}{h\nu} \right) + 4P_{APO}P_S \left(\frac{\eta e}{h\nu} \right)^2 + 4P_{APO}{}^2 \Delta\nu \left(\frac{\eta e}{h\nu} \right)^2 \right\} \right] B , \tag{2.15}$$

where $\Delta\nu$ is the linewidth of the received ASE including that from the optical filter in the EDFA. The second through fourth terms in $I_{NPO,d}{}^2$ correspond to the shot noise produced by the ASE current, the ASE-signal beat noise, and the ASE-ASE beat noise [2-23].

SNR of D-OTDR with EDFA as inline amplifier

When an EDFA is used as an inline amplifier, as shown in Fig. 2.4(b), it amplifies both the pulsed signal light and the backscattered signal light by a factor of g. Consequently, the backscattered signal light power at the receiver is $g^2 P_S$. The ASE radiated toward the receiver reaches it through the coupler. The ASE radiated toward the test fiber, on the other hand, is reflected by it, amplified by the EDFA, and then transmitted to the receiver through the coupler. The total ASE power density at the receiver is thus given by

$$2P_{API} = 2T_1(1+gT_2)(g-1)\mu h\nu . \tag{2.16}$$

The SNR is given by

$$SNR_{\mathrm{d,I}} = \frac{I_{SI,d}{}^2}{I_{NI,d}{}^2}, \tag{2.17}$$

where $I_{SI,d}^2$ and $I_{NI,d}^2$ are the mean square signal current and noise current, respectively, and are defined as the following:

$$I_{SI,d}{}^2 = g^4 I_{Sd}{}^2, \tag{2.18}$$

$$I_{NI,d}{}^2 = I_{Nd}{}^2 + \left[M^{2+y} \left\{ 4eP_{AI}\Delta\nu\left(\frac{\eta e}{h\nu}\right) + 4P_{AI}P_S\left(\frac{\eta e}{h\nu}\right)^2 + 4P_{AI}{}^2\Delta\nu\left(\frac{\eta e}{h\nu}\right)^2 \right\} \right] B . \tag{2.19}$$

SNR of D-OTDR with EDFA as pre-amplifier

When an EDFA is used as a pre-amplifier, as shown in Fig. 2.4(c), it amplifies the backscattered signal light by a factor of g. The ASE radiated toward the receiver reaches it directly. The ASE power density at the receiver is then given by

$$2P_{APR} = 2(g-1)\mu h\nu . \tag{2.20}$$

The SNR is given by

$$SNR_{\mathrm{d,PR}} = \frac{I_{SPR,d}{}^2}{I_{NPR,d}{}^2}, \tag{2.21}$$

where $I_{SPR,d}^2$ and $I_{NPR,d}^2$ are the mean square signal current and noise current, respectively, and are defined as the following:

$$I_{SPR,d}{}^2 = g^2 I_{Sd}{}^2, \tag{2.22}$$

$$I_{NPR,d}{}^2 = I_{Nd}{}^2 + \left[M^{2+y} \left\{ 4eP_{APR}\Delta\nu\left(\frac{\eta e}{h\nu}\right) + 4P_{APR}P_S\left(\frac{\eta e}{h\nu}\right)^2 + 4P_{APR}{}^2\Delta\nu\left(\frac{\eta e}{h\nu}\right)^2 \right\} \right] B . \tag{2.23}$$

SNR improvement ratio (SNIR)

The SNR improvement ratios (SNIRs) in the post-, inline-, and pre-amplifier cases are obtained by using Eqs.(2.9), (2.13), (2.17), and (2.21). The SWDR improvements for these three cases are obtained by logarithmic transformation of the SNIRs, adapting the SWDR description commonly used for OTDR:

$$SNIR_{\mathrm{d,PO}} = 5\log\left[\frac{SNR_{\mathrm{d,PO}}}{SNR_{\mathrm{d}}}\right]^{1/2} \quad \text{(dB)}, \tag{2.24}$$

$$SNIR_{\mathrm{d,I}} = 5\log\left[\frac{SNR_{\mathrm{d,I}}}{SNR_{\mathrm{d}}}\right]^{1/2} \quad \text{(dB)}, \tag{2.25}$$

$$SNIR_{\mathrm{d,PR}} = 5\log\left[\frac{SNR_{\mathrm{d,PR}}}{SNR_{\mathrm{d}}}\right]^{1/2} \quad \text{(dB)}. \tag{2.26}$$

The SWDR improvements for these three cases are obtained by logarithmic transformation of the SNIRs, adapting the SWDR description commonly used for OTDR. Figure 2.5 shows the calculated SWDR improvements achieved by using an EDFA as (a) a post-amplifier and (b) an inline amplifier, for typical parameter values of T_1, T_2, i_d, η, μ, and $\Delta\nu$, as a function of the gain g (in dB).

For the post-amplifier case, the SWDR improvement increases almost linearly with g when g is less than 25 dB. In the region over 25 dB, the SWDR improvement gradually saturates and then depends on the population inversion factor μ of the EDFA and the bandwidth $\Delta\nu$ of the optical filter.

For the inline-amplifier case, the SWDR improvement increases almost linearly with g when g is less than 25 dB, which is similar to the characteristics for the post-amplifier case. The EDFA population inversion factor μ and the optical filter bandwidth $\Delta\nu$, however, influence the SWDR improvement throughout the whole range of g. Therefore, a narrow-bandwidth optical filter is required.

For the pre-amplifier case, Eqs. (2-12) and (2-20) indicate that P_{APR} is very much larger than P_{APO}, because T_1 and T_2 are usually smaller than 1. Therefore, the SWDR improvement is smaller than that for the post-amplifier case.

Figure 2.6 shows the SWDR improvements for the post- and inline-amplifier cases as a function of the gain g. When g is less than 25 dB, the SWDR improvement is greater with the inline amplifier than with the post-amplifier. This is because the inline amplifier amplifies both the signal pulse and the backscattered signal. If there is a large Fresnel reflection at the end face of the test fiber, i.e., if T_2 = 0.1, the SWDR improvement in both cases saturates when g is larger than 15 dB.

With an EDFA post-amplifier, an optical switch synchronously pulse-driven with the signal pulse can eliminate the residual ASE in the time domain [2-14], [2-15]. Therefore, the SWDR improvement can be increased. With an inline amplifier, such optical switch technology cannot be applied, thus limiting the SWDR improvement.

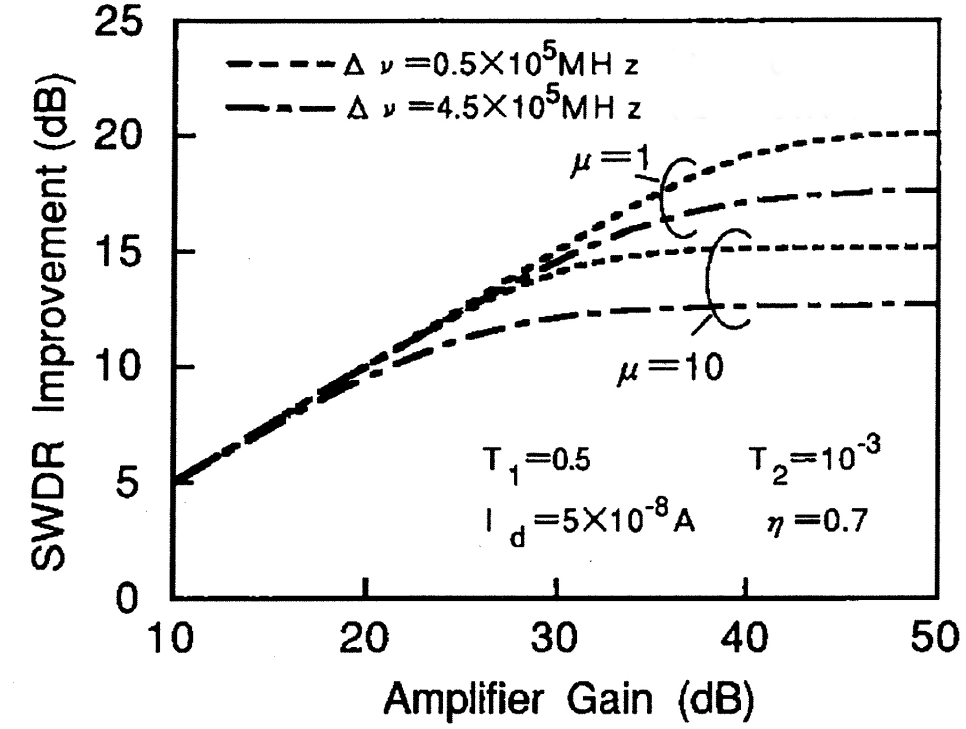

(a) LD post-amplifier

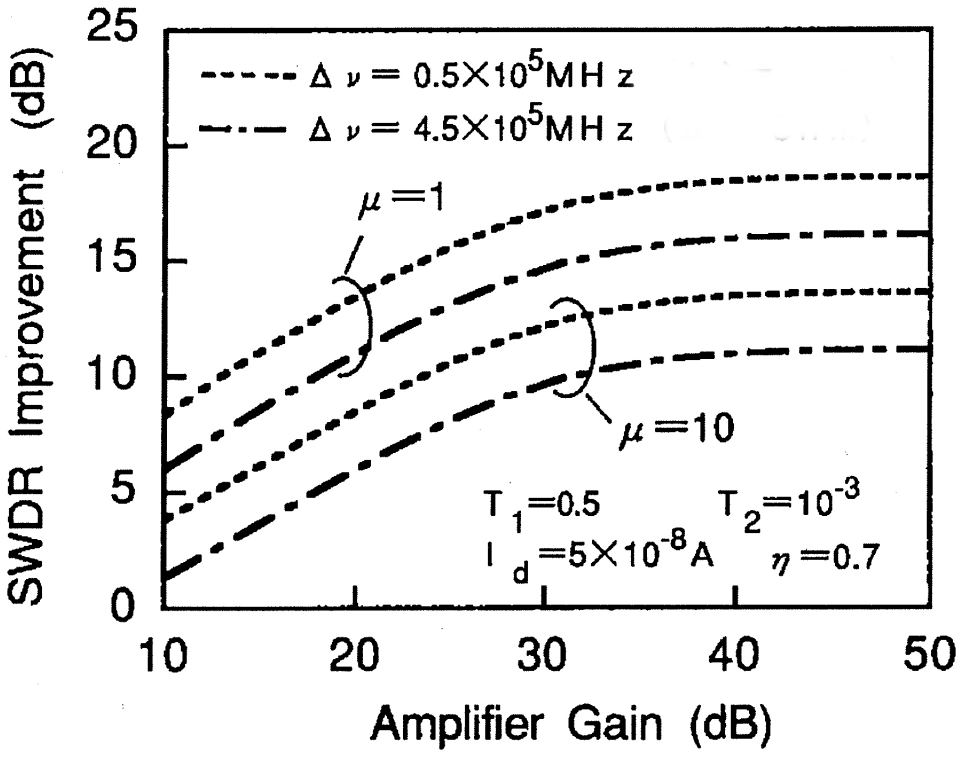

(b) In-line-amplifier

Figure 2.5 Calculated SWDR improvement achieved with EDFAs

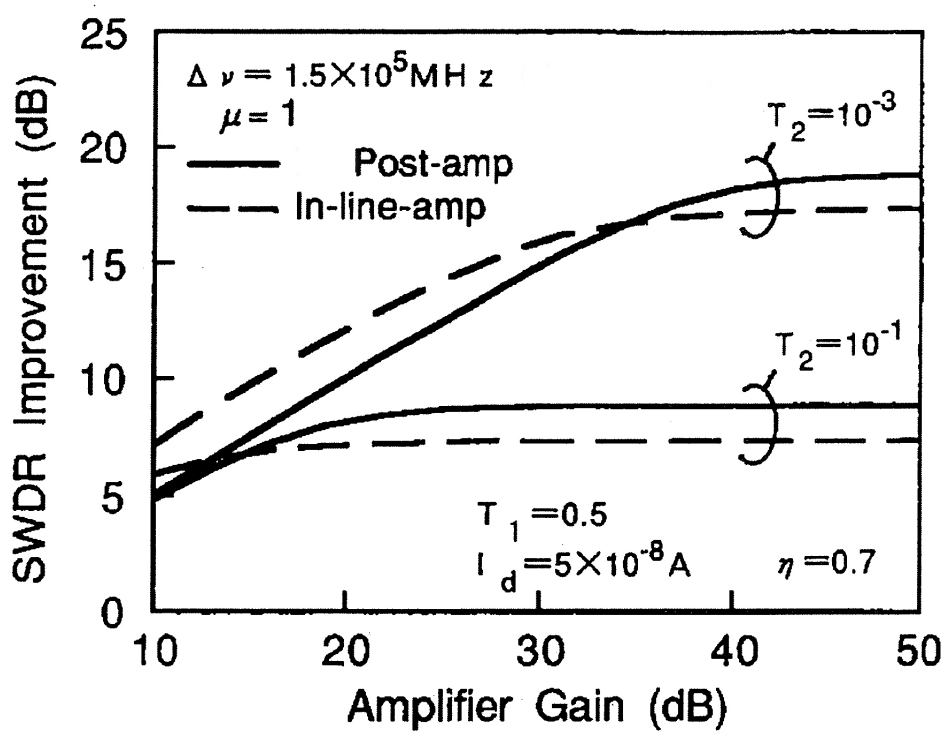

Figure 2.6 Comparison of calculated SWDR improvements achieved with an EDFA as a post-amplifier or an inline amplifier

2.4.2. SNR improvement of C-OTDR with EDFAs

Y. Koyamada et al. previously reported a numerical evaluation of the dynamic range enhancement of C-OTDR with EDFAs [2-24]. Therefore, this subsection simply reviews those results.

Figure 2.7 shows three possible arrangements by which EDFAs can be incorporated into C-OTDR: as (a) a post-amplifier, (b) an inline amplifier, and (c) a pre-amplifier. Since the sensitivity of C-OTDR is limited by the shot noise, the use of an EDFA as a pre-amplifier is ineffective for improving the SWDR. Here, only the first two cases are considered.

Let P_S and P_{LO} be the backscattered signal light power and the local oscillator light power, respectively, measured at the receiver of C-OTDR without EDFAs. The SNR at the output of the receiver is given by

$$SNR_{\mathrm{C}} = \frac{{I_{SC}}^2}{{I_{NC}}^2}, \tag{2.27}$$

where ${I_{SC}}^2$ and ${I_{NC}}^2$ are the mean square signal current and noise current, respectively, and are defined as the following:

$${I_{SC}}^2 = \left[2P_S P_{LO} \left(\frac{\eta e}{h\nu} \right) \right], \tag{2.28}$$

$${I_{NC}}^2 = \left[\frac{4Fk_B T}{R_L} + 2e\left\{ i_d + \left(P_{LO} + P_S\right)\left(\frac{\eta e}{h\nu} \right) \right\} \right] B. \tag{2.29}$$

The advantage of coherent detection is that, by increasing P_{LO}, SNR_{C} is increased until ${I_{NC}}^2$ is dominated by the last term in Eq. (2.29). When this condition is satisfied, the SNR is given by

$$SNR_{\mathrm{C}} = \frac{\eta P_S}{h\nu B}, \tag{2.30}$$

which corresponds to the quantum limit of detection. In the case of heterodyne-detection OTDR, the bandwidth B replaces $2B$. Assuming $SNR_{\mathrm{C}} = 1$, $B = 1$ MHz, $\nu = 194$ THz (1.55 μm), and $\eta = 0.8$, the calculated minimum detectable power is -98 dBm. After averaging the polarization-dependent fluctuation and the heterodyne detection efficiency due to phase mismatch between the backscattered signal and the LO, the sensitivity is reduced by 6 dB. Thus, the minimum detectable power is -92 dBm. Compared with D-OTDR, as described in section 2.4.1, the minimum detectable power of C-OTDR is improved by over 20 dB with a bandwidth of 1 MHz, i.e., a 100-m spatial resolution.

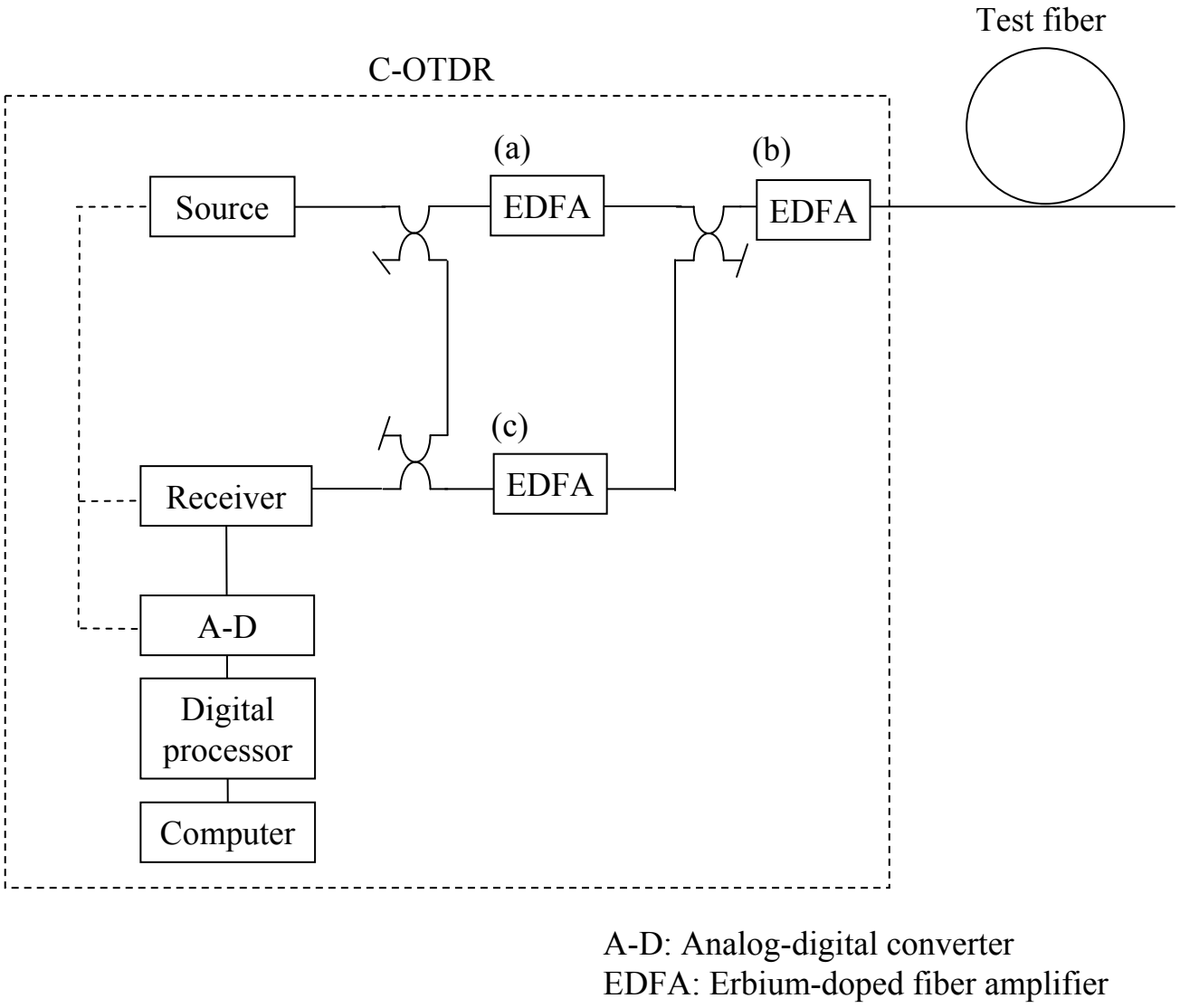

Figure 2.7 Arrangement for incorporating EDFAs into C-OTDR

SNR of C-OTDR with EDFA as post-amplifier

When an EDFA is used as a post-amplifier, as shown in Fig. 2.7(a), the signal pulses are amplified by a factor of g and sent into the test fiber, and the backscattered signal light power at the receiver becomes gP_S. In a manner similar to the D-OTDR numerical evaluation discussed in section 2.4.1, the SNR can be derived as

$$SNR_{\mathrm{C,PO}} = \frac{I_{SPO,C}{}^2}{I_{NPO,C}{}^2}, \tag{2.31}$$

where $I_{SPO,C}{}^2$ and $I_{NPO,C}{}^2$ are the mean square signal current and noise current, respectively, and are defined as the following:

$$I_{SPO,C}{}^2 = gI_{SC}{}^2, \tag{2.32}$$

$$I_{NPO,C}{}^2 = I_{NC}{}^2 + \left[4eP_{APO}\Delta\nu\left(\frac{\eta e}{h\nu}\right) + 4P_{APO}P_S\left(\frac{\eta e}{h\nu}\right)^2 + 4P_{APO}P_{LO}\left(\frac{\eta e}{h\nu}\right)^2 + 4P_{APO}{}^2\Delta\nu\left(\frac{\eta e}{h\nu}\right)^2 \right] B$$

, (2.33)

where $2P_{APO}$ is defined by Eq. (2.12). The second through fifth terms in $I_{NPO,C}{}^2$ correspond to the shot noise produced by the ASE current, the ASE-signal beat noise, the ASE-LO beat noise, and the ASE-ASE beat noise [2-23].

SNR of C-OTDR with EDFA as inline amplifier

When an EDFA is used as an inline amplifier, as shown in Fig. 2.7(b), it amplifies both the pulsed signal light and the backscattered signal light by a factor of g. The backscattered signal light power at the receiver is then g^2P_S. The total ASE power density at the receiver, $2P_{AI}$, is given by Eq. (2.16), and the SNR is given by

$$SNR_{\mathrm{C,I}} = \frac{I_{SI,C}{}^2}{I_{NI,C}{}^2}, \tag{2.34}$$

where $I_{SI,d}{}^2$ and $I_{NI,d}{}^2$ are the mean square signal current and noise current, respectively, and are defined as the following:

$$I_{SI,C}{}^2 = g^2 I_{SC}{}^2, \tag{2.35}$$

$$I_{NI,C}{}^2 = I_{NC}{}^2 + \left[4eP_{AI}\Delta\nu\left(\frac{\eta e}{h\nu}\right) + 4P_{AI}P_S\left(\frac{\eta e}{h\nu}\right)^2 + 4P_{AI}P_{LO}\left(\frac{\eta e}{h\nu}\right)^2 + 4P_{AI}{}^2\Delta\nu\left(\frac{\eta e}{h\nu}\right)^2 \right] B. \tag{2.36}$$

SNR improvement ratio (SNIR)

The SNIRs in the post- and inline-amplifier cases are obtained by using Eqs. (2.27), (2.31), and (2.34). The SWDR improvements for these cases are given by logarithmic transformation of the SNIRs, adapting the SWDR description commonly used for OTDR:

$$SNIR_{\mathrm{C,PO}} = 5\log\left[\frac{SNR_{\mathrm{C,PO}}}{SNR_{\mathrm{C}}}\right] \ (\mathrm{dB}), \tag{2.37}$$

$$SNIR_{\mathrm{C,I}} = 5\log\left[\frac{SNR_{\mathrm{C,I}}}{SNR_{\mathrm{C}}}\right] \ (\mathrm{dB}). \tag{2.38}$$

For the post-amplifier case, from Eq. (2.33), $I_{NPO,C}^2$ is dominated by I_{NC}^2 and $4P_{APO}P_{LO}\,(\eta e/hv)^2B$ (the ASE-LO beat noise). Therefore, $SNR_{\mathrm{C,PO}}$, hardly changes, even if Δv is reduced by using an optical filter. The SWDR improvement, $SNIR_{\mathrm{C,PO}}$, defined by Eq. (2.37), increases almost linearly with g up to about 15 dB when g is less than 30 dB; in this region, $I_{NPO,C}^2$ is dominated by I_{NC}^2. Next, $SNIR_{\mathrm{C,PO}}$ saturates at around g = 50 dB; in this region, $I_{NPO,C}^2$ is dominated by $4P_{APO}P_{LO}\,(\eta e/hv)^2B$. SWDR improvement of more than 15 dB is thus possible by applying an EDFA as a post-amplifier, without using any devices to suppress ASE. As mentioned in section 2.4.1, further improvement is possible by using optical switches to reduce the residual ASE [2-14], [2-15].

For the inline-amplifier case, the SNR improvement, $SNIR_{\mathrm{C,I}}$, defined by Eq. (2.38), increases almost linearly with g when g is less than 25 dB; in this region, $I_{NI,C}^2$ is dominated by $4P_{AI}\,P_{LO}\,(\eta e/h\nu)^2B$ (the ASE-LO beat noise). It reaches a maximum at around g = 30-33 dB and then decreases as g increases above 35 dB; in this region, $I_{NI,C}^2$ is dominated by $4P_{AI}^2\,\Delta\nu\,(\eta e/h\nu)^2B$ (the ASE-ASE beat noise).

Comparing these two cases and considering the possibility of further SWDR improvement, it can be concluded that application of EDFAs as post-amplifiers in C-OTDR is the more effective technique.

Furthermore, comparing the SWDR improvement achieved by applying EDFAs in both D-OTDR and C-OTDR, the results show that the post-amplifier is the most effective application for both forms of OTDR. Further improvement in the inline-amplifier application requires an EDFA with a narrow-band optical filter. In the low-gain region, the inline amplifier is still useful for increasing the SWDR. Therefore, chapter 3 considers the feasibility of combining both EDFA applications in C-OTDR.

2.5. Feasibility of D-OTDR with EDFAs as post-amplifier

The feasibility of enhancing D-OTDR by applying an EDFA as a post-amplifier is examined experimentally.

2.5.1. Optical pulse enhancement with EDFAs

Figure 2.8 show the experimental setup for measuring the characteristics of optical pulse amplification. The EDFA consisted of a 90-ppm erbium-doped single-mode fiber (EDF) with a length of 150 m, two optical isolators embedded at each end of the EDF to achieve stable operation, a 1.48-μm FP-LD for EDFA pumping, and a 1.55-/1.48-μm WDM coupler. A 1.55-μm FP-LD and a DFB-LD were used to provide the pulsed light source. These sources were driven in a pulsed mode, and optical pulses with low repetition were launched into the EDFA. An acousto-optic switch (AO-SW) in a pulsed mode was driven synchronously with the pulsed light source. This could reduce the residual ASE from the EDFA. The resultant optical pulse power was measured by an optical power meter (OPM).

Here, two type of pulsed light source were used. One was the FP-LD, with a wavelength of 1.554 μm and a linewidth of 14 nm. The pulse power was 10 dBm. The other was the DFB-LD, with an external cavity having a linewidth of less than 3 kHz. The CW light from the DFB-LD was introduced into the AO-SW driven in a pulsed mode, and optical pulses were produced. In this case, the optical pulse power was -10 dBm.

Figure 2.9 shows the optical spectra of the FP-LD (a) with and (b) without the AO-SW, as measured with an optical spectrum analyzer instead of by the OPM shown in Fig. 2.8. The pulse width was 1 μs, and the pulse period was 0.41 ms, giving a duty of -26 dB. With the AO-SW, the 1.48-μm pump light was reduced by about 20 dB as compared with the spectrum for the case without the AO-SW. This indicates the feasibility of the time-domain filtering of the AO-SW.

Figure 2.10 shows the measured pulsed signal gain characteristics of the EDFA as a function of the pump light power of the 1.48-μm LD. For the FP-LD, the pulse gain linearly increased when the pump power was 10-40 mW. In the region of pump power over 40 mW, the gain gradually saturated. For the DFB-LD, the pulse gain linearly increased.

To increase the pulse power amplified by the EDFA, two EDFAs were concatenated. The first EDFA had a 70-ppm EDF with a length of 300 m. A 23-dB gain was obtained

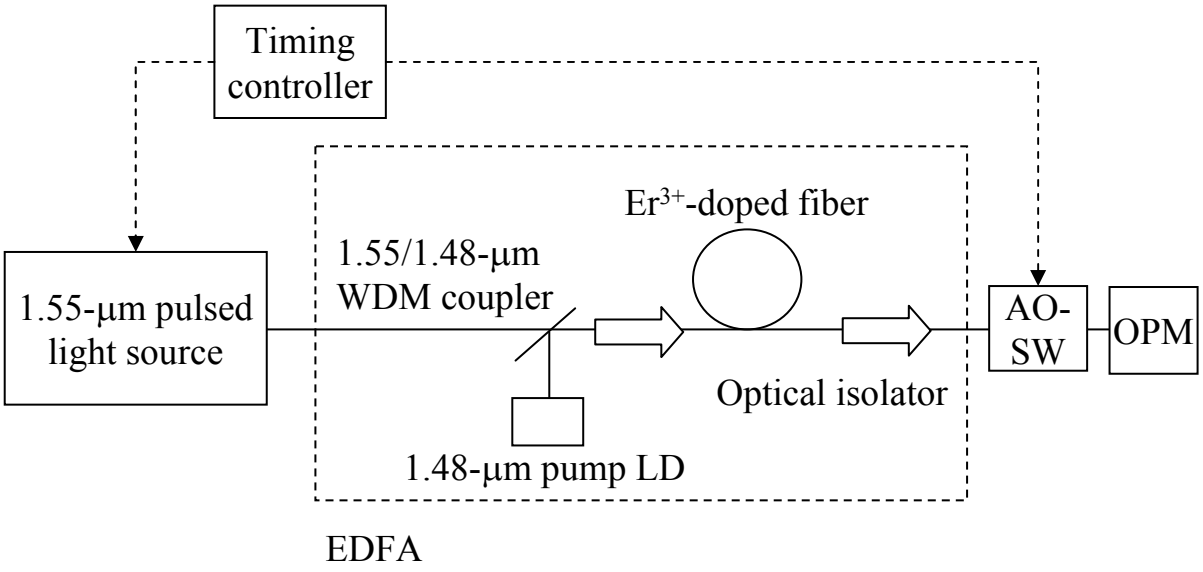

Figure 2.8 Experimental setup for measuring characteristics of optical pulse amplification

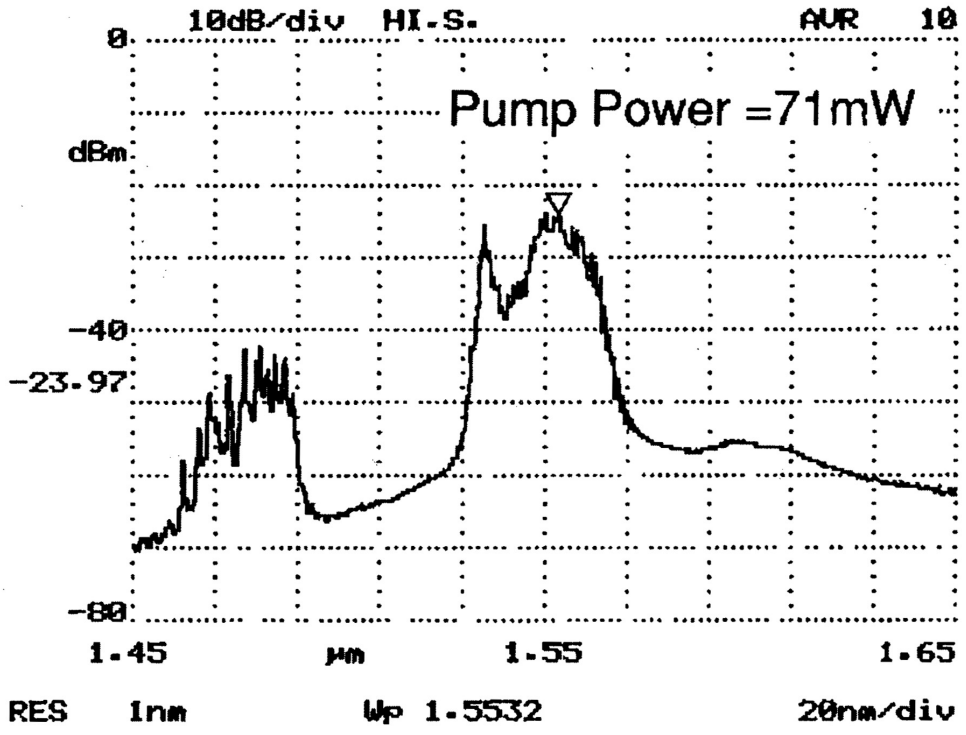

(a) With AO-SW

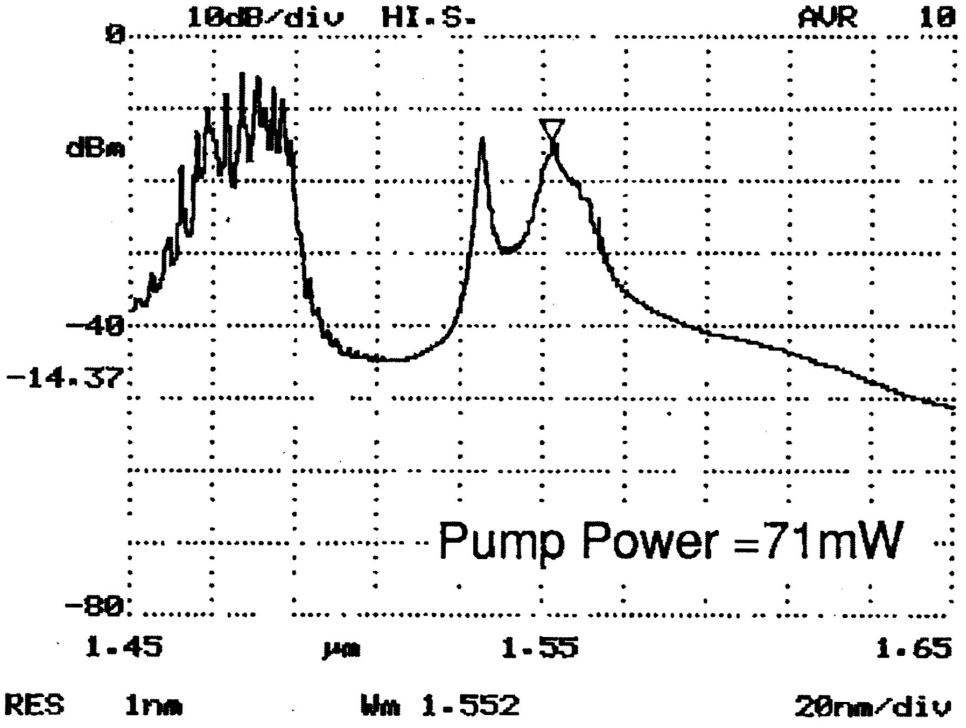

(b) Without AO-SW

Figure 2.9 Amplified spectra of FP-LD output pulsed signal
(a) with AO-SW and (b) without AO-SW

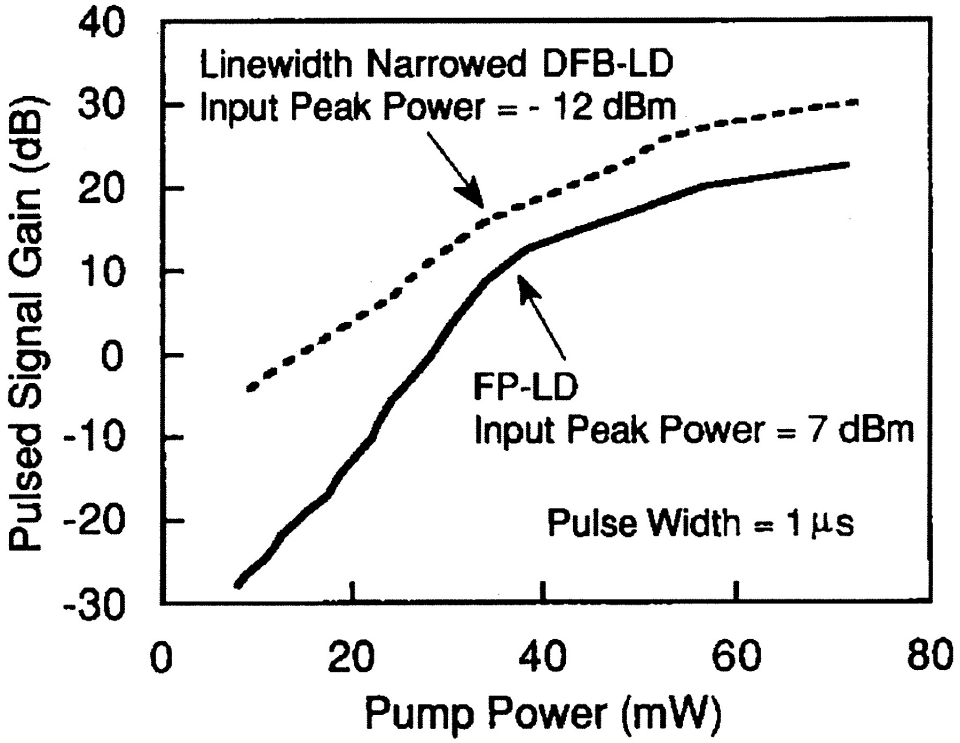

Figure 2.10 Measured pulsed signal gain characteristics

with a pump power of 71 mW. The second EDFA was the one described above, with the gain characteristics shown in Fig. 2.10.

Figure 2.11 shows the pulse gain characteristics of the two concatenated EDFAs as a function of the output power of the pulsed signal. The pulsed light source was the FP-LD. For a 10-μs pulse width, the gain decreased in the region over an output power of 15 dBm, and the output power saturated at 22 dBm. For a 1-μs pulse width, the gain began to slightly saturate over an output power of around 24 dBm. Finally, a 31-dB gain and 30-dBm output power were obtained.

Figure 2.12 shows the pulse shapes amplified by the two concatenated EDFAs for pulse widths of 1 μs, 10 μs, 50 ns, and 200 ns. The results show that the peak powers of each pulse had approximately the same value, and that the powers within the pulses decreased exponentially.

2.5.2. High performance of D-OTDR with two concatenated EDFAs

To the examine the feasibility of enhancing D-OTDR with two concatenated EDFAs and AO-SW filtering technology, a conventional OTDR was modified by adding the two concatenated EDFAs, as described in section 2.5.1.

Figure 2.13 shows the experimental setup for D-OTDR with the concatenated EDFAs. The pulsed light from the 1.55-μm FP-LD was amplified by the two EDFAs. The AO switches, AO-SW1 and AO-SW2, were driven synchronously with the pulsed FP-LD to eliminate the residual ASE in the time domain. The fundamental port of AO-SW2 introduced the backscattered signals from the test fiber into the APD receiver. The test fiber consisted of three single-mode optical fibers wound around a bobbin, and each fiber was spliced with directional couplers with a loss of several decibels.

Figure 2.14 shows OTDR traces, measured with the setup shown in Fig. 2.13, for pulse widths of (a) 50 ns, (b) 200 ns, and (c) 1 μs with 2^{16} integrations. The pulse period was 0.41 ms, and the pump power of the 1.48-μm LD was 71 mW. The pulse power with a pulse width of 1 μs was 27 dBm.

Table 2.1 summarizes the SWDR improvements achieved for D-OTDR. The measured SWDR is defined by the difference between the initial Rayleigh backscattered signal level and the peak level of the OTDR receiver noise, as described in section 2.2.2. The measured value here was the difference between the SWDR with EDFAs and the SWDR without EDFAs. The predicted value was half of the measured pulse gain. For a 1-μs pulse width, the SWDR was 30.5 dB and the improvement was 8.5 dB, which agrees with the predicted value. This means that the effect of ASE was

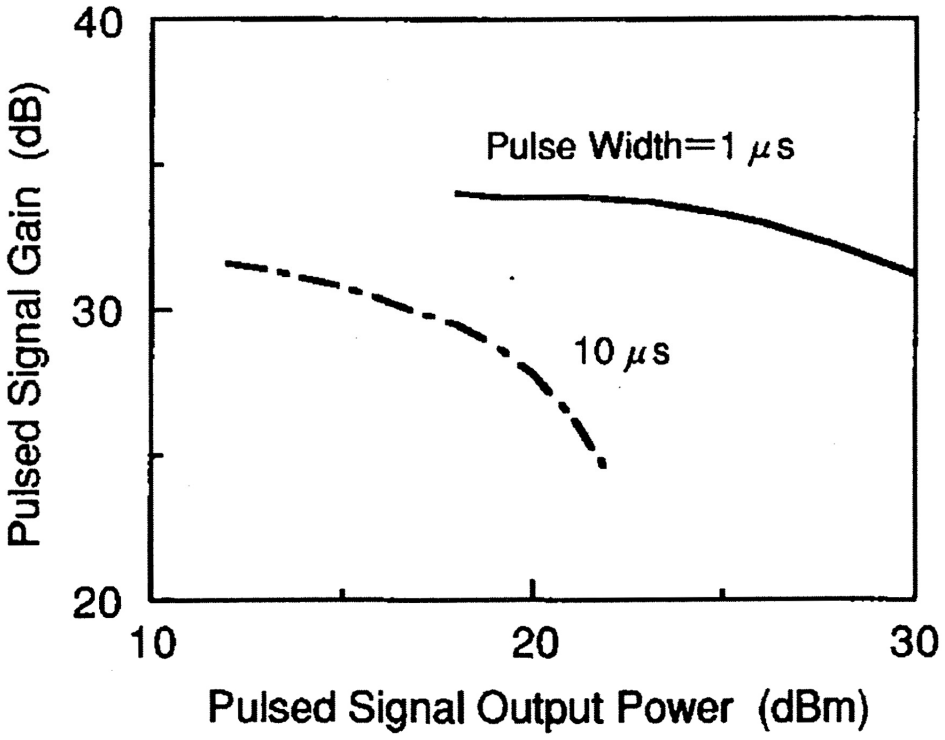

Figure 2.11 Measured pulsed signal gain characteristics as a function of signal output power

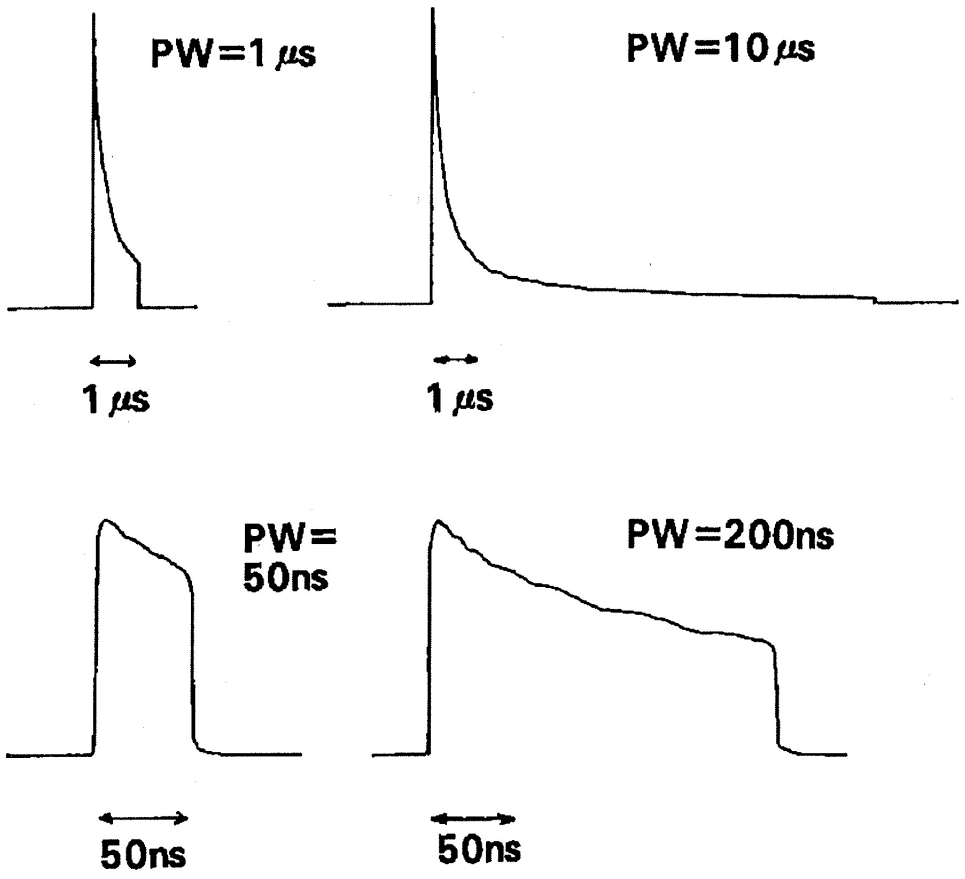

Figure 2.12 Pulse shapes amplified with two concatenated EDFAs

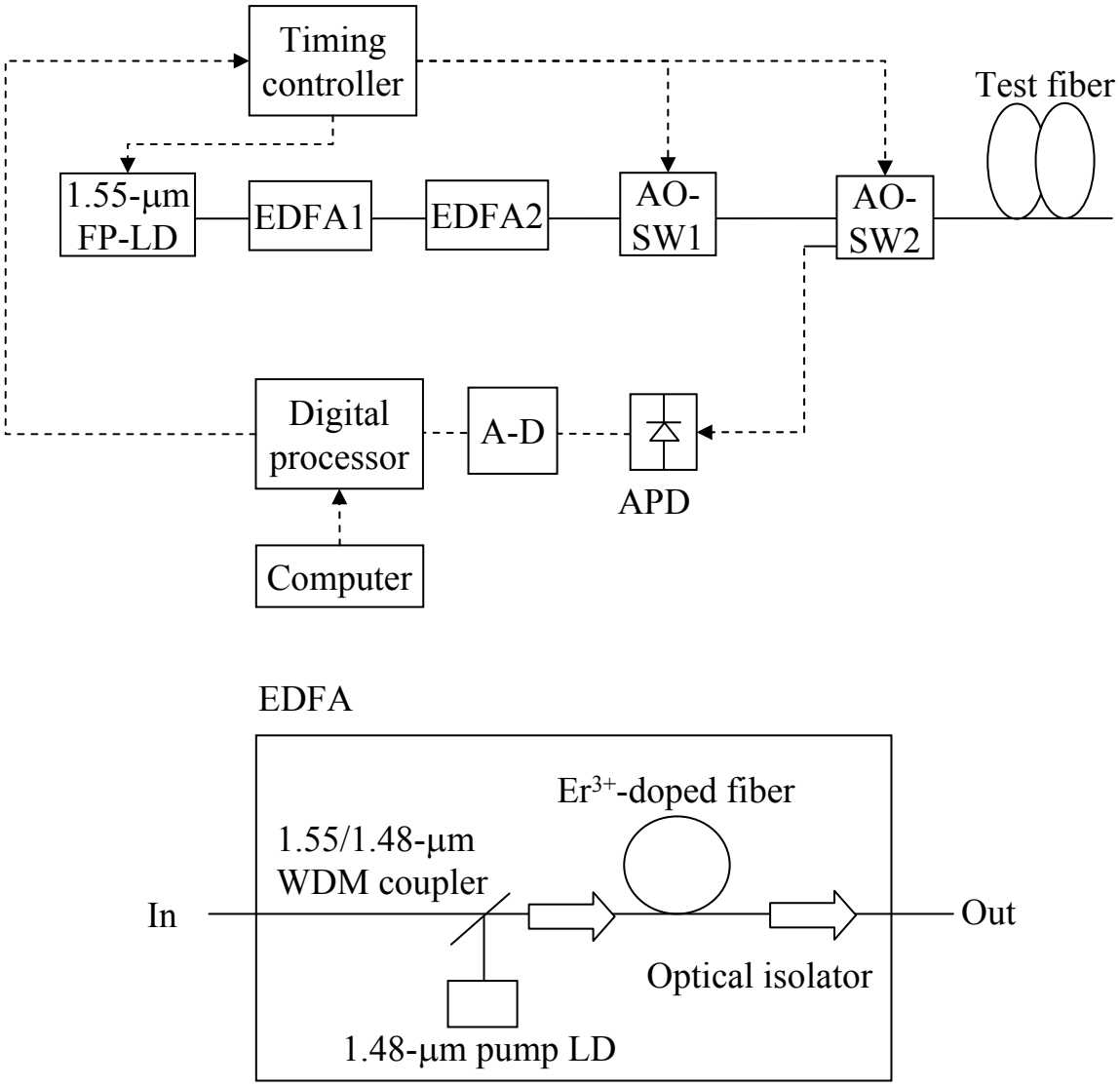

Figure 2.13 Experimental setup for D-OTDR with EDFAs

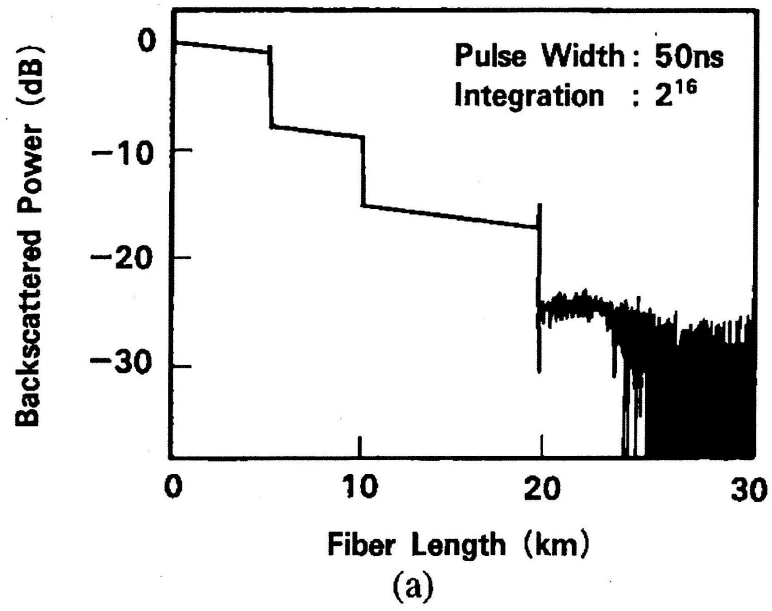

(a)

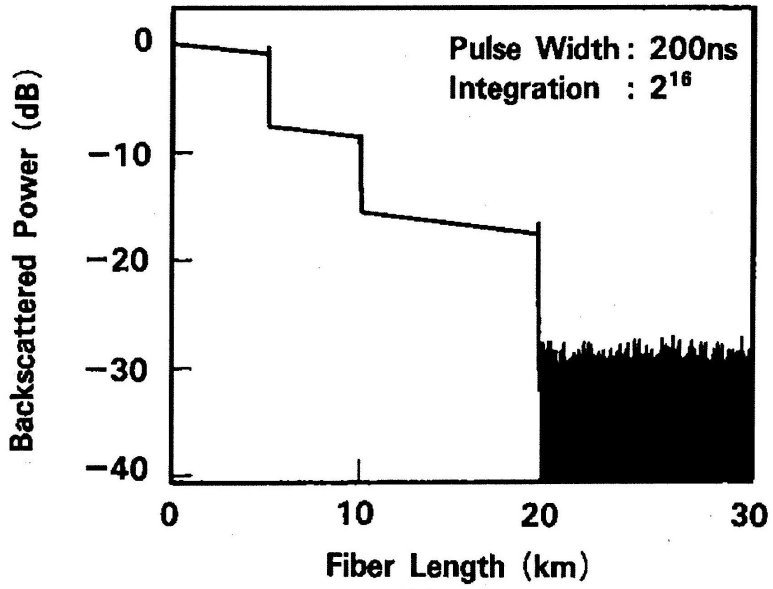

(b)

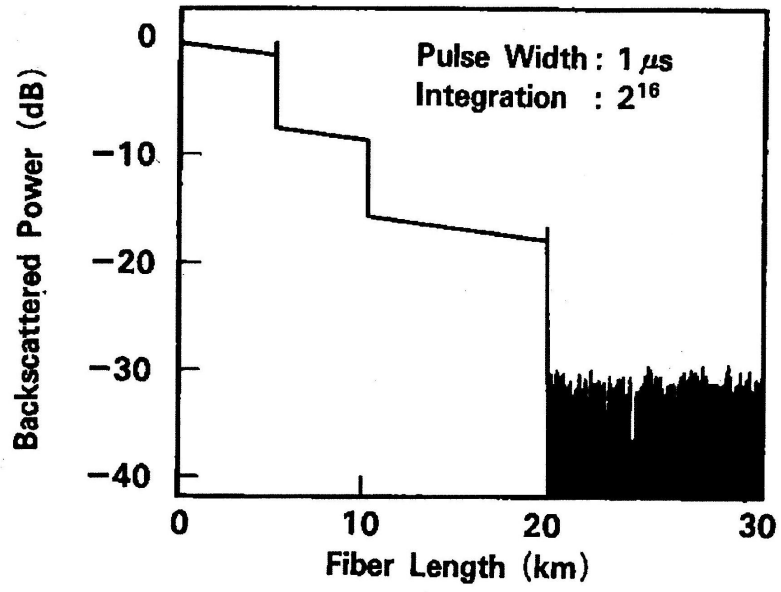

(c)

Figure 2.14 Backscattered traces from D-OTDR with EDFAs

Table 2.1 SWDR improvements for D-OTDR enhanced with EDFAs

Pulse width	SWDR (dB)		SWDR improvement (dB)	
	with EDFA (S1)	without EDFA (S0)	Measured value (S1-S0)	Predicted value (g/2)
50 ns	24.9	14.8	10.1	9.1
200 ns	28.6	18.8	9.8	9.3
1 μs	30.5	22.0	8.5	8.6

negligible. For shorter pulse widths, the SWDR improvement was larger than that for a 1-μs pulse width. This was because the waveform distortion for a short pulse width is smaller than that for a 1-μs pulse width, and the resulting pulse gain is larger.

2.6. Feasibility of C-OTDR with EDFAs as post-amplifier

Figure 2.15 shows an experimental setup for C-OTDR with two EDFAs used as a post-amplifier. A DFB-LD coupled to a 1-km length of fiber to narrow the linewidth was used as a signal and local oscillator. The linewidth was less than 3 kHz, the output power was about 1 dBm, and the wavelength was changed to around 1.55 μm by changing the temperature of the DFB-LD with an LD temperature controller. The CW light from the DFB-LD was divided by a 3-dB fused fiber directional coupler (FCl) into two paths: the signal path, and the LO path. The signal pulses were produced by an AO switch (AO-SW1) operating in a pulsed mode. They were amplified by the two EDFAs joined by AO-SW2 and then launched into the test fiber through an optical bandpass filter (OBPF) and FC2. The returned backscattered signal light was mixed with the optical LO signal by FC3 and detected by a double balanced p-i-n FET receiver. The detected backscattered signals were electrically amplified and mixed with the electrical LO signal, and their high frequency parts were eliminated by an LPF and introduced to the A-D converter. The digitized backscattered signals were squared and integrated to improve the SNR and finally displayed on the computer monitor as an OTDR trace after logarithmic transformation. A polarization controller was inserted between FC1 and the first EDFA to change the SOP of the signal pulse. The minimum detectable power was -92 dBm for a receiver bandwidth of l MHz

Each amplifier consisted of a 90-ppm EDF with a length of 150 m, pumped by an FP-LD at 1.48 μm. The gains of amplifiers l and 2 were 28 dB and 25 dB, respectively, for an output pump power of 100 mW. The gain of the second amplifier was smaller than that of the first because of the gain saturation induced by the large input signal. AO-SW2, which operated in a pulsed mode synchronized with the signal pulses passing through it, was placed between the EDFAs to suppress the ASE from the first EDFA [2-14]. Also, a 1-nm-bandwidth BPF was placed next to the second EDFA to eliminate its ASE and the 1.48-μm pump lights. The launch power was -14 dBm without the EDFAs. A launch power of approximately 26 dBm was achieved with the EDFAs, indicating amplification by 40 dB, where the gross gain of the two EDFAs was 53 dB, as mentioned above. The losses of AO-SW2 and the BPF and the connection loss were 8 dB, 4 dB, and 1 dB, respectively. Figure 2.16 shows the pulse

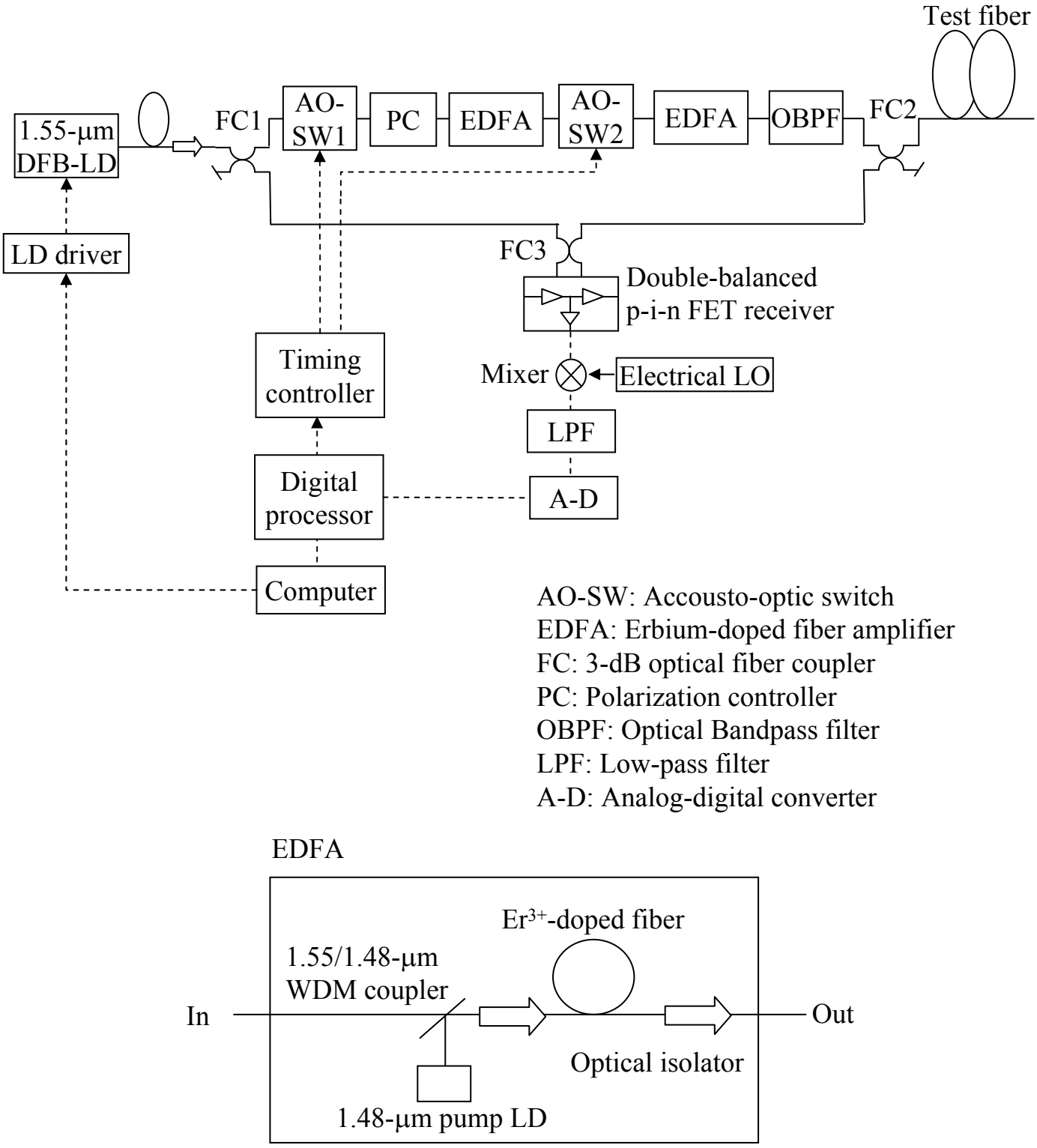

Figure 2.15 Experimental setup for C-OTDR with two EDFAs as a post-amplifier

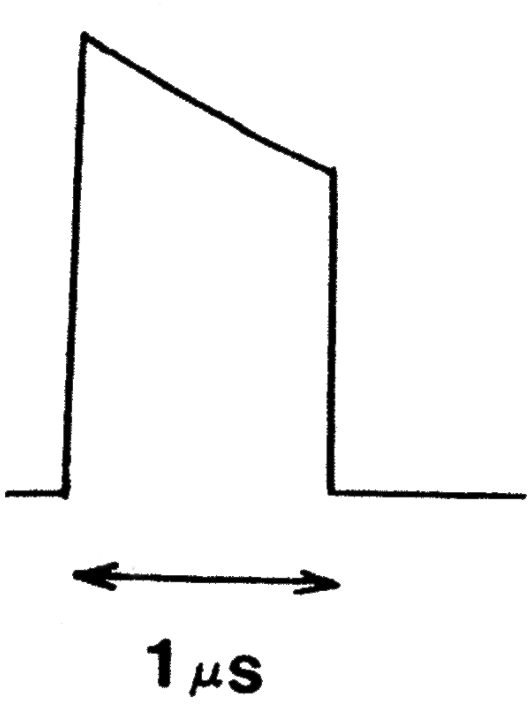

Figure 2.16 Amplified pulse shape from the second EDFA

shape of the output signal from the second EDFA. The shape of the 1-μs-width pulse was distorted by the gain saturation of the second EDFA.

The optical frequency was up-converted by 120 MHz by AO-SW1 at 1.55 μm. AO-SW2 was designed to down-convert the optical frequency by 115 MHz. The resulting beat frequency generated by the backscattered signal and the optical LO signal was 5 MHz. This low frequency made it easy to design the coherent receiver and the electrical amplifier.

Figure 2.17 show the backscattered traces from the C-OTDR setup without and with the EDFAs. The measurements were performed on a 40-km-long single-mode fiber consisting of seven sections joined using 3-dB FCs with a loss of about 3.5 dB. The launched pulse width was 1 μs, and the frequency bandwidth was 1 MHz, both of which allowed a 100-m spatial resolution. The number of integrations was 2^{12}(=4 x 10^3), and the temperature of the DFB-LD and the signal pulses SOP were fixed during the experiment. The SWDR without the EDFAs, measured from the initial backscattering level to the noise floor level, was found to be 16 dB, as shown in Fig. 2.17(a). The SWDR with the EDFAs was 36 dB, as shown in Fig. 2.17(b), for an improvement of 20 dB. Consequently, the results confirmed that the whole 40-dB increase in the launched power with the EDFAs contributed to improving the dynamic range of C-OTDR. Furthermore, the use of EDFAs did not increase the noise level of the backscattered signals. If the integrations number increases from 2^{12} to 2^{18}, the SWDR could be improved by 4.5 dB. This suggests the possibility of an SWDR over 40 dB.

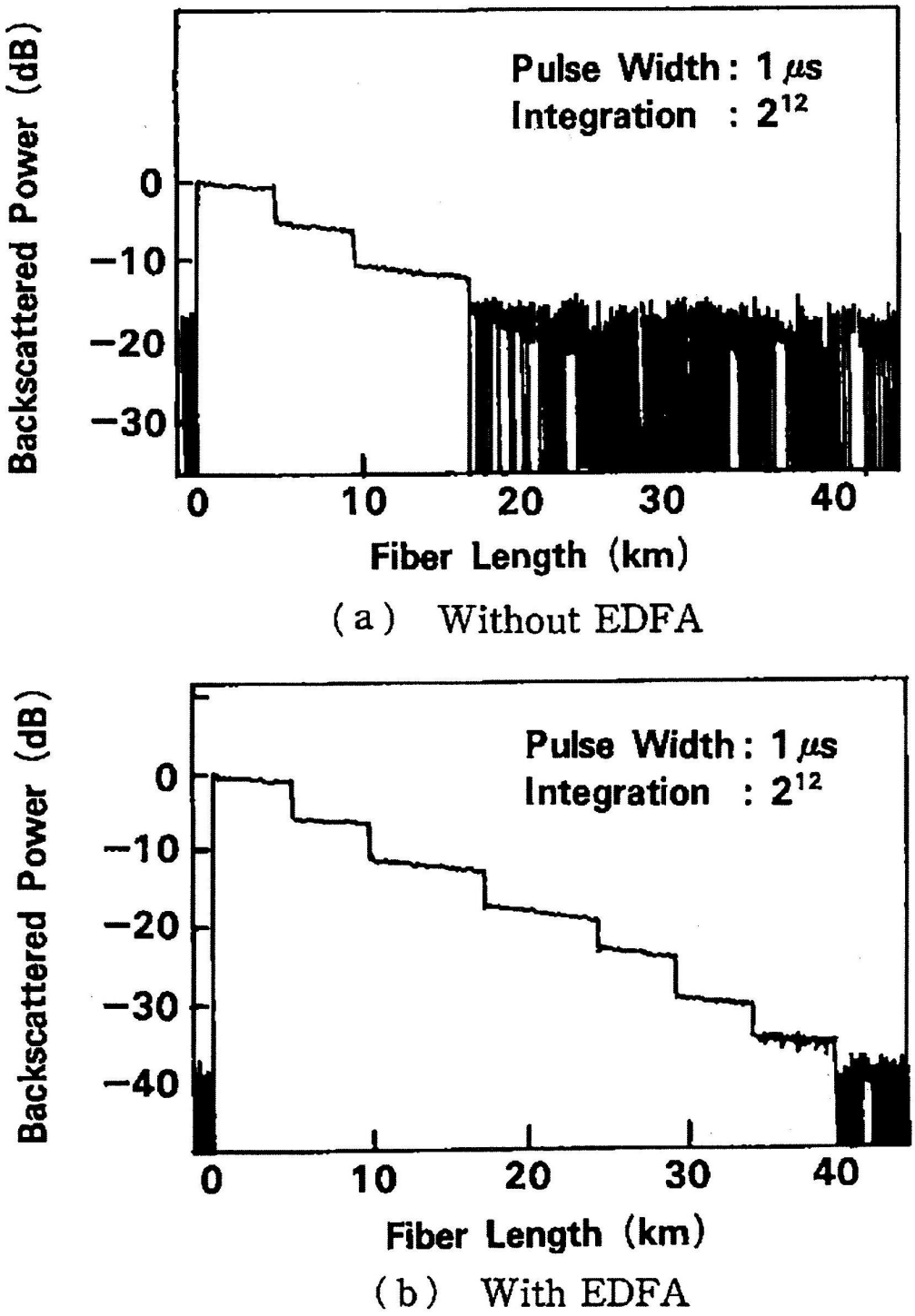

Figure 2.17 Backscattered C-OTDR traces (a) without EDFAs, and (b) with EDFAs

2.7. Nonlinear phenomena in optical fiber and pulse power limit

In section 2.2.2, the SWDR of OTDR was defined by Eq. (2.4). The SWDR increases with the incident pulse power. As mentioned in sections 2.5 and 2.6, a high-power signal pulse could be obtained using EDFAs. The pulse power could possibly reach about 30 dBm. Very high power in a small fiber core, however, can cause significant nonlinear effects, such as stimulated Raman scattering (SRS) and stimulated Brillouin scattering (SBS) [2-25], [2-26]. These phenomena limit the allowable launched pulse power in the test fiber. Both the forward SRS and the backward SBS must be considered for coherent light pulses sent from C-OTDR, though only the former must be considered for incoherent light pulses sent from D-OTDR.

Y. Koyamada et al. predicted the critical power theoretically. The critical power of SBS occurring in a conventional single-mode fiber is about 28 dBm for a 1-μs pulse width [2-24].

Figure 2.18 shows the beat signals measured by the double-balanced FET receiver in the C-OTDR described above for a 1-μs pulse width with a pulse power of (a) 15 dBm, (b) 21 dBm, (c) 24 dBm, and (d) 28 dBm. For case (c), the beat signals decreased, even though the incident pulse power theoretically increases under the condition that the SBS did not occur. Since the test fiber consisted of about 100 km of dispersion-shifted fiber (DSF), the interaction length was sufficiently long. Therefore, other nonlinear phenomena are predicted to have occurred in the DSF, rather than SBS or SRS.

Figure 2.19 shows the beat signals measured by the double-balanced FET receiver in the C-OTDR for a 100-ns pulse width with a pulse power of (a) 24 dBm and (b) 25 dBm. These results also support the above prediction.

Clarification of the SWDR limit of C-OTDR required a detail investigation of the occurrence of nonlinear phenomena in a DSF is required. Chapter 3 gives the results of investigating the performance limits of C-OTDR, including these nonlinear phenomena.

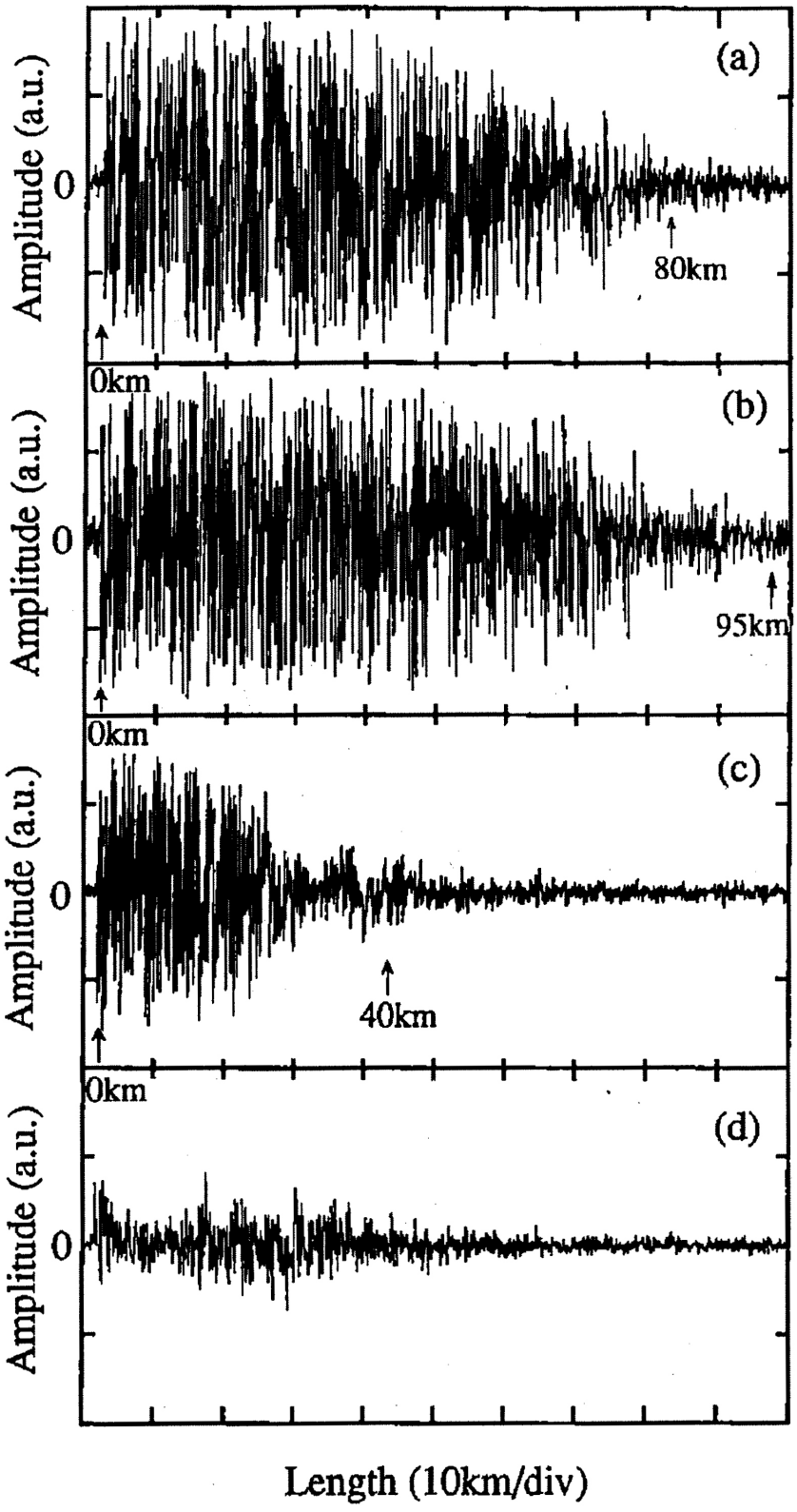

Figure 2.18 Beat signals measured by C-OTDR with a 1-μs pulse width

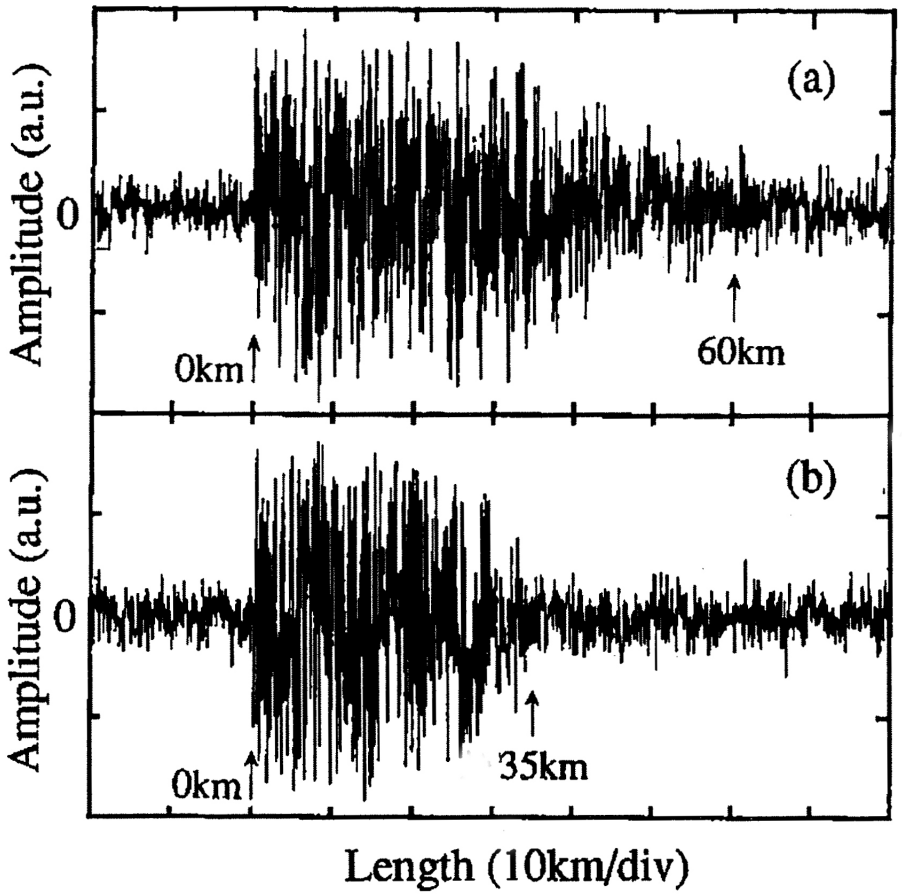

Figure 2.19 Beat signals measured by C-OTDR with a 100-ns pulse width

2.8. Conclusions

The results of theoretical and experimental studies have been described for D-OTDR and C-OTDR enhanced with EDFAs.

(1) The use of EDFAs as post-amplifiers is the most effective technique of incorporating EDFAs for both D-OTDR and C-OTDR.

(2) It was confirmed experimentally that the two concatenated EDFAs with a synchronously driven AO-SW could produce a 30-dBm high-power signal pulse light with low ASE.

(3) Distortion of the amplified signal pulse in the saturation regime was found experimentally. The power within the pulse decreased exponentially, and the leading edge of the pulse peak intensity was independent of the pulse width.

(4) For D-OTDR with a 1-μs pulse width and 2^{16} integrations, the SWDR and its improvement were 30.5 and 8.5 dB, respectively, with two concatenated EDFAs and an AO-SW. With a narrower pulse width, the improvement increased.

(5) The C-OTDR with a 36-dB SWDR has been constructed using two concatenated EDFAs and an AO-SW to reduce the ASE noise. This suggests the possibility of an SWDR over 40 dB.

(6) Although it has been theoretically predicted that the critical powers of SBS and SRS limit the incident pulse power in C-OTDR, the critical power at which such nonlinear phenomena occurred in a DSF was found experimentally to be lower that these critical powers. This result provides new criteria for the SWDR limit of C-OTDR enhanced with EDFAs.

2.9. References

[2-1] R. J. Mears, L. Reekie, I. M. Jauncey, and D. N. Payne, "Low-noise erbium-doped fibre amplifier operating at 1.54 μm," Electron. Lett., vol. 23, no. 19, pp. 1026-1028, 1987.

[2-2] Special issue on Optical Amplifiers; IEEE J. Lightwave Technol., vol. LT-9, no. 2, 1991.

[2-3] R. A. Jensen, D. G. Duff, J. J. Risko, and C. R. Davidson, "Possibility of upgrade of the first installed amplifier system," Tech. Dig. OAA'95, pp. 9-12, 1995.

[2-4] K. Iwatsuki, S. Saito, K. Suzuki, A. Naka, S. Kawai, T. Matsuda, and S. Nishi, "Field demonstration Gb/s 2700 km soliton transmission through commercial submarine optical amplifier system with distributed fiber dispersion and 90 km amplifier spacing," in the proc. of ECOC'95, vol. PD I-6, 1995.

[2-5] N. Sato ed., "Optical Fiber Technologies toward IT Era," Chapter 7, IEICE 2001. (in Japanese)

[2-6] M. Murakami, T. Takahashi, M. Aoyama, M. Amemiya, M. Sumida, Ohkawa, Y. Fukada, T. Imai, and M. Aiki, "2.5Gbit/s-9720km, 10Gbit/s-6480km transmission in the FSA commercial system with 90km spaced optical amplifier repeater and dispersion-manage cables," Electron. Lett., vol. 31, no. 10, pp. 814-15, 1995.

[2-7] P. Healey, "Review of long wavelength single-mode optical fiber reflectometry techniques," IEEE J. Lightwave Technol., vol. LT-3, no. 4, pp. 876-886, 1985.

[2-8] M. Tateda and T. Horiguchi, "Advances in optical time-domain reflectometry," IEEE J. Lightwave Technol., vol. LT-7, no. 8, pp. 1217-1224, 1989.

[2-9] M. P. Gold and A. H. Hartog, "Improved-dynamic-range single-mode OTDR at 1.3 μm," Electron. Lett., vol. 20, pp. 285-287, 1984.

[2-10] M. Nakazawa, M. Tokuda, K. Washio, and Y. Asahara, "130-km-long fault location for single-mode optical fiber using 1.55-μm Q-switched Er^{3+}:glass laser," Optics Lett., vol. 9, no. 7, pp. 312-314, 1984.

[2-11] ITU-T Recommendation G.664, "Optical safety procedures and requirements for optical transport systems," 2006.

[2-12] IEC 60825-2, "Safety of laser products - Part 2: Safety of optical fiber communication systems," 2007.

[2-13] J. King, D. F. Smith, K. Richards, P. Timson, R. E. Epworth, and S. Wright, "Development of coherent OTDR instrument," IEEE J. Lightwave Technol.,

vol. LT-5, no. 4, pp. 616-624, 1987.

[2-14] Y. Koyamada and H. Nakamoto, "High performance single mode OTDR using coherent detection and fibre amplifiers," Electron. Lett., vol. 26, no. 9, pp. 573-574, 1990.

[2-15] L. C. Bank and D. M. Spirit, "OTDR performance enhancement through erbium fibre amplification," Electron. Lett., vol. 25, no. 25, pp. 1693-1694, 1989.

[2-16] P. Healey, "Fading in heterodyne OTDR," Electron. Lett., vol. 20, no. 1, pp. 30-32, 1984.

[2-17] IEC 61746 Ed.1: Calibration of optical time domain reflectometers (OTDRs) 2001-09.

[2-18] K. Aoyama, K. Nakagawa, and T. Itoh, "Optical time domain reflectometry in a single-mode fiber," IEEE Journal of Quantum Electronics, vol. 17, no. 6, pp. 862-868, 1981.

[2-19] E. Brinkmeyer, "Backscattering in single-mode fibers," Electron. Lett., vol. 16, no. 9, pp. 329-330, 1980.

[2-20] L. Goldberg, H. F. Taylor, and J. F. Weller, "Feedback effects in a laser diode due to Rayleigh backscattering from an optical fibre," Electron. Lett., vol. 18, no. 9, pp. 353-354, 1982.

[2-21] H. Izumita, S. Furukawa, Y. Koyamada, and I. Sankawa, "Fading Noise Reduction in Coherent OTDR," IEEE Photon. Technol. Lett., vol. 4, no. 2, pp. 201-203, 1992.

[2-22] A. Yariv, "Introduction to optical electronics," 3rd edition, Holt, Rinehart and Winston, Inc., 1986.

[2-23] T. Okoshi and K. Kikuchi, "Coherent optical fiber communications," KTK Scientific Publishers, 1988.

[2-24] Y. Koyamada, H. Nakamoto, and N. Ohta, "High performance coherent OTDR enhanced with erbium doped fiber amplifiers," J. Opt. Commun., vol. 13, no. 4, pp. 127-133, 1992.

[2-25] R. G. Smith, "Optical power handling capacity of low loss optical fibers as determined by stimulated Raman and Brillouin scattering," Applied Optics, vol. 11, no. 11, pp. 2489-2494, 1972.

[2-26] R. H. Stolen, "Nonlinearity in fiber transmission," Proc. IEEE, vol. 68, no. 10, pp. 1232-1236, 1980.

Chapter 3. The performance limit of C-OTDR with optical fiber amplifiers due to optical nonlinear phenomena

This chapter describes theoretical and experimental studies on optical nonlinear phenomena stimulated by a high-power coherent pulse launched into a single-mode optical fiber. It also clarifies the critical power for degradation in the performance of C-OTDR as a result of these phenomena.

3.1. Introduction

Optical time-domain reflectometry (OTDR) is a commonly used technique for characterization and fault location in optical fiber transmission systems. Many studies have been undertaken to extend the dynamic range of OTDR [3-1]. Its performance is significantly improved by using coherent detection [3-2] and optical fiber amplifiers [3-3]. Coherent detection is a promising technique for improving the receiver sensitivity up to the quantum limit, which is a big advantage for direct detection. Erbium-doped fiber amplifiers (EDFAs) have the potential for high gain and high saturation output power. Coherent-detection OTDR (C-OTDR) with EDFAs has demonstrated a single-way dynamic range (SWDR) of over 30 dB [3-4]-[3-6].

An optical pulse can be amplified to more than 1 W by using EDFAs. The high-power optical pulse with a narrow linewidth required for coherent detection stimulates optical nonlinear phenomena in a single-mode optical fiber [3-7]. These phenomena significantly degrade the performance of C-OTDR. It is important to clarify the critical power inducing these phenomena, which are the origin of the SWDR limit of C-OTDR with EDFAs.

This chapter describes theoretical and experimental studies on the optical nonlinear phenomena stimulated by launching a high-power coherent pulse into a single-mode optical fiber. The chapter also clarifies the critical power for degradation in the performance of C-OTDR as a result of these phenomena. Section 3.2 shows theoretically that the performance of C-OTDR is degraded by the effects of optical nonlinear phenomena, such as self-phase modulation (SPM), four-wave mixing (FWM), stimulated Brillouin scattering (SBS), and stimulated Raman scattering (SRS). Section 3.3 confirms experimentally that these phenomena degrade the performance of C-OTDR, and that the critical powers for SPM and FWM are lower than those for SBS and SRS. This section also considers these critical powers theoretically. Section 3.4 demonstrates high performance of C-OTDR with EDFAs for pulse widths of 10 μs, 4 μs, 1 μs, and 100 ns, limited by the effects of the nonlinear phenomena.

3.2. Degradation of the performance of C-OTDR by optical nonlinear phenomena

3.2.1. Self-phase modulation

Self-phase modulation (SPM) occurs due to the power dependence of the refractive index of a single-mode optical fiber [3-8]. When an optical pulse with a power gradient within the pulse width is incident to the optical fiber, the optical frequency of the transmitted optical pulse passing through the optical fiber is shifted by SPM. The optical frequency shift $\delta\nu$ is [3-8]

$$\delta\nu = \frac{n_2 L_{eff}}{A\lambda}\frac{\partial p(t)}{\partial t}, \tag{3.1}$$

$$L_{eff} = \frac{1-\exp(-\alpha L)}{\alpha}, \tag{3.2}$$

where A is the effective cross section area, which is approximated by $A=\pi a_m^2$, a_m is the mode-field radius, $p(t)$ is the optical pulse power at time t, n_2 is the nonlinear refractive index of the optical fiber, λ is the wavelength of the incident optical pulse, L_{eff} is the effective length, L is the length of the optical fiber, and α is its attenuation coefficient. Equation (3.1) shows that the optical frequency shift increases in proportion to the power gradient of the optical pulse and the effective length.

The Rayleigh backscattered signals from the optical fiber have the same optical frequency shift as the optical pulse propagating in the optical fiber. Since a stable frequency difference between the Rayleigh backscattered signal and the local oscillator is needed for coherent detection, the optical frequency shift of the Rayleigh backscattered light caused by SPM degrades the sensitivity of C-OTDR.

The Rayleigh backscattered signals in the receiver bandwidth are proportional to the integral of the instantaneous power spectrum over the frequency. The instantaneous power spectrum of the Rayleigh backscattered signals in the frequency domain is the square of a SINC function with a period of the inverse of the incident optical pulse width ($1/\tau$) [3-9]. In C-OTDR, the receiver bandwidth B is usually set to $1/\tau$. When the optical frequency of the Rayleigh backscattered signal is shifted by $\delta\nu$, the detected signal power decreases in proportion to the function:

$$S(\delta\nu) = \int_{-B}^{B}\left[\frac{\sin(\pi(\nu-\delta\nu)/B)}{\pi(\nu-\delta\nu)/B}\right]^2 d\nu, \tag{3.3}$$

where ν is the frequency. Let the detection coupling coefficient for the optical

frequency shift be $\eta(\delta\nu)$. It is derived as $S(\delta\nu)$ normalized by $S(0)$.

$$\eta(\delta\nu) = \frac{S(\delta\nu)}{S(0)} \tag{3.4}$$

Equation (3.4) shows the sensitivity degradation of C-OTDR due to the optical frequency

Figure 3.1 shows the calculated sensitivity degradation as a function of the optical frequency shift $\delta\nu$ normalized by the receiver bandwidth B. When the critical frequency shift $\delta\nu_c$ is defined to make the sensitivity degradation less than 0.05 dB, $\delta\nu_c/B$ is 0.4. Therefore, the critical power gradient of the incident optical pulse is derived from Eq.(3.1) as

$$\left.\frac{\partial p(t)}{\partial t}\right|_c = \frac{\lambda A}{n_2 L_{eff}}\delta\nu_c = \frac{\lambda A}{n_2 L_{eff}}0.4B. \tag{3.5}$$

Equation (3.5) shows that the critical power gradient is proportional to the receiver bandwidth, so the condition is much more severe for a narrow bandwidth receiver (i.e., an incident optical pulse with a long pulse width). For example, for a receiver bandwidth B of 1 MHz (i.e., 1 μs pulse width), the critical power gradient is $4.7\text{x}10^4$ W/s, assuming that an optical pulse with a wavelength = 1.551 μm is incident to a standard single-mode optical fiber with an effective cross section area A = 50 μm^2, optical fiber length L = 100 km, and nonlinear index $n_2 = 3.2\text{x}10^{-20}$ m^2/W [3-7]. For a 100 ns pulse width, however, the critical power gradient is 10 times that for the 1 μs pulse width.

3.2.2. Four-wave mixing

Four-wave mixing (FWM) is a parametric interaction which generates new frequencies on both sides of the pump frequency [3-10]. The energy from a pump light wave at frequency ν_0 is transformed into two side-bands located symmetrically at frequencies ν_0-ν_s and ν_0+ν_s. The low frequency side-band at ν_0-ν_s and the high frequency one at ν_0+ν_s are referred to as the Stokes and anti-Stokes bands, respectively.

When phase matching is achieved by the nonlinear phenomena of SPM, the FWM frequency shift ν_s [3-10],[3-11] is

$$\nu_s = \frac{1}{2\pi}\sqrt{\frac{2\gamma P_i}{|\beta_2|}}, \tag{3.6}$$

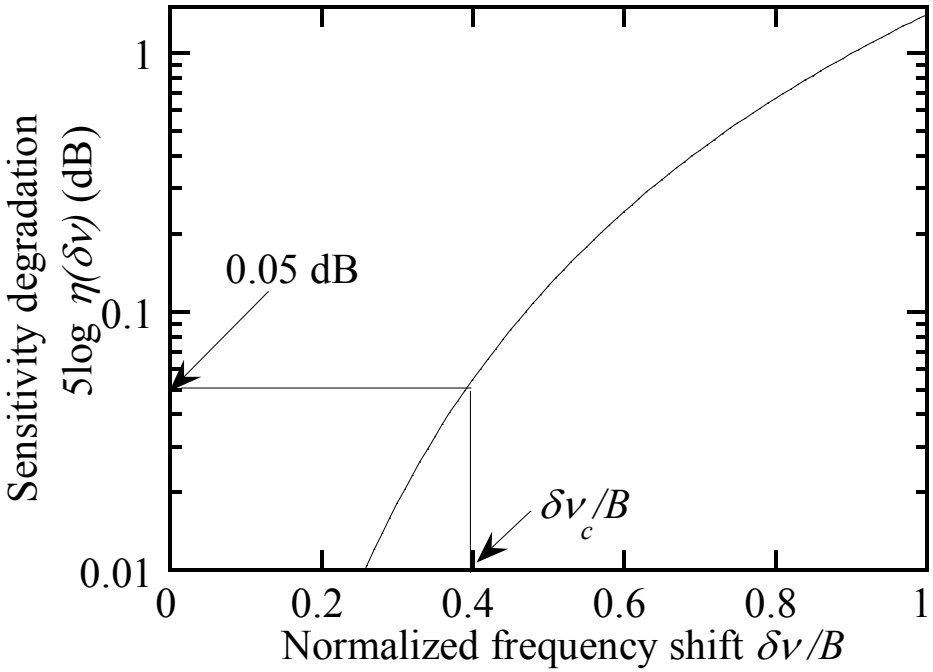

The horizontal scale is optical frequency shift $\delta\nu$ normalized by the receiver bandwidth B.
The vertical scale is the calculated sensitivity degradation in dB.
$\delta\nu_c$ is the critical frequency shift, which is defined to make the sensitivity degradation less than 0.05 dB.

Figure 3.1 Calculated sensitivity degradation as a function of the optical frequency shift $\delta\nu$.

$$\gamma = \frac{2\pi n_2}{\lambda A}, \tag{3.7}$$

$$\beta_2 = -\frac{\lambda^2}{2\pi c} D, \tag{3.8}$$

and the bandwidth (FWHM) $\Delta\nu_s$ [3-10],[3-11] is approximately

$$\Delta\nu_s = \frac{\nu_s}{2}, \tag{3.9}$$

where P_i is the incident optical power, c is the velocity of light in vacuum, and D is the dispersion of the optical fiber.

When the Stokes light and the anti-Stokes light are generated as a result of FWM, which is a parametric interaction between the incident optical pulse and amplified spontaneous emission (ASE), the power of the Rayleigh backscattered signal detected in the receiver bandwidth decreases and the performance of C-OTDR is degraded.

3.2.3. Stimulated Raman scattering and stimulated Brillouin scattering

Once stimulated Raman scattering (SRS) and stimulated Brillouin scattering (SBS) occur in the optical fiber, the energy of the incident optical pulse is transferred to the Stokes light [3-12]. The critical incident pulse power in C-OTDR enhanced with EDFAs is theoretically given by that for SRS or SBS [3-13].

The critical power for SRS for a non-polarization-maintaining single-mode fiber has been derived as [3-12]

$$P_r = 2\frac{16A\alpha}{g_r}, \tag{3.10}$$

where g_r is the Raman gain coefficient for SRS. The critical power is independent of the incident pulse width. If we assume a standard single-mode optical fiber with an effective cross section area A = 50 μm^2 (mode-field radius a_m = 4 μm), an attenuation coefficient α = 4.8x10^{-5} m^{-1} (0.21 dB/km) at 1.55 μm, and a Raman gain coefficient g_r = 6.5x10^{-14} m/W [3-7], then the critical power for SRS is calculated to be 1.18 W (30.7 dBm). The critical power for SBS for a non-polarization-maintaining single-mode fiber for a pulse with a pulse width τ has been derived as [3-13]

$$P_b = 2\frac{21A}{g_b\left(\frac{\tau c}{2n}\right)}, \tag{3.11}$$

where g_b is the Brillouin gain coefficient for SBS. Equation (3.11) shows that the

critical power for SBS depends on the pulse width. Assuming a standard single-mode fiber with a Brillouin gain coefficient $g_b = 4.5\text{x}10^{-11}$ m/W [3-12] and a core refractive index $n = 1.45$ at 1.55 μm, the critical power of SBS for pulse widths $\tau = 1$ μs and $\tau =$ 100 ns was calculated to be 451 mW (26.5 dBm) and 45.1 mW (36.5 dBm), respectively.

3.3. Experiments

Experiments were performed in order to clarify the critical conditions of the incident optical pulse for degrading the performance of C-OTDR due to the nonlinear phenomena in the optical fiber.

3.3.1. Experimental set-up

Figure 3.2 shows the experimental set-up for C-OTDR with EDFAs. A DFB-LD was coupled to a 1 km long fiber to reduce the linewidth [3-14] and, as a result, the linewidth was less than 10 kHz. The CW light from the DFB-LD was divided by a 3-dB fused fiber directional coupler (FC1) into two paths: a signal path and a local oscillator (LO) path. The signal pulses were produced by an optical waveguide switch made of $LiNbO_3$ (EO-SW) operating in a pulsed mode. The pulse period was 2 ms. The signal pulses were amplified by two post-amplifiers (EDFA1 and EDFA2) and an in-line amplifier (EDFA3). An acousto-optic switch (AO-SW), operating in a pulse mode synchronized with the EO-SW, eliminated the amplified spontaneous emission (ASE) from EDFA1. The optical frequency of the signal pulses was shifted by 120 MHz at the AO-SW. The amplified signal pulses were launched into a 100 km long test fiber.

The Rayleigh backscattered signals from the test fiber were mixed with the local oscillator by FC2 and detected with a double balanced p-i-n-FET receiver. The detected signals were mixed with the 120-MHz electrical local oscillator. A low-frequency-pass filter (LPF) eliminated their high frequency parts and the resulting signals were introduced into an analog to digital (A-D) converter. The digitized signals were squared and integrated, and finally displayed on a computer monitor as a conventional OTDR trace.

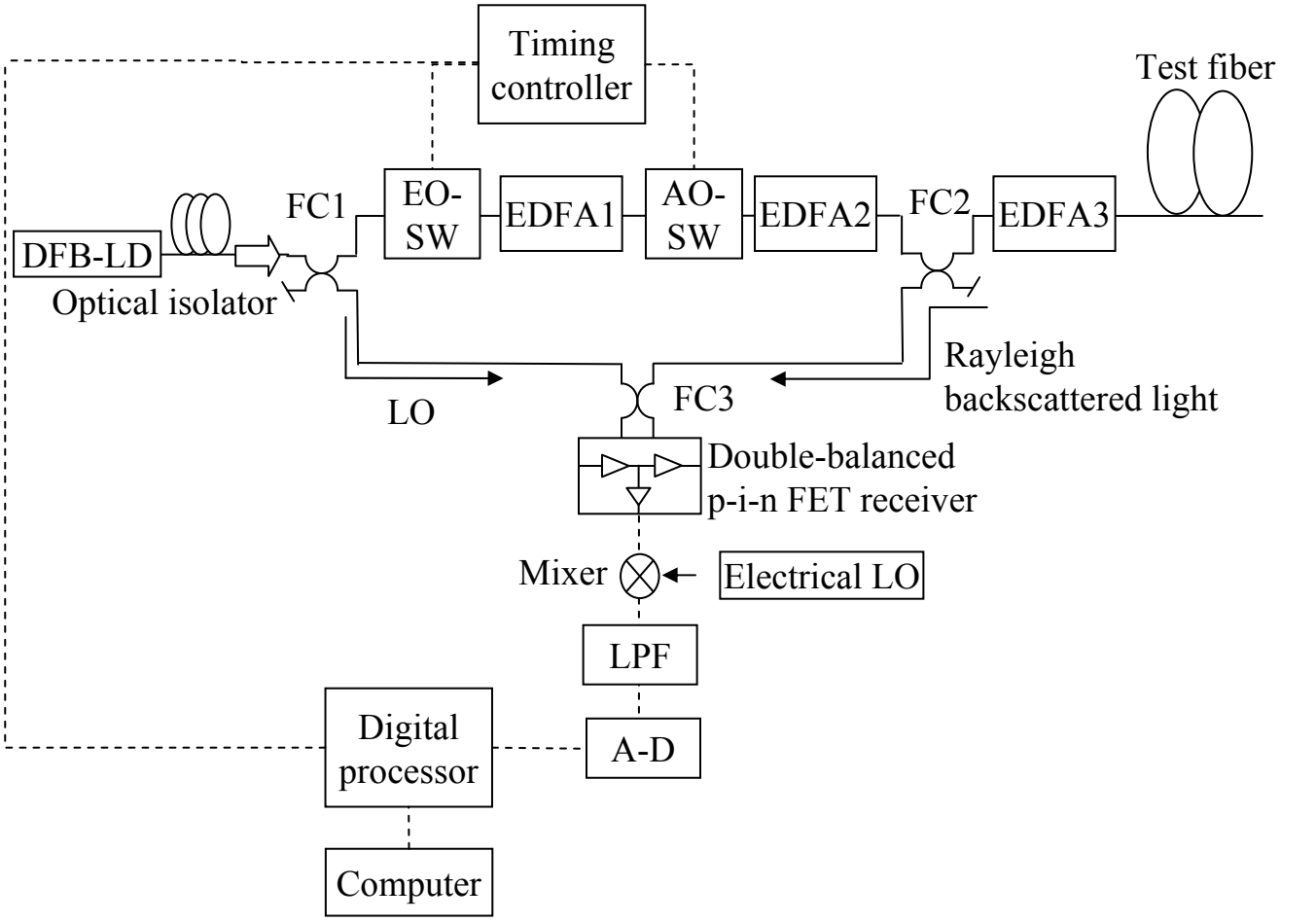

Figure 3.2 Experimental set-up for C-OTDR enhanced with EDFAs.

3.3.2. Experimental results

For a 1-μs pulse width

Figure 3.3 shows the C-OTDR traces measured for a 1-μs pulse width. In trace (a), the incident pulse power was 21 dBm. The total loss of the test fiber was found to be 22 dB from the C-OTDR trace, which agreed with the total loss measured with the optical power meter. The single-way dynamic range (SWDR) was about 39 dB after 2^{18} integrations. There is a little amplitude fluctuation in the C-OTDR trace due to the fading noise [3-9]. In trace (b), the incident pulse power was 24 dBm. Compared with trace (a), the attenuation curve of the optical fiber on the C-OTDR trace gradually became distorted from 10 km to 100 km. The total measured loss of the optical fiber was 24 dB, which was 2 dB larger than that of (a). This was because the Rayleigh backscattered signal power in the receiver bandwidth was decreased by the effect of the nonlinear phenomena.

Figure 3.4(1) shows the incident optical pulse waveforms with a pulse width of 1 μs and averaged pulse power over the pulse width of (a) 21 dBm, (b) 24 dBm, and (c) 28 dBm. The power of the optical pulse amplified by EDFAs in the saturation regime gradually decreased from the head of the pulse to its tail, due to a reduction in the inversion population in the erbium-doped fiber. The power gradient within the pulse width increased in proportion to the pulse power. In these experiments, the power gradient within the pulse width was approximately constant, and the power gradient k with the pulse width of τ was determined as

$$k = \frac{p(0) - p(\tau)}{\tau}. \tag{3.12}$$

From Fig. 3.4(1), the measured power gradient k for (a) was 2.91×10^4 W/s, which is less than the theoretical critical power gradient calculated in section 3.2.1. The measured power gradients for (b) and (c) were 6.64×10^4 W/s and 3.46×10^5 W/s, respectively, which are larger than the theoretical critical power gradient.

Figure 3.4(2) shows the transmitted optical pulse waveforms passing through the test fiber. In (a), the distortion of the pulse waveform was small in comparison with the incident optical pulse waveform shown in Fig. 3.4(1). In (b), the tail of the pulse was slightly rounded due to SBS. In (c), the pulse waveform was significantly distorted. The power of the head of the incident pulse was about 30 dBm from Fig. 3.4(1) and reached the calculated critical power for SRS. So the power of the head of the pulse was converted into Stokes light in the 1.65 μm wavelength band as shown in Fig. 3.4(4). The power of the tail of the incident pulse was about 26 dBm and reached the

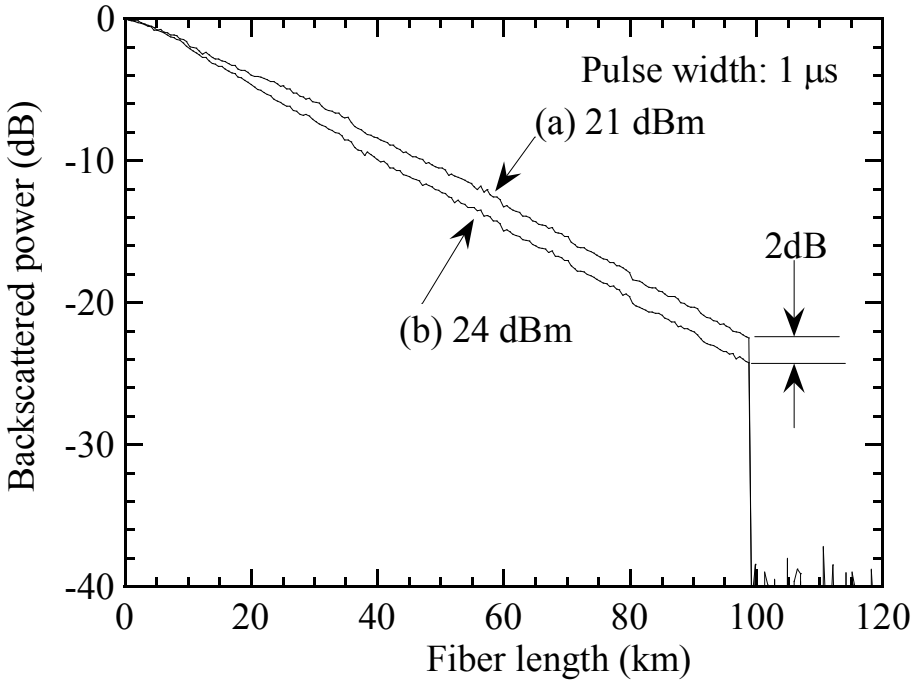

Figure 3.3 C-OTDR trace with 1-μs pulse width for incident pulse power of (a) 21 dBm, and (b) 24 dBm.

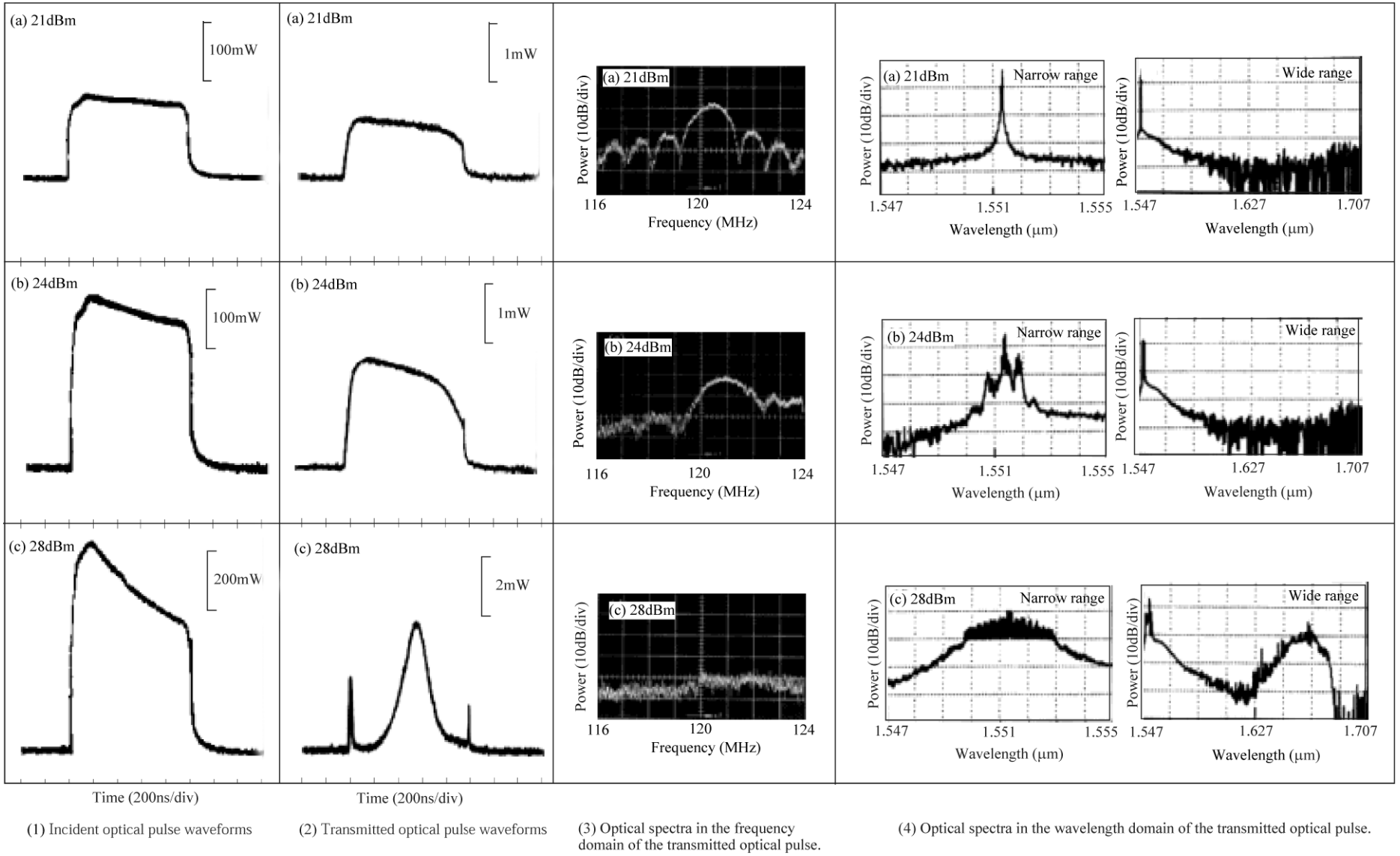

Figure 3.4 Experimental results for 1-μs optical pulse at (a) 21 dBm, (b) 24 dB and (c) 28 dBm.
(1) Incident optical pulse waveforms,
(2) Transmitted optical pulse waveforms,
(3) Optical spectra in the frequency domain of the transmitted optical pulse,
(4) Optical spectra in the wavelength domain of the transmitted optical pulse.

calculated critical power for SBS for a 1 μs pulse width. So the power of the tail was reduced by the backward SBS.

Figure 3.4(3) shows the optical spectra in the frequency domain of the transmitted optical pulse. These spectra were measured using the set-up shown in Fig. 3.5. In (a), the optical spectrum was in the form of the square of a SINC function with center frequency of 120.4 MHz and period of 1 MHz. The center optical frequency was shifted by 0.4 MHz in comparison with the optical frequency shift of 120 MHz at the AO-SW, which was caused by the effect of SPM. In (b), the center optical frequency was shifted by 1 MHz. In (c), the optical frequency shift was even greater.

Figure 3.4(4) shows the optical spectrum in the wavelength domain of the transmitted optical pulse. In (a), the center wavelength of the transmitted pulse was 1.5513 μm. No Stokes or anti-Stokes light was generated. In (b), two side-bands were generated, one on either side of the center wavelength, as a result of FWM. In (c), Stokes light with a center wavelength of 1.65 μm was generated by SRS.

The test fiber in this experiment had a length L = 100 km, the attenuation coefficient $\alpha = 4.8\text{x}10^{-5}$ m^{-1}, and effective cross section A = 50 μm^2 (the mode-field radius a_m = 4 μm) at the wavelength of λ = 1.5513 μm. Assuming the test fiber to be a standard single-mode fiber with nonlinear refractive index $n_2 = 3.2\text{x}10^{-20}$ m^2/W [3-7], the optical frequency shift δv was calculated using Eqs. (3.1) and (3.2), as a function of the power gradient k (Figure 3.6). The measured optical frequency shift is also plotted. The calculated result roughly agrees with the experimental values. The reasons for the discrepancy between the measured and the calculated values plotted in Figure 3.6 were: (1) the measured power gradient k, which was approximated as shown in Eq. (3.12) for simplicity, was smaller than the exact one because the power of the amplified optical pulse exponentially decreased from the head of the pulse to its tail, and (2) the nonlinear refractive index n_2 of the Ge-doped core fiber (in this experiment) was different from that of a pure Si core fiber (in Ref. [3-7]), which was used in the calculation.

These experiments clarify that the critical condition for degrading the performance of C-OTDR combined with EDFAs is given by the optical frequency shift of the Rayleigh backscattered signals caused by the effect of SPM. The critical power gradient of the incident pulse amplified using the EDFAs in this experiment was $2.91\text{x}10^4$ W/s and the pulse power for this critical condition was lower than the critical power for the other nonlinear phenomena.

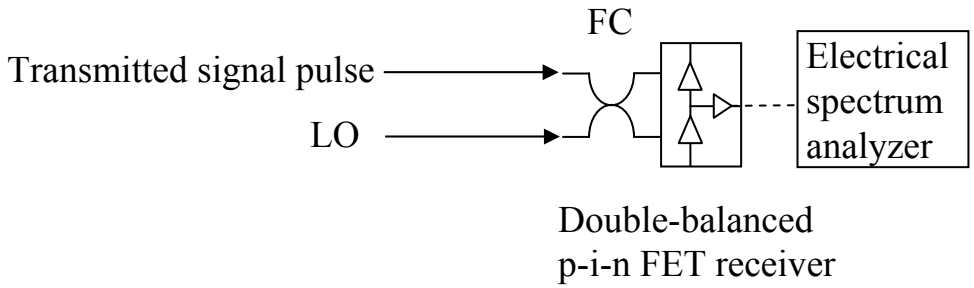

Figure 3.5 Experimental set-up for measuring optical spectrum in the frequency domain.

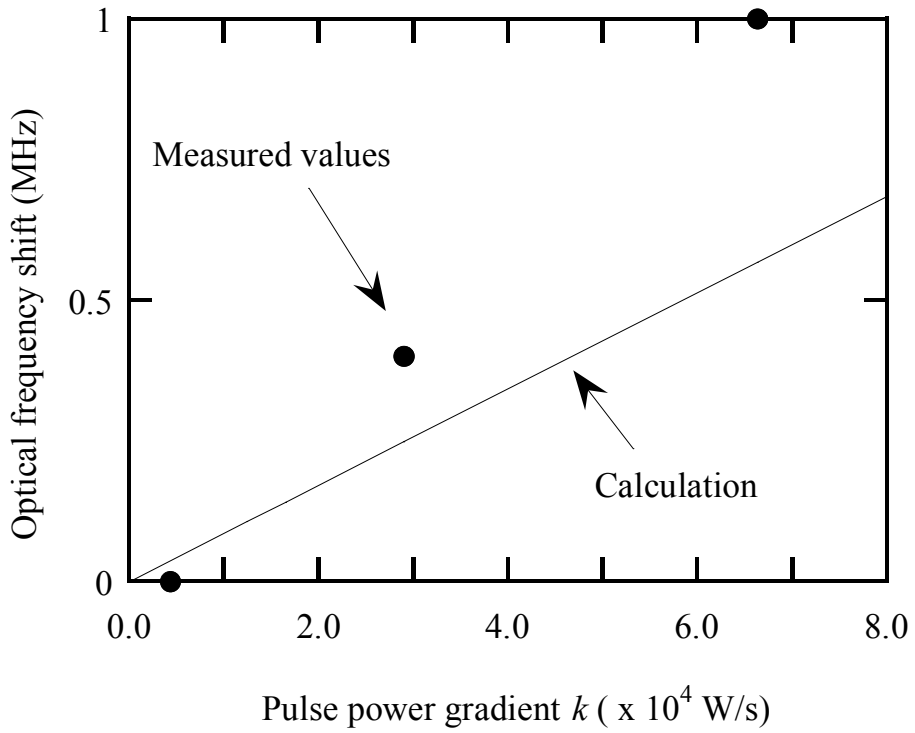

Figure 3.6 Optical frequency shift as a function of pulse power gradient.

For a 100-ns pulse width

Experiments were also performed for a 100 ns pulse width. Figure 3.7 shows the C-OTDR traces after 2^{18} integrations. In trace (a), the incident pulse power was 24 dBm. The total loss of the test fiber was found to be 22 dB, which agreed with the previous experimental results shown in Fig. 3.3(a). The SWDR was about 29 dB. In trace (b), the incident pulse power was 25 dBm. The C-OTDR trace was distorted and at 20 km shifted down by about 2 dB. The total measured loss of the test fiber was 2.5 dB greater than that of (a). The reason for this is that the detected signal power was decreased by the nonlinear phenomena.

Figure 3.8(1) shows the incident optical pulse waveforms. The power gradient of the pulse was negligible in both (a) and (b). Figure 3.8(2) shows the transmitted optical pulse waveforms. The transmitted pulse waveform was unchanged from the incident optical pulse in both cases. Figure 3.8(3) shows the optical spectra in the frequency domain. They had the form of the square of a SINC function with center frequency of 120 MHz and period of 10 MHz. The optical frequency shift of the transmitted optical pulse was also negligible in both cases. Figure 3.8(4) shows the optical spectra in the optical wavelength domain. In (a), the side-bands were very small. In (b), Stokes and anti-Stokes lights were generated on either side of the center wavelength as a result of FWM, which causes the incident optical pulse to interact parametrically with the ASE. The power levels of the Stokes and anti-Stokes lights were 15 dB higher than the ASE level. The optical wavelength shift (the optical frequency shift) between the signal and the Stokes or anti-Stokes light was about 0.5 nm (62 GHz) and the Stokes bandwidth was about 0.25 nm (32 GHz).

The test fiber was composed of several 5-20 km dispersion-shifted single-mode fibers with typical dispersion D = -1.50 ps/(km·nm). From Eqs. (3.6) and (3.9), the calculated frequency shift and the Stokes bandwidth at the incident pulse power of P_i = 316 mW (25dBm) were 147 GHz and 74 GHz, respectively. The reasons for the difference between the measured value and the calculated one were: (1) the coefficient n_2 of the Ge-doped core fiber (in this experiment) was different from that of a pure Si core fiber, (2) there was some fluctuation of the dispersion in the test fiber, and (3) the parametric gain of FWM was suppressed by polarization mismatch between the signal pulse and the ASE.

These experiments show that the critical condition for a 100 ns pulse width is given by FWM, which leads to the generation of the Stokes and anti-Stokes light. The FWM critical power for the incident pulse amplified with the EDFAs in this experiment was lower than the critical power for the other nonlinear phenomena.

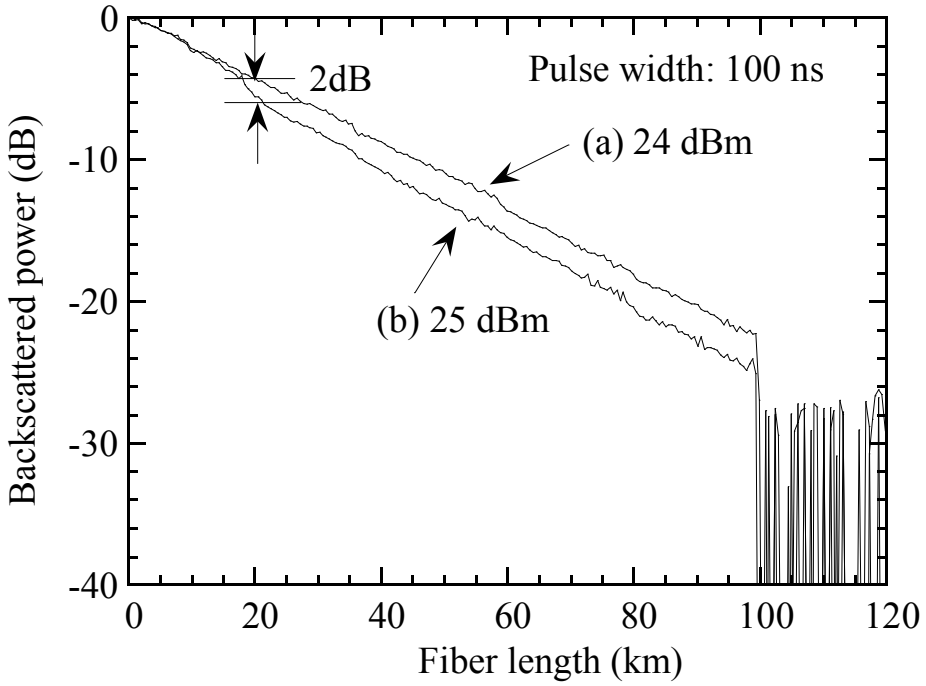

Figure 3.7 C-OTDR trace with 100-ns pulse width for incident pulse power of (a) 24 dBm, and (b) 25 dBm.

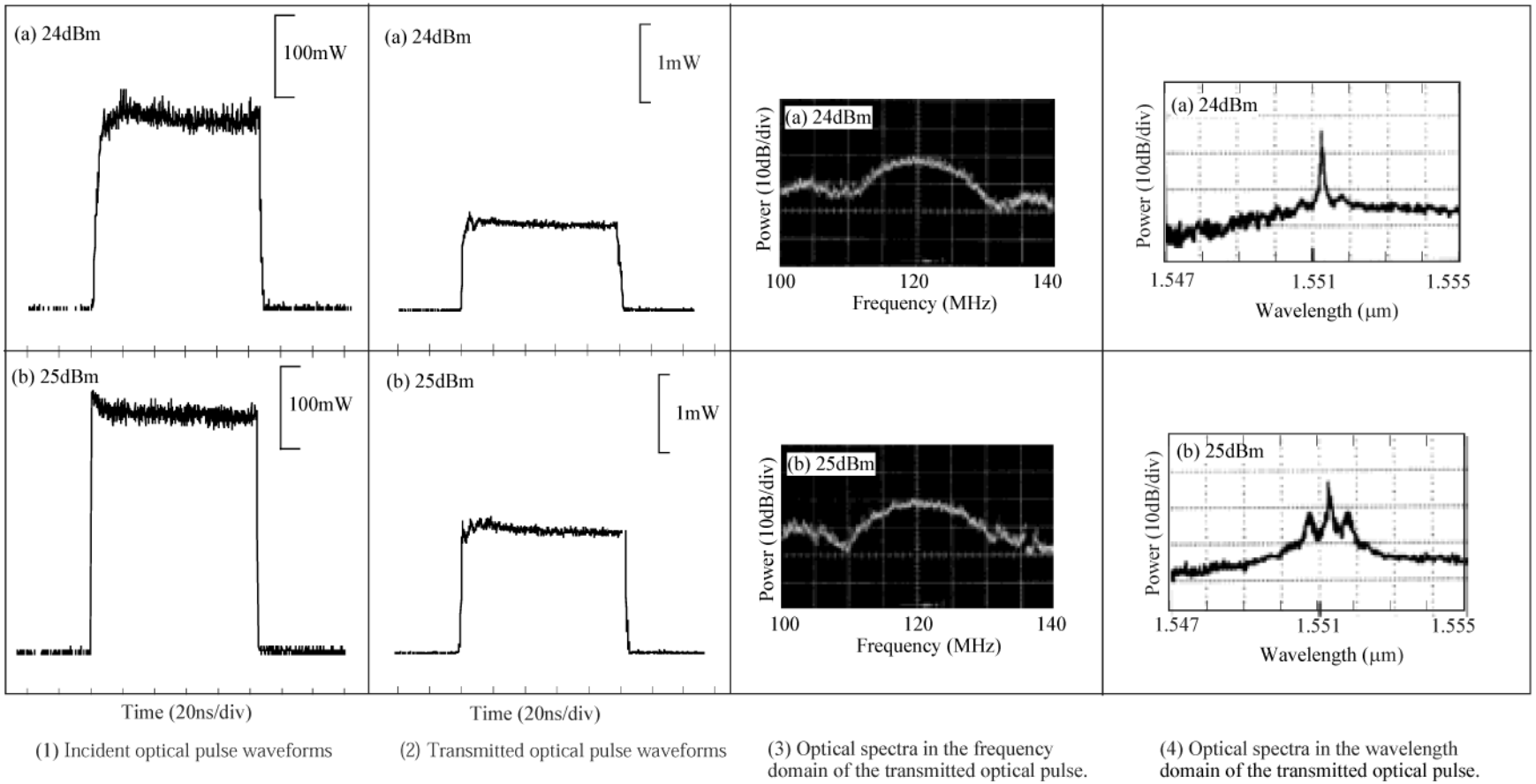

Figure 3.8 Experimental results for 100 ns optical pulse at (a) 24 dBm, and (b)25 dBm.
(1) Incident optical pulse waveforms,
(2) Transmitted optical pulse waveforms,
(3) Optical spectra in the frequency domain of the transmitted optical pulse,
(4) Optical spectra in the wavelength domain of the transmitted optical pulse.

3.4. Performance limit of C-OTDR enhanced with EDFAs due to nonlinear phenomena

3.4.1. Critical incident pulse power for pulse widths of longer than 1μs

The previous experimental results showed that the critical incident pulse power for a 1-μs pulse width (i.e., 1-MHz receiver bandwidth) was about 21 dBm, limited by the effect of SPM. The measured critical power gradient was 2.9×10^4 W/s. Since the critical condition for the effect of SPM is more severe for a narrow bandwidth (i.e., a long pulse width), the critical conditions for pulse widths of 4 μs and 10 μs were measured. For a 4-μs pulse width (i.e., 250-kHz receiver bandwidth), the measured critical power gradient k_c was 4.4×10^3 W/s, for which the optical frequency shift normalized by the receiver bandwidth ($\delta v/B$) was less than 0.4. The pulse power of the critical incident pulse amplified with EDFAs in this experiment was 18.1 dBm. For a 10-μs pulse width (i.e., 100-kHz receiver bandwidth), the measured critical power gradient k_c was 2.1×10^3 W/s and the pulse power of the critical incident pulse amplified with EDFAs in this experiment was 16.7 dBm.

Figure 3.9 shows the calculated critical power for SBS, that for SRS, and plots of experimental critical pulse powers for SPM and FWM as a function of the receiver bandwidth. For a 1-μs or longer pulse width (i.e., a 1-MHz or narrower receiver bandwidth), the critical pulse power for SPM was lower than those of SBS or SRS. For a 100 ns (i.e., a 10-MHz bandwidth), the critical pulse power for FWM was also lower than those for SBS or SRS.

3.4.2. Performance of C-OTDR at critical incident pulse power

Figure 3.10 shows the C-OTDR traces for a 1-μs pulse width after 2^{18} integrations. The SWDR was found to be 39 dB and the attenuation curve in the C-OTDR trace indicates the characteristics of the test fiber. The incident pulse had pulse power of 20.7 dBm and a power gradient of 2.9×10^4 W/s, which was the critical condition for the effect of SPM. The minimum power detectable by the receiver was about -85 dBm for 1-MHz bandwidth.

Figure 3.11 shows the C-OTDR trace for a 4-μs pulse width. The critical power gradient of the incident pulse was 4.4×10^3 W/s, for which the optical frequency shift normalized by the bandwidth ($\delta v/B$) was less than 0.4, and the incident pulse power was 18.1 dBm. The SWDR was found to be 44 dB. The degradation by SPM was

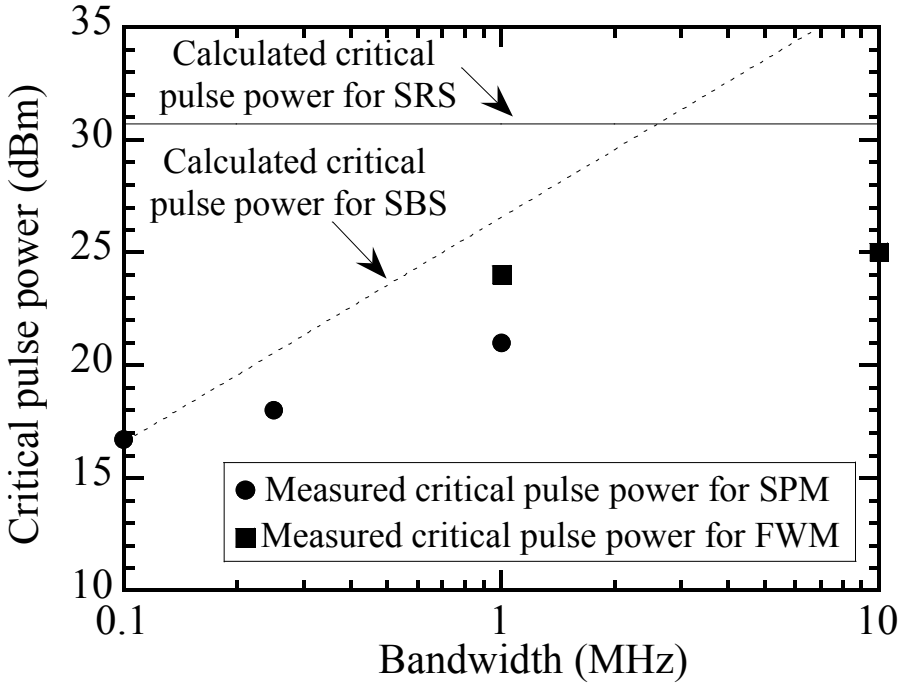

The solid line is the calculated critical pulse power of SRS using Eq. (3.10),
The dotted line is the calculated critical pulse power of SBS using Eq. (3.11) as a function of bandwidth (i.e. inverse of pulse width: $1/\tau$),
The circles (●) are the measured critical pulse power for SPM,
The squares (■) are the measured critical pulse power for FWM.

Figure 3.9 Critical pulse power of nonlinear phenomena as a function of bandwidth (i.e., inverse of pulse width: $1/\tau$).

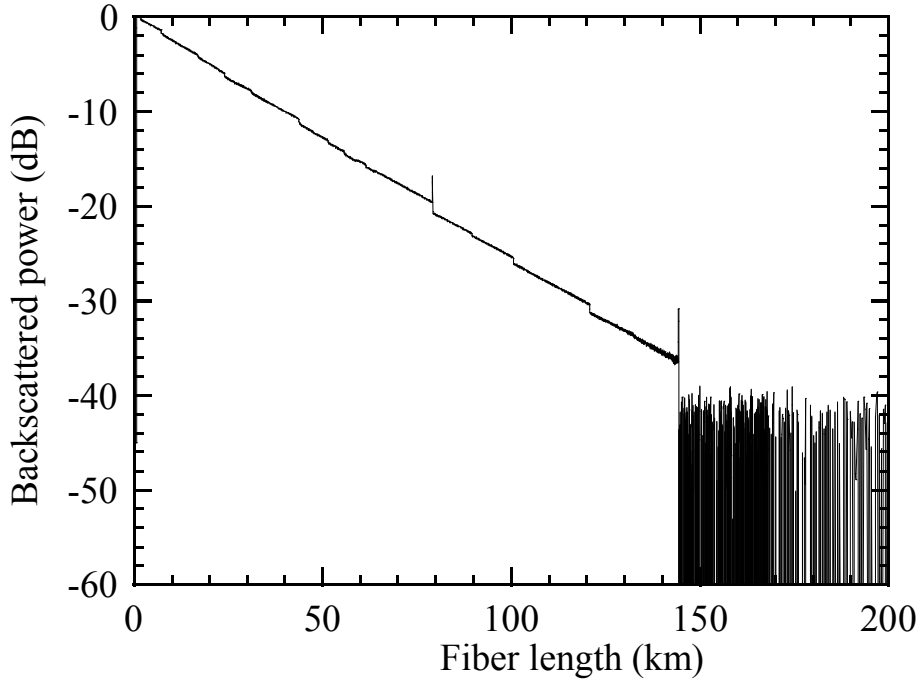

Figure 3.10 C-OTDR trace with pulse width of 1-μs.

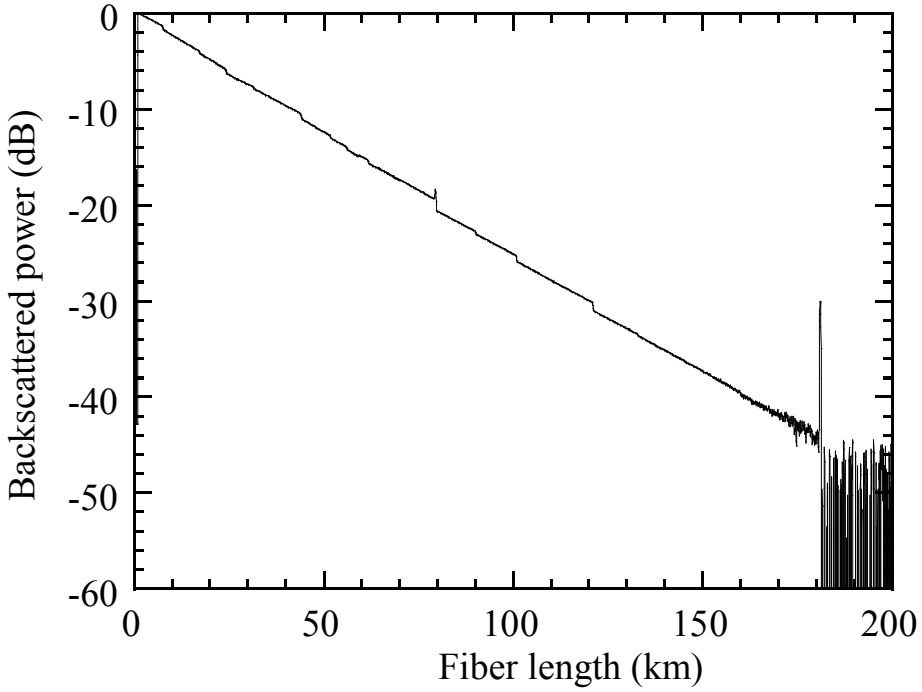

Figure 3.11 C-OTDR trace with pulse width of 4-μs.

negligible.

Figure 3.12 shows the C-OTDR trace for a 10-μs pulse width. The critical power gradient of the incident pulse was 2.1×10^3 W/s at which the incident pulse power was 16.7 dBm in this experiment. The SWDR was found to be 48 dB and the degradation by SPM was also negligible.

Figure 3.13 shows the C-OTDR trace for a 100 ns pulse width. The incident pulse power was 24 dBm, which was limited by the effect of FWM according to the previous results. The minimum power detectable by the receiver for 10 MHz bandwidth was about -72 dBm. The SWDR was found to be about 29 dB.

For 10-μs, 4-μs, 1-μs and 100-ns pulse widths, we have demonstrated the critical pulse power and the performance limit of C-OTDR enhanced with EDFAs due to the effect of SPM and FWM.

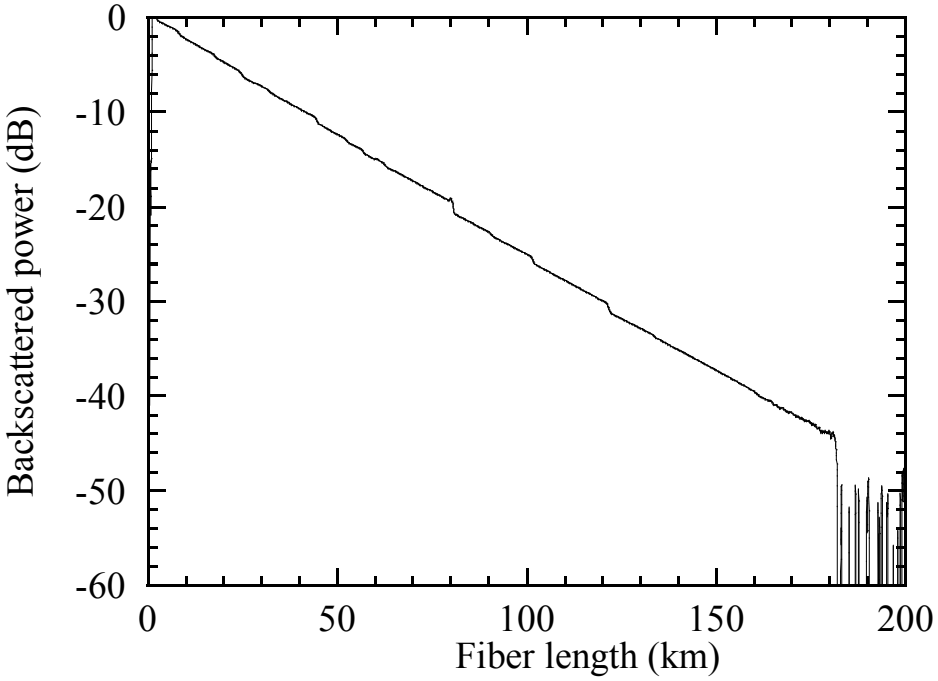

Figure 3.12 C-OTDR trace with pulse width of 10-μs.

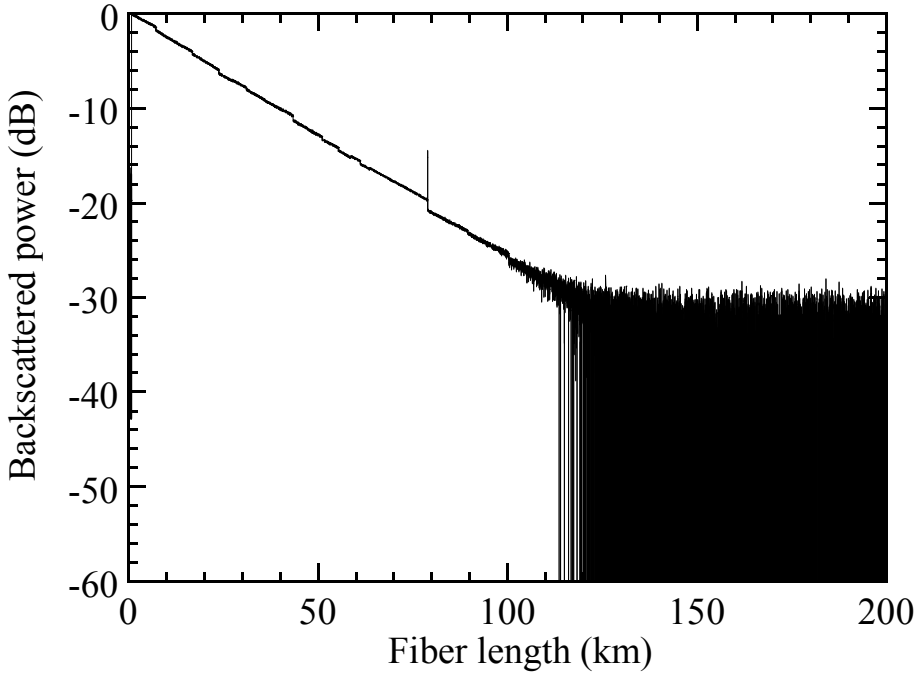

Figure 3.13 C-OTDR trace with pulse width of 100-ns.

3.5. Conclusions

This chapter has clarified theoretically and experimentally that the critical conditions at which the performance of C-OTDR with EDFAs is degraded by the effects of optical nonlinear phenomena in a single-mode optical fiber are given by the effects of SPM and FWM. For a 1-μs pulse width, the incident pulse power was limited by the effect of SPM. When an optical pulse with a power gradient within the pulse width was incident into a single-mode fiber, the optical frequency of the backscattered signal was shifted by SPM, and the center frequency of the signal moved outside the receiver band, thus degrading the sensitivity of C-OTDR. The effect of SPM on sensitivity was greater for a narrow bandwidth (i.e., a long pulse width). For a 100-ns pulse width, the incident pulse power was limited by FWM, which caused the incident optical pulse to interact with the amplified spontaneous emission and be converted to Stokes and anti-Stokes light. The critical powers for SPM and FWM were lower than those for SBS and SRS.

Through this chapter, the high performance of C-OTDR enhanced with EDFAs has been demonstrated. The SWDRs of C-OTDR for pulse widths of 10 μs, 4 μs, 1 μs, and 100 ns after 2^{18} integrations were 48 dB, 44 dB, 39 dB, and 29 dB, respectively, which are believed to represent the highest performance of any C-OTDR with EDFAs.

The above 48-dB-SWDR C-OTDR with a pulse width of 10 μs can be applied to monitor the 160-km repeaterless optical transmission systems deployed in NTT trunk lines in Japan.

3.6. References

[3-1] M. Tateda and T. Horiguchi, "Advances in optical time-domain reflectometry," IEEE J. Lightwave Technol., vol. LT-7, no. 8, pp. 1217-1224, 1989.

[3-2] P. Healey and D.J. Malyon, "OTDR in single-mode fiber at 1.5 μm using heterodyne detection," Electron. Lett., vol. 18, no. 12, pp. 862-863, 1982.

[3-3] L. C. Bank and D. M. Spirit, "OTDR performance enhancement through erbium fibre amplification," Electron. Lett., vol. 25, no. 25, pp. 1693-1694, 1989.

[3-4] Y. Koyamada and H. Nakamoto, "High performance single mode OTDR using coherent detection and fibre amplifiers," Electron. Lett., vol. 26, no. 9, pp. 573-574, 1990.

[3-5] S. Furukawa, H. Izumita, I. Sankawa, and Y. Koyamada, "High dynamic range, low fading noise coherent OTDR using erbium fiber amplification and LD temperature changing techniques," in the proc. of ECOC'91/IOOC'91, Mo.C1-3, pp. 81-84, 1991.

[3-6] H. Izumita, Y. Koyamada, I. Sankawa, and S. Furukawa, "A coherent optical time-domain reflectometer with a 40-dB dynamic range enhanced with erbium-doped fiber amplifiers," in the technical digest of OFC'92, WK6, p. 147, 1992.

[3-7] R. H. Stolen, "Nonlinearity in fiber transmission," Proc. IEEE, vol. 68, no. 10, pp.1232-1236, 1980.

[3-8] H. Stolen and Lin Chinlon, "Self-phase-modulation in silica optical fibers," Phys. Rev. A, vol. 17, No. 4, pp.1448-1453, 1978.

[3-9] P. Healey, "Fading in heterodyne OTDR," Electron. Lett., vol. 20, no. 1, pp.30-32, 1984.

[3-10] R. H. Stolen and J. E. Bjorkholm, "Parametric amplification and frequency conversion in optical Fibers," IEEE J. Quantum Electron., Vol. QE-18, No. 7, pp. 1062-1072, 1982.

[3-11] G. P. Agrawal, "Nonlinear Fiber Optics," Academic Press, 1989.

[3-12] R. G. Smith, "Optical power handing capacity of low loss optical fiber as determined by stimulated Raman and Brillouin scattering," Appl. Opt. vol. 11, no. 11, pp.2489-2499, 1972.

[3-13] Y. Koyamada, H. Nakamoto, and N. Ohta, "High performance coherent OTDR enhanced with erbium doped fiber amplifiers," J. Opt. Commun., vol. 13, no. 4. pp. 127-133. 1992.

[3-14] J. Mark, E. Bodtker and B. Tromborg, "Measurement of Rayleigh backscatter-induced linewidth reduction," Electron. Lett., vol. 21, no. 22, pp. 1008-1009, 1985.

Chapter 4. Amplitude fluctuation in C-OTDR and its reduction technique

This chapter provides a stochastic description of the amplitude fluctuation and estimates it theoretically. An effective reduction technique, in which an RF current pulse is induced in the drive current of the laser diode (LD) C-OTDR source while changing the LD temperature, is proposed, and reduction of the amplitude fluctuation is experimentally demonstrated.

4.1. Introduction

Optical time-domain reflectometry (OTDR) is a commonly used technique for fault location and characterization in optical fiber transmission systems. Many studies have been undertaken to extend the dynamic range of OTDR [4-1]. Coherent detection is a promising technique for improving the receiver sensitivity up to the quantum limit, which is advantageous for direct detection [4-2]-[4-7]. Coherent-detection OTDR (C-OTDR) enhanced with erbium-doped fiber amplifiers (EDFAs) has been demonstrated to achieve a single-way dynamic range (SWDR) of over 40 dB [4-6],[4-7].

A problem with C-OTDR is the occurrence of amplitude fluctuation, which leads to a reduction in measurement accuracy. This fluctuation is caused by the following factors: (1) fading noise resulting from the interference of Rayleigh backscattered light [4-8]; (2) the polarization-dependent fluctuation caused by the state of polarization (SOP) mismatch between the Rayleigh backscattered light and the local oscillator (LO) light; and (3) the fluctuation of the heterodyne detection efficiency, caused by the relative phase change between the Rayleigh backscattered signal and the LO. The amplitude fluctuation in C-OTDR has been reported to be about 0.2–0.3 dB [4-3],[4-9]. This fluctuation must be reduced before C-OTDR can be practically applied in optical fiber networks.

This chapter provides a stochastic description of the amplitude fluctuation and estimates it theoretically. It also proposes an effective reduction technique, in which an RF current pulse is induced in the drive current of the laser diode (LD) C-OTDR source while changing the LD temperature. Furthermore, the chapter experimentally demonstrates reduction of the amplitude fluctuation. Section 4.2 derives a stochastic formula for amplitude fluctuation in the C-OTDR trace, by using the probability density functions for each factor, and it evaluates the amplitude fluctuation

theoretically. Section 4.3 describes techniques for reducing the effects of each factor and calculates the amplitude fluctuation with integrations. Section 4.4 theoretically investigates asynchronous optical frequency hopping, which increases the inclination of the C-OTDR trace and reduces the measurement accuracy. This section also proposes a new technique for reducing the amplitude fluctuation by stimulating synchronous optical frequency hopping with no inclination increase. Finally, section 4.5 reports experiments which demonstrate a reduction in the amplitude fluctuation in C-OTDR.

4.2. Stochastic description of the amplitude fluctuation in the C-OTDR trace

4.2.1. Amplitude fluctuation in the C-OTDR trace

Figure 4.1 shows the C-OTDR configuration. A CW light from a narrow linewidth source with an optical frequency of ν is divided by a 3-dB fused-fiber directional coupler (FC1) into two paths; a signal path and a local oscillator (LO) path. The signal pulse is produced by an acousto-optic switch (AO-SW) which is an acousto-optic modulator (AOM) made of $PbMoO_4$ operated in a pulsed mode. The optical frequency of the signal pulse is shifted by the modulation frequency ν_A of the AO-SW. The beam waist and the rise-time of the AOM used in the experiment were about 0.5 mm and 60 ns, respectively. The rise-time can be improved by employing a smaller beam waist. However, the deflection efficiency is degraded and the resulting insertion loss increases. For a 100 ns or shorter pulse width, we used an optical waveguide switch made of $LiNbO_3$ (EO-SW) operating in a pulsed mode synchronized with the AO-SW in order to reshape the signal pulse. The rise-time and insertion loss of the EO-SW were 4 ns and 3.5 dB, respectively.

When a signal pulse with a unit pulse power is launched into the test fiber and passes through FC2 at time t = 0, the Rayleigh backscattered signal, $E_b(t)\cdot\exp(j2\pi(\nu+\nu_A)t+\varphi(t))$, at time t is mixed with the LO light, $E_{LO}\cdot\exp(j2\pi\nu t)$, by FC3 and is detected with a double balanced p-i-n FET receiver. The detected signal current $i(t)$ is proportional to the square of the total signal field and is shown as,

$$i(t) = \left(\frac{\eta e}{h\nu}\right)\left[{E_{LO}}^2 + E_b(t)^2 + 2E_{LO}E_b(t)\cos\theta(t)\cos(2\pi\nu_A t + \varphi(t))\right], \quad (4.1)$$

where $\theta(t)$ and $\varphi(t)$ are the relative polarization angle and the relative phase between the backscattered signal and the LO light, respectively. The ac signal of the last term in

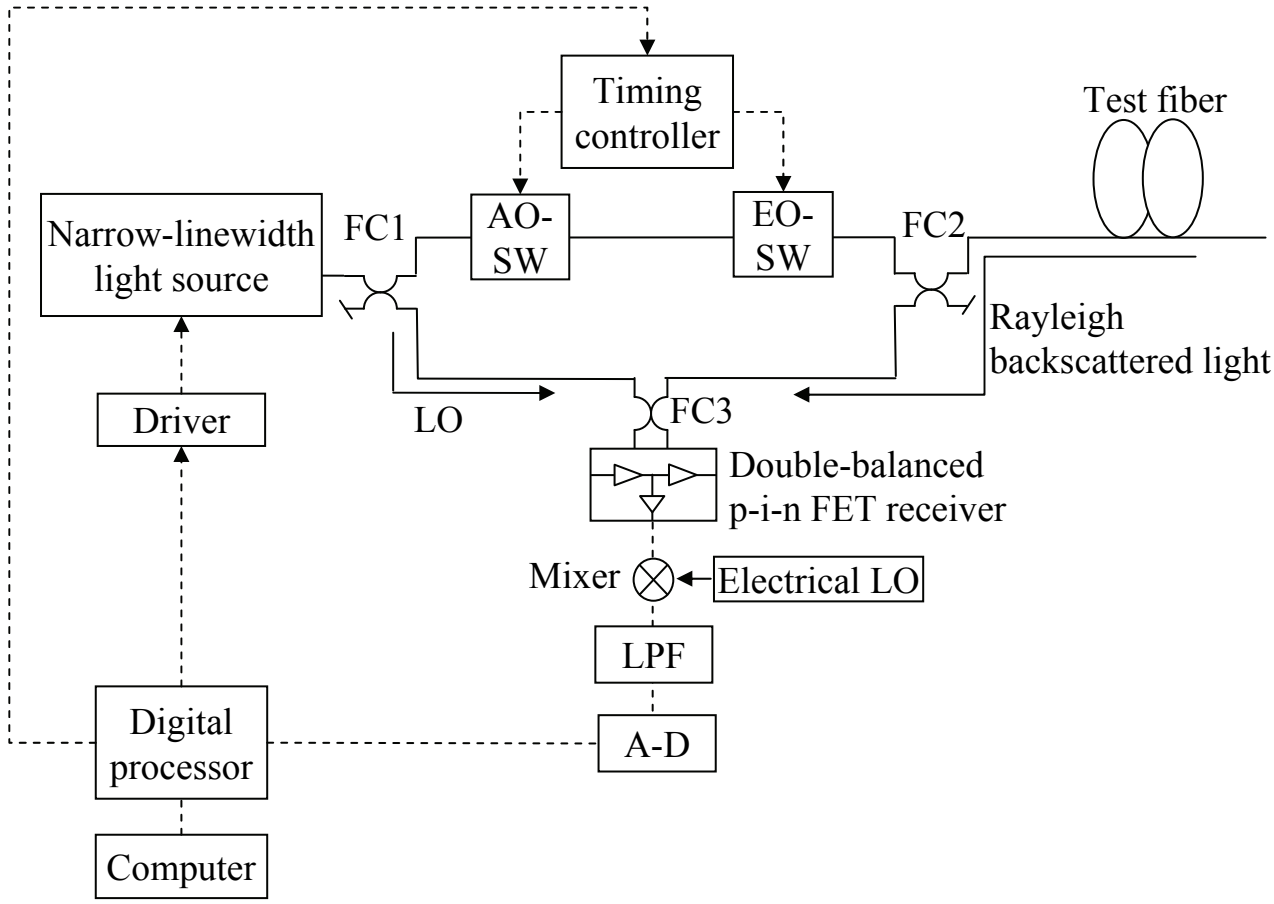

AO-SW: Accousto-optic switch
EO-SW: Optical waveguide switch made of $LiNbO_3$
FC: 3-dB optical fiber coupler
LPF: Low-pass filter
A-D: Analog-digital converter

Figure 4.1 Configuration of C-OTDR

Eq. (4.1) is converted to a baseband signal by mixing it with the electrical LO with a frequency of ν_A. A low frequency pass filter (LPF) eliminates its high frequency part. The baseband signal, $E_{LO}\cdot E_b(t)\cdot\cos\theta(t)\cdot\cos\varphi(t)$, is introduced into an analog to digital (A-D) converter. The square of the baseband signal is integrated to improve the signal-to-noise ratio (SNR). Finally the squared signal, $E_{LO}^2\cdot E_b(t)^2\cdot\cos^2\theta(t)\cdot\cos^2\varphi(t)$, is displayed on a computer CRT as a conventional OTDR trace. The C-OTDR trace $S(t)$ in dB is shown as

$$S(t) = 5\log\left(E_{LO}{}^2 E_b(t)^2 \cos^2\theta(t)\cos^2\varphi(t)\right). \text{ (dB)} \tag{4.2}$$

When the test fiber attenuation is taken into account, the Rayleigh backscattered signal power $E_b(t)^2$ observed at the input fiber end at time t is shown as [4-1]

$$E_b(t)^2 = E_R(t)^2 \exp\left(-2\alpha\left(\frac{ct}{2n}\right)\right), \tag{4.3}$$

where $E_R(t)$ is the amplitude of the Rayleigh backscattered signal from the scattering volume at the location z (=ct/(2n)) in the test fiber, c is the light velocity in a vacuum, n is the refractive index of the test fiber and α (m^{-1}) is the attenuation coefficient of the test fiber. Therefore, the C-OTDR trace $S(t)$ is derived from Eqs. (4.2) and (4.3), and is given as

$$S(t) = -\left(10\alpha\log e\right)\left(\frac{ct}{2n}\right) + 5\log\left(E_R(t)^2\cos^2\theta(t)\cos^2\varphi(t)\right), \text{ (dB)} \tag{4.4}$$

where the LO light power is $E_{LO}{}^2 = 1$ for simplicity. The first term in Eq. (4.4) implies the attenuation characteristics of the test fiber, and time t corresponds to the location z (=ct/(2n)) in the test fiber. The second term involves three variables; $E_R(t)$, $\cos\theta(t)$, and $\cos\varphi(t)$. The stochastic nature of this term is the origin of the amplitude fluctuation in the C-OTDR trace.

4.2.2. Stochastic formulas for the amplitude fluctuation

The amplitude fluctuation must be described stochastically before it can be estimated theoretically. The second term in Eq. (4.4) includes three variables and the fluctuation of this term causes the amplitude fluctuation in the C-OTDR trace. In this thesis, the amplitude fluctuation is regarded as the square root of the variance of $E_R(t)^2\cdot\cos^2\theta(t)\cdot\cos^2\varphi(t)$ in the second term of Eq. (4.4). Therefore, the amplitude fluctuation Δ in dB is shown as

$$\Delta = 5\log(m+\sigma) - 5\log(m) = 5\log\left(1+\frac{\sigma}{m}\right), \text{ (dB)} \tag{4.5}$$

where m is the mean of $E_R(t)^2 \cdot \cos^2\theta(t) \cdot \cos^2\varphi(t)$ $(=X^2)$, σ is the square root of the variance of X^2 and the amplitude X is

$$X = E_R(t)\cos\theta(t)\cos\varphi(t). \tag{4.6}$$

Since the variables $E_R(t)(=u)$, $\cos\theta(t)(=v)$, $\cos\varphi(t)(=w)$ vary independently, the probability density function $P(X)$ can be described as the joint probability density function [4-10],

$$P(X) = p_1(u)p_2(v)p_3(w), \tag{4.7}$$

where $p_1(u)$, $p_2(v)$ and $p_3(w)$ are the probability density functions for the variables u, v and w, respectively. Then, the mean m of X^2 is

$$m = \left\langle X^2 \right\rangle = \int X^2 P(X)dX = \int u^2 v^2 w^2 p_1(v)p_2(u)p_3(w)dvdudw, \tag{4.8}$$

and the square root σ of the variance of X^2 is

$$\sigma = \sqrt{\left\langle X^4 \right\rangle - \left\langle X^2 \right\rangle^2}, \tag{4.9}$$

$$\left\langle X^4 \right\rangle = \int X^4 P(X)dX = \int u^4 v^4 w^4 p_1(v)p_2(u)p_3(w)dvdudw. \tag{4.10}$$

If the probability density functions $p_1(u)$, $p_2(v)$ and $p_3(w)$ are determined, the amplitude fluctuation (Δ) can be calculated by Eqs. (4.5), and (4.8) - (4.10).

4.2.3. Calculation of the amplitude fluctuation

The amplitude fluctuation is calculated under the following conditions: (a) without using an amplitude fluctuation reduction technique, (b) with a reduction technique (e.g. the polarization-diversity detection technique described in section 4.3.2) to reduce the fluctuation in the optical detection efficiency caused by a change in the polarization mismatch, (c) with a reduction technique (e.g. the phase-diversity detection technique described in section 4.3.3) to reduce the fluctuation in the heterodyne detection efficiency caused by the relative phase change and (d) with both techniques to reduce the detection efficiency fluctuation caused by the polarization mismatch change and the relative phase change.

With (a), since the Rayleigh backscattered signal, $E_R(t)$, from a single-mode optical fiber has Rayleigh statistics [4-8], the probability density function $p_1(u)$ is derived as

$$p_1(u) = \frac{u}{a^2}\exp\left(-\frac{u^2}{2a^2}\right), \tag{4.11}$$

where a is constant. The SOP mismatch $\theta(t)$ described in Eq. (4.6) is changed by the

birefringence and mechanical vibration in the test fiber. Hence the probability density function $p_2(v)$ is derived as,

$$p_2(v) = \frac{1}{\pi\sqrt{1-v^2}}, \tag{4.12}$$

while $\theta(t)$ is uniformly distributed with the interval $(-\pi,\pi)$ [4-10],[4-11]. Since the relative phase $\varphi(t)$ described in Eq. (4.6) is randomized by the phase noise in the test fiber, the probability density function $p_3(w)$ is, simultaneously, derived as,

$$p_3(w) = \frac{1}{\pi\sqrt{1-w^2}}, \tag{4.13}$$

while $\varphi(t)$ is uniformly distributed with the interval $(-\pi,\pi)$ [4-10],[4-11]. Therefore, the amplitude fluctuation Δ, which depends on σ/m, is derived from Eqs. (4.5), (4.8) and (4.9) after calculating $<X^2>$ and $<X^4>$ by inserting Eqs. (4.11) - (4.13) into Eqs. (4.8) and (4.10). Thus, the calculated σ/m and Δ values are 1.9 and 2.3 dB, respectively.

For (b), the optical detection efficiency, which depends on the change in the SOP mismatch, is stabilized and $\cos\theta(t)$ (= v) in Eq. (4.4) can be regarded as a constant c_1. The second term of Eq. (4.4) is rewritten as $5\log(E_R(t)^2\cdot\cos^2\varphi(t))+5\log(c_1^2)$. The amplitude fluctuation in this case is caused by the first term of $5\log(E_R(t)^2\cdot\cos^2\varphi(t))$. Therefore, in calculating the amplitude fluctuation, the variable $\cos\theta(t)$ (= v) and the probability density function $p_2(v)$ must be omitted from Eqs. (4.6)-(4.10). The σ/m and Δ values are simultaneously determined as with (a), and they are 1.4 and 1.9 dB, respectively.

For (c), the heterodyne detection efficiency, which depends on the relative phase, is stabilized and $\cos\varphi(t)$ (= w) in Eq. (4.4) can be regarded as a constant c_2. The second term of Eq. (4.4) is rewritten as $5\log(E_R(t)^2\cdot\cos^2\theta(t))+5\log(c_2^2)$. The amplitude fluctuation in this case is caused by the first term of $5\log (E_R(t)^2\cdot\cos^2\theta(t))$. Therefore, in calculating the amplitude fluctuation, the variable $\cos\varphi(t)$ (= w) and the probability density function $p_3(w)$ must be omitted from Eqs. (4.6) - (4.10) as with (b). The σ/m and Δ values are calculated simultaneously and are 1.4 and 1.9 dB, respectively.

For (d), the detection efficiency fluctuation caused by the SOP mismatch and the relative phase change is reduced. $\cos\theta(t)$ (= v) and $\cos\varphi(t)$ (= w) in Eq. (4.4) can be regarded as a constant c_3. The second term of Eq. (4.4) is rewritten as $5\log(E_R(t)^2) + 5\log(c_3^2)$. The amplitude fluctuation in this case is caused by the first term of $5\log(E_R(t)^2)$. Therefore, in calculating the amplitude fluctuation, the variables $\cos\theta(t)$ (= v) and $\cos\varphi(t)$ (= w) and the probability density functions $p_2(v)$ and $p_3(w)$ must be omitted from Eqs. (4.6) - (4.10). The σ/m and Δ values are calculated simultaneously and are 1 and 1.5 dB, respectively.

The calculated σ/m values for (a)-(d) indicate the amplitude fluctuation in the C-OTDR trace with only one measurement and are the fundamental values for calculating the amplitude fluctuation with N integrations.

4.3. Techniques for reducing amplitude fluctuation in C-OTDR with *N* integrations

4.3.1. Optical frequency domain integration technique for reducing the amplitude fluctuation caused by interference between Rayleigh backscattered lights

The amplitude fluctuation in the C-OTDR trace, caused by interference between the Rayleigh backscattered lights, decreases in proportion to the square root of the number of independent Rayleigh backscattered signals [4-8],[4-9]. For a signal pulse with a pulse width of τ, the optical frequency change by $1/\tau$ in Hz produces an independent Rayleigh backscattered signal [4-12]. Therefore, it can be reduced by changing the optical frequency of the signal pulse during the integration of the Rayleigh backscattered signals [4-13]. This technique corresponds to the integration of the Rayleigh backscattered signals over the optical frequency domain, and we call it the optical frequency domain integration technique. In order to reduce the amplitude fluctuation effectively, an optical frequency change is required every time a signal pulse is launched.

4.3.2. Polarization dependent fluctuation reduction techniques

The state of polarization (SOP) mismatch between Rayleigh backscattered light and LO light changes the optical heterodyne detection efficiency. Since the SOP of Rayleigh backscattered light is changed by a small birefringence and mechanical vibration in the test fiber, the polarization dependent fluctuation is distributed along the test fiber and can not be reduced by temporal averaging.

A polarization scrambler randomizes the SOP of the Rayleigh backscattered signals [4-14]. Therefore, the relative SOP angle $\theta(t)$ described in Eq. (4.6) is uniformly distributed with the interval $(-\pi,\pi)$ and the probability density function is shown as Eq.(4.12). This corresponds to condition (a) in section 4.2.3. Averaging the signals with the randomized SOP can reduce the polarization dependent fluctuation. We call this the scrambling SOP technique.

When the polarization dependent fluctuation distributed along the test fiber is stable during the measurement period, it can be reduced by averaging the orthogonal SOP of the Rayleigh backscattered signals [4-13] (which we call the orthogonal SOP averaging technique). The polarization-diversity detection technique can also effectively reduce the polarization dependent fluctuation and improve the sensitivity [4-15]. The application of the orthogonal SOP averaging technique or the polarization-diversity detection technique stabilizes the optical heterodyne detection efficiency and the variable *v* described in Eq.(4.6) is constant. This corresponds to condition (b) in section 4.2.3.

4.3.3. Relative phase dependent fluctuation reduction techniques

The relative phase between the Rayleigh backscattered signal and the LO changes the heterodyne detection efficiency. The phase-diversity detection technique stabilizes the heterodyne detection efficiency and reduces the relative phase dependent fluctuation [4-16]. Therefore, the variable *w* described in Eq. (4.6) is constant. This corresponds to condition (c) in section 4.2.3. However, the relative phase dependent fluctuation is reduced by temporal averaging because the relative phase is randomized by the phase noise in the test fiber. Thus, the relative phase $\varphi(t)$ described in Eq. (4.6) is uniformly distributed with the interval $(-\pi,\pi)$ and the probability density function is shown as Eq. (4.13). This corresponds to condition (a) in section 4.2.3.

4.3.4. Amplitude fluctuation with *N* integrations

When the independent random variables of *Xi* (i=1,2,3,...,*N*) are averaged with a constant variance σ^2, the variance of the averaged variables is σ^2/N [4-10],[4-11]. Therefore, the amplitude fluctuation decreases in proportion to the inverse of the square root of the averaging number *N* of independent Rayleigh backscattered signals and the amplitude fluctuation with *N* integrations is derived from Eq. (4.5),

$$\Delta = 5\log\left(1+\frac{\sigma/m}{\sqrt{N}}\right). \text{(dB)} \qquad (4.14)$$

Table 4.1 shows the calculated amplitude fluctuation with *N* integrations when the above reduction techniques are applied. For (a), when optical frequency domain integration is applied with the scrambling SOP technique and temporal averaging, the amplitude fluctuation with *N* integrations is as shown by Eq. (4.14) at σ/m of 1.9. For (b), when optical frequency domain integration is applied with the

Table 4.1 The amplitude fluctuation with N integrations and its reduction techniques

Technique for reducing amplitude fluctuation due to interference between Rayleigh lights	Technique for reducing polarization dependent fluctuation	Technique for reducing relative phase dependent fluctuation	Calculated amplitude fluctuation with N integrations (dB)	Condition in section 4.2.3
Optical frequency domain integration $p_1(u)=\frac{u}{a^2}\exp\left(-\frac{u^2}{2a^2}\right)$	Scrambling SOP technique $v=\cos\theta(t)$ $p_2(v)=\frac{1}{\pi\sqrt{1-v^2}}$	Temporal averaging for randomized relative phase $w=\cos\varphi(t)$ $p_3(w)=\frac{1}{\pi\sqrt{1-w^2}}$	σ/m=1.9 $\Delta=5\log\left(1+\frac{1.9}{\sqrt{N}}\right)$	(a)
		Phase-diversity detection technique w=const.	σ/m=1.4 $\Delta=5\log\left(1+\frac{1.4}{\sqrt{N}}\right)$	(c)
	Polarization - diversity detection technique or Orthogonal SOP averaging technique v=const.	Temporal averaging for randomized relative phase $w=\cos\varphi(t)$ $p_3(w)=\frac{1}{\pi\sqrt{1-w^2}}$	σ/m=1.4 $\Delta=5\log\left(1+\frac{1.4}{\sqrt{N}}\right)$	(b)
		Phase-diversity detection technique w=const.	σ/m=1 $\Delta=5\log\left(1+\frac{1}{\sqrt{N}}\right)$	(d)

polarization-diversity detection technique or the orthogonal SOP averaging technique, the amplitude fluctuation is as shown by Eq. (4.14) at σ/m of 1.4. For (c), when optical frequency domain integration is used with the scrambling SOP technique and the phase-diversity detection technique, the amplitude fluctuation is as shown by Eq. (4.14) at σ/m of 1.4. For (d), when optical frequency domain integration is used with the polarization-diversity detection technique (or the orthogonal SOP averaging technique) and the phase-diversity detection technique, the amplitude fluctuation is as shown by Eq. (4.14) at σ/m of 1.

4.4. A new technique for reducing amplitude fluctuation

4.4.1. Reduction in amplitude fluctuation limited by the inclination increase caused by asynchronous optical frequency hopping

The optical frequency of a conventional DFB-LD with a narrow linewidth hops to a different frequency when the LD temperature is changed [4-13]. Therefore, the amplitude fluctuation can be reduced by changing the LD temperature during the integration of Rayleigh backscattered signals. However, this optical frequency hopping does not occur synchronously with the launch of the signal pulse. The optical frequency hopping rate r (s^{-1}) is defined as the number of optical frequency hops in a unit of time. The number N of independent backscattered signals can then be derived from Eq. (A3) in Appendix A, as follows,

$$N = N_0\left(1-\exp(-rT)\right), \tag{4.15}$$

where T is the signal pulse period and N_0 is the averaging number. Equation (4.15) shows that the independent backscattered signal number increases when the optical frequency hopping rate is increased. The amplitude fluctuation Δ is derived from Eqs. (4.14) and (4.15) as,

$$\Delta = 5\log\left(1+\frac{\sigma/m}{\sqrt{N_0\left(1-\exp(-rT)\right)}}\right). \tag{4.16}$$

Equation (4.16) shows that the amplitude fluctuation can be reduced effectively by increasing the optical frequency hopping rate.

Coherent detection also requires optical frequency stability while the test fiber is being measured. If the optical frequency of the DFB-LD hops to a different frequency during the round-trip of the Rayleigh backscattered signals returning from the far end of the test fiber, the beat signal between the Rayleigh backscattered signal and the LO

light moves out of the receiver bandwidth after the optical frequency hopping occurs, and the resulting signal power decreases. Since the probability of optical frequency hopping becomes higher as a function of the round-trip time, the signal power of the C-OTDR trace decreases gradually from the input end of the test fiber to the other end. Therefore, the inclination of the C-OTDR trace increases, which reduces the accuracy of the attenuation coefficient measurement for the test fiber. The inclination increase Δk of the C-OTDR trace is derived from Eq. (B2) in Appendix B,

$$\Delta k = 5r\frac{n}{c}\log e \text{ , (dB/m)} \tag{4.17}$$

which only depends on the optical frequency hopping rate r. Figure 4.2 shows the calculated inclination increase Δk as a function of the optical frequency hopping rate. When we define the upper limit of the optical frequency hopping r_c so that the inclination increase is less than 0.001 dB/km, $r_c = 92$ (s^{-1}). This limits the reduction in the amplitude fluctuation.

The reason for the inclination increase is that the optical frequency hopping is asynchronous with the launch of the signal pulse. In order to reduce the amplitude fluctuation effectively without an inclination increase, the optical frequency hopping must be synchronized with the launch and the optical frequency hopping rate must be increased.

4.4.2. A new source setup for stimulating synchronous optical frequency hopping

This section proposes a new technique for reducing the amplitude fluctuation in a C-OTDR trace by stimulating synchronous optical frequency hopping during an LD temperature change. Figure 4.3 shows a new source setup for stimulating the optical frequency hopping which is synchronized with the timing of the signal pulse launch by inducing an RF current pulse in the LD drive current. An RF signal of 1 MHz from a synthesizer is introduced into a gate switch driven in a pulsed mode. The RF current pulse with a pulse width of 10 μs is produced by the gate switch synchronized with a timing signal and is induced in a LD drive current by a bias-T. The 1.55 μm DFB-LD is coupled to a 1 km long optical fiber to reduce the linewidth [4-17] which, as a result, is less than 10 kHz. The LD temperature can be changed by the temperature controller. Figure 4.4 shows the optical frequency shift of the DFB-LD measured with a conventional optical spectrum analyzer as a function of the LD temperature. The optical frequency shift was about 147 GHz with an LD temperature change from 27 °C to 14 °C.

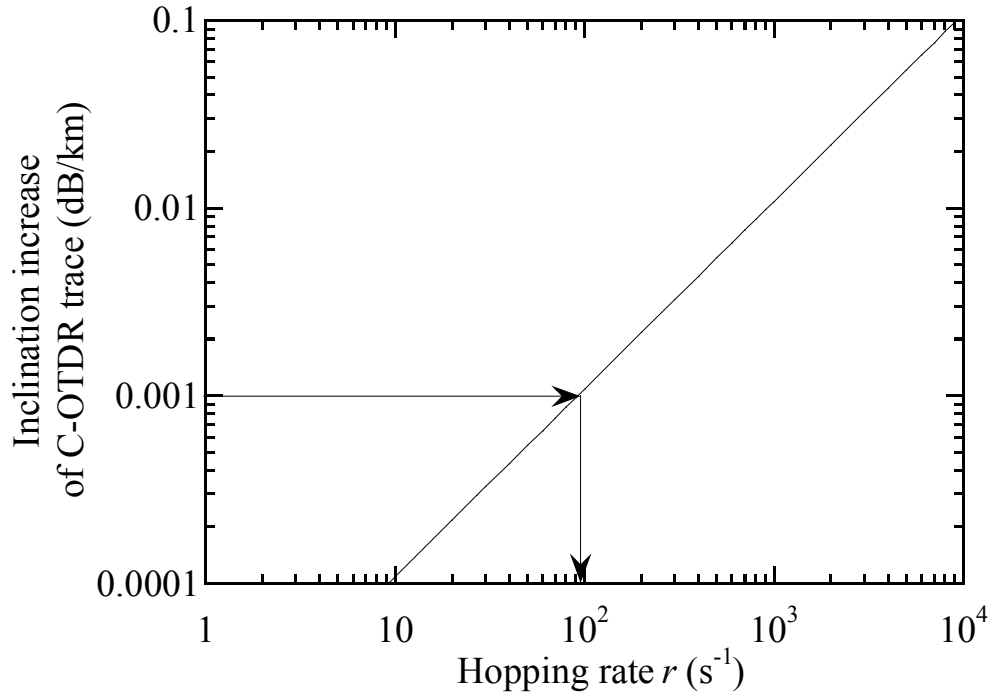

Figure 4.2 Calculated inclination increase as a function of the optical frequency hopping rate

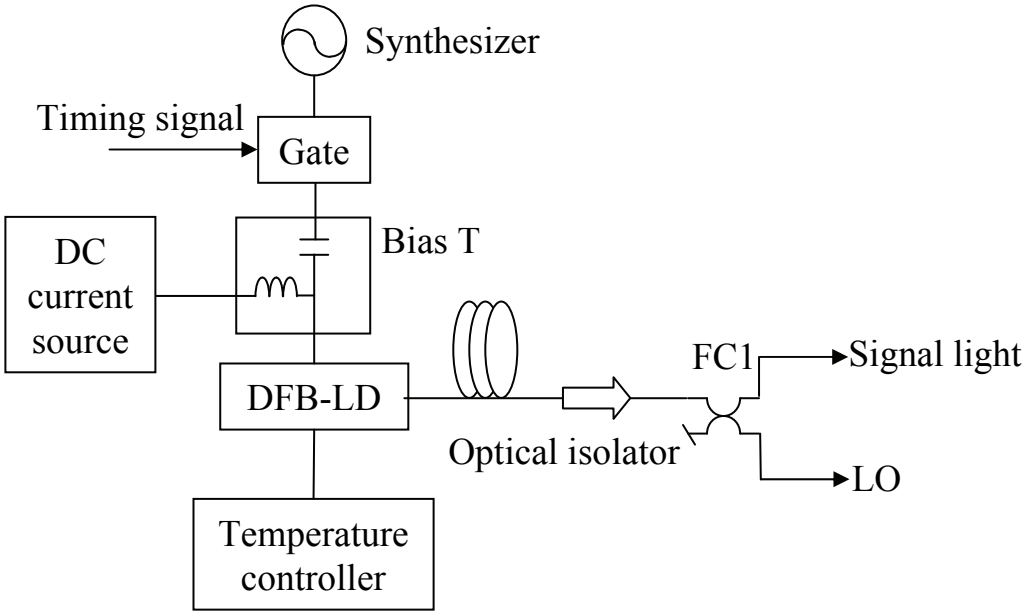

Figure 4.3 Signal source setup for stimulating synchronous optical frequency hopping

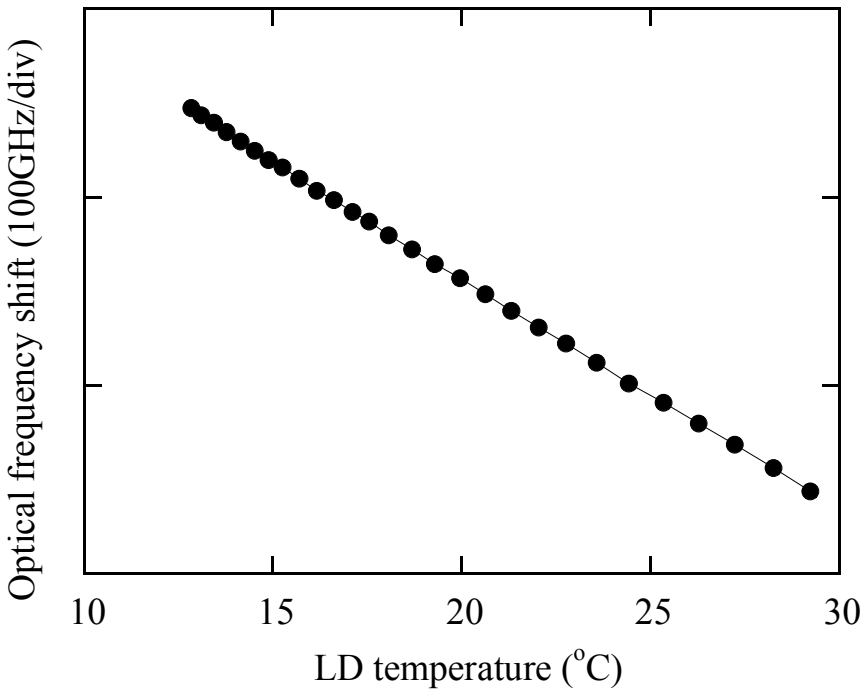

Figure 4.4 Optical frequency shift of DFB-LD as a function of LD temperature

4.4.3. Measurement of the optical frequency hopping rate

Optical frequency hopping without induced RF current pulse

Figure 4.5 shows an experimental setup for measuring the optical frequency hopping of the C-OTDR source. The CW light from the source, as shown in Fig. 4.3, is divided by FC1 into two paths: a signal path and a local oscillator (LO) path. The optical frequency of the signal light is shifted by f_a = 120 MHz at an acousto-optic modulator (AOM). The signal light is launched into a delay-line consisting of a 100-km long optical fiber. The transmitted signal light is mixed with the LO light by FC2 and detected with a double balanced p-i-n FET receiver. The detected signal is mixed with the f_L = 119.985-MHz electrical LO. A low-frequency-pass filter (LPF) with a bandwidth B of 1 MHz eliminates its high frequency part. The resulting signal with a f_b (= f_a - f_L =15 kHz) sine waveform is detected using a conventional digital sampling oscilloscope (DSO).

Figure 4.6 shows the beat signal waveforms with (a) the LD temperature stabilized at 27 °C and (b) an LD temperature change from 27 °C to 14 °C in 66 seconds without inducing RF current pulses. For (a), there was a break in the continuous beat signal waveform in the measuring period of 100 ms. The distortion of the beat signal waveform was caused by the phase noise of the signal light passing through the delay-line. For (b), when the LD temperature was changed from 27 °C to 14 °C, the optical frequency shifted by about 147 GHz. If the optical frequency shift is continuously swept in proportion to the LD temperature change, the frequency shift is 2.2 MHz/ms in this experiment and the frequency of the beat signal between the transmitted signal light and the LO light is 121.9 MHz. This means that the resulting baseband signal with a frequency of 1.9 MHz is eliminated by the LPF with a bandwidth of 1 MHz. However, in Fig. 4.6(b), three breaks were measured in the baseband beat signal. This means that the optical frequency did not change continuously and hopped to a different frequency as a result of changing the LD temperature. Simultaneous measurements were performed 100 times. The optical frequency hopping rate is defined as the mean value of the number of the optical frequency hops per unit of time. The measured optical frequency hopping rates for (a) and (b) were 10 s^{-1} and 27 s^{-1}, respectively, and these values are less than the calculated upper limit of the optical frequency hopping. Therefore, the inclination increase of the C-OTDR trace under conditions (a) and (b) is negligible.

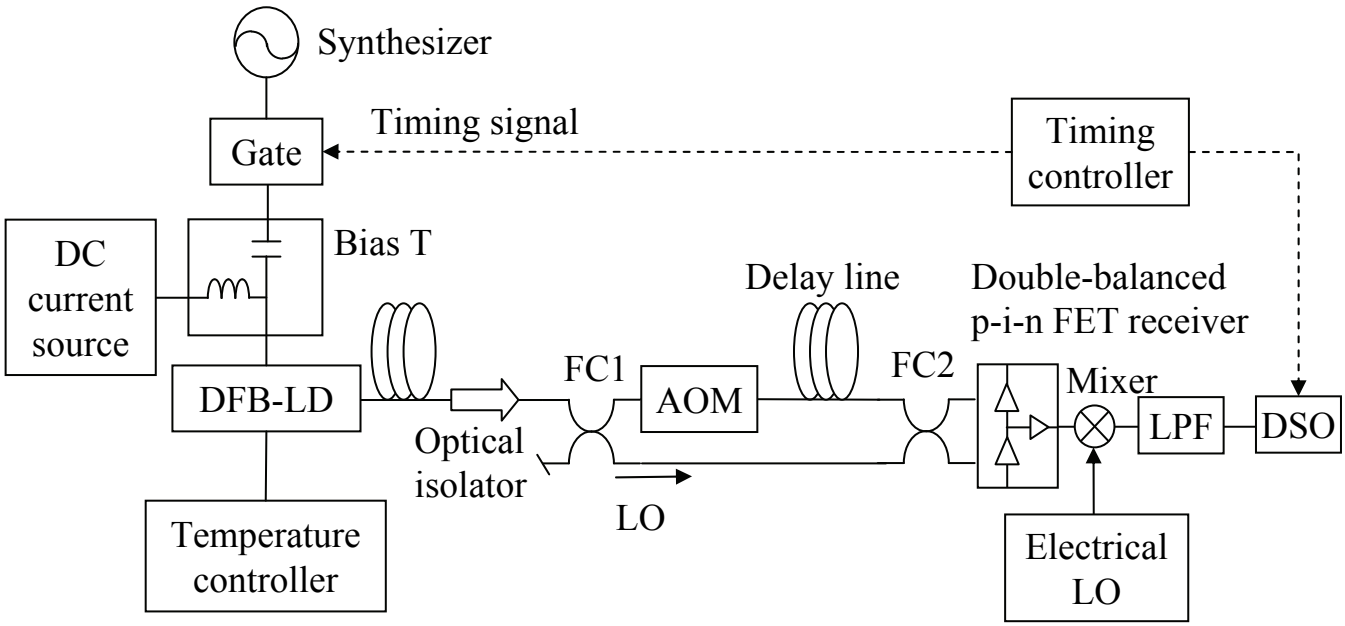

AOM: Accousto-optic modulator
DSO: Digital sampling oscilloscope

Figure 4.5 Experimental setup for measuring optical frequency hopping

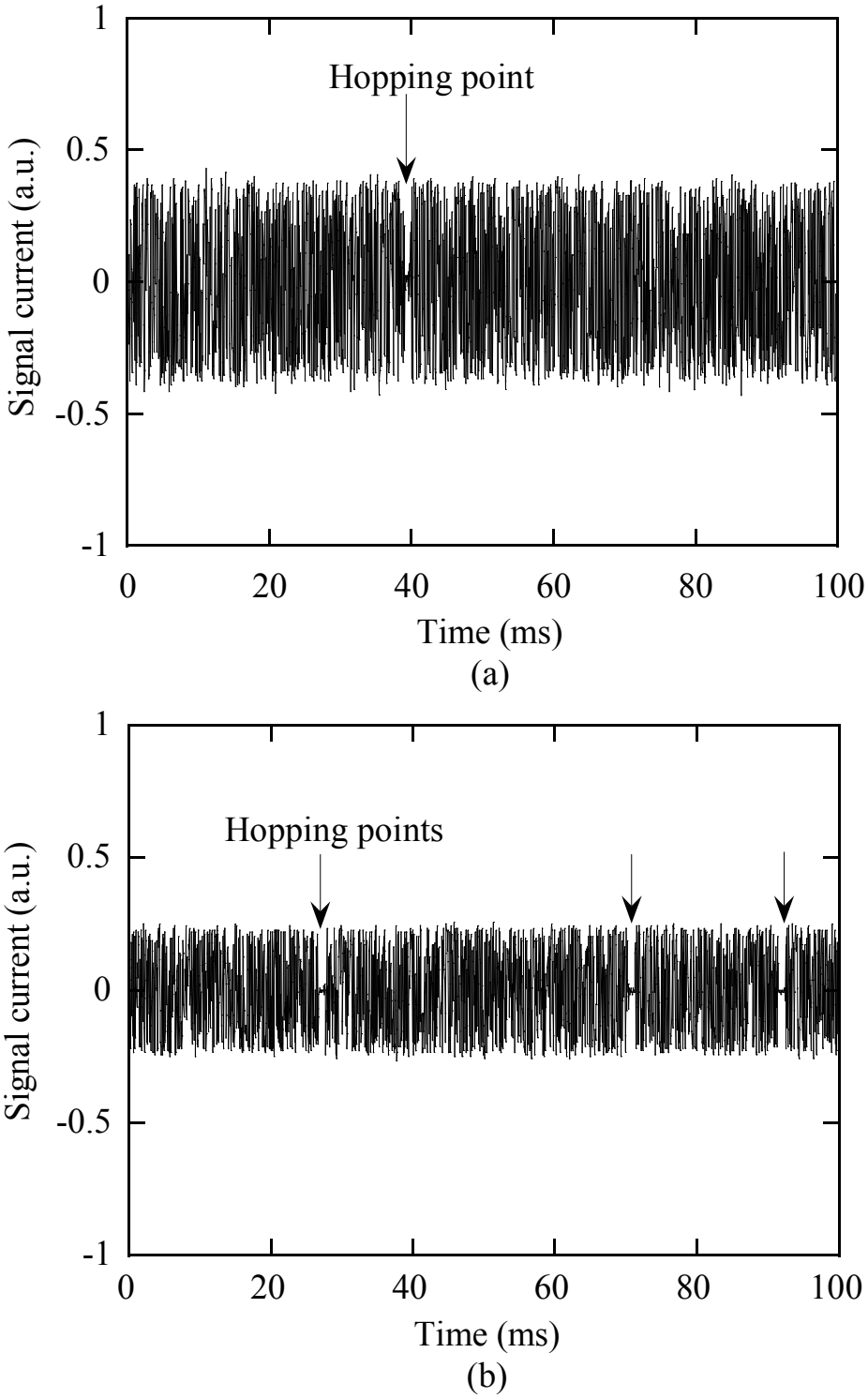

Figure 4.6 Measured beat signals
(a) with LD temperature stabilized at 27 ºC
(b) with LD temperature changed from 27 ºC to 14 ºC

Optical frequency hopping with induced RF current pulse

Figure 4.7 shows a timing chart for (a) the transmitted signal, (b) the LO light and (c) the beat signal between the transmitted signal and the LO light. The RF current pulse is induced in the LD drive current with a period of T = 1 ms. The transmitted signal (a) has a 500-μs time-delay (=0.5T) from the LO light (b). f_i (i=0,1,2,…) denotes the optical frequency from time (i-1)T to time iT. If we assume that the optical frequency f_i is sequentially changed to a different frequency every time the RF current pulse is induced and is stabilized until the next RF current pulse is induced, the frequency of the beat signal f_b changes with a period of T/2 as shown in Fig. 4.7(c). For odd numbered segments, the frequency f_b is (f_{i-1}-f_i+f_a). If the optical frequency change (f_{i-1}-f_i) is greater than the bandwidth B, the baseband beat signal moves outside the bandwidth and the signal does not appear. Therefore, the disappearance of the baseband beat signal means that optical frequency hopping occurs. For even numbered segments, the frequency of the baseband beat signal is f_a. If the optical frequency of the source is unchanged until the next RF current pulse is induced, the baseband beat signal appears. Otherwise, the optical frequency of the source is unstable.

Figure 4.8 shows the measured baseband beat signal with a bandwidth of B = 1 MHz. The amplitude, pulse width and frequency of the induced RF current pulse were 27.5 mA, 10 μs and 1 MHz, respectively. The DC bias I_{DC} was 50 mA and the DFB-LD threshold current I_{th} was 20 mA.

The 15 kHz beat signals with a beat length of 450 μs appeared in the 2nd and 4th segments, which means that the optical frequency was unchanged until the next RF current pulse was induced. The beat length was found to be less than the delay-time by about 50 μs because the induced RF current pulse generated unstable regions. The beat signal did not appear for the 1st, 3rd and 5th segments. This means that the optical frequency hopped to a different frequency by more than the bandwidth of 1 MHz every time an RF current pulse was induced with a pulse period of 1 ms.

In order to clarify the dependence of the optical frequency hopping on the amplitude of the RF current pulse, the experiment shown in Fig. 4.8 was performed 100 times and we measured the probability of the optical frequency hopping in odd numbered segments. Figure 4.9 shows the measured probability of the optical frequency hopping as a function of the RF modulation degree of m, where m is $I_{RF}/(I_{DC}-I_{th})$, I_{RF} is the amplitude of the RF current pulse, I_{DC} is the DC bias and I_{th} is the threshold current of the DFB-LD. For (a) where the LD temperature is stabilized at 27 °C and (b) where the LD temperature change is from 27 °C to 14 °C, the probability of optical frequency hopping in the expected region (odd numbered segments) gradually saturated at 0.4

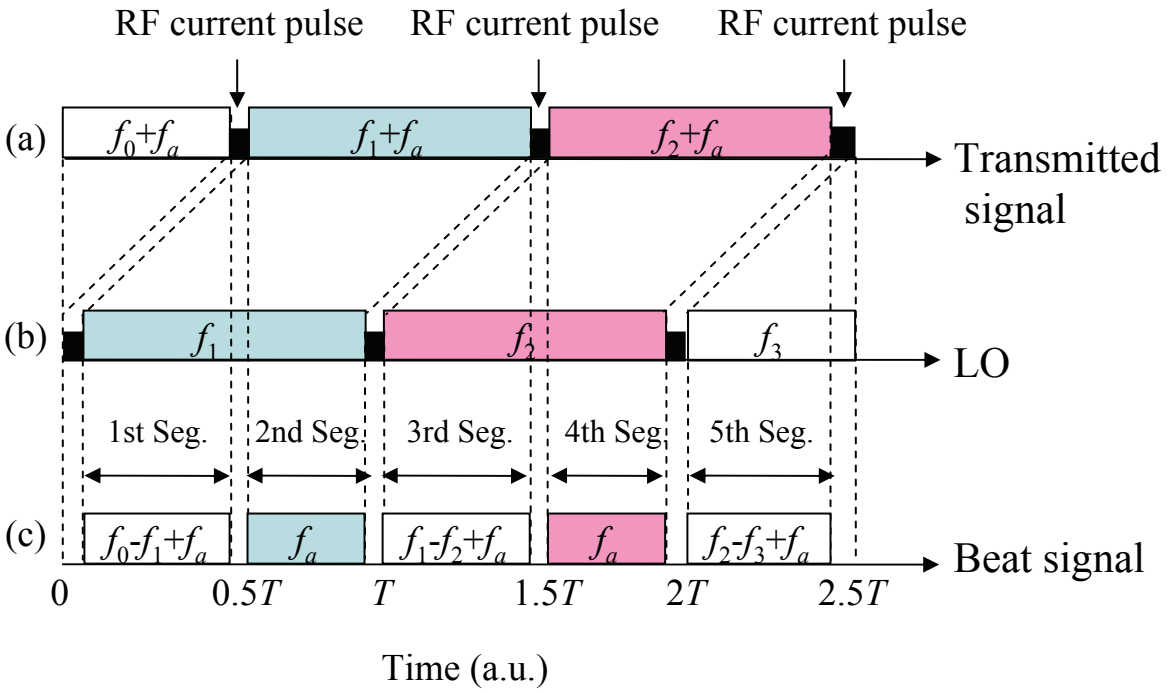

Figure 4.7 Timing chart for (a) transmitted signal, (b) LO light and (c) beat signal

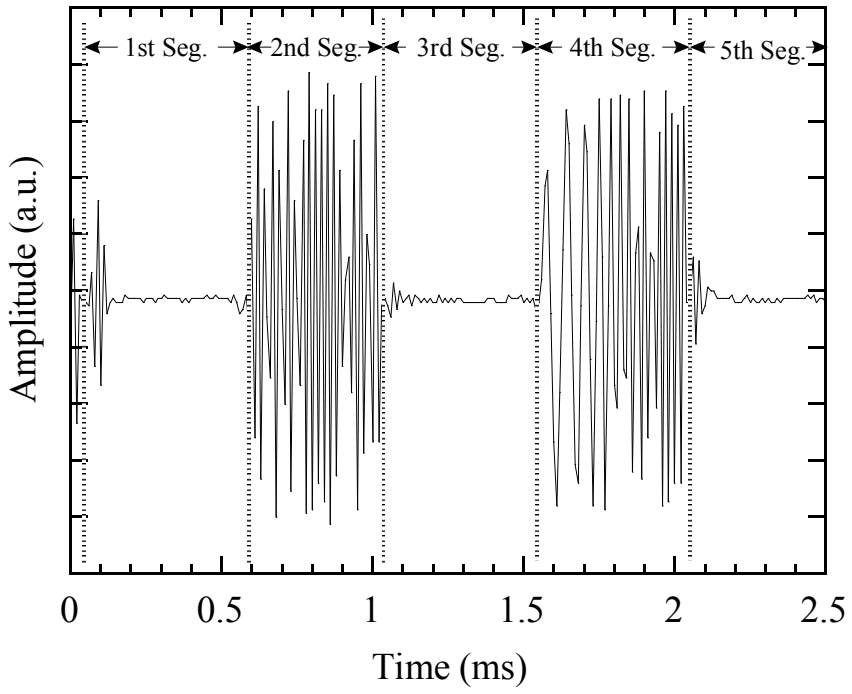

Figure 4.8 Measured beat signals with a bandwidth of 1 MHz

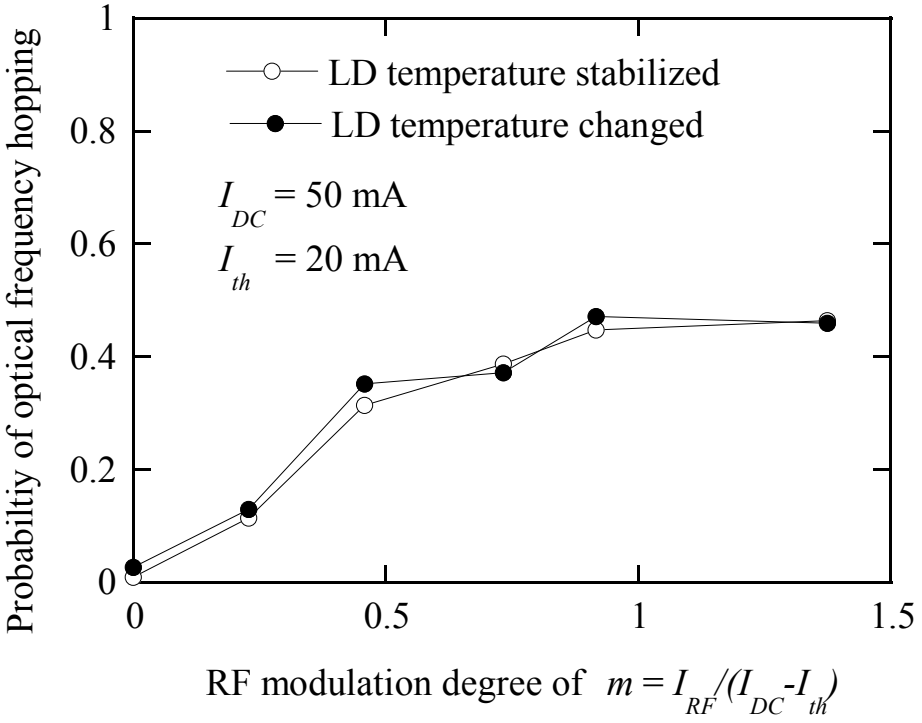

Figure 4.9 Probability of optical frequency hopping vs. RF modulation degree of *m*
(a) with LD temperature stabilized at 27 ºC
(b) with LD temperature changed from 27 ºC to 14 ºC

around the RF modulation degree of m =1. The optical frequency hopping in the unexpected region (even numbered segments) increased slightly. However, it is negligible for an RF modulation degree of $m < 1$. The probability 0.4 in 1 ms at m = 0.92 corresponds to an optical frequency hopping rate of 511 s^{-1} from Eq. (4.15), which was more than 20 times greater than that when no RF current pulse was induced as shown in the previous subsection. This experiment revealed that inducing an RF current pulse is effective for stimulating optical frequency hopping synchronized with the timing of a signal pulse launch.

4.4.4. Unstable optical frequency region caused by induced RF current pulse

Measurements were performed using the C-OTDR with the source shown in Fig. 4.3, and by inducing an RF current pulse synchronized with the timing signal and changing the LD temperature. Figure 4.10 shows the C-OTDR trace for a 10 km test fiber with 2^{10} integrations. The RF modulation degree was m = 0.92 and the LD temperature was changed from 27 °C to 14 °C. Ghost signals were found at (a) and (b). The (a) region was produced by the RF modulation. The signals in region (b) are believed to be chirped LO light multi-reflected within the receiver or between the receiver and the FCs. The existence of the unstable region agreed with the fact that the beat length was shortened by about 50 μs as shown in Fig. 4.8. In order to avoid this unstable region, the signal pulse was produced by an AO-SW driven with a delay of 200 μs in relation to the timing of the induced RF current pulse. Therefore, a conventional C-OTDR trace can be found in the time region with a 200 μs delay in relation to the unstable region.

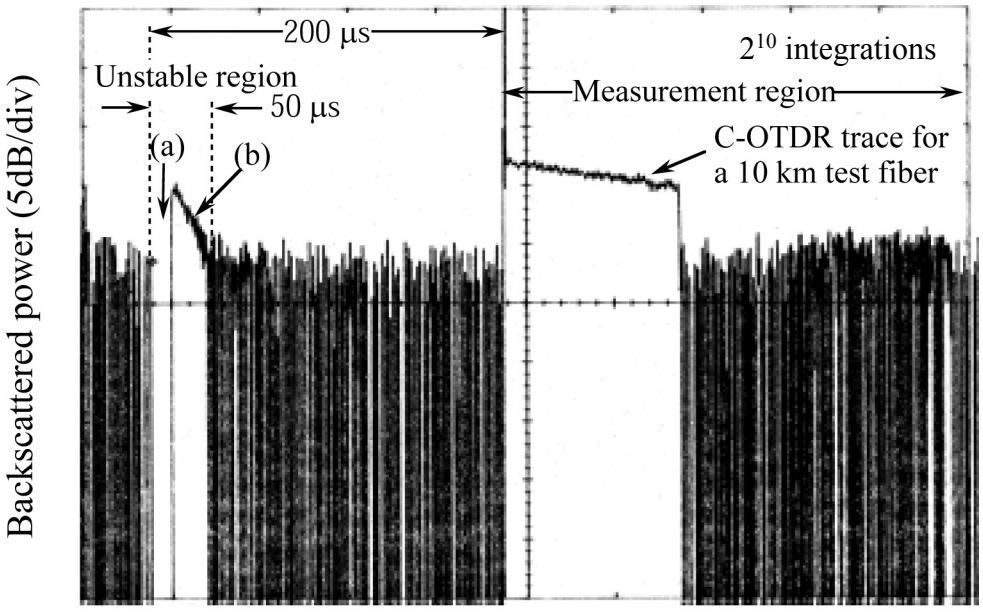

Figure 4.10 Measured unstable region in C-OTDR trace

4.5. Measurements of the amplitude fluctuation in the C-OTDR trace

In order to estimate the reduction in the amplitude fluctuation with C-OTDR employing the source as shown in Fig. 4.3 for signal pulse widths of 1 μs, 100 ns and 30 ns, we undertook measurements under the following conditions, (a) with the LD temperature stabilized at 27 °C, (b) with the LD temperature changed from 27 °C to 14 °C, (c) with the LD temperature stabilized at 27 °C and an induced RF current pulse and (d) with the LD temperature changed from 27 °C to 14 °C and an induced RF current pulse. The pulse width of the RF current pulse was 10 μs and the RF modulation degree was 0.92. The signal pulse period T was 1 ms. The averaging times N_0 was 2^{16}. The test fiber was a 10 km long dispersion-shifted optical fiber with an attenuation coefficient of 0.21 dB/km. In this experiment, the amplitude fluctuation of the C-OTDR trace was defined as the root mean square (rms) of the difference between the linear regression line and the measured data.

Figure 4.11 shows the measured C-OTDR traces for a 1-μs pulse width. For (a), the optical frequency hopping rate was 10 s^{-1} and the amplitude fluctuation was 0.20 dB. For (b), the optical frequency hopping rate was 27 s^{-1} and the amplitude fluctuation was 0.08 dB. For (c) and (d), the probability of the optical frequency hopping was 0.4. This corresponds to an optical frequency hopping rate of 511 s^{-1}, which is over the optical frequency hopping rate limit of 92 s^{-1}. However, the increase in the inclination of the C-OTDR trace due to the optical frequency hopping was negligible because the hopping was synchronized with the timing of the signal pulse launch and the optical frequency was stable until the next signal pulse was launched. The amplitude fluctuations for (c) and (d) were 0.12 dB and 0.03 dB, respectively. Although the probability of the optical frequency hopping for (c) was the same as that for (d), the amplitude fluctuation for (c) was not reduced to be as much as that for (d). This is believed to be because the optical frequency hopping occurs within a narrow frequency range and the number of the independent backscattered signals does not increase. For (d), however, the optical frequency of the signal pulse hops more than 1 MHz when an RF current pulse is induced during the LD temperature change and the number of independent backscattered signals increased. Therefore, the amplitude fluctuation in the C-OTDR trace was reduced effectively by the synchronous optical frequency hopping technique.

Figure 4.12 shows C-OTDR traces for a 100-ns pulse width. The measured amplitude fluctuations for (a) - (d) were 0.43 dB, 0.09 dB, 0.24 dB and 0.04 dB, respectively. For (d), the probability of the optical frequency hopping by more than 10

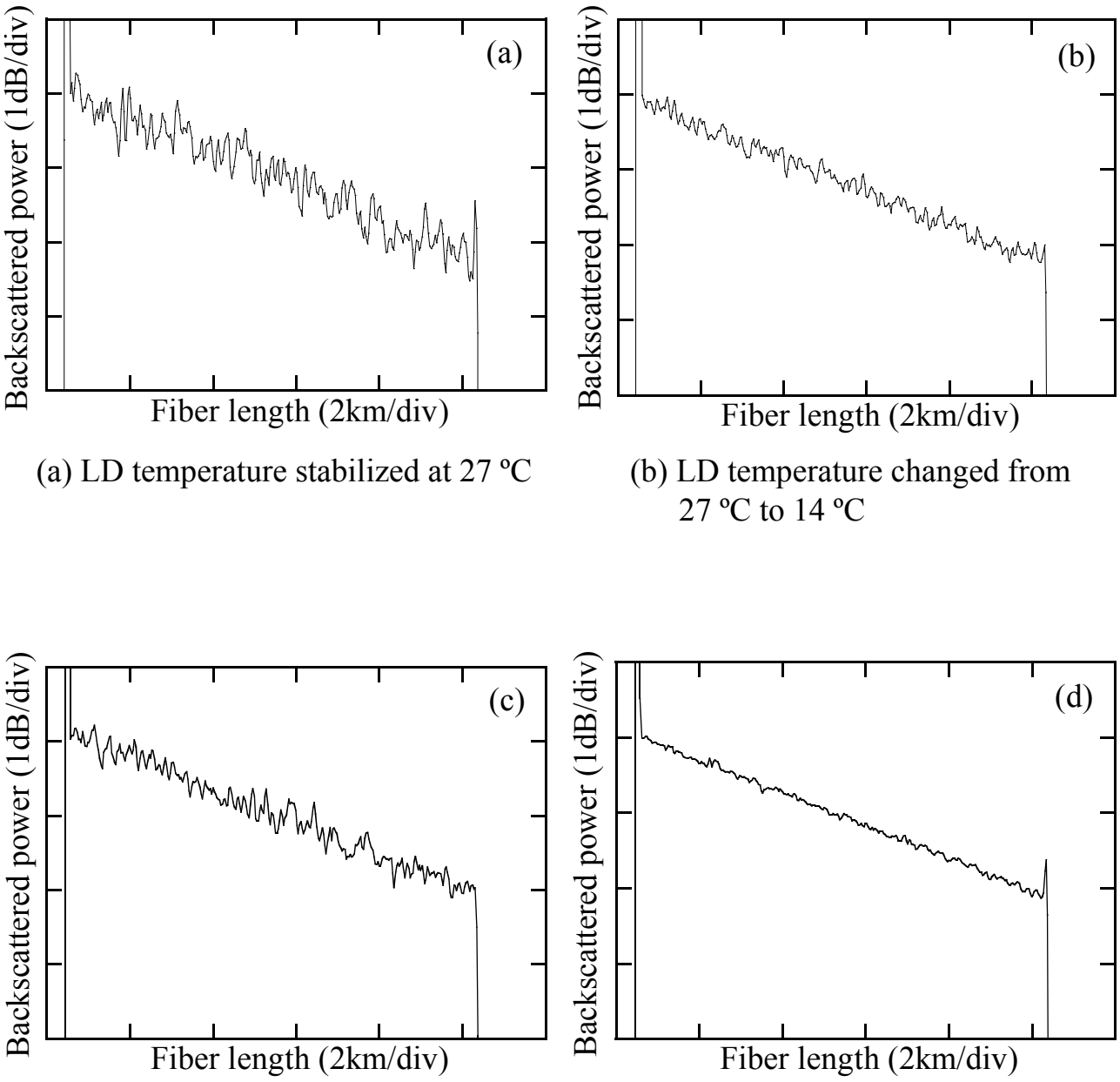

(a) LD temperature stabilized at 27 ºC

(b) LD temperature changed from 27 ºC to 14 ºC

(c) Stabilized LD temperature and induced RF current pulse

(d) LD temperature changed from 27 ºC to 14 ºC and induced RF current pulse

Figure 4.11 C-OTDR traces for 1 μs pulse width
(a) with LD temperature stabilized at 27 ºC
(b) with LD temperature changed from 27 ºC to 14 ºC
(c) with stabilized LD temperature and induced RF current pulse
(d) with LD temperature changed from 27 ºC to 14 ºC and induced RF current pulse

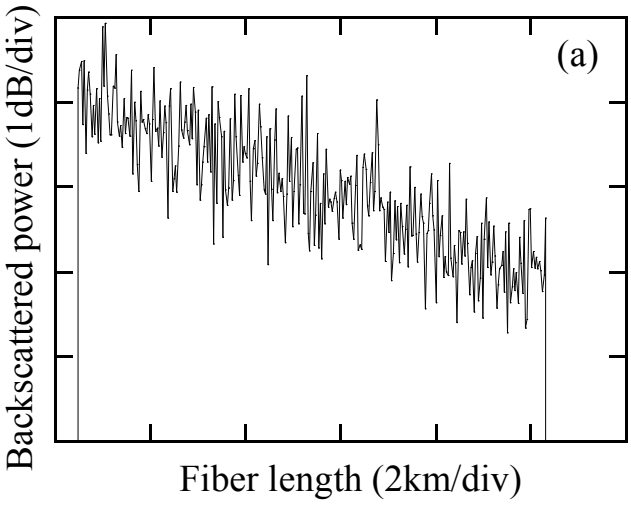

(a) LD temperature stabilized at 27 ºC

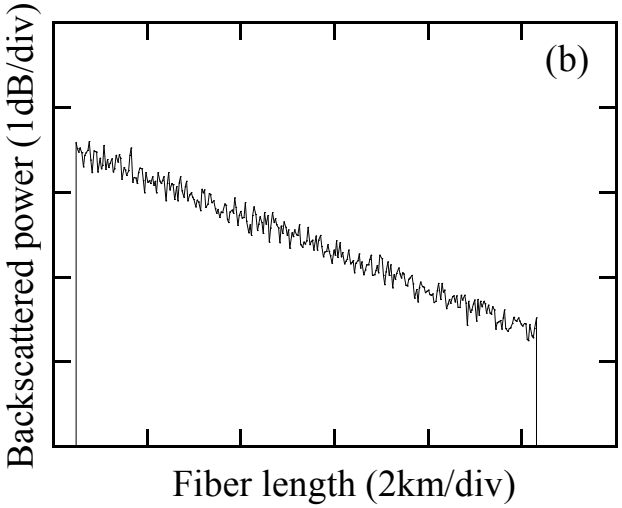

(b) LD temperature changed from 27 ºC to 14 ºC

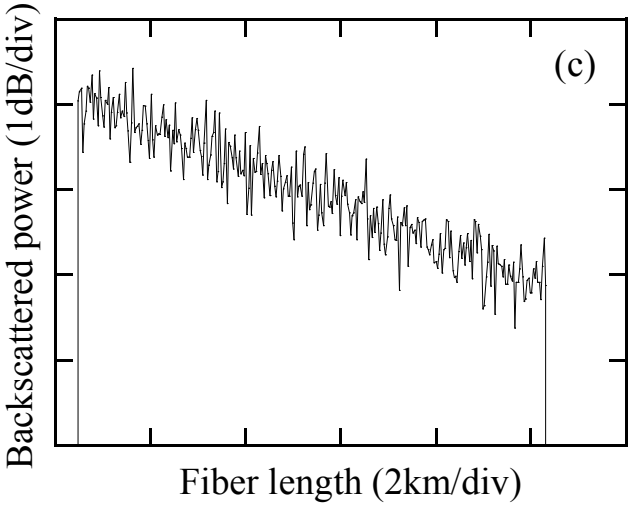

(c) Stabilized LD temperature and induced RF current pulse

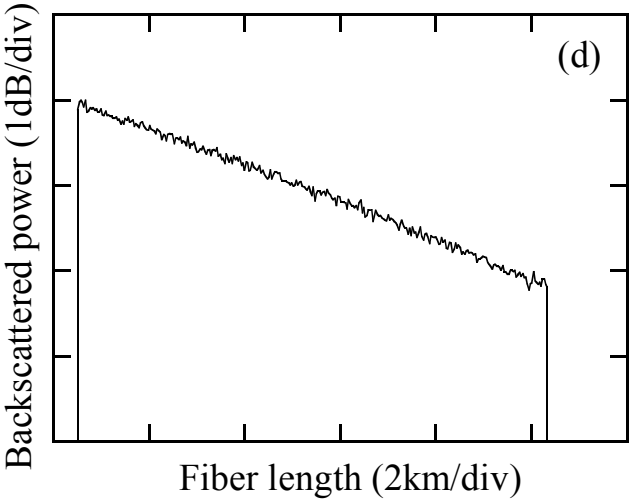

(d) LD temperature changed from 27 ºC to 14 ºC and induced RF current pulse

Figure 4.12 C-OTDR traces for 100 ns pulse width
(a) with LD temperature stabilized at 27 ºC
(b) with LD temperature changed from 27 ºC to 14 ºC
(c) with stabilized LD temperature and induced RF current pulse
(d) with LD temperature changed from 27 ºC to 14 ºC and induced RF current pulse

MHz was about 0.3 measured with the measurement setup shown in Fig. 4.5 with an LPF bandwidth of 10 MHz. This corresponds to an optical frequency hopping rate of 357 s^{-1}. The measured inclination increases for (a) - (d) were negligible.

Figure 4.13 shows C-OTDR traces for a 30-ns pulse width. The measured amplitude fluctuations for (a) - (d) were 0.59 dB, 0.09 dB, 0.44 dB and 0.05 dB, respectively. For (d), the measured probability of the optical frequency hopping by more than 33 MHz was about 0.2. This corresponds to an optical frequency hopping rate of 223 s^{-1}. The measured inclination increases for (a) - (d) were also negligible.

Figure 4.14 shows the calculated amplitude fluctuation with T =1 ms and $N_0 = 2^{16}$ as a function of the optical frequency hopping rate. Since the test fiber was wound around a bobbin with a radius of 30 cm, the polarization-dependent fluctuation was averaged for the pulse width in this experiment and was negligible. Therefore, in the calculation, σ/m was set at 1.4 as described in section 4.3.2. The measured amplitude fluctuations with a pulse width of 1 μs, 100 ns and 30 ns were also plotted.

For (a), the measured amplitude fluctuations were larger than the calculated values. This was because the averaging number of the independent backscattered signal is small since the optical frequency hopping occurred in a narrow frequency range. Optical frequency hopping over a wide frequency range is required in order to reduce the amplitude fluctuation by averaging the independent Rayleigh backscattered signals. This requirement is more severe when the pulse width is shorter. For (b), the amplitude fluctuations for pulse widths of 1 μs, 100 ns and 30 ns were reduced and were good agreement with the calculated values. For (c) and (d), the probability of optical frequency hopping is defined by N/N_0 and the optical frequency hopping rate is calculated by using Eq. (4.15) , with T = 1 ms. The amplitude fluctuation for (c) was not reduced due to the narrow-range optical frequency hopping such as that for (a). For (d), the calculated optical frequency hopping increased 20 times more than that for (a). The measured amplitude fluctuation for a 1-μs pulse width was reduced to 1/7 that for (a). With a pulse width of 100 ns and 30 ns, it was reduced to 1/11 of that for (a).

This section has demonstrated experimentally that the proposed technique of inducing an RF current pulse during an LD temperature change stimulates optical frequency hopping synchronized with the timing of the signal pulse launch and reduces amplitude fluctuation effectively without any inclination increase which reduces the accuracy when measuring the attenuation in a test fiber.

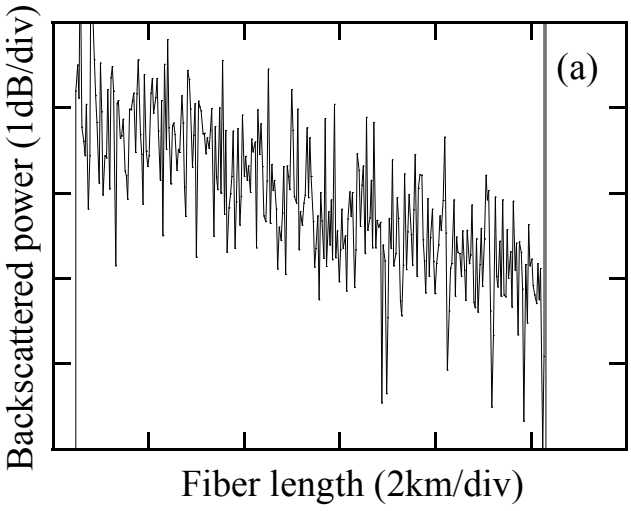

(a) LD temperature stabilized at 27 ºC

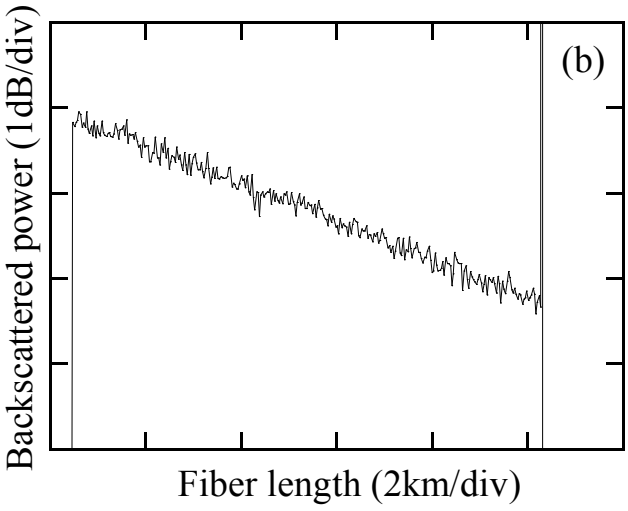

(b) LD temperature changed from 27 ºC to 14 ºC

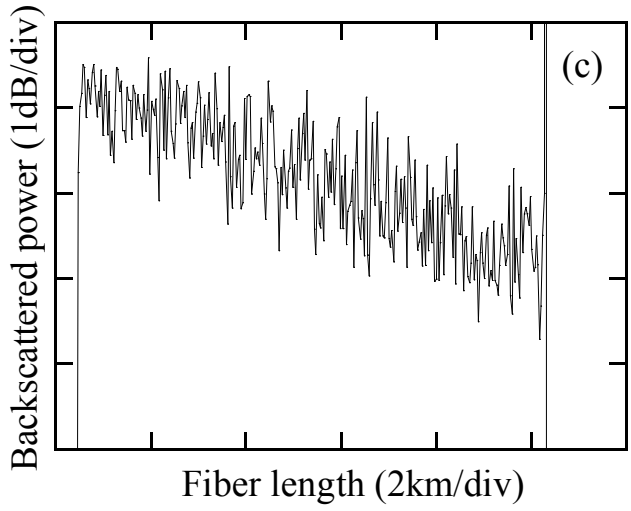

(c) Stabilized LD temperature and induced RF current pulse

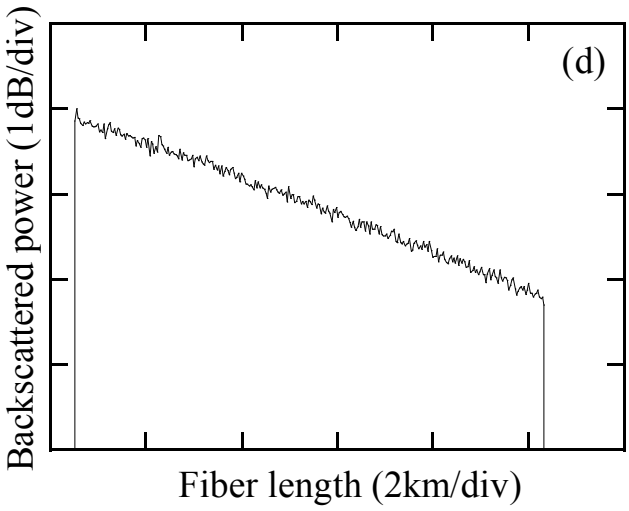

(d) LD temperature changed from 27 ºC to 14 ºC and induced RF current pulse

Figure 4.13 C-OTDR traces for 30 ns pulse width
(a) with LD temperature stabilized at 27 ºC
(b) with LD temperature changed from 27 ºC to 14 ºC
(c) with stabilized LD temperature and induced RF current pulse
(d) with LD temperature changed from 27 ºC to 14 ºC and induced RF current pulse

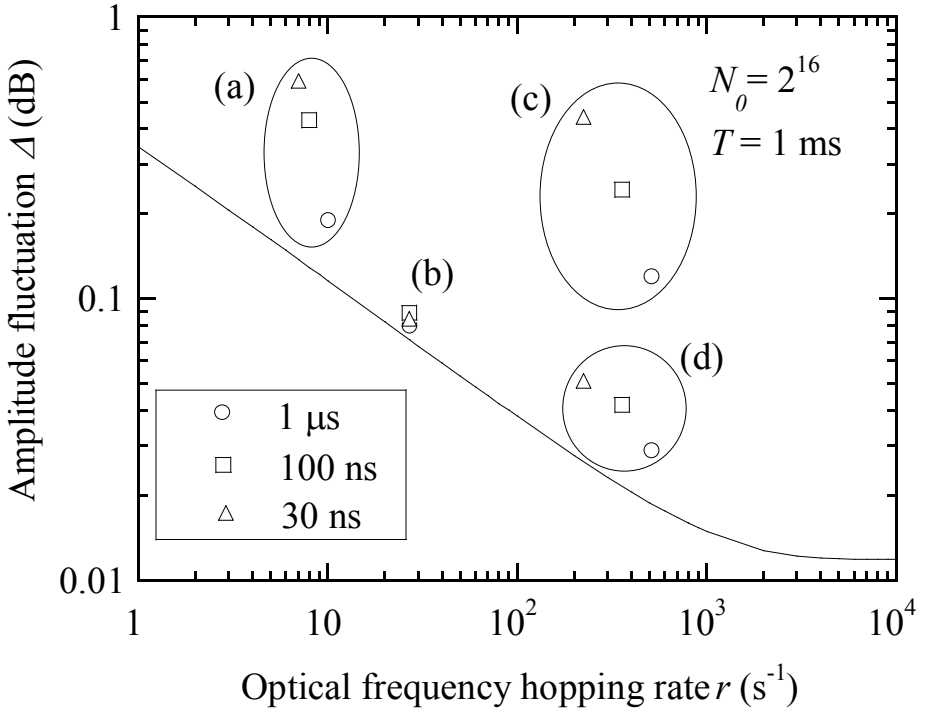

Figure 4.14 Amplitude fluctuation in C-OTDR as a function of optical frequency hopping rate.

Solid line is calculated amplitude fluctuation (σ/m = 1.4)
(a) with LD temperature stabilized at 27 ºC
(b) with LD temperature changed from 27 ºC to 14 ºC
(c) with stabilized LD temperature and induced RF current pulse
(d) with LD temperature changed from 27 ºC to 14 ºC and induced RF current pulse

4.6. Conclusions

The amplitude fluctuation in a C-OTDR trace has been described with the probability density functions for each of the factors which cause the fluctuation and was estimated theoretically when reduction techniques were applied. It was thus found theoretically that an optical frequency domain integration technique which uses the asynchronous optical frequency hopping of the source can reduce the amplitude fluctuation but leads to an increase in the inclination of the C-OTDR trace, which reduces the measurement accuracy.

Therefore, this chapter proposed a new reduction technique in which an RF current pulse is induced in the drive current of an LD during an LD temperature change. This stimulates the optical frequency hopping synchronized with the timing of the launch of the signal pulse and increases the number of independent Rayleigh backscattered signals. The technique was found experimentally to reduce the amplitude fluctuation without increasing the inclination of the C-OTDR trace. The amplitude fluctuation for a 1-μs pulse width was reduced to 0.03 dB, which was about 1/7 of that with the LD temperature stabilized. For 100-ns and 30-ns pulse widths, the fluctuations were reduced to 0.04 dB and 0.05 dB, respectively, which were about 1/11 of those with the LD temperature stabilized.

Appendices

A. Relationship between optical frequency hopping rate and number of independent Rayleigh backscattered signals

It is assumed that optical frequency hopping changes the optical frequency by more than the receiver bandwidth and gives rise to independent Rayleigh backscattered signals before and after the optical frequency hopping. The optical frequency hopping rate r (s^{-1}) is defined as the mean value of the number of optical frequency hops per unit of time, obtained from a sufficiently large number of measurements.

The optical frequency of the source must be stabilized during the round-trip of the signal pulse when measuring a test fiber by C-OTDR. $P_r(t)$ is the probability function where the optical frequency is stabilized during the delay time t after launching the signal pulse into the test fiber. Then, the number N of independent Rayleigh backscattered signals is derived as,

$$N = N_0\left(1 - P_r(T)\right), \tag{A1}$$

where N_0 is the averaging number of the Rayleigh backscattered signals and T is the signal pulse period.

Next, the probability $P_r(t)$ is determined. The probability at an incremental interval dt passed time t is $P_r(t+dt)$ and decreases by $r \cdot P_r(t) \cdot dt$ due to the optical frequency hopping during the interval dt. Hence, the probability $P_r(t+dt)$ at time $t+dt$ is shown as

$$P_r(t+dt) = P_r(t) - rP_r(t)dt .$$

Therefore, the differential equation is derived as

$$\frac{dP_r(t)}{dt} = -rP_r(t).$$

The solution with the initial condition $P_r(0)=1$ is shown as

$$P_r(t) = \exp(-rt) . \tag{A2}$$

From Eqs. (A1) and (A2), the number of independent Rayleigh backscattered signals is

$$N = N_0\left(1 - \exp(-rT)\right). \tag{A3}$$

B. Inclination increase in C-OTDR trace as a function of the optical frequency hopping rate

When there is no optical frequency hopping during the delay time t_e corresponding to the round-trip time of the Rayleigh backscattered signal returning from the far end of the test fiber, the probability, by which the Rayleigh backscattered signal is detected in C-OTDR, is described by $P_r(t_e)$ which is derived in Appendix A. Let the test fiber length to be L, then the delay time t_e is $2nL/c$, where n is the refractive index of the test fiber and c is the velocity of light in a vacuum.

When the Rayleigh backscattered signals are averaged, the signal-to-noise ratio of the C-OTDR is improved by $5\log\sqrt{N_0}$ in dB where N_0 is the number of averaged Rayleigh backscattered signals. If the optical frequency hopping occurs during the delay time, the Rayleigh backscattered signal after the hopping can not be detected and the signal power decreases. Therefore, the signal-to-noise ratio improvement ratio (SNIR) at the far end of the test fiber in the C-OTDR trace decreases by the amount $5\log\sqrt{N_0} - 5\log\sqrt{N_0 P_r(t_e)}$ in dB. The decrease in the SNIR causes to an inclination increase in the C-OTDR trace. This increase Δk is shown by

$$\Delta k = \frac{5\log\left(\sqrt{P_r(t_e)}\right)}{L} \text{ (dB/m) .} \tag{B1}$$

From Eqs. (A2) and (B1), the inclination increase Δk is derived as

$$\Delta k = 5r\frac{n}{c}\log e \text{ (dB/m),} \tag{B2}$$

which is proportional to the optical frequency hopping rate r.

4.7. References

[4-1] M. Tateda and T. Horiguchi, "Advances in optical time-domain reflectometry," IEEE J. Lightwave Technol. vol. LT-7, no.8, pp.1217-1224, 1989.

[4-2] P. Healey and D. J. Malyon, "OTDR in single-mode fiber at 1.5 μm using heterodyne detection," Electron. Lett., vol. 18, no. 12, pp. 862-863, 1982.

[4-3] Y. Koyamada and H. Nakamoto, "High performance single mode OTDR using coherent detection and fibre amplifiers," Electron. Lett., vol. 26, no. 9 pp. 573 - 574, 1990.

[4-4] S. Furukawa, H. Izumita, I. Sankawa, and Y. Koyamada, "High dynamic range, low fading noise coherent OTDR using erbium fiber amplification and LD temperature changing techniques," in the proc. of ECOC'91/IOOC'91, Mo.C1-3, pp. 81-84, 1991.

[4-5] Y. Koyamada, H. Nakamoto, and N. Ohta, "High performance coherent OTDR enhanced with erbium doped fiber amplifiers," J. Opt. Commun., vol. 13, no. 4, pp. 127-133, 1992.

[4-6] H. Izumita, Y. Koyamada, S. Furukawa, and I. Sankawa, "The performance limit of coherent OTDR enhanced with optical fiber amplifiers due to optical nonlinear phenomena," IEEE J. Lightwave Technol., vol. 12, no. 7, pp. 1230-1238, 1994.

[4-7] H. Izumita, Y. Koyamada, I. Sankawa, and S. Furukawa, "A coherent optical time-domain reflectometer with a 40-dB dynamic range enhanced with erbium-doped fiber amplifiers," in the technical digest of OFC'92, WK6, p. 147, 1992.

[4-8] P. Healey, "Fading in heterodyne OTDR," Electron. Lett., vol. 20, no. 1, pp. 30 - 32, 1984.

[4-9] J. King, D. F. Smith, K. Richards, P. Timson, R. E. Epworth, and S. Wright, "Development of coherent OTDR instrument," IEEE J. Lightwave Technol., vol. LT-5, no. 4, pp. 616-624, 1987.

[4-10] A. Papoulis, "Probability, Random Variables, and Stochastic Processes," 1984, McGraw-Hill, Inc.

[4-11] J. S. Bendat and A. G. Piersol, "RANDOM DATA: Analysis and Measurement Procedures," 1971, Johm Wiley & Sons, Inc.

[4-12] K. Shimizu, T. Horiguchi and Y. Koyamada, "Characteristics and reduction of coherent fading noise in Rayleigh backscattering measurement for optical fiber and components," IEEE J. Lightwave Technol., vol. LT-10, no. 7, pp. 982 -

987, 1992.

[4-13] H. Izumita, S. Furukawa, Y. Koyamada, and I. Sankawa, "Fading Noise Reduction in Coherent OTDR," IEEE Photon. Technol. Lett., vol. 4, no. 2, pp. 201-203, 1992.

[4-14] E. Brinkmeyer and J. Strecker, "Reduction of polarization sensitivity of optical time-domain reflectometers for single-mode fibers," IEEE J. Lightwave Technol., vol. LT-4, no. 5, pp. 513 - 515, 1986.

[4-15] T. Imai, T. Matsumoto and K. Iwashita, "Polarization diversity technique for coherent optical detection," in the proc. of OFS'86, P-4, pp. 274-276, 1986.

[4-16] G. Hodgkinson, R.A. Harmon and D. W. Smith, "Demodulation of optical DPSK using in-phase and quadrature detection," Electron. Lett., vol. 21, no. 19, pp. 867-868,1985.

[4-17] J. Mark, E. Bodtker and B. Tromborg, "Measurement of Rayleigh backscatter-induced linewidth reduction," Electron. Lett., vol. 21, no. 22, pp. 1008-1009, 1985.

Chapter 5. Applications: Enhanced C-OTDR for long span optical transmission lines containing optical fiber amplifiers

High performance coherent-detection optical time-domain reflectometry (C-OTDR), described in chapters 3 and 4, can be applied to monitor long-haul optical transmission lines containing (a) in-line amplifiers as 1R repeaters and (b) a distributed Raman amplifier (DRA). This chapter describes implementation of C-OTDR, which is based on delayed self-heterodyne detection using acousto-optic (AO) switches, for use in testing optical fiber cable spans in transmission lines containing optical fiber amplifiers.

5.1. Introduction

Optical transmission systems containing erbium-doped fiber amplifiers (EDFA) have been developed for use in long-haul submarine cable transmission systems [5-1]-[5-5]. A fault location technique using optical time-domain reflectometry (OTDR) was investigated for use in these systems in which an optical backscattering path is employed between optical pair lines in a repeater in order to detect backscattered light beyond the repeaters [5-6]-[5-7]. This was performed with coherent-detection OTDR (C-OTDR) using frequency-shift-keying (FSK) probe light generated by a distributed Bragg reflector (DBR) laser diode with a line width of 5 MHz [5-6]-[5-7] and conventional OTDR [5-8]. Since these OTDR had small dynamic ranges, the maximum measurable fiber span was only about 40 km. To measure a fiber span of 100 km, it is necessary to increase the dynamic range of the OTDR.

As described in chapters 3 and 4, the advanced C-OTDR employing delayed self-heterodyne detection using acousto-optic (AO) switches and EDFAs had a single-way dynamic range (SWDR) of 48 dB with a pulse width of 10 μs, and the fading noise on the C-OTDR trace was greatly reduced. These results make C-OTDR an attractive way to monitor optical transmission systems containing optical fiber amplifiers as 1R repeaters. When launching an OTDR pulse with low pulse repetition into an optical transmission line containing EDFAs optimized in continuous wave (CW) gain mode, the leading edge intensity of the OTDR pulse increases with every pass through a repeater. This optical surge, caused by the accumulated difference between the pulse gain and CW gain of the EDFAs, breaks the feedback circuits in the repeaters. To keep the probe power from the C-OTDR as uniform as possible and to avoid any optical surges, C-OTDR multiplexing of dummy light is proposed in section

5.2. This section also describes the performance and feasibility of enhanced C-OTDR for application to monitoring optical fiber cable spans in transmission systems containing repeaters based on EDFAs.

In the 2000s, the number of broadband services users in Japan has increased rapidly [5-9] and exceeded 28 million by the end of September, 2007, including over 10 million fiber to the home (FTTH) service users [5-10]. The demand for trunk line communications will rapidly increase. Using a WDM repeaterless transmission system with a distributed Raman amplifier (DRA) and remotely pumped EDFAs is a cost effective way of meeting this demand [5-11]-[5-13]. In order to design the WDM transmission system and support long-haul fiber lines through preventive maintenance, we will require high performance fiber measurement techniques. The C-OTDR with EDFAs is a promising approach for increasing the SWDR, as described in chapter 3. This C-OTDR has narrowband filtering characteristics and eliminates amplified spontaneous emission (ASE) noise from the DRA and EDFA, which would otherwise reduce the dynamic range.

Section 5.3 describes a highly developed C-OTDR with low fading noise and demonstrates measurement, from the end of a test fiber, of a 340-km optical fiber line with a remotely pumped EDFA and a DRA.

5.2. Monitoring long-haul optical transmission lines containing in-line amplifiers as 1R repeaters

5.2.1. Requirements and configuration of C-OTDR for optical transmission lines containing EDFAs

Figure 5.1 shows the measurement setup for using enhanced C-OTDR with fiber spans in a transmission system containing optical fiber amplifiers as 1R repeaters. The downstream line and upstream line are accommodated in a repeater, which uses EDFAs for compensating the loss of the fiber span. The EDFAs in the repeater contain optical isolators and auto-level control (ALC) circuits to stabilize the gain characteristics of the communication signal light passing through the repeater.

A probe light launched from the C-OTDR into the first fiber span of the downstream line is amplified at the EDFA in the first repeater. The amplified probe light propagates further along the downstream line. Since the optical isolator in the EDFA rejects any backscattered light from the second and subsequent spans of the transmission line, the repeater requires a backscattered path. Thus, the backscattered path incorporated in the

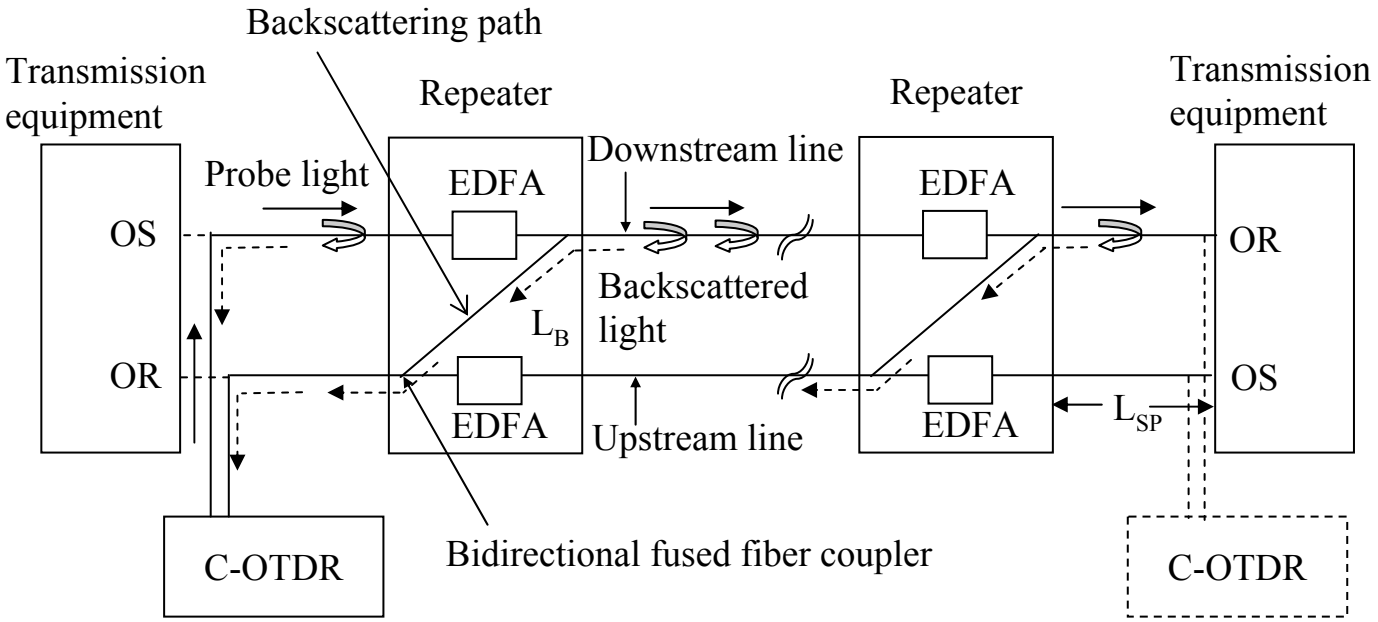

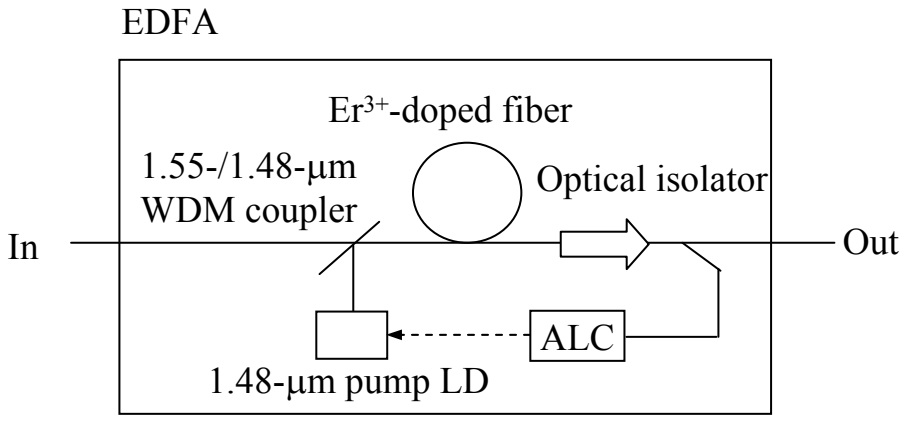

EDFA: Erbium-doped fiber amplifier
ALC: Auto-level control circuit
OS: Optical source
OR: Optical receiver

Figure 5.1 Measurement setup for using enhanced C-OTDR for optical fiber spans in an optical transmission system containing optical fiber amplifiers as 1R repeaters

repeater connects the downstream and upstream lines via a bidirectional fused fiber coupler with a typical coupling ratio of 1:10. The backscattered light generated in the second and subsequent spans of the downstream line propagates back along the upstream line via the backscattering paths. The resultant backscattered light is introduced into the backscattered light port of the C-OTDR receiver. To avoid interference noise, an optical isolator is embedded in this port (as shown in Fig. 5.2). To test fiber spans along the upstream line, another C-OTDR is placed at the other end of the optical transmission system, as shown by the broken lines in Fig. 5.1.

When launching OTDR pulses with low pulse repetition into an optical transmission line containing EDFAs optimized in CW gain mode, the leading edge intensity of the OTDR pulses increases with every pass through a repeater. This optical surge, caused by the accumulated difference between the gain of the pulsed light and the gain of the CW light in the EDFA, breaks the ALC circuit after passing through several repeaters. Therefore, it is necessary to keep the probe power from the C-OTDR as uniform as possible to avoid any optical surges.

Figure 5.2 shows the configuration of the enhanced C-OTDR for optical transmission lines with EDFAs. A distributed feedback laser diode (DFB-LD) with an external cavity generates 1552-nm CW laser light, whose linewidth is narrowed to less than 10 kHz. This CW laser light is used as the signal and local oscillator (LO) light for heterodyne detection. An AO switch (AO-SW1) is driven in pulse mode to produce signal pulses. These signal pulses are introduced into a second AO switch (AO-SW2) operated synchronously with AO-SW1. The optical frequency shift of the signal pulse is 35 MHz, because AO-SW1 provides an upshift of 120 MHz and AO-SW2 provides a downshift of 85 MHz. CW dummy light generated by another DFB-LD operating at a wavelength of 1554 nm is added to the signal pulses via the fundamental port of AO-SW2. A 1-nm optical band pass filter (OBPF) with a center wavelength of 1554 nm reduces the sideband of the dummy light by about 20 dB. This enables keeping the optical probe power from the OTDR as uniform as possible and reduces the beat noise between the LO light and backscattered light generated by the sideband light of the dummy light source. A polarization controller (PC) is incorporated to reduce polarization fluctuation in the C-OTDR trace, described in chapter 4. The resultant probe light is amplified by an EDFA and launched into the downstream line through a 3-dB optical fiber coupler (FC2). An optical isolator is connected to the other side of FC2 to avoid sending probe light into the upstream line. Otherwise, the probe light propagating along the downstream and upstream lines is mixed at the second and subsequent fiber spans via the backscattered paths, causing interference noise.

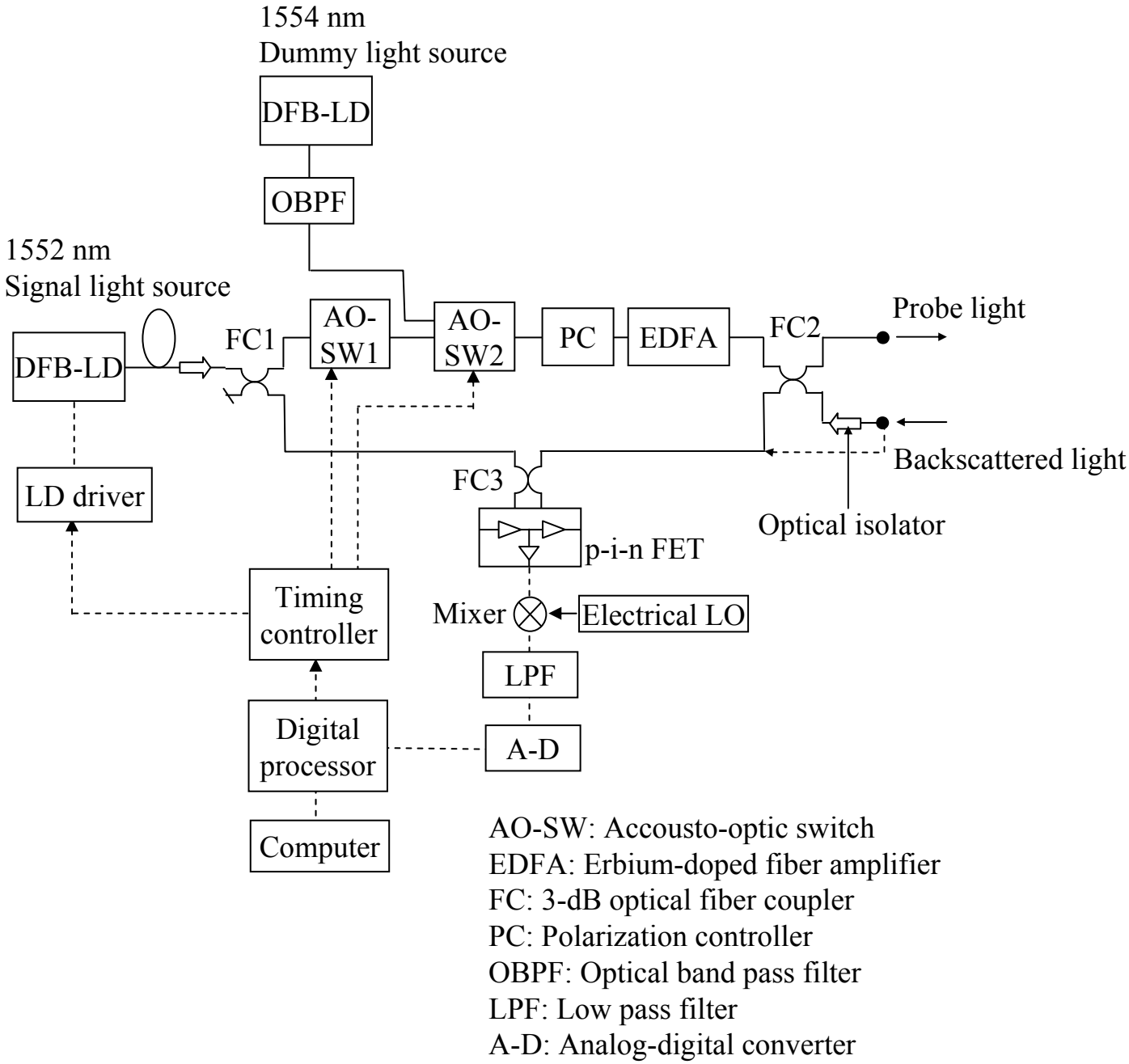

Figure 5.2 Configuration of an enhanced C-OTDR for an optical transmission system containing optical fiber amplifiers as 1R repeaters

The backscattered signal light from the downstream and upstream lines is then mixed with the LO light by FC3 and detected by a double-balanced p-i-n FET receiver. The beat signals are down-converted to a baseband signal by an electrical local oscillator and a mixer. The high frequency components are eliminated by a low-pass filter (LPF), digitized by an analog-to-digital (A-D) converter, and finally squared, integrated, transformed logarithmically, and displayed as an OTDR trace. Since the backscattered light from the dummy light source has a different wavelength from that of the signal pulses, the frequency of the beat signals between the LO light and backscattered light from the dummy lights is so extremely high that the beat signals' effect on the OTDR trace is negligible. The beat noise between the LO light and the ASE from the EDFAs in the repeaters significantly degrades the receiver sensitivity, as discussed in chapter 2.

5.2.2. Required dynamic range and performance evaluation of C-OTDR for optical transmission lines containing EDFAs

If the EDFA in a repeater compensates for the loss of the fiber span, the probe light power at the output port of the repeater remains at the initial launching power. The backscattered light from the fiber span via the backscattered path in the n-th repeater propagates along the upstream line and pass through n - 1 repeaters. The EDFAs also compensate for the loss of the fiber spans from the (n - 1)-th repeater to the second repeater in the upstream line. Consequently, taking into account both the loss of the first fiber span and the loss of the backscattering path in the n-th repeater, the SWDR required for the C-OTDR, *SWDRreq*, is given by

$$SWDRreq = \alpha_f L_{SP} + (\alpha_f L_{SP} + L_{BP})/2 + D_d, \quad (5.1)$$

where α_f is the average fiber loss (in dB/km), L_{SP} is the fiber span length, L_{BP} is the loss of the backscattering path, and D_d is the decrease in dynamic range caused by the accumulation of ASE noise from the EDFAs in the upstream line. The first term in Eq. (5.1) indicates the single-way loss of the n-th fiber span. The second term corresponds to the loss of the first fiber span and the loss of the backscattering path in the n-th repeater. From Eq. (5.1), when C-OTDR is applied to transmission lines where α_f = 0.21 dB/km, *Lsp* = 80 km, L_{BP} = 20 dB, and the dynamic range decrease is assumed to be zero (i.e., D_d = 0 dB), an SWDR of 35.2 dB is required.

To evaluate the SWDR of the proposed C-OTDR as shown in Fig. 5.2, experiments using a 180-km dispersion-shifted fiber were performed. Figure 5.3 shows the waveform of the probe light with a 10-μs signal pulse from AO-SW2. The signal pulse

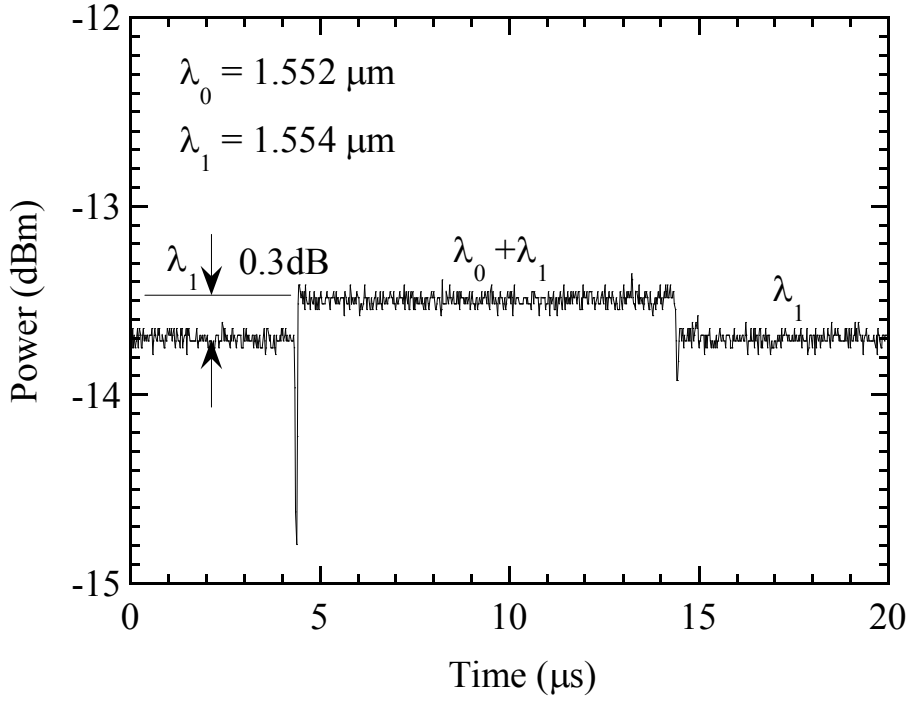

Figure 5.3 Waveform of probe light obtained with a 10-μs signal pulse from AO-SW2 in C-OTDR

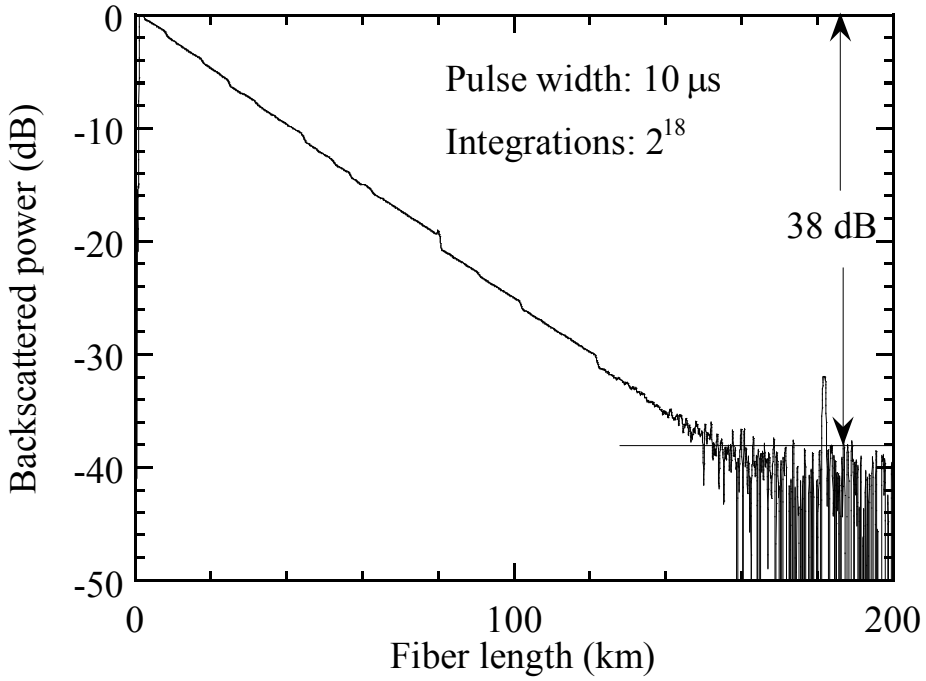

Figure 5.4 C-OTDR trace from a 180-km test fiber

repetition rate was 4 ms. The difference between the power levels of the signal pulse and the dummy light was negligible. The probe light was introduced into the EDFA in the C-OTDR. The gain of the EDFA was about 23 dB, and the power of the probe light launched into the test fiber was about 6 dBm.

The SWDR of the C-OTDR was experimentally measured by connecting the test fiber at the port of the downstream line. Figure 5.4 shows the resulting C-OTDR trace for 2^{18} integrations. With a 10-μs pulse width and a receiver bandwidth of 100 kHz, an SWDR of about 38 dB was achieved. This value is slightly lower than that calculated by assuming the quantum limit of the receiver sensitivity [5-17].

For C-OTDR applied to transmission lines with EDFAs, the dynamic range of the upstream line with a 10-μs pulse width was assumed as 37 dB, because of the 2-dB loss of the optical isolator at the input port from the upstream line. These results confirm that the proposed C-OTDR has the required SWDR for testing optical fiber lines containing repeaters with a fiber span of 80 km.

5.2.3. Feasibility of applying C-OTDR to test optical transmission lines with optical repeaters containing EDFAs

Figure 5.5 shows the experimental setup for monitoring the downstream line in second section (i.e., section #2) of an optical transmission line with optical repeaters containing EDFAs. The optical transmission line in the first section (i.e., section #1) was composed of two dispersion-shifted optical fibers and optical attenuators. The total fiber length was 25 km. The loss of both the downstream line and the upstream line in section #1 was 18.5 dB after adjusting the attenuation of the optical attenuators. The gain of EDFA1 in the repeater was about 18 dB. Probe light from the C-OTDR launched with a power of about 6 dBm, propagated further along the downstream line as a result of EDFA amplification. The downstream line in section #2 was composed of an 80-km dispersion-shifted optical fiber with a loss of 21 dB. The backscattered light generated from the fiber in section #2 was introduced into the upstream line in section #1 via the backscattered path in the repeater. The loss of the backscattering path, including the two directional fused fiber couplers, was 20 dB. To reject the backscattered light from the downstream line in section #1, the fiber end of the upstream line was directly connected to the signal input port of FC3 in the C-OTDR as shown in Fig. 5.2.

Figure 5.6 shows a C-OTDR trace with a 10-μs pulse width and 2^{18} integrations for the cases of (a) having EDFA2 off and (b) having EDFA2 on. For case (a), the

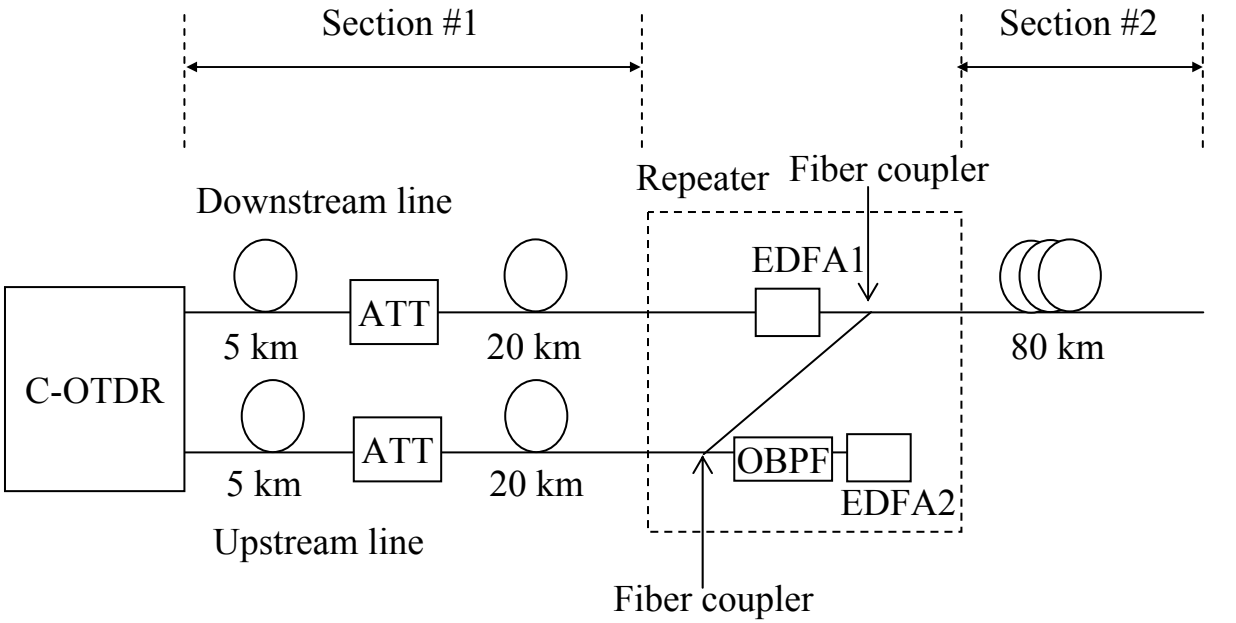

Figure 5.5 Experimental setup for using enhanced C-OTDR to test optical fiber lines containing EDFAs as 1R repeaters

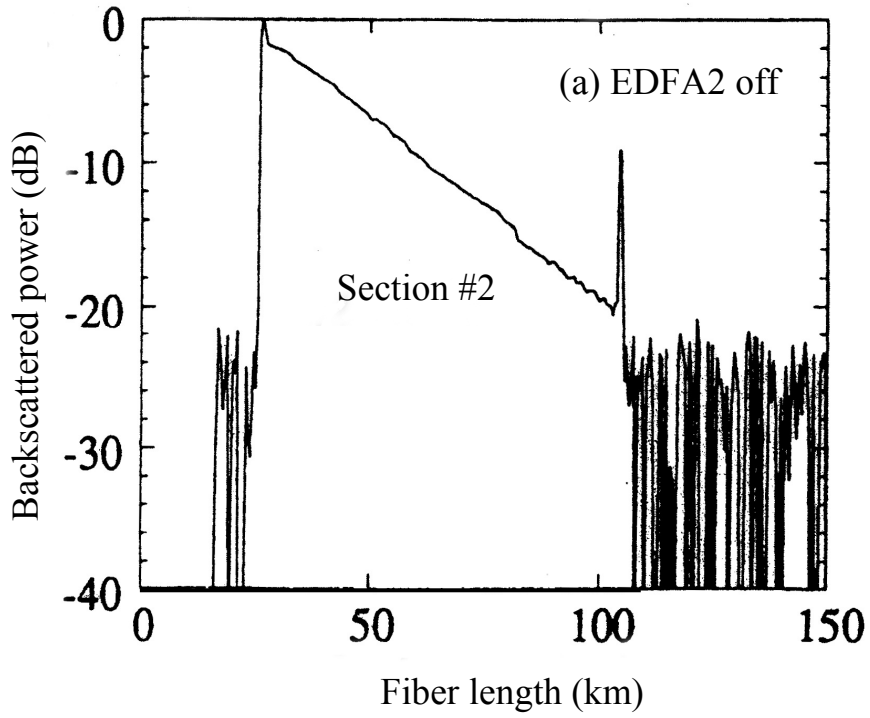

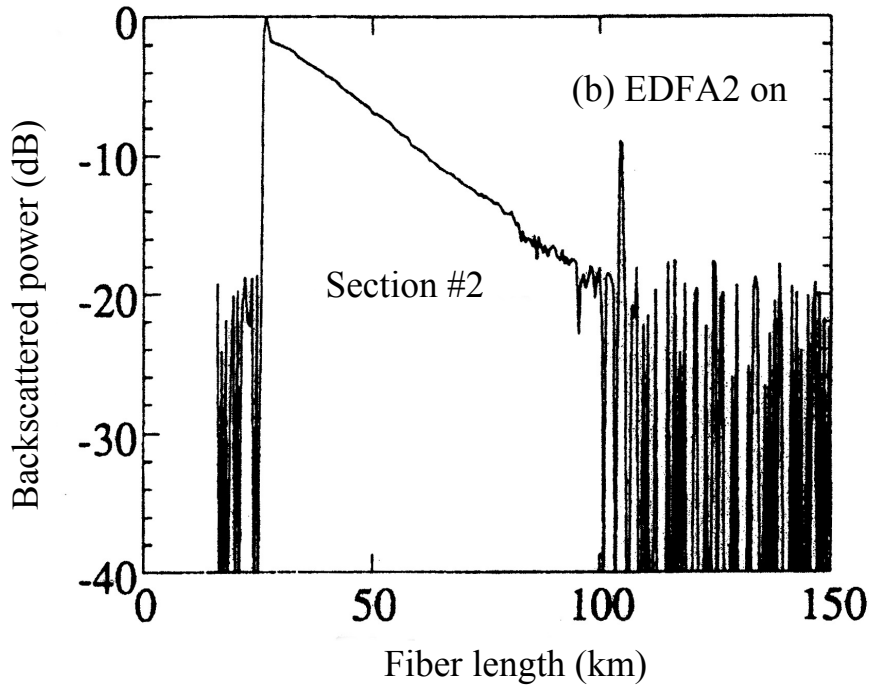

Figure 5.6 C-OTDR traces from section #2 of the test optical fiber line containing EDFAs, with (a) EDFA2 off and (b) EDFA2 on

backscattered light from the 80-km fiber of the downstream line in section #2 was clearly observed. For case (b), the noise level increased by about 2 dB in comparison with the C-OTDR trace for case (a). This was because the beat noise between the optical LO light and the ASE noise from the EDFA2 became larger than the shot noise of the optical LO light in the receiver.

When the dynamic range decrease due to the EDFAs is assumed to be zero, the measurable portion of each fiber span is estimated as about 90 km, which is longer than the value obtained in the experiment. Although the measurable portion of the fiber span was less than 100 km, in practice there is no problem with locating a cable fault in a whole span of 100 km. Since the measurable portion using the C-OTDR is over 80 km, another C-OTDR located at the other end of the transmission system can be used to test the last 20 km of a span. Consequently, the results confirm the feasibility of applying the proposed C-OTDR to monitor an optical transmission line with repeaters containing EDFAs and a span of 100 km.

After further investigation based on this study [5-18]-[5-20], the highly developed C-OTDR was deployed for testing the commercial optical amplifier submarine transmission system that connected Kagoshima and Okinawa in Japan in 1995. This 890-km optical transmission line had nine repeaters and ten fiber spans with an average fiber length of 90 km [5-21].

5.3. Measurement of 340 km optical fiber line with a remotely pumped EDFA and DRA by C-OTDR

5.3.1. High dynamic range C-OTDR with low fading noise

Figure 5.7 shows the configuration of an enhanced C-OTDR with low fading noise. CW laser light at 1554 nm is generated by an InGaAsP multiple quantum well (MQW) DFB-LD with an external cavity and has its linewidth reduced to less than 10 kHz. An AO switch (AO-SW1) is used to divide this light into two paths: the signal path, and the LO path. At the same time, AO-SW1 produces signal pulses, whose optical frequency is shifted up by 80 MHz. The pulses are then transmitted to the test fiber through AO-SW2, which is designed to down-convert the optical frequency by 120 MHz. As a result, the optical frequency shift of the signal pulses is 40 MHz. An EDFA located between AO-SW1 and AO-SW2 amplifies the optical power of the signal pulses along the signal path. The backscattered signal light is mixed with the optical LO by a double balanced p-i-n FET receiver.

The 40-MHz beat signals are down-converted to a baseband signal by mixing them with an electrical LO signal, and the high-frequency components are eliminated by a 100-kHz LPF. The filtered signal is then introduced into an analog-to-digital (A-D) converter. The digitized backscattered signals are squared, integrated, and finally displayed on a computer CRT as an OTDR trace after logarithmic transformation.

Figure 5.8 shows the measured C-OTDR trace for a test fiber with a pulse width of 10 μs and 2^{18} integrations. The launched power of the signal pulses was about 18 dBm. The test fiber was a 300-km pure silica core fiber (PSCF) with a fiber loss coefficient of about 0.178 dB/km at a wavelength of 1550 nm. The dispersion of the fiber was about 18.7 ps/nm/km. In fact, the C-OTDR had a high sensitivity of -99 dBm with a bandwidth of 100 kHz when the LO light power was about 3 dBm. It achieved an SWDR of about 46 dB and a distributed fiber loss over approximately 260 km of fiber.

This C-OTDR has a function for reducing fading noise. A polarization controller (PC) is inserted into the LO path to change the state of polarization (SOP). The randomized SOP reduces the polarization-dependent fluctuation, and the fading noise can be reduced by applying the synchronous optical frequency hopping method described in chapter 4.

Figure 5.9 shows the amplitude fluctuation in the C-OTDR trace with 2^{16} integrations for the region of 4-14 km. The measured root mean square (RMS) of the fading noise fluctuation was 0.04 dB.

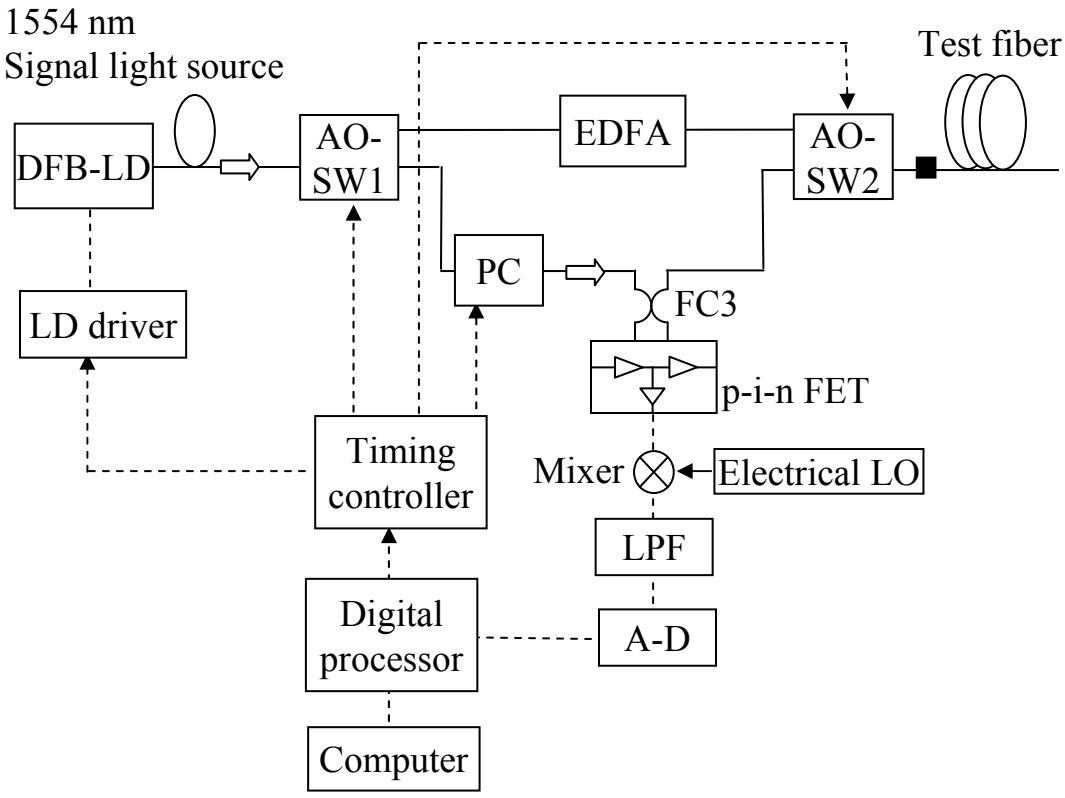

Figure 5.7 Configuration of the enhanced C-OTDR with low fading noise

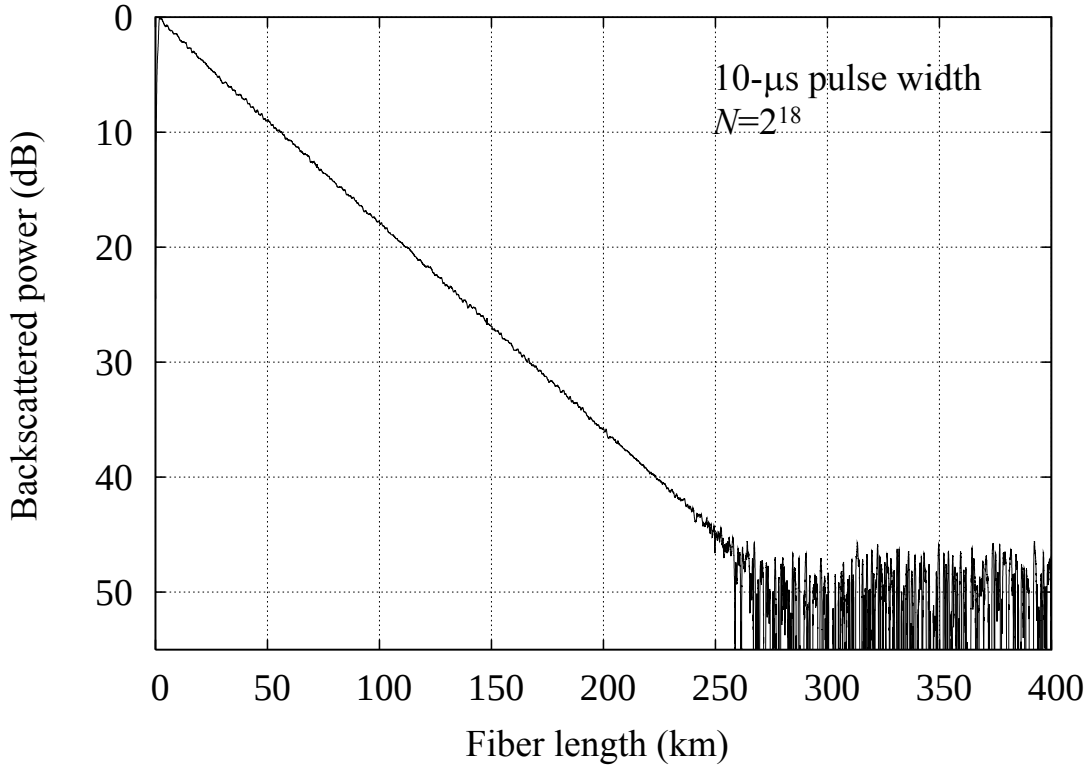

Figure 5.8 C-OTDR trace obtained with 10-μs pulse width and 2^{18} integrations

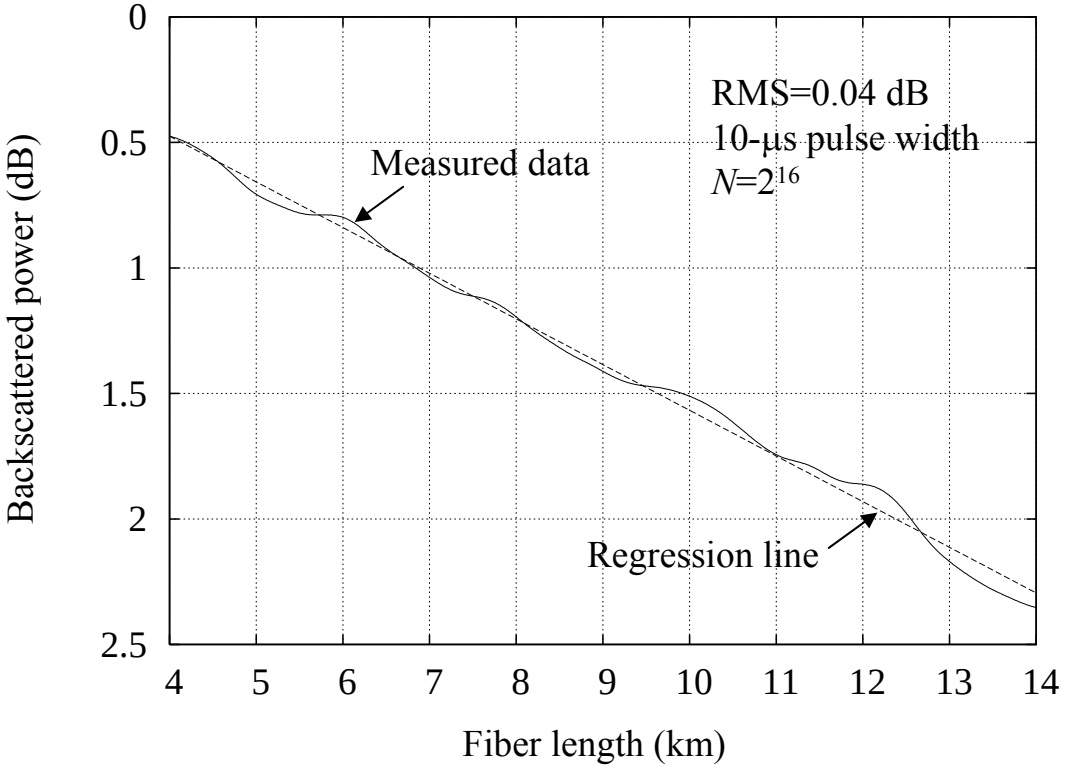

Figure 5.9 C-OTDR trace for the region of 4-14 km

These results demonstrate that this C-OTDR, with high dynamic range and low fading noise and enhanced with an EDFA post-amplifier, can be applied to monitor long-haul optical fiber cables.

5.3.2. Measurement of 340-km test fiber with a remotely pumped EDFA and a DRA

Figure 5.10 shows the experimental setup for measuring a 340-km long-haul test fiber with a remotely pumped EDFA and a DRA. The test fiber line consisted of an 82.1-km PSCF and a 258.2-km PSCF with the remotely pumped EDFA placed between them. The PSCF loss coefficient was about 0.195 dB/km at a wavelength of 1480 nm. Pump light at a wavelength of 1480 nm was introduced into the 82.1-km PSCF.

Figure 5.11 shows the resulting C-OTDR trace with a 10-μs pulse width for operating pump light with an optical power of 24 dBm. The number of integrations was $N = 2^{16}$. We clearly obtained fiber loss distribution for the 340-km test fiber with a remotely pumped EDFA. The Rayleigh backscattered signals were amplified by the DRA in the region of 258-340 km. The measured EDFA gain of G1 and DRA gain of G2 were about 18.9 and 5.9 dB, respectively. These values match the original gain characteristics of the remotely pumped EDFA and the DRA with 1.48-μm pump light and a power of 24 dBm.

The highly developed C-OTDR was employed in the monitoring a 340-km repeaterless optical transmission system with a remotely pumped EDFA and a DRA, which connected the islands of Okinawa and Miyako-jima in Japan in 2005 [5-22].

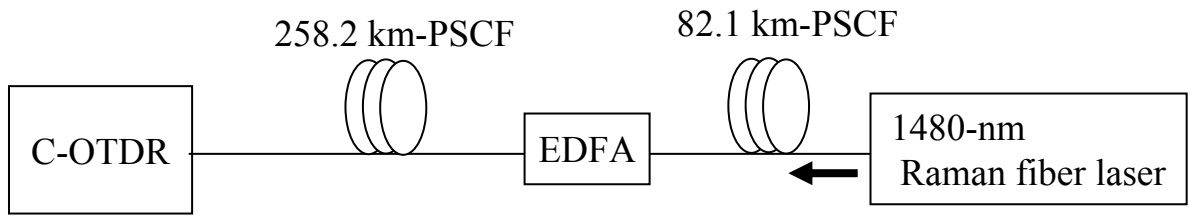

Figure 5.10 Experimental setup for measuring the 340-km test fiber with remotely pumped EDFA and DRA

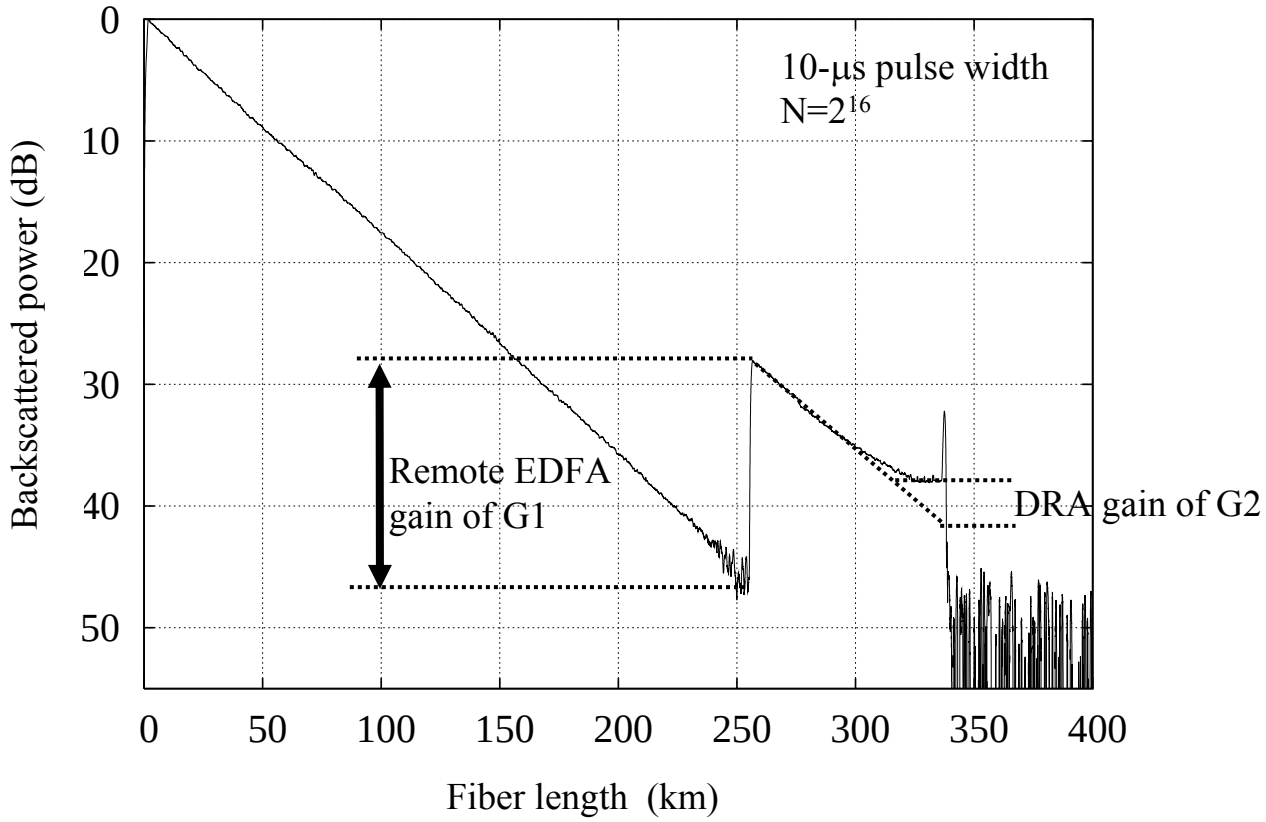

Figure 5.11 C-OTDR trace for the 340-km test fiber

5.4. Conclusions

This chapter described the application of coherent-detection optical time-domain reflectometry (C-OTDR) for monitoring long-haul optical transmission lines containing (1) in-line amplifiers as 1R-repeaters and (2) distributed Raman amplifier (DRA).

(1) An enhanced C-OTDR with high dynamic range, for use in optical transmission lines containing optical fiber amplifiers, was implemented and evaluated. The C-OTDR was constructed by applying conventional acousto-optic (AO) modulation for heterodyne detection and an erbium-doped fiber amplifier (EDFA) to increase the probe power. Optical dummy light was added between signal pulses to keep the optical probe power as uniform as possible. The single-way dynamic range (SWDR) of the C-OTDR was quite large, 37 dB, with a probe power of 6 dBm. By applying the C-OTDR to optical transmission lines with fiber spans of 80 km and backscattering paths with loss of about 20 dB, the C-OTDR was confirmed capable of testing fiber spans with distances of 90 km, which is twice the previously reported value. Since the measurable portion using the C-OTDR is over 80 km, another C-OTDR located at the other end of the transmission system can be used to test the last 20 km of a span. Consequently, the proposed C-OTDR can monitor an optical transmission line with repeaters containing EDFAs and a span of 100 km.

(2) The C-OTDR was further developed to achieve a 46-dB SWDR and low fading noise, and measurement of a 340-km long optical fiber line containing a remotely pumped EDFA and a DRA was demonstrated. This highly developed C-OTDR is a powerful tool for designing and maintaining a repeaterless optical transmission system with a remotely pumped EDFA and a DRA.

5.5. References

[5-1] K. Hagimoto, S. Nishi, and K. Nakagawa, "An optical bit-rate flexible transmission system with 5-Tb/s-km capacity employing multiple in-line erbium-doped fiber amplifiers," IEEE J. Lightwave Technol. vol. 8, no. 9, pp. 1387-1395, 1990.

[5-2] S. Saito, M. Murakami, A. Naka, Y. Fukada, T. Imai, M. Aiki, and T. Ito, "Inline amplifier transmission experiments over 4500 km at 2.5 Gb/s," IEEE J. Lightwave Technol. vol. 10, no. 8, pp. 1117-1126, 1992.

[5-3] M. Aiki. S. Saito, Y. Hayashi, and T. Ito, "Future evolution of optical amplifier submarine systems," in the proc. of SubOptic'93, Apr., pp. 281-285, 1993.

[5-4] P. K. Runge and E. K. Stafford, "AT&T optical amplifier systems," in the proc. of SubOptic'93, Apr., pp. 72-77, 1993.

[5-5] H. Wakabayashi, Y. Namihira. S. Akiba, and S. Yamamoto, "OS-A optical amplifier submarine cable systems," in the proc. of SubOptic'93, Apr., pp. 85-90, 1993.

[5-6] Y. Horiuchi, S. Yamamoto, S. Akiba, and H. Wakabayashi, "Highly accurate fault localization over 4580 km optical amplifier system using coherent Rayleigh backscatter reflectometry," in the proc. of ECOC'93, MoC1.3, pp. 5-8, 1993.

[5-7] Y. Horiuchi, S. Ryu, K. Mochizuki, and H. Wakabayashi, "Novel coherent heterodyne optical time domain reflectometry for fault localization of optical amplifier submarine cable systems," IEEE Photon. Technol. Lett., vol. 2, no. 4, pp. 291-293, 1990.

[5-8] Y. Sato and K. Aoyama, "OTDR in optical transmission systems using Er-doped fiber amplifiers containing optical circulators," IEEE Photon. Technol. Lett., vol. 3, no. 11, pp. 1001-1003, 1991.

[5-9] Y. Maeda and K. Nakanishi, "Deployments of broadband optical access network systems in NTT, Japan," in the proc. of ECOC2003, vol. 5, pp. 16-19, 2003.

[5-10] "Number of Broadband Service Contracts, Etc. (as of the end of September 2007)," MIC (Ministry International Affairs and Communications, Japan Government) Press release – Telecom, December 18, 2007.

[5-11] H. Masuda, H. Kawakami, S. Kuwahara, A. Hirano, K. Sato, and Y. Miyamoto, "1.28 Tbit/s (32/spl times/43 Gbit/s) field trial over 528 km (6/spl times/88 km) DSF using L-band remotely-pumped EDF/distributed Raman hybrid inline amplifiers," Electron. Lett., vol. 39, no. 23, pp. 1680-1670, 2003.

[5-12] P. B. Hansen, A. Stentz, T. N. Nielsen, R. Espindola, L. E. Nelson, and A. A

Abramov, "Dense wavelength-division multiplexed transmission in “zero-dispersion” DSF by means of hybrid Raman/erbium-doped fiber amplifiers," in the proc. of OFC, PD8, 1999.

[5-13] K. Aida, S. Nishi, Y. Sato, K. Hagimoto, and K. Nakagawa, "1.8 Gb/s 310 km fiber transmission without outdoor repeater equipment using a remotely pumped in-line Er-doped fiber amplifier in an IM/DIRECT-DETECTION system," in the proc. of ECOC’89, PDA-7, pp. 29-32, 1989.

[5-14] Y. Koyamada and H. Nakamoto, "High performance single mode OTDR using coherent detection and fiber amplifiers," Electron. Lett., vol. 26, no. 9, pp. 573-574, Apr. 1990.

[5-15] S. Furukawa, H. Izumita, I. Sankawa, andY. Koyamada, "High dynamic range, low fading noise coherent OTDR using erbium fiber amplifier and LD temperature changing techniques," in the proc. of ECOC91/IOOC91, MoCl-3, pp. 81-84 1991.

[5-16] H. Izumita, Y. Koyamada, I. Sankawa, and S. Furukawa, "Coherent optical time-domain reflectometer with a 40-dB dynamic range enhanced with erbium-doped fiber amplifiers," in the technical digest of OFC'92, WK6, p. 147, 1992.

[5-17] Y. Koyamada, H. Nakamoto, and N. Ohta, "High performance coherent OTDR enhanced with erbium doped fiber amplifiers," J. Opt. Commun., vol. 13, no. 4, pp. 127-133, 1992.

[5-18] S. Furukawa, K. Tanaka, Y. Koyamada, and M. Sumida, "High dynamic range coherent OTDR for fault location in optical amplifier systems," in the proc. of IMTC/94 Hamamatsu, Japan, pp. 106-109, 1994.

[5-19] S. Furukawa, K. Tanaka, Y. Koyamada, and M. Sumida, "Enhanced coherent OTDR for long span optical transmission lines containing optical fiber amplifiers," IEEE Photon. Technol. Lett., vol. 7, no. 5, pp. 540-542, 1995.

[5-20] M. Sumida, S. Furukawa, K. Tanaka, and M. Amemiya, “Fault location on optical amplifier submarine transmission systems,” IEICE Trans., vol. J78-B-I, no. 12, pp. 745-752, 1995.(in Japanese)

[5-21] M. Sumida, S. Furukawa, K. Tanaka, and M. Aiki, "High-accurate fault location technology using FSK-ASK probe backscattering reflectometry in optical amplifier submarine transmission systems," IEEE J. Lightwave Technol. vol. 14, no. 10, pp. 2108-2116, 1996.

[5-22] NTT WEST News Release 24/Dec./2003, in Japanese, http://www.ntt-west.co.jp/news/0312/031224.html.

Chapter 6. Applications: Fiber-distributed strain measurement techniques using upgraded C-OTDR enhanced with sideband generation technique or wideband coherent receiver

This chapter describes applications of the highly developed coherent-detection optical time-domain reflectometry (C-OTDR) for distributed strain measurement in an optical fiber in order to evaluate the reliability of the fiber. Optical frequency conversion techniques using the sideband generation technique or a wideband coherent receiver are proposed. These techniques enable upgrading C-OTDR to Brillouin OTDR (B-OTDR), in order to measure the optical frequency shift and power of spontaneous Brillouin scattering, which is related to the tensile strain in an optical fiber. To reduce the accuracy degradation due to environmental temperature changes, a simultaneous measurement technique for separating strain and temperature is also proposed and discussed.

6.1. Introduction

In preventive maintenance of optical fiber networks, technologies for measuring the strain distributed in an optical fiber are very important for evaluating the reliability of optical fiber cables [6-1]-[6-3]. In 1989, it was reported that the Brillouin frequency shift in silica fibers varies greatly with the strain and temperature [6-4],[6-5]. Then, many approaches have been proposed for measuring fiber-distributed strain by using Brillouin scattering in single-mode optical fibers [6-6]. This was due to the great advantages of distributed fiber sensors using Brillouin scattering in an optical fiber: (1) strain is a very important parameter for evaluating the reliability of optical fibers; (2) Brillouin frequency shift measurement does not require calibration of the optical fiber loss and (3) conventional low-loss communication wavelength regions can be used for this sensing, because the optical frequency shifts of the Stokes and anti-Stokes light of Brillouin scattering are within those wavelength bands.

Figure 6.1 shows a fiber-distributed sensing method using OTDR and backscattering. When launching pulsed light into a single-mode optical fiber, backscattered light is detected at the input end of the optical fiber, as a function of the round-trip time corresponding to the fiber length. Backscattering in an optical fiber includes Rayleigh, Raman, and Brillouin scattering. Rayleigh backscattering consists of elastically scattered light, with the same wavelength as the incident light. Raman- and Brillouin-scattered light originates from inelastically scattering caused by interaction

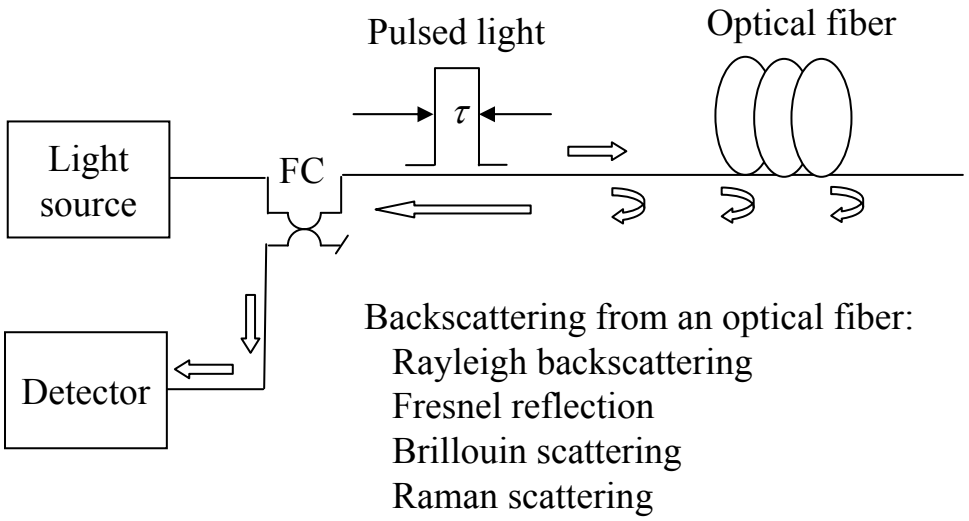

Figure 6.1 Sensing method using OTDR and backscattering

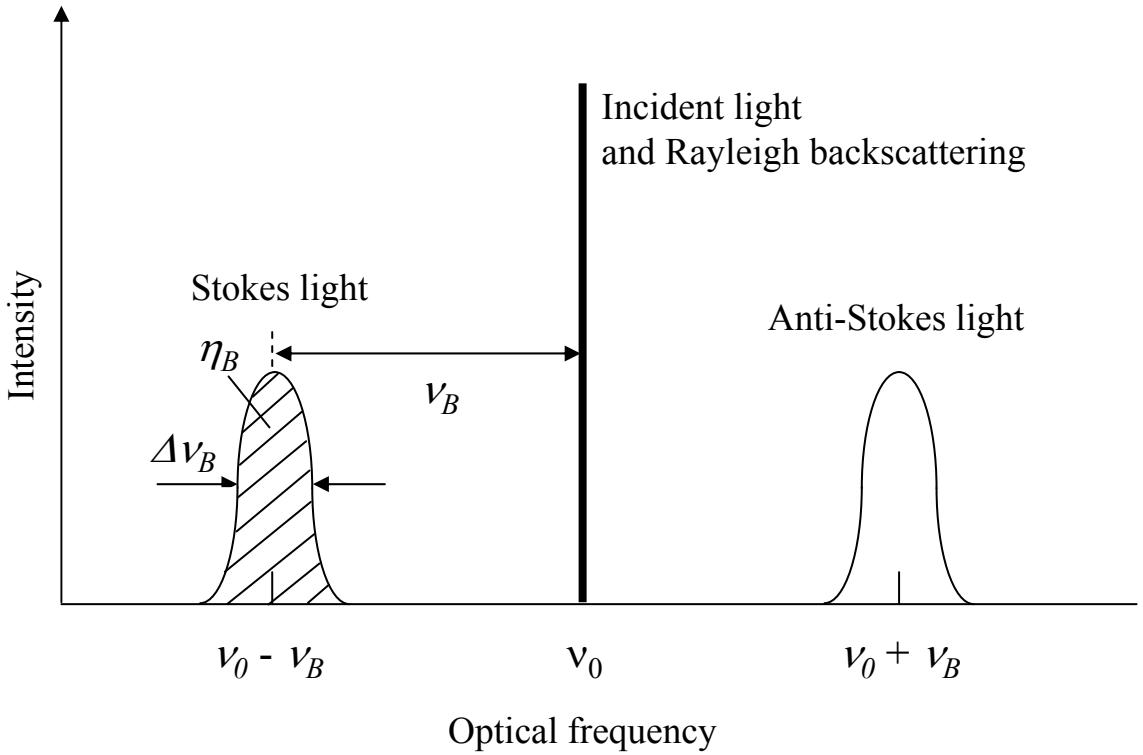

η_B: Power of spontaneous Brillouin backscattered light
ν_B : Brillouin frequency shift
$\Delta\nu_B$: Linewidth of spontaneous Brillouin backscattered light

Figure 6.2 Spectra of Brillouin scattering from an optical fiber

with optical and acoustic phonons, respectively [6-7]. Since the power of Raman and Brillouin backscattering is significantly weaker than that of Rayleigh backscattering in silica fibers, Rayleigh backscattering is the dominant backscattering mechanism in OTDR.

Figure 6.2 shows spectra of Brillouin scattering from an optical fiber, which is characterized by the Brillouin frequency shift v_B, the Brillouin linewidth Δv_B, and the Brillouin scattering coefficient η_B. The Brillouin frequency shift v_B, which is maximized when the light is scattered in a backward direction, is given by [6-8]

$$v_B = 2nV_a/\lambda, \tag{6.1}$$

where n is the fiber-core refractive index, V_a is the velocity of sound, and λ is the light wavelength. For typical values of n = 1.45 and V_a = 5.96 km/s for silica glass, the calculated Brillouin frequency shift v_B is approximately 11.2 GHz at a wavelength of 1.55 μm.

To detect weak Brillouin scattering, a high-sensitivity detection technique and a filtering technique are required to separate the weak Brillouin backscattered light from other backscattered light. To meet these requirements, Brillouin gain spectroscopy and a coherent heterodyne detection method was proposed [6-9], [6-10].

Brillouin optical time-domain analysis (B-OTDA) is a promising method, with high dynamic range, for measuring the strain and temperature distribution in an optical fiber by Brillouin gain spectroscopy [6-9],[6-11],[6-12]. This method uses stimulated Brillouin amplification caused by counter-propagating pump light in order to obtain large Brillouin signals. There is, however, an operational limit to this method, because it must access both ends of the optical fiber. By used a cleaved end of a test fiber, a distributed fiber sensor, based on Brillouin gain spectrum analysis with probe and delayed pump pulses generated by a $LiNbO_3$ (LN) intensity modulator (EOM), was proposed and makes single-fiber-end measurement possible [6-13]-[6-15]. Since a reflection from the far end of the test fiber is required, this approach cannot be applied to optical fibers with large loss or no reflection at the far end.

A C-OTDR has the potential of high dynamic range, as described in chapters 2 and 3. The receiver sensitivity can be improved up to the shot noise limit. B-OTDR using a coherent detection technique to measure spontaneous Brillouin backscattered light from one end of an optical fiber and obtain the strain and temperature distribution in the optical fiber was proposed for the first time in a co-authored paper [6-10].

Figure 6.3 illustrates the operation of B-OTDR. When measuring the Brillouin backscattering with a spectrum bandwidth of Δv_B, the optical frequency shift is swept around the Brillouin frequency shift v_B. The optical frequency difference between the

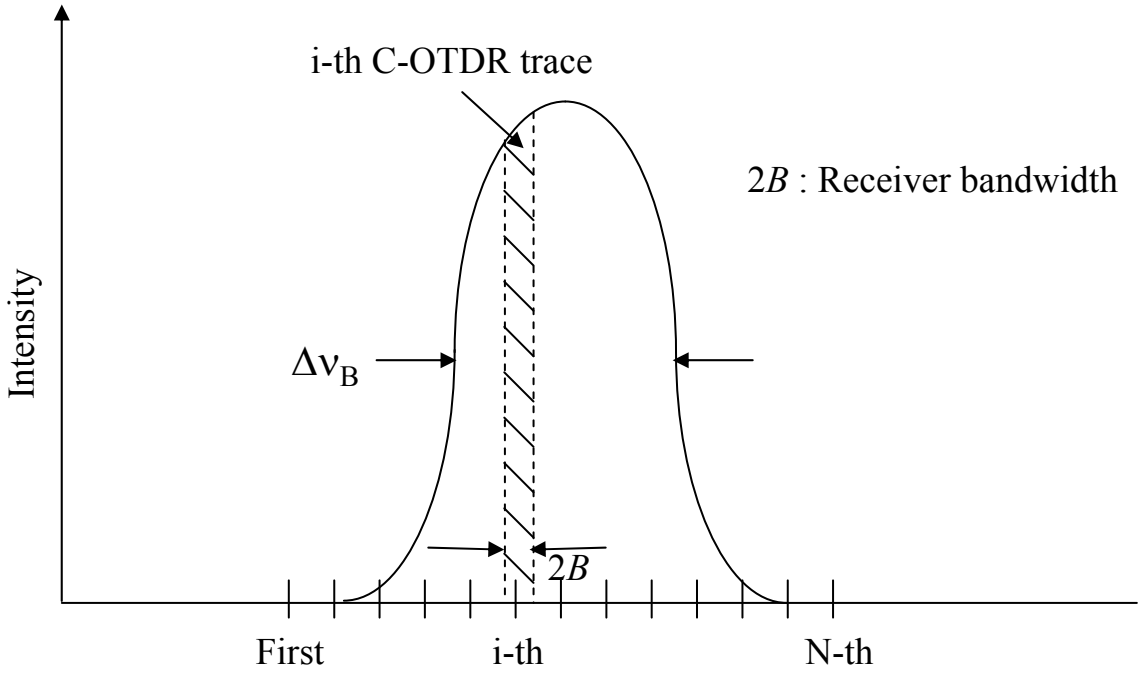

(a) Brillouin spectrum distribution composed of incrementally measured C-OTDR traces as a function of the optical frequency shift

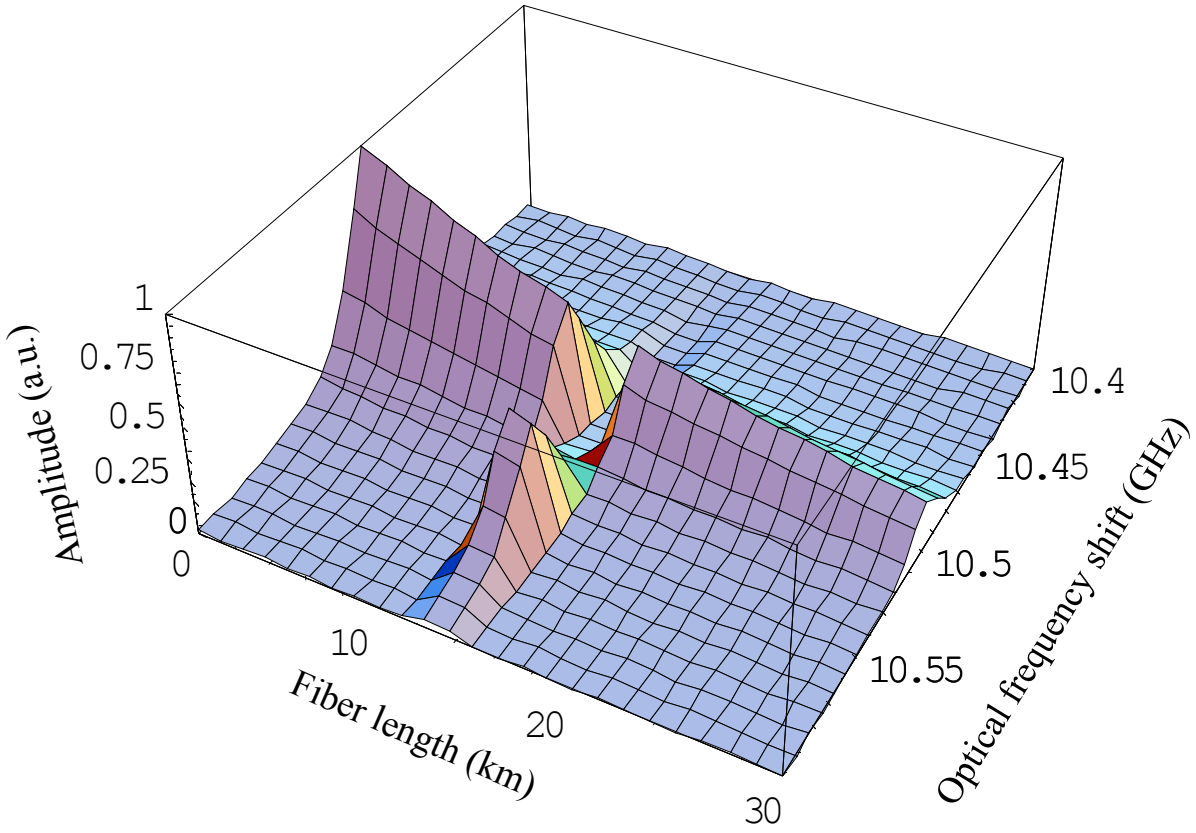

(b) 3D schematic of the Brillouin spectrum distributed along the test fiber, with a 0.1% tensile strain applied in the 12- to 15-km region

Figure 6.3 Operation of B-OTDR

signal light and the local oscillator (LO) light is controlled by a sophisticated optical frequency controller consisting of two laser sources [6-10], or by an optical frequency translator [6-16], as shown in Fig. 6.4. Since the bandwidth in C-OTDR is 1 MHz for a 1-μs pulse width (i.e., a 100-m spatial resolution), the filtering performance of C-OTDR is sufficiently narrower than the bandwidth of $\Delta\nu_B$ (e.g., 30 MHz at a wavelength of 1.55 μm). The resultant incrementally measured C-OTDR traces as a function of the optical frequency shift provide the Brillouin spectrum distribution in the optical fiber. If a tensile strain of 0.1 % is applied to the 12- to 15-km region in the optical fiber, the Brillouin frequency shift in that region is increased by approximately 50 MHz, as shown in Fig. 6.3(b). This is because the Brillouin frequency shift varies linearly with the strain and temperature over wide ranges, with strain and temperature coefficients of 493 MHz/% and 1 MHz/°C at 1.55 μm for a silica-based single-mode fiber [6-12].

There are several problems, however, with previously proposed B-OTDR approaches: (1) the complexity of optical frequency control between the probe light and local light as shown in Fig. 6.4; (2) the lack of a loss measurement function, unlike conventional OTDR; (3) fixed-wavelength operation, preventing in-service line monitoring; and (4) degradation of the strain measurement accuracy because of environmental temperature changes.

This chapter discusses improvements in B-OTDR. First, the required single-way dynamic range (SWDR) for upgrading C-OTDR to B-OTDR is theoretically investigated in section 6.2, because B-OTDR is based on C-OTDR technologies. Since the optical frequency of spontaneous Brillouin backscattered light is down-shifted by approximately 11 GHz from that of 1.55-μm input light, the frequency of the beat signal between the spontaneous Brillouin backscattered light and LO light in coherent self-heterodyne B-OTDR is extremely high, and the beat signal can hardly be detected with the conventional double-balanced receiver used in C-OTDR. Therefore, an optical frequency shifter, which up-shifts the frequency of the signal light by approximately 11 GHz, is required in order to reduce the beat signal frequency to the intermediate frequency (IF) bandwidth of the receiver [6-16]. A previously reported optical frequency translator produces a pulse train with a sequential frequency shift by circulating a signal pulse around an optical loop incorporating an acousto-optic (AO) modulator, as shown in Fig. 6.4(b) [6-16]. An erbium-doped fiber amplifier (EDFA) is required, however, to compensate the loss of the optical loop, and the delay time at the translator increases the measurement time.

Section 6.3 proposes an optical frequency shifter using the sideband generation

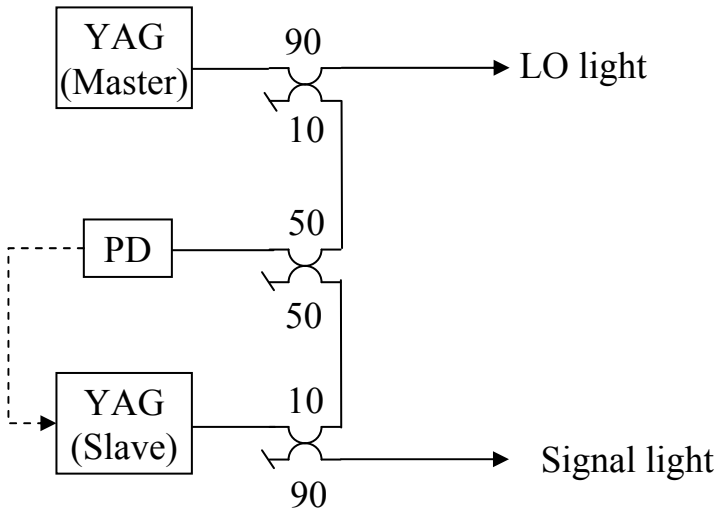

(a) Master and slave sources of YAG lasers with a feedback circuit for the beat frequency between the two lasers in B-OTDR [6-10]

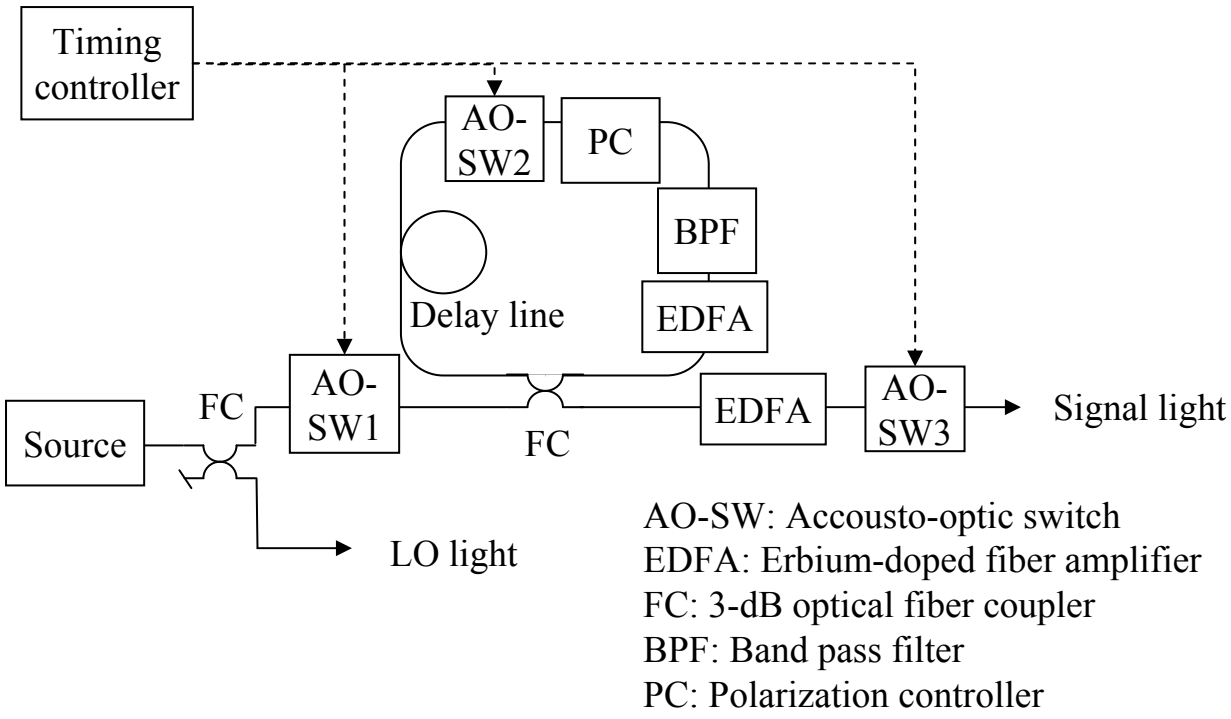

(b) Optical frequency translator composed of an EDFA, a BPF, AO-SWs, and a delay line in the optical loop for delayed self-heterodyne detection in B-OTDR [6-16]

Figure 6.4 Previous approaches to control the optical frequency difference between signal light and LO light in B-OTDR

technique with a high-speed $LiNbO_3$ phase modulator (LN-PM). This section also discusses the frequency resolution and stability of the shifter. By applying this shifter to self-heterodyne detection B-OTDR, the tensile strain distribution in an optical fiber is measured.

Another simple approach detects the spontaneous Brillouin backscattered light by using self-heterodyne C-OTDR. Section 6.4 proposes the application of an advanced wideband double-balanced receiver to B-OTDR. Measurement of the fiber-distributed strain in a 30-km dispersion-shifted fiber (DSF) demonstrates the feasibility of this approach.

To achieve in-line monitoring for preventive maintenance in an optical fiber network, U-band operation, standardized in ITU-T L.41, is a promising approach [6-17]-[6-19]. The key B-OTDR technologies for measuring the strain and optical loss distribution in an optical fiber are (1) an optical frequency shifter and (2) a high-gain optical amplifier [6-20]. The proposed shifter using an LN-PM, described in section 6.3, has the optical characteristics of low loss and low wavelength dependence. According to certain drive conditions for the LN-PM, discussed in section 6.3, B-OTDR enhanced with the LN-PM can be applied to measure the Rayleigh backscattering as well as spontaneous Brillouin backscattering, which provides the strain and loss distributions in the optical fiber. Furthermore, by using several optical switches, a 1.55- and 1.65-μm B-OTDR for measuring both the strain and optical fiber loss distributions can be constructed by using the expensive double-balanced receiver and the LN-PM for both 1.55-μm- and 1.65-μm-band operation.

Section 6.5 demonstrates 1.65-μm B-OTDR with the optical frequency shifter using the LN-PM and a high-performance Raman fiber amplifier (RFA). The combined 1.55-/1.65-μm B-OTDR is also described, and strain and optical loss distribution measurements of 30- and 100-km-long optical fibers demonstrate the feasibility of this B-OTDR approach.

Temperature fluctuation degrades the measurement accuracy of the Brillouin frequency shift caused by strain, because the shift varies with both strain and temperature [6-4]-[6-5]. Therefore, it is necessary for B-OTDR to distinguish between strain and temperature. An attractive solution is the simultaneous use of changes in the Brillouin frequency shift ν_B and changes in the Brillouin scattering coefficient η_B [6-21]-[6-23]. Few studies, however, have focused on exploiting any possible η_B dependence for distributed sensing. Therefore, section 6.6 discusses simultaneous measurement of ν_B and η_B for separating strain and temperature.

6.2. Required SWDR for upgrading C-OTDR to B-OTDR

The single-way dynamic range of B-OTDR ($SWDR_{BOTDR}$) is given by [6-10], [6-16]

$$SWDR_{\mathrm{BOTDR}} = \frac{\left[P_0 + R_B + T_s - L_c - P_{\min} + \frac{SNIR_{AVE}}{2} - \frac{SNR_R}{2} \right]}{2} \text{ (dB).} \quad (6.2)$$

P_0: Incident pulse power (dBm).

R_B: Spontaneous Brillouin backscattering factor (dB), defined below.

T_S: Brillouin scattering selection ratio (dB), defined below.

L_C: Directional coupler loss (dB).

P_{min}: Minimum detectable power of receiver with SNR = 1 (dBm).

$SNIR_{AVE}$: Electrical signal-to-noise improvement ratio by signal averaging (dB).

SNR_R: Electrical signal-to-noise ratio required for strain and temperature measurement (dB), defined below.

$$R_B = 10\log\left[\alpha_B S \frac{c\tau}{2n} \right] \text{ (dB),} \quad (6.3)$$

$$T_S = 10\log\left[\frac{2B}{\pi \Delta \nu_B} \right] \text{ (dB),} \quad (6.4)$$

$$SNR_R = 20\log\left[\left(\frac{\Delta \nu_B}{\sqrt{2}\delta \nu_B} \right)^4 \right] \text{ (dB),} \quad (6.5)$$

where α_B is the fiber-attenuation coefficient for spontaneous Brillouin scattering, which is approximately 1.23×10^{-6} m^{-1} [6-25], S is the ratio of the backscattered power to the total scattered power [6-26], c is the light velocity in vacuum, τ is the pulse width, n is the refractive index of the optical fiber core, B is the bandwidth of the receiver, $\Delta\nu_B$ is the Brillouin linewidth, and $\delta\nu_B$ is required frequency resolution of B-OTDR.

The single-way dynamic range of C-OTDR ($SWDR_{COTDR}$) was given in chapter 2 as

$$SWDR_{\mathrm{COTDR}} = \frac{\left[P_0 + R_R - L_c - P_{\min} + \frac{SNIR_{AVE}}{2} \right]}{2} - M_P \text{ (dB),} \quad (6.6)$$

$$R_R = 10\log\left[\alpha_R S \frac{c\tau}{2n} \right] \text{ (dB),} \quad (6.7)$$

where α_R is the fiber-attenuation coefficient for Rayleigh scattering, and M_P is the margin (in dB) for defining the noise level as 99.7% of the peak noise level, not as a signal-to-noise ratio (SNR) of 1. Assuming a Gaussian noise distribution, 99.7% of all

noise samples are included within three standard deviations. This corresponds to M_P = 2.4 dB.

Combining Eqs. (6.1), (6.3)-(6.5), and (6.7) with Eq. (6.6), the SWDR of B-OTDR is derived as the following:

$$SWDR_{\mathrm{BOTDR}} = SWDR_{\mathrm{COTDR}} + 5\log[\alpha_B/\alpha_R] + 5\log\left[\frac{2B}{\pi\Delta\nu_B}\right] - 5\log\left[\left(\frac{\Delta\nu_B}{\sqrt{2}\delta\nu_B}\right)^4\right] + M_P. \quad (6.8)$$

The minimum required SWDR ($SWDR_{min}$) of C-OTDR for upgrading to B-OTDR is given by the condition of $SWDR_{BOTDR} \geq 0$ in Eq. (6.8), that is,

$$SWDR_{\mathrm{min}} = 5\log[\alpha_R/\alpha_B] - 5\log\left[\frac{2B}{\pi\Delta\nu_B}\right] + 5\log\left[\left(\frac{\Delta\nu_B}{\sqrt{2}\delta\nu_B}\right)^4\right] - M_P. \quad (6.9)$$

For measurement with a 1-μs pulse width, the bandwidth B is 1 MHz and the spatial resolution is 100 m. A strain measurement resolution of 0.02% in the optical fiber corresponds to the required frequency resolution of $\delta\nu_B$ = 9.86 MHz by using a strain coefficient of 493 MHz/% at 1.55 μm [6-12]. For this strain resolution, the calculated $SWDR_{min}$ is over 20 dB, assuming that the parameters are set to typical values: α_B = $1.23\text{x}10^{-6}$ m^{-1}, $\alpha_R = 3.9\text{x}10^{-5}$ m^{-1}, and $\Delta\nu_B$ = 30 MHz. The advanced C-OTDR described in chapter 3 has an SWDR 39 dB with a 100-m spatial resolution. Therefore, this advanced C-OTDR can be applied to measure the strain distribution with a 0.02% resolution over a 90-km-long optical fiber.

6.3. B-OTDR with optical frequency shifter using sideband generation technique

6.3.1. Proposed B-OTDR configuration

Figure 6.5 shows an experimental setup for B-OTDR with an optical frequency shifter using the sideband generation technique. A 1.55-μm distributed feedback laser diode (DFB-LD) with an external cavity had a linewidth of less than 10 kHz. The continuous wave (CW) light from the DFB-LD is divided by a 3-dB fiber coupler (FC1) into two paths: the signal path, and the LO path. The frequency of the signal light is up-shifted by the optical frequency shifter, composed of an LN-PM and a polarization controller (PC). A 1-μs signal pulse is produced by an acousto-optic switch (AO-SW1) operating in pulsed mode and amplified by an EDFA. A second acousto-optic switch (AO-SW2), operating in pulsed mode and synchronized with AO-SW1, eliminates the amplified spontaneous emission from the EDFA. The modulation frequency of both acousto-optic switches is 120 MHz. The up-shifted signal pulse is then launched into a test fiber. The spontaneous Brillouin backscattered light from the test fiber is mixed with the LO light by FC3 and detected by a double-balanced p-i-n field-effect transistor (FET) receiver. A 90-MHz electrical LO mixes the detected signals, and a 1-MHz low-pass filter (LPF) eliminates their high-frequency components. The resulting signals are then introduced into an analog-digital (A-D) converter. The digitized signals are squared and integrated, and finally, displayed on a computer monitor.

6.3.2. Optical frequency shifter using sideband generation technique

Figure 6.6 shows the optical frequency shifter using the sideband generation technique, and the drive conditions for the LN-PM in the shifter. The structure of the optical frequency shifter for B-OTDR, consisting of the 14-GHz-bandwidth LN-PM and a PC, is simple, and in the experiments, the insertion loss was about 3 dB. The PC adjusts the state of polarization (SOP) of the signal light to the transverse magnetic (TM) mode of the LN-PM. The launched signal light, with unit amplitude and optical frequency v_0, is converted to nth-order sideband light with an amplitude of $Jn(\pi V/V_\pi)$ and a frequency of $v_0 + nv_s$ [6-27], where v_s is the modulation frequency, V is the drive voltage of the LN-PM, V_π is the drive voltage at which the signal phase is shifted by half the signal wavelength, and $Jn()$ denotes an nth-order Bessel function. The

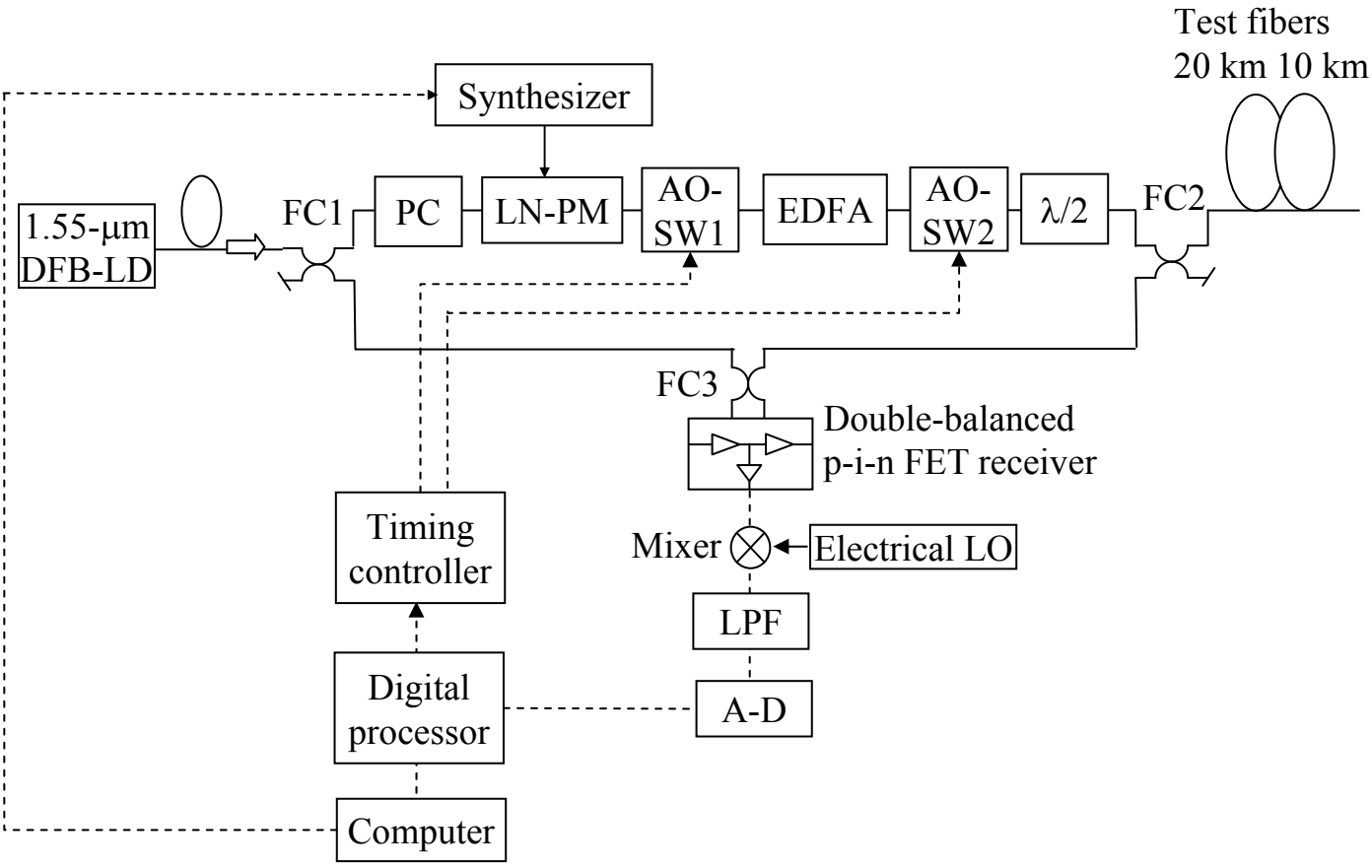

Figure 6.5 Experimental setup for B-OTDR with the sideband generation technique

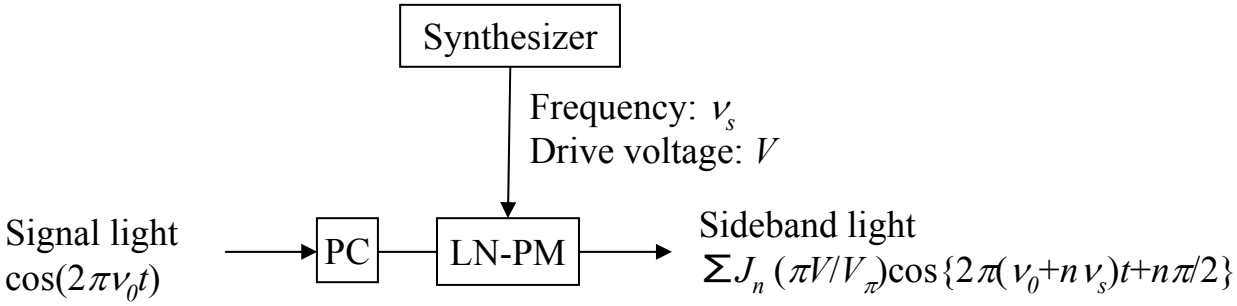

To maximize the cross talk between the fundamental and 1st-order sideband light, tune drive voltage of V such that $\pi V/V_\pi$=2.4048.

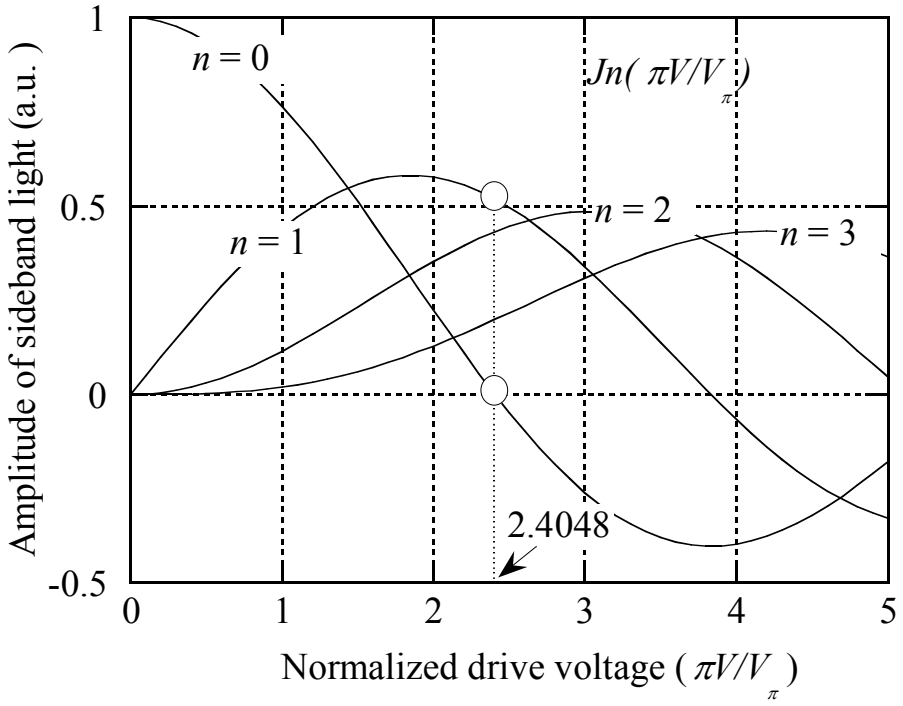

Figure 6.6 Optical frequency shifter using the sideband generation technique, and the drive conditions for the LN-PM in the shifter

Table 6.1 Frequency conditions for LN-PM in B-OTDR

	Beat frequency between backscattered signals and the LO	Detectable beat frequency in B-OTDR receiver	Condition
Brillouin scattering	$n\nu_s + 2\nu_a - \nu_B < B_{IF}$	$\nu_s + 2\nu_a - \nu_B$	n=1
Rayleigh scattering	$n\nu_s + 2\nu_a < B_{IF}$	$2\nu_a$	n=0

generated sideband signals are launched into the acousto-optic modulators (AO-SW1 and AO-SW2 in Fig. 6.5), operating in pulsed mode with a frequency of v_a, and the resulting signal pulse has an optical frequency of $v_0 + nv_s + 2v_a$. When the drive frequency v_s is set near the Brillouin frequency shift v_B, only the first-order sideband signal ($n = 1$) is valid for the optical frequency shifter, because the frequency, $v_s + 2v_a - v_B$, of the beat signal between the Brillouin backscattered signal and the LO light is less than the IF bandwidth of the receiver. The higher-order sideband signals ($n \geq 2$) generate extremely high-frequency beat signals, so the detected beat signals are negligible. Although a beat signal with a frequency of $2v_a$ is also generated between the Rayleigh backscattered light and the LO light by the fundamental signal ($n = 0$), this signal can be eliminated with a conventional electrical filter. This is a significant advantage arising from the use of coherent detection. Table 6.1 summarizes the frequency conditions for the LN-PM in B-OTDR when measuring Brillouin scattering and Rayleigh scattering.

Figure 6.7 shows the spectrum of 10.480-GHz phase-modulated signal light from the LN-PM, measured with a scanning Fabry-Perot interferometer with a free spectral range (FSR) of 8000 GHz and a finesse of 5000. For the result shown in Fig. 6.7(a), the PC adjusted the SOP of the signal light to the transverse electric (TE) mode of the LN-PM, and the fundamental signal was observed. For the result shown in Fig. 6.7(b), the PC adjusted the SOP of the signal light to the TM mode of the LN-PM. First- and second-order sideband signals were generated, and the fundamental signal was sufficiently suppressed. In this case, to maximize the isolation between the first-order sideband signal ($n = 1$) and the fundamental signal ($n = 0$), the drive voltage V was set to $x_0 V_\pi/\pi$, where $x_0 = 2.4048$ was the first zero of the fundamental signal amplitude $J_0(x_0)$.

Optical frequency shift and linewidth of the first-order sideband signal from the LN-PM was measured by using a self-heterodyne laser linewidth measurement technique with a 120-MHz AO modulator and a 50-km delay line [6-28]. The modulation frequency v_s of the LN-PM was set to 10.480 GHz. Figure 6.8 shows the measured power spectrum of the beat signal between the generated first-order sideband signal and the LO light. The frequency of the beat signal was 10.599 998 GHz. The half width at half maximum of the power spectrum was less than 10 kHz, which corresponds to the linewidth of the first-order sideband signal light. Therefore, the frequency resolution of this shifter was as much as twice the linewidth of the B-OTDR source, that is 20 kHz. The frequency stability and repeatability depends on the characteristics of the synthesizer which drives the LN-PM. To evaluate the stability of

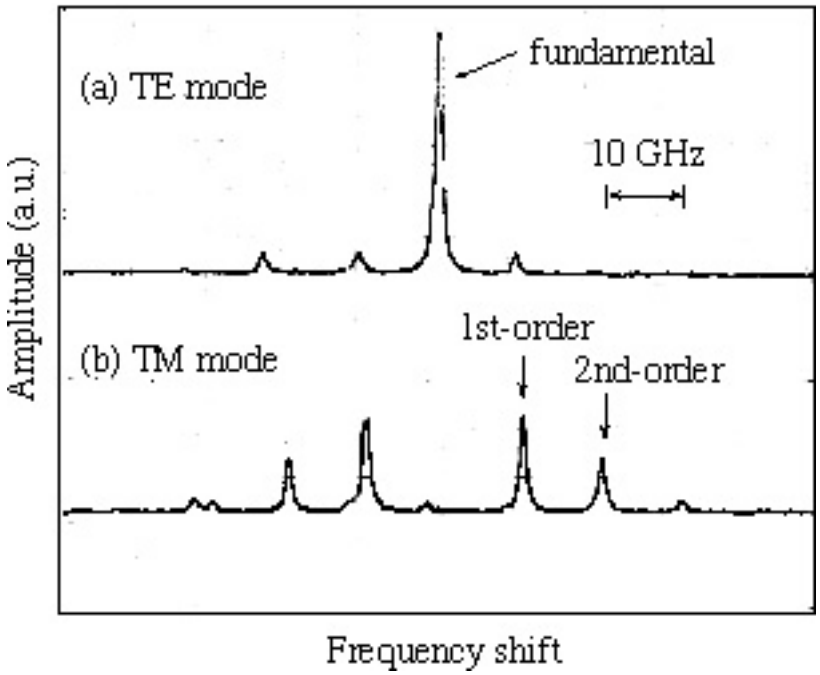

Figure 6.7 Modulated signal spectra

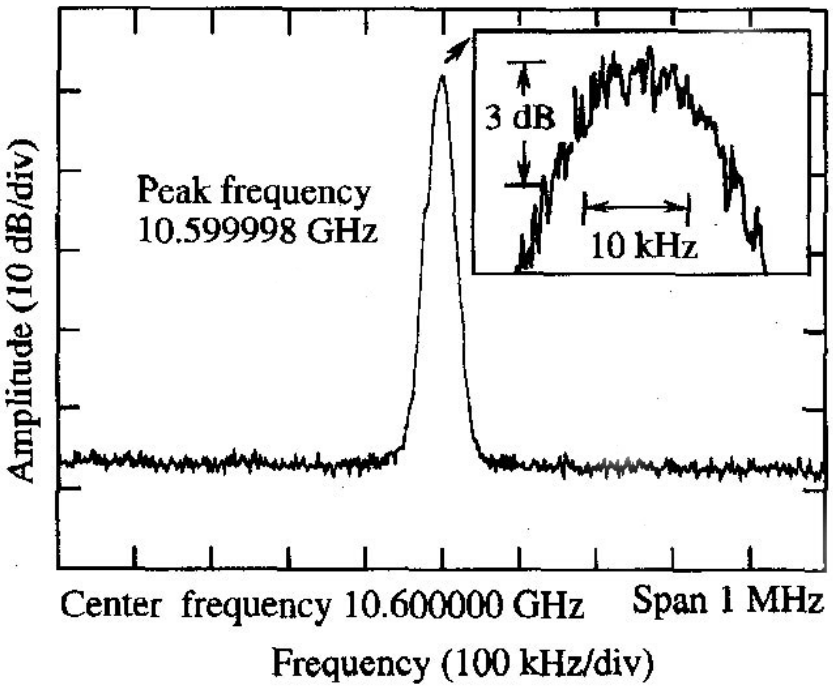

Figure 6.8 Spectrum of the beat signal between the modulated signal and the LO

the shifter's frequency, the spectrum of the beat signal was monitored. The peak frequency was found to change by less than 2 kHz over one hour. This optical frequency shifter, with a high frequency resolution and good stability, can improve the frequency resolution in B-OTDR and enhance the dynamic range of B-OTDR [6-29].

6.3.3. Measurement of distributed tensile strain in optical fiber by B-OTDR

Measurements were performed on a test fiber composed of 20-km and 10-km lengths of DSF. The two fibers were wound around bobbins with a radius of 30 cm and spliced together.

Figure 6.9 shows the measured spontaneous Brillouin backscattered signals for various frequency shifts, each with 2^{16} integrations. To reduce the polarization-dependent fluctuation of the B-OTDR sensitivity, the $\lambda/2$ plate was periodically rotated by 45° every 2^{15} integrations, as described in chapter 4. The optical frequency shift was changed from 10.49 to 10.60 GHz in 10-MHz steps. The peak of the Brillouin spectrum gradually shifted from the input end to the 20-km point. The cause is believed to be the increasing tension in the test fibers wound around the bobbins.

Figure 6.10 shows Brillouin spectra measured with a frequency step of 1 MHz and Lorentzian form fitting curves at: (a) 1 km, (b) 10 km, (c) 19 km, and (d) 25 km. The measured Brillouin frequency shifts in (a)-(d) were (a) 10.537 GHz, (b) 10.542 GHz, (c) 10.556 GHz, and (d) 10.540 GHz, respectively, which are in good agreement with the values measured by Brillouin optical time-domain analysis (B-OTDA) [6-12]. This corresponds to 0.039% strain with a tensile strain coefficient of 493 MHz/% at a wavelength of 1.55 μm [6-12].

Figure 6.11 shows the distribution of the measured Brillouin frequency shift and the relative tensile strain in the test fiber. The fluctuation in the Brillouin frequency shift was ±1 MHz, corresponding to ±0.002% strain fluctuation.

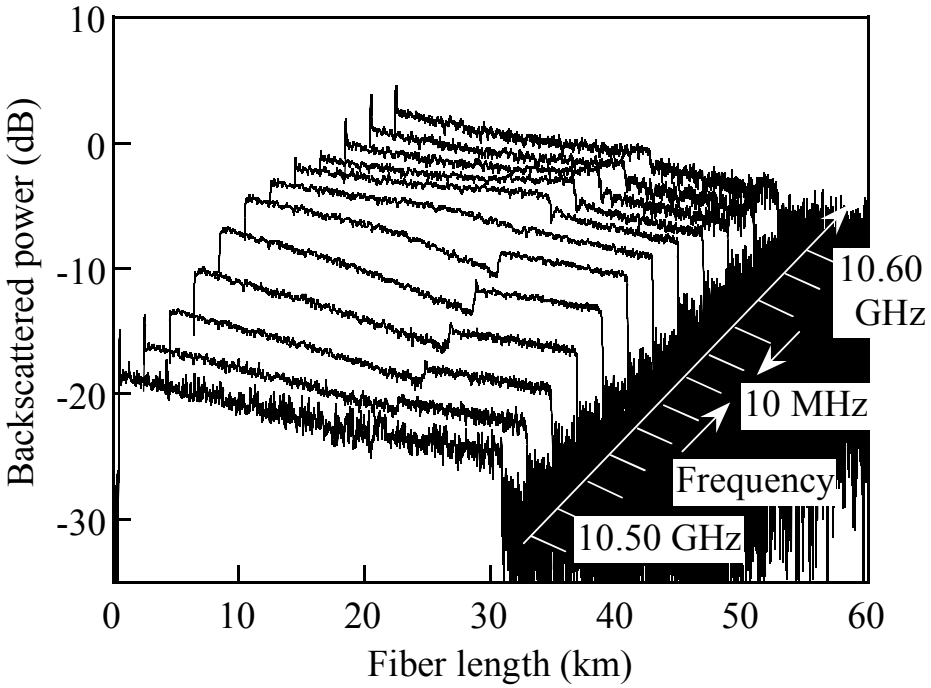

Figure 6.9 Brillouin OTDR traces

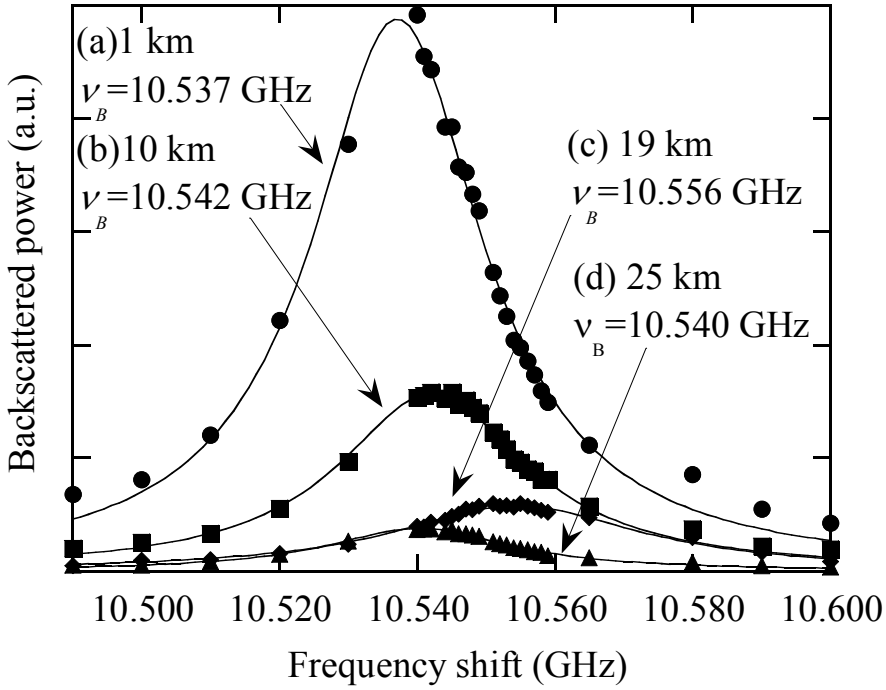

Figure 6.10 Brillouin spectra at (a) 1 km (b) 10 km, (c) 19 km, and (d) 25 km

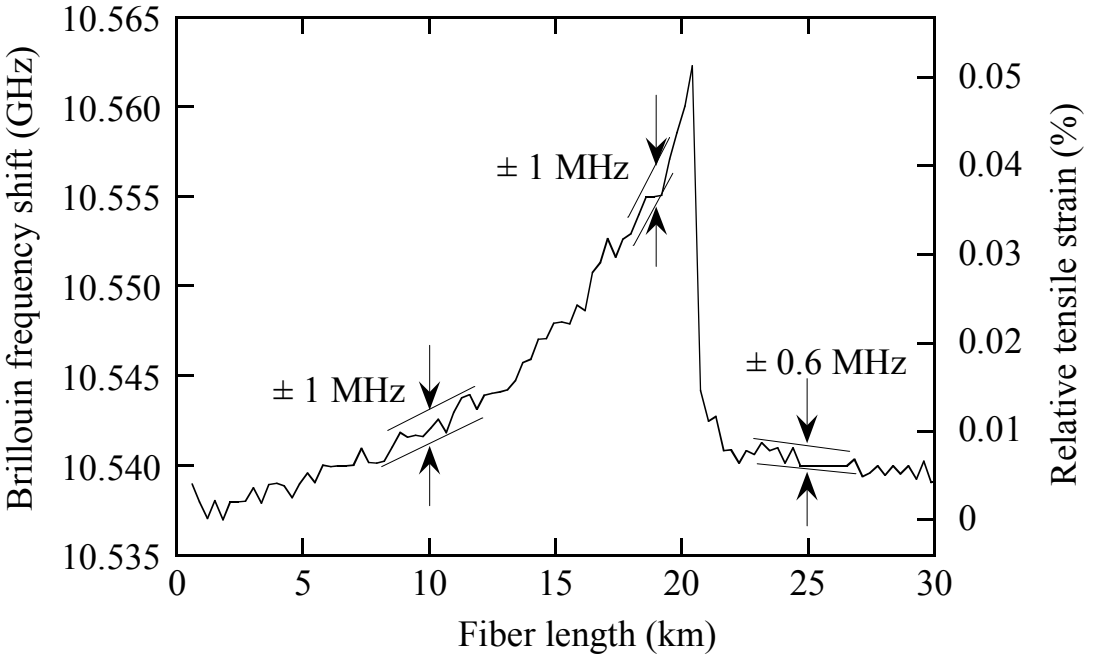

Figure 6.11 Distribution of measured Brillouin frequency shift and relative tensile strain

6.4. B-OTDR using 20-GHz wideband balanced receiver

6.4.1. Configuration of B-OTDR with wideband balanced receiver

Figure 6.12 shows an experimental setup for B-OTDR with a wideband balanced receiver. The 1.55-μm DFB-LD with an external cavity had a linewidth of less than 10 kHz. The CW light from the DFB-LD was amplified by an EDFA and divided by a 98:2 directional FC into two paths: the signal path, and the LO path. The powers of the signal light and LO light are 20 dBm and 7 dBm, respectively. A 1-μs signal pulse is produced by an AO switch (AO-SW) operating in pulsed mode. The modulation frequency of AO-SW is 120 MHz. The probe signal pulse is launched into the test fiber. The spontaneous Brillouin backscattered light from the test fiber is mixed with the LO light by a 3-dB FC and detected by a wideband double-balanced receiver. The wideband balanced receiver has a cutoff frequency of over 20 GHz and a common mode rejection ratio (CMRR) of about 20 dB. The detected signals, with an IF of approximately 11 GHz, are mixed with the electrical LO signal from the synthesizer, and a 1-MHz LPF eliminates their high-frequency parts. The resulting signals are then introduced to an A-D converter. The digitized signals are squared and integrated, and finally displayed on a computer monitor.

6.4.2. Strain measurement in 30-km DSF by B-OTDR with wideband balanced receiver

Figure 6.13 shows the measured Brillouin backscattered signals for various frequency shifts, each with 2^{16} integrations. By changing the synthesizer frequency, the frequency of the electrical LO was changed from 10.520 to 10.600 GHz in 5-MHz steps. The peak frequencies in the Brillouin spectra gradually shifted from the input end to the 20-km point of the fiber, which was wound around a bobbin under tension. Figure 6.14 shows the measured Brillouin spectra and Lorentzian fitting curves at (a) 1 km, (b) 10 km, (c) 19 km, and (d) 25 km. The measured Brillouin frequency shifts were (a) 10.551 GHz, (b) 10.556 GHz, (c) 10.570 GHz, and (d) 10.554 GHz. There was a difference of 19 MHz between the Brillouin frequency shifts for cases (a) and (c). This corresponds to 0.039% strain with a tensile strain coefficient of 493 MHz/% at a wavelength of 1.55 μm, which is in good agreement with the value measured by B-OTDR with an optical frequency shifter, as described in section 6.3.

This B-OTDR has very simple configuration because there is no additional optical

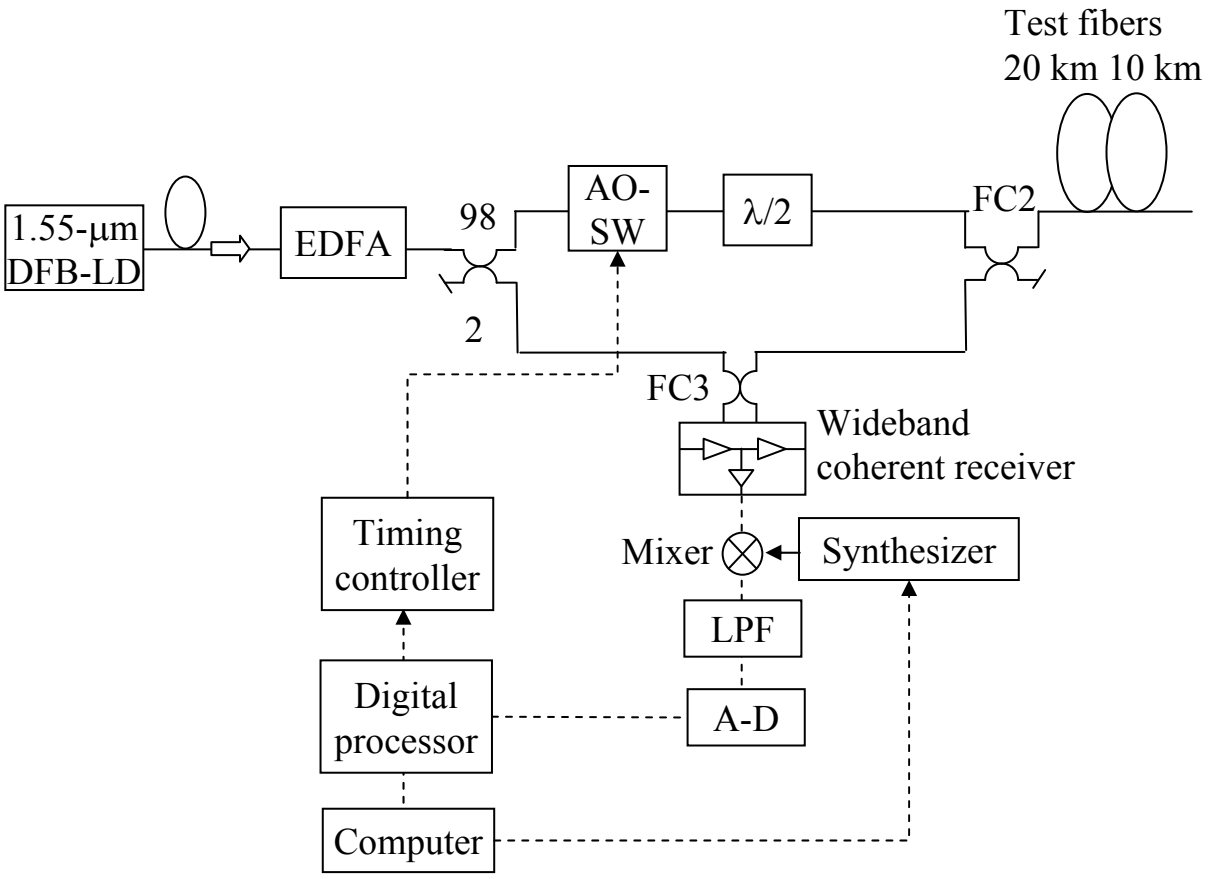

AO-SW: Accousto-optic switch
EDFA: Erbium-doped fiber amplifier
FC: 3-dB optical fiber coupler
λ/2 : Half-wavelength plate
LPF: Low pass filter
A-D: Analog-digital converter

Figure 6.12 Configuration of B-OTDR using wideband coherent receiver

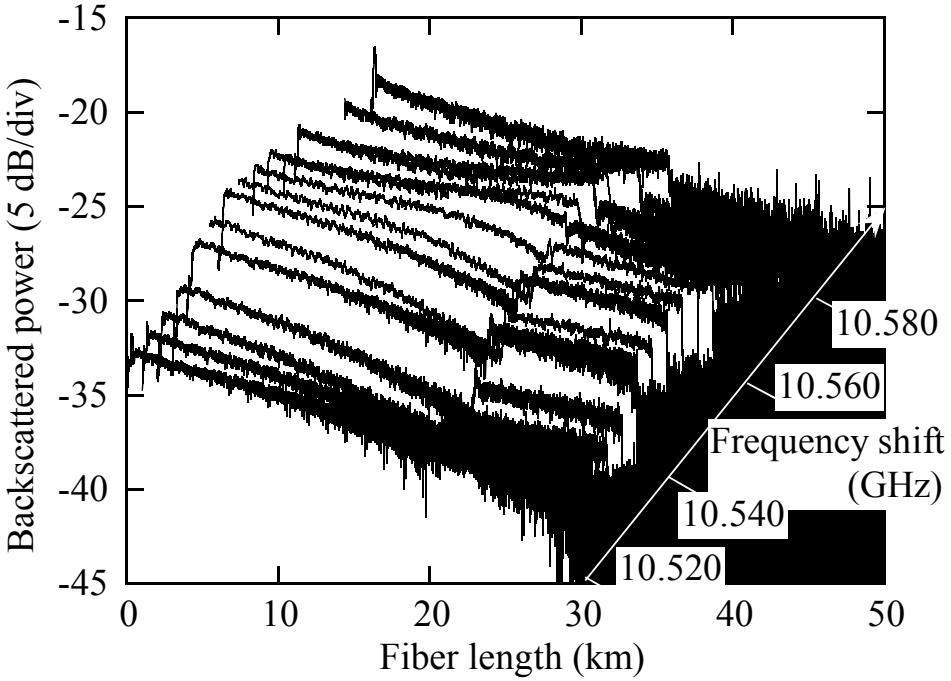

Figure 6.13 B-OTDR traces for a 30-km DSF

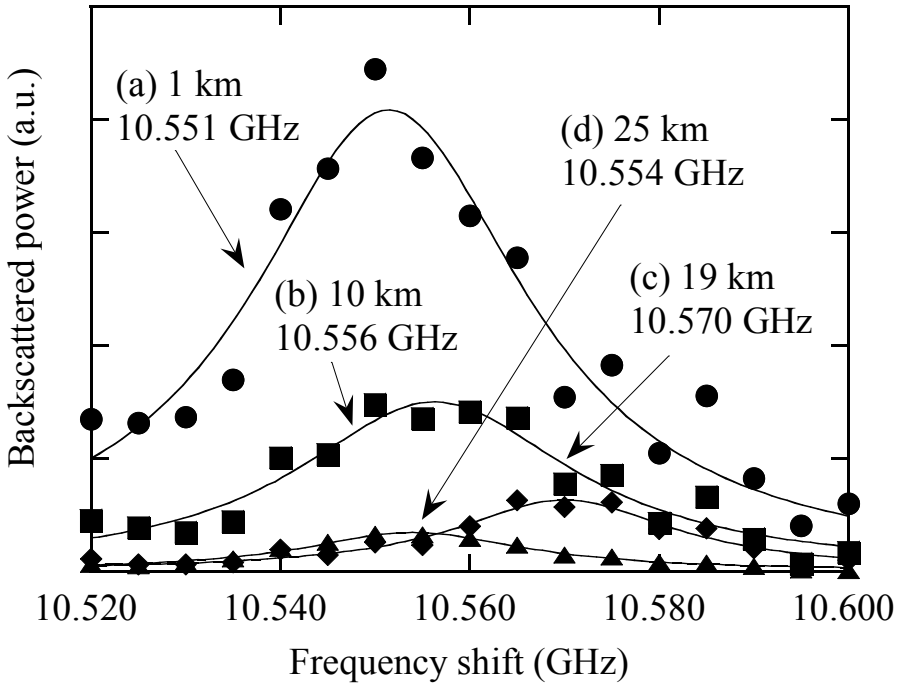

Figure 6.14 Brillouin spectra at (a) 1 km, (b) 10 km, (c) 19 km, and (d) 25 km.

frequency shifter. To improve the dynamic range of B-OTDR, the noise of the wideband balanced receiver should be reduced. For this purpose, one effective approach is incorporating a narrow-bandwidth amplifier with an IF of approximately 11 GHz in the wideband balanced receiver. This approach, however, degrades the capability of loss measurement by detecting the Rayleigh backscattered signal. Current commercial B-OTDR uses this configuration.

6.5. B-OTDR enhanced with synchronous pumped RFA and LN-PM for measuring strain distribution and optical fiber loss

6.5.1. Configuration of 1.65-μm-band B-OTDR

Figure 6.15 shows an experimental setup for 1.65-μm-band B-OTDR using self-heterodyne detection. The 1.647 μm DFB-LD with an external cavity has a linewidth of less than 20 kHz. The signal light is modulated by the LN-PM at a frequency of approximately 10 GHz. The 1st-order upper sideband light from the LN-PM is used as B-OTDR probe light in order to down-shift the Brillouin beat signal frequency. Then, the fundamental light is suppressed by adjusting the LN-PM drive voltage. A 1-μs signal pulse is produced by an AO switch (AO-SW) with a 120-MHz modulation frequency and amplified by a 25-dB-gain RFA using an 8.7-km-long high numerical aperture (NA) single-mode fiber. The RFA is synchronously pumped by a 28-dBm quasi-rectangular pulsed light, generated by a 1.48-μm bidirectionally pumped Er-/Al-co-doped fiber amplifier (denoted as EDFA in Fig. 6.15) and an optical pulse from a 1.54-μm Fabry-Perot laser diode (FP-LD) [6-20],[6-30]. The total power of the 1.65-μm incident signal pulse is about 13 dBm. The spontaneous Brillouin backscattered light generated by the 1st-order sideband light pulse from the test fiber is mixed with the LO light and detected by a double-balanced p-i-n FET receiver in the 210-MHz IF band with 1-MHz bandwidth. The Rayleigh backscattered light can be heterodyne detected in the 120-MHz IF band without driving the LN-PM. In this configuration, the Rayleigh backscattered signals generated by the residual unmodulated light can be suppressed when measuring weak Brillouin signals. The test fiber is formed by splicing together 20-km and 10-km DSFs. These two fibers are wound around bobbins, the former under slight tension and the latter tension free.

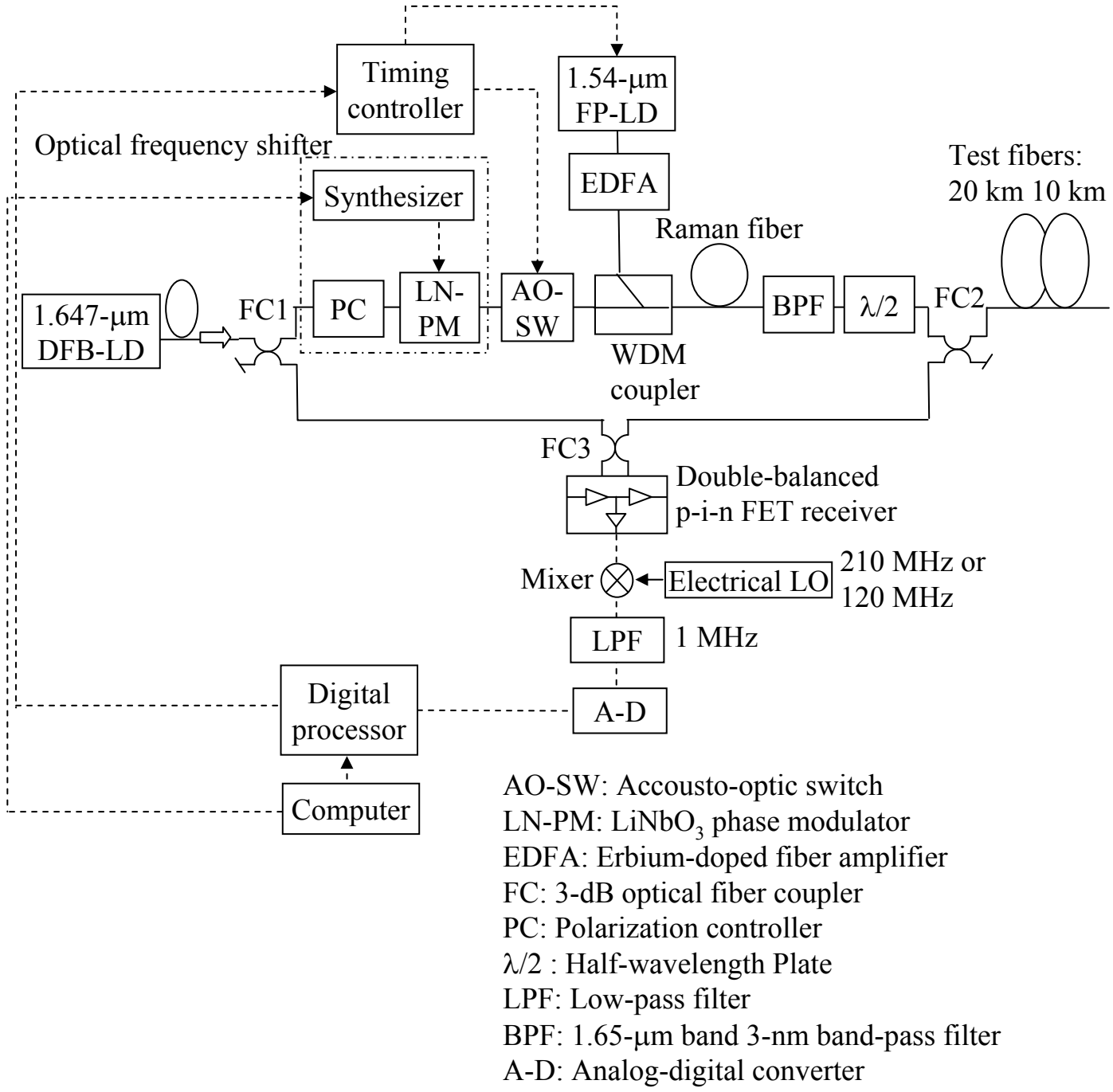

Figure 6.15 Experimental setup for 1.65-μm-band B-OTDR

6.5.2. Measurement of strain distribution and optical fiber loss by 1.65-μm-band B-OTDR

Figure 6.16(1) shows the measured Brillouin backscattered signals for various frequency shifts, each with 2^{16} integrations. The optical frequency shift of the incident signal pulse was changed from 9.89 GHz to 9.97 GHz in 5-MHz steps by changing the modulation frequency of the LN-PM. The peak frequencies in the Brillouin spectra gradually shifted from the input end to the 20-km point of the fiber, which was wound around a bobbin under tension. Figure 6.16(2) shows the measured Brillouin spectra and Lorentzian fitting curves at (a) 10 km, (b) 18.7 km and (c) 25 km. The measured Brillouin frequency shift ν_B was (a) 9.935 GHz, (b) 9.949 GHz, and (c) 9.934 GHz. There was a difference of 14 MHz between the Brillouin frequency shifts for cases (a) and (b), corresponding to 0.03% strain with a tensile strain coefficient of 463 MHz/% at a wavelength of 1.65 μm.

Figure 6.17 shows the measured Rayleigh backscattered signals from a 102-km DSF, with 2^{18} integrations. The signal pulse width was 1 μs. The SWDR was about 30 dB with a 100-m spatial resolution. These results indicate the first successful demonstration of 1.65-μm-band B-OTDR, which is capable of measuring both fiber-distributed strain and optical loss.

6.5.3. Configuration of 1.55-/1.65-μm B-OTDR

In-service testing requires a measurement wavelength differing from the communication signal wavelength. The B-OTDR operating at 1.55 or 1.65 μm for offline and online services, respectively, was constructed. Figure 6.18 shows the experimental setup for 1.55/1.65-μm B-OTDR. The 1.551/1.647-μm DFB-LDs with an external cavity has a linewidth of less than 20 kHz. One port (0) of an optical path switch (OpSW) is open for the 1.55-μm mode. The other port (1) is open for the 1.65-μm mode. An optical frequency shifter operating in the 1.55- and 1.65-μm bands, is constructed with a wavelength-independent bulk-type polarizer (PL) and an LN-PM. The 1.551- and 1.647-μm signal light is modulated at a frequency of approximately 10 GHz. The 1st-order upper sideband light is used as the B-OTDR probe light. The fundamental light is suppressed by adjusting the LN-PM drive voltage. A 1-μs signal pulse is produced by an AO switch (AO-SW) with a 120-MHz modulation frequency. In the 1.55- and 1.65-μm modes, an EDFA is used as an optical fiber amplifier for the 1.55-μm-band signal and for the pump light of an RFA, respectively. The total power

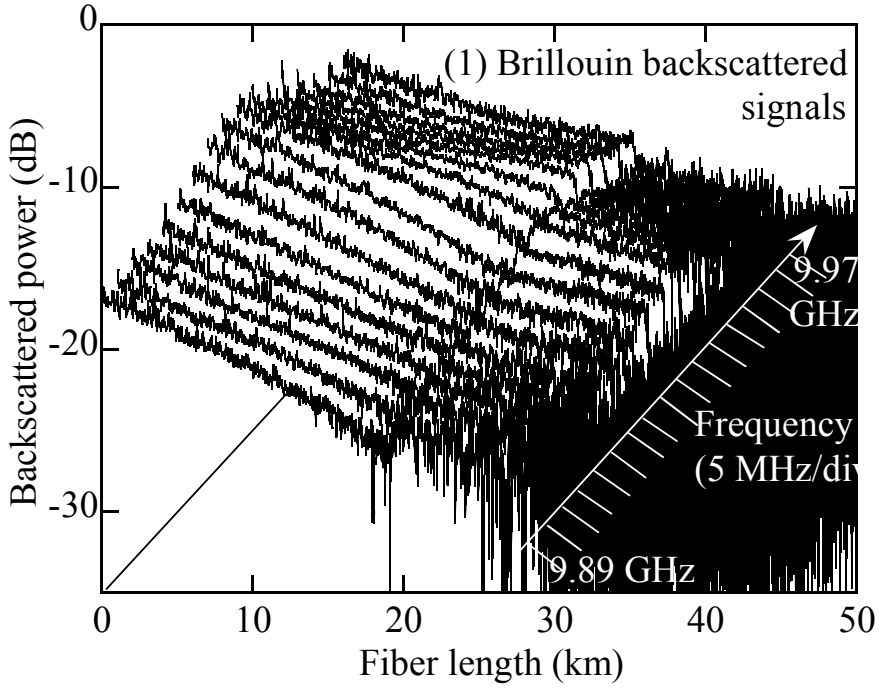

(1) Fiber-distributed Brillouin backscattered signal power vs. optical frequency shift

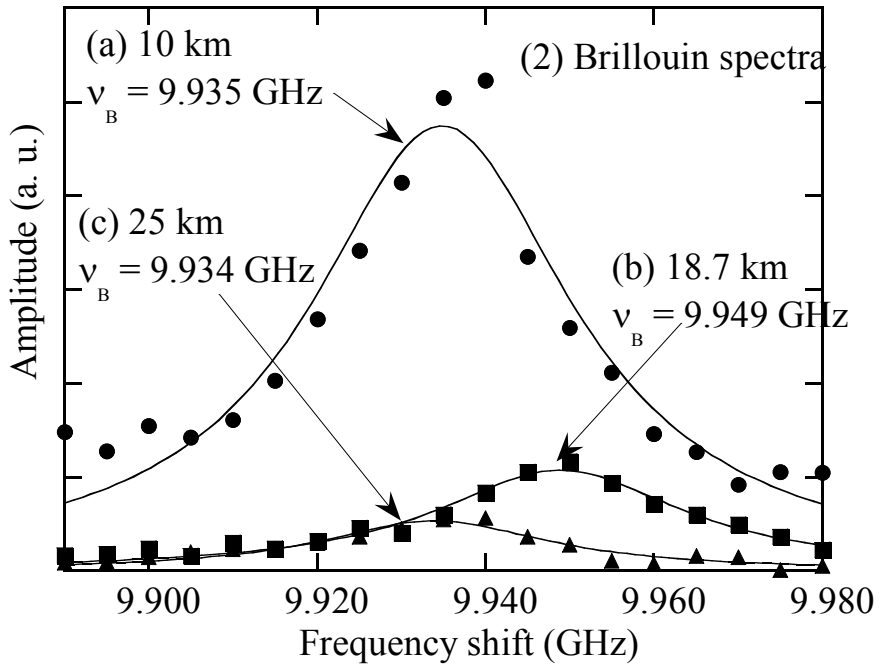

(2) Brillouin spectra at (a) 10 km, (b) 18.7 km, and (c) 25 km

Figure 6.16 1.65-μm B-OTDR traces for a 30-km DSF

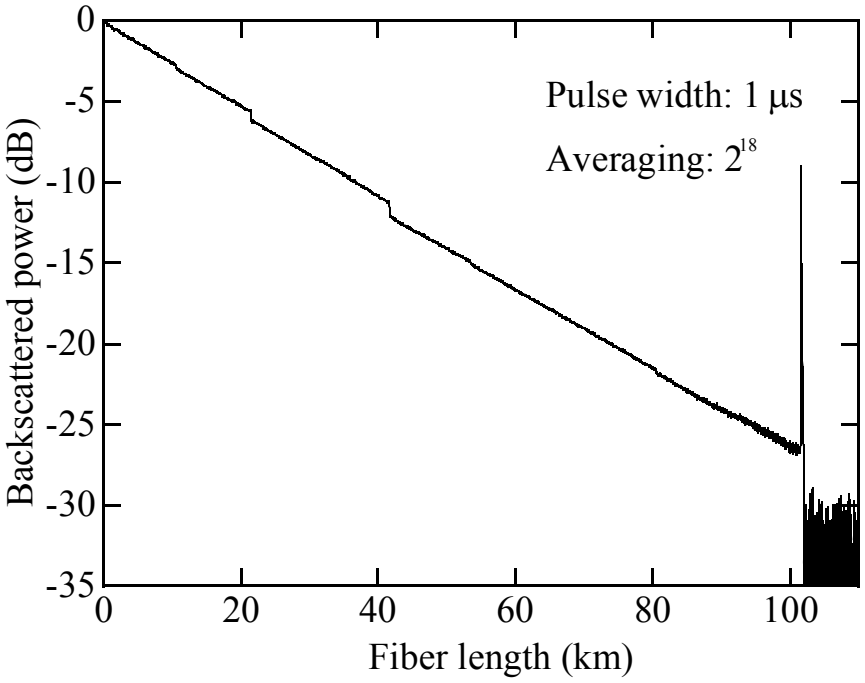

Figure 6.17 Rayleigh backscattered signals from a 102-km DSF

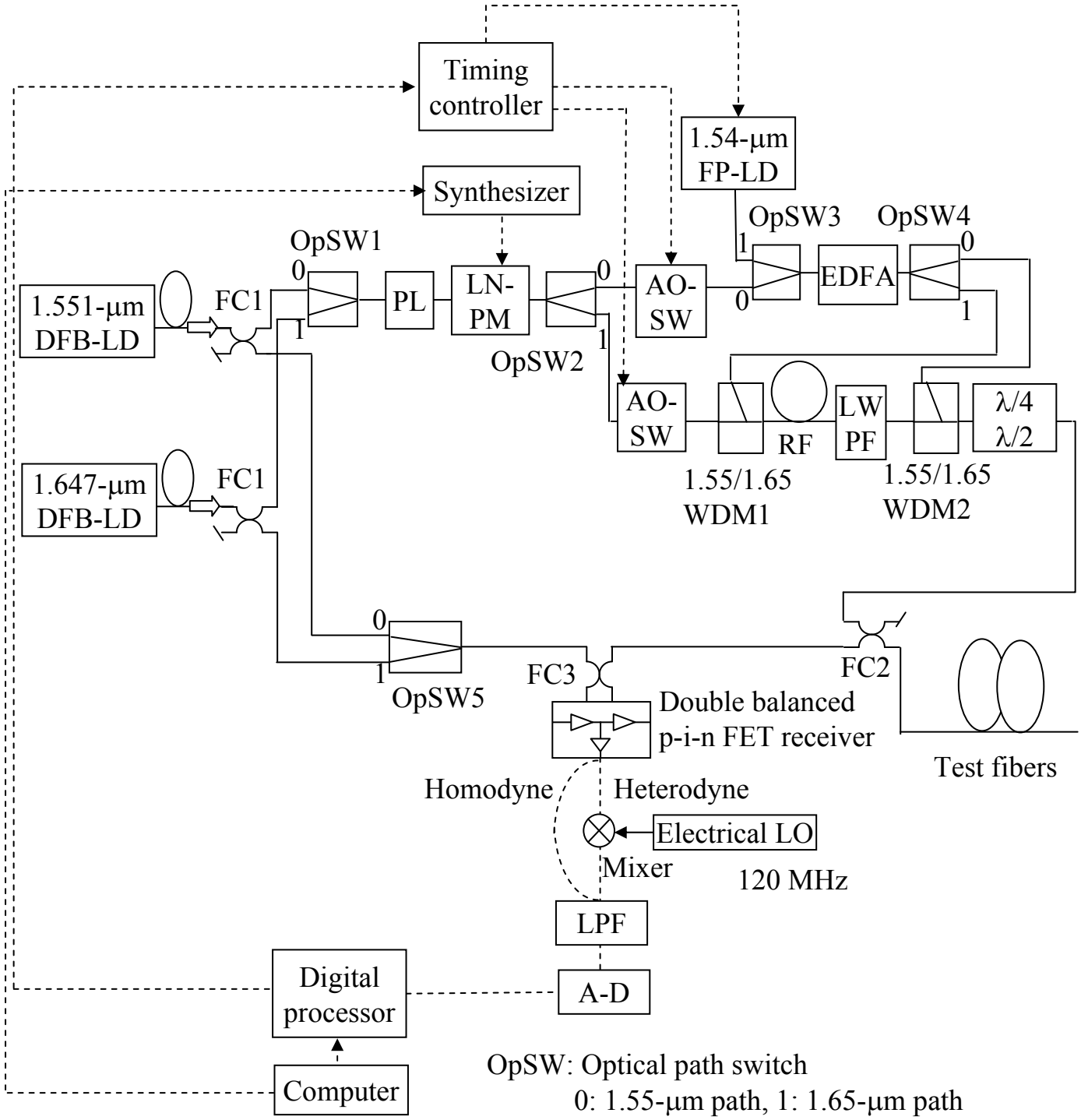

Figure 6.18 Experimental setup for 1.55-/1.65-μm B-OTDR

of the 1.55-/1.65-μm incident signal pulse is about 11 dBm. The spontaneous Brillouin backscattered light is mixed with the LO light and detected by a homodyne receiver with a 1-MHz bandwidth. The Rayleigh backscattered light can be heterodyne detected in the 120-MHz IF band without driving the LN-PM. The test fiber is formed by splicing together 20-km and 10-km DSFs.

6.5.4. Measurement of strain distribution and optical fiber loss by 1.55-/1.65-μm B-OTDR

Figure 6.19 shows the measured Brillouin backscattered signals for various frequency shifts, each with 2^{16} integrations, at (a) 1.55 μm and (b) 1.65 μm. The optical frequency shift step of the incident signal pulse was 5 MHz, obtained by changing the modulation frequency of the LN-PM. The peak frequencies in the Brillouin spectra gradually shifted because of the slight tension. When the wavelength-dependence was taken into account, the measured distribution of the Brillouin frequency shift at 1.55 μm from the 0- to 20-km points was in good agreement with the distribution measured at 1.65 μm.

Figure 6.20 shows the measured Rayleigh backscattered signals from a 102-km DSF, with 2^{18} integrations, at (a) 1.55 μm and (b) 1.65 μm. The signal pulse width was 1 μs. The SWDR was about (a) 33 dB and (b) 30 dB, with a 100-m spatial resolution.

These results confirm the feasibility of the proposed B-OTDR employing the optical frequency shifter incorporating an LN-PM and optical fiber amplifier technologies.

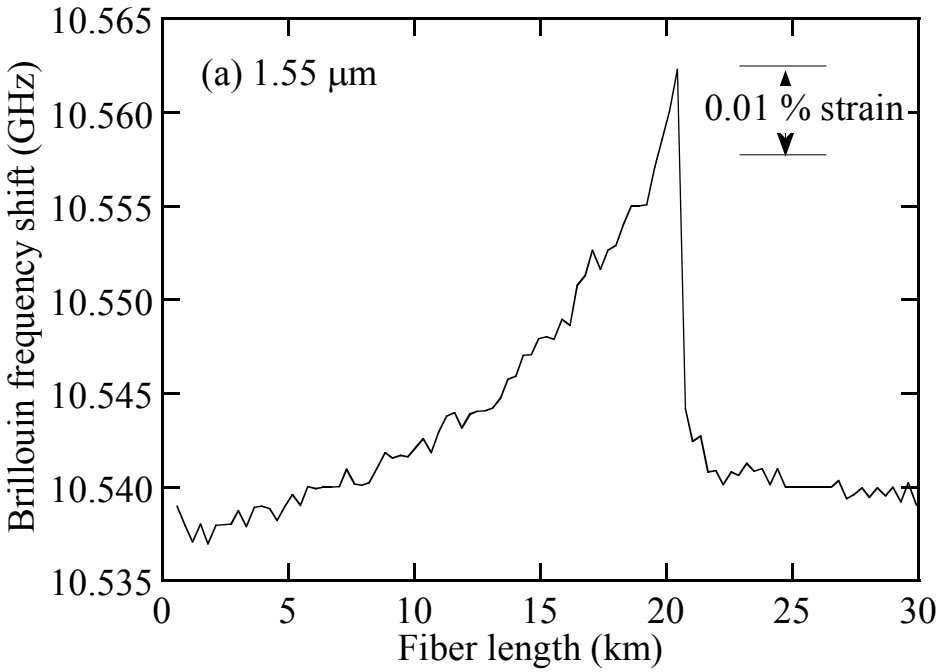

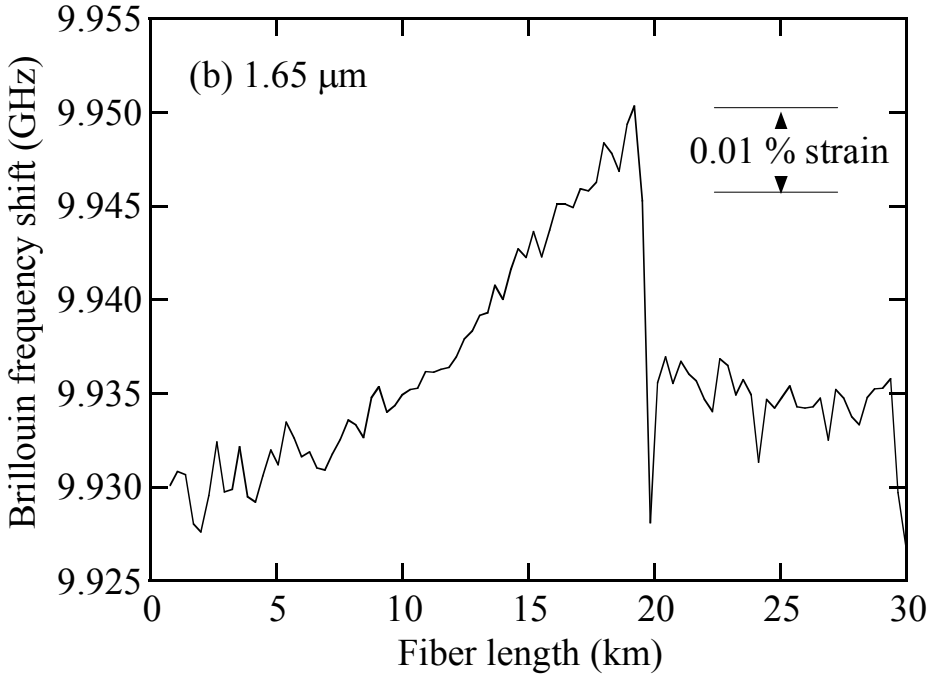

Figure 6.19 B-OTDR traces at (a) 1.55 μm and (b) 1.65 μm

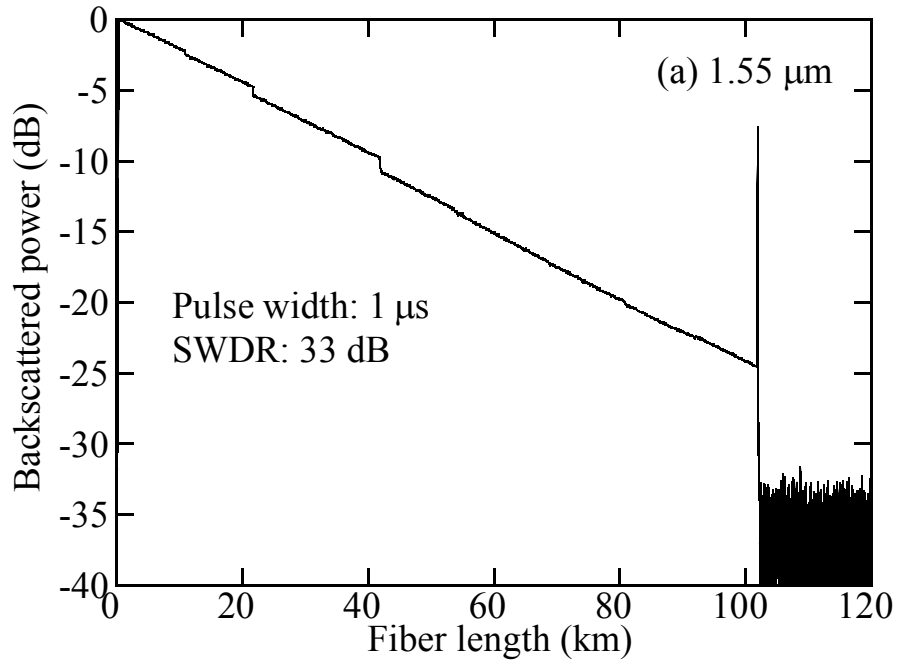

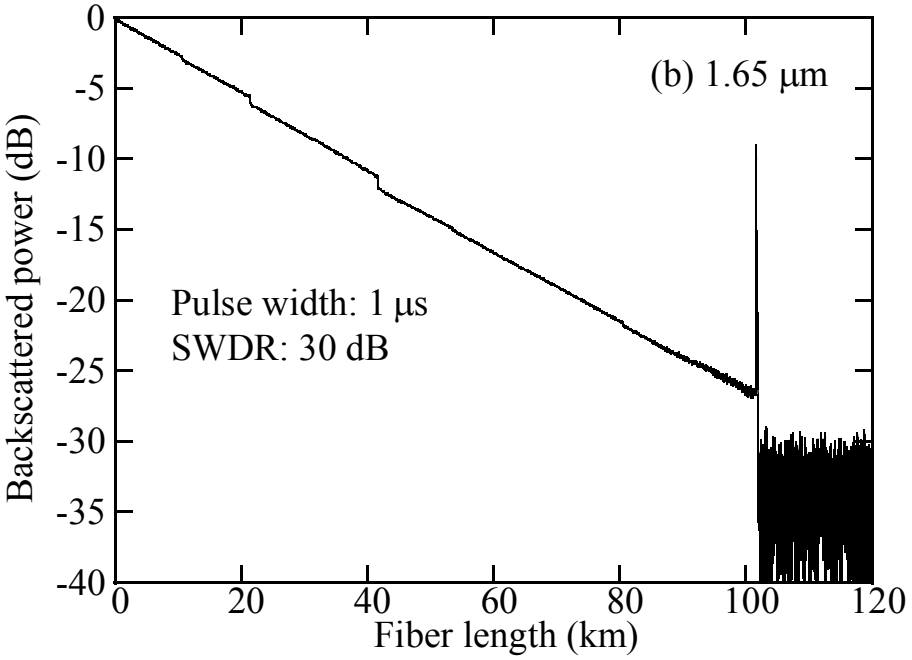

Figure 6.20 Rayleigh backscattered signals from a 102-km DSF at (a) 1.55 μm and (b) 1.65 μm.

6.6. Temperature-dependence reduction method for B-OTDR by simultaneous measurement of Brillouin frequency shift and power

6.6.1. Theoretical background for simultaneously measuring strain and temperature from Brillouin frequency shift and power

Since the Brillouin frequency shift varies with both the strain and the temperature, the accuracy of B-OTDR is degraded by the temperature dependence when measuring the strain distribution to evaluate the reliability of an optical fiber. Use of a tension-free reference fiber is one solution for calibrating the temperature, but this method is not applicable for installed fiber cables. Use of a Raman technique for temperature monitoring [6-31] is another solution, because the Raman scattering coefficient has large temperature dependence and appears to have negligible strain dependence. Simultaneous measurements of the changes in the Brillouin frequency shift ν_B and the changes in the Brillouin scattering coefficient η_B thus provides an attractive way to measure the strain compensating the temperature dependence [6-22],[6-23].

The changes in the Brillouin frequency shift, $\delta\nu_B$, in the Brillouin scattering coefficient, $\delta\eta_B$, and changes in the strain, $\delta\varepsilon$, and in the temperature, δT, are expressed by a matrix equation [6-22],[6-23]:

$$\begin{bmatrix} \delta\nu_{\mathrm{B}} \\ \delta\eta_B \end{bmatrix} = \begin{bmatrix} C1 & C2 \\ C3 & C4 \end{bmatrix} \begin{bmatrix} \delta\varepsilon \\ \delta T \end{bmatrix}, \tag{6.10}$$

where $C1$ and $C2$ are the strain and temperature coefficients of ν_B, and $C3$ and $C4$ are those of η_B. The values of both $\delta\varepsilon$ and δT can be determined by using inversion of the matrix in Eq. (6.10) when $C1C4\text{-}C2C3 \neq 0$.

The values of $C3$ and $C4$ have been reported recently [6-21],[6-23], with the values obtained from the direct detection method and a scanning Fabry-Perot filter. Since coherent detection has a better frequency resolution than that of a Fabry-Perot filter, B-OTDR using coherent detection should have better performance in terms of strain measurement than when a Fabry-Perot filter is used.

6.6.2. Measurement of Brillouin scattering coefficient via strain and temperature

Measurement of the Brillouin scattering coefficient was performed with a setup combining that shown in Fig. 6.15 with another EDFA and an LN intensity modulator (EO-SW) operating in pulsed mode and synchronized with the AO-SW. The EO-SW reshapes the signal pulse and eliminates amplified spontaneous emission (ASE) from the EDFAs. The total power of the 1.55-μm incident signal pulse with a pulse width of 100 ns is about 18 dBm. The spontaneous Brillouin backscattered light is detected using a homodyne receiver with a 10-MHz bandwidth.

The three-section test fiber consists of a 510-m UV-coated 0.25-mm-ϕ single-mode optical fiber, which is tension free. The second section of the test fiber was placed in an oven whose temperature was controlled from 10 to 50°C. The other sections remained at a room temperature of about 28°C.

The Brillouin backscattered signals were measured for various frequency shifts, each with 2^{18} integrations. Figure 6.21 shows that the Brillouin frequency shift in section 2 varied as a function of temperature. Figure 6.22 shows the measured Brillouin spectra and Lorentzian fitting curves for section 2 at (a) 10, (b) 20, (c) 30, (d) 40, and (e) 50°C. Figure 6.23 shows that the temperature coefficient for ν_B was $C2$ = 1.08 MHz/°C. As the temperature increased, the peak power of the Brillouin spectrum increased, while the linewidth decreased. Figure 6.24 shows the temperature coefficient for η_B as a function of temperature. The temperature coefficient of the total Brillouin scattering power was 0.39%/°C. This agrees well with the previously reported values of 0.32%/°C [6-21] and 0.36%/°C [6-23].

After this investigation, simultaneous measurement of strain-induced changes in ν_B and η_B by the coherent detection method was performed and reported in a co-authored paper [6-24]. The strain coefficient $C4$ was found to be -7.8%/% (strain), which is in good agreement with the previously reported value of -7.7%/% (strain) [6-23].

Finally, Figure 6.25 shows a viewgraph of the prototype 1.55-μm B-OTDR enhanced with the proposed optical frequency shifter.

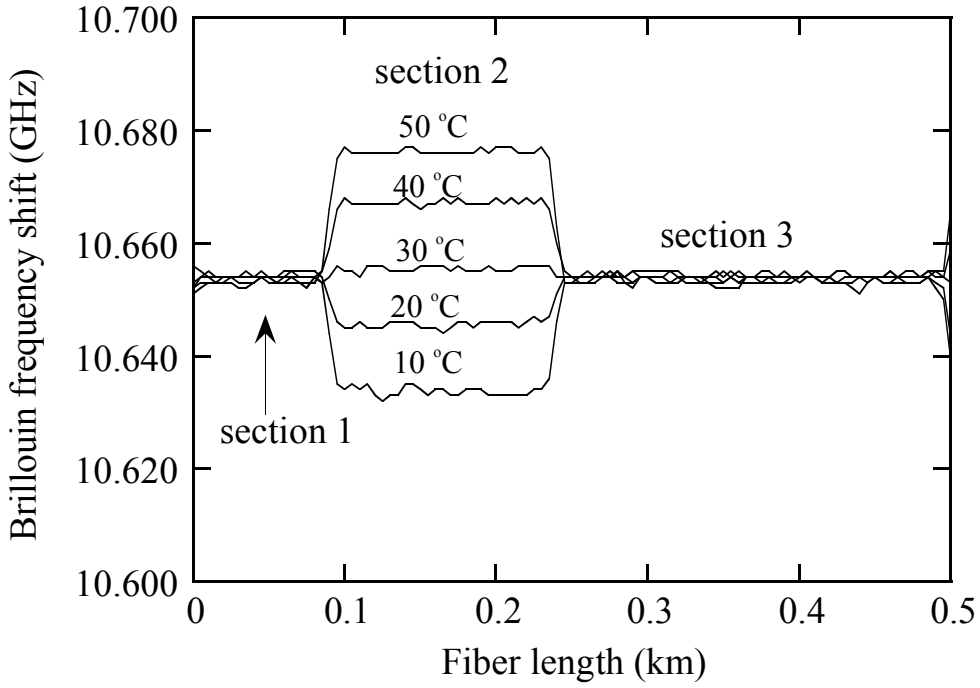

Figure 6.21 Brillouin frequency shift distribution

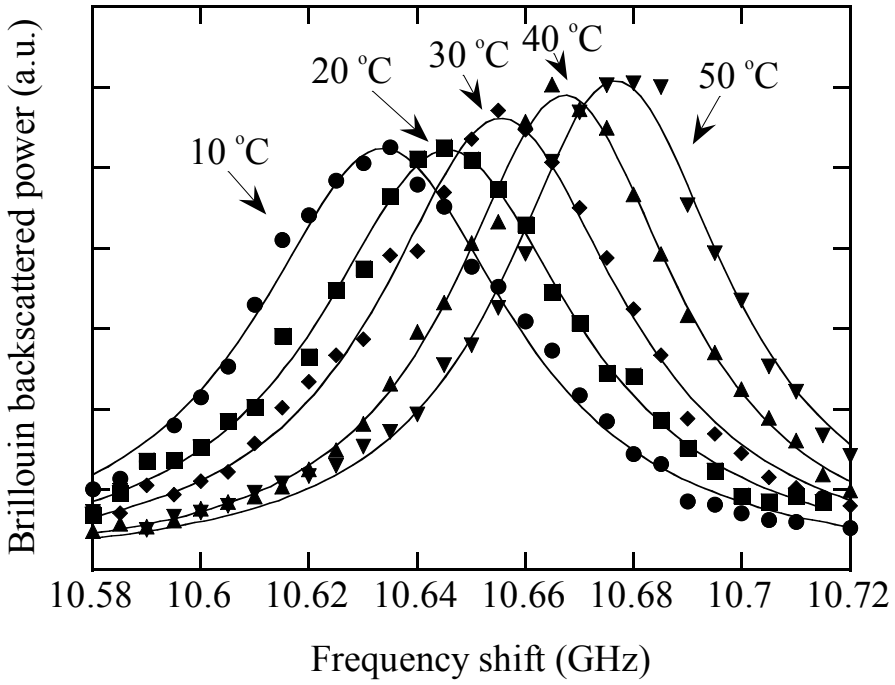

Figure 6.22 Measured Brillouin spectra and Lorentzian form fitting curves for section 2 at (a) 10ºC, (b) 20ºC, (c) 30ºC, (d) 40ºC and (e) 50ºC

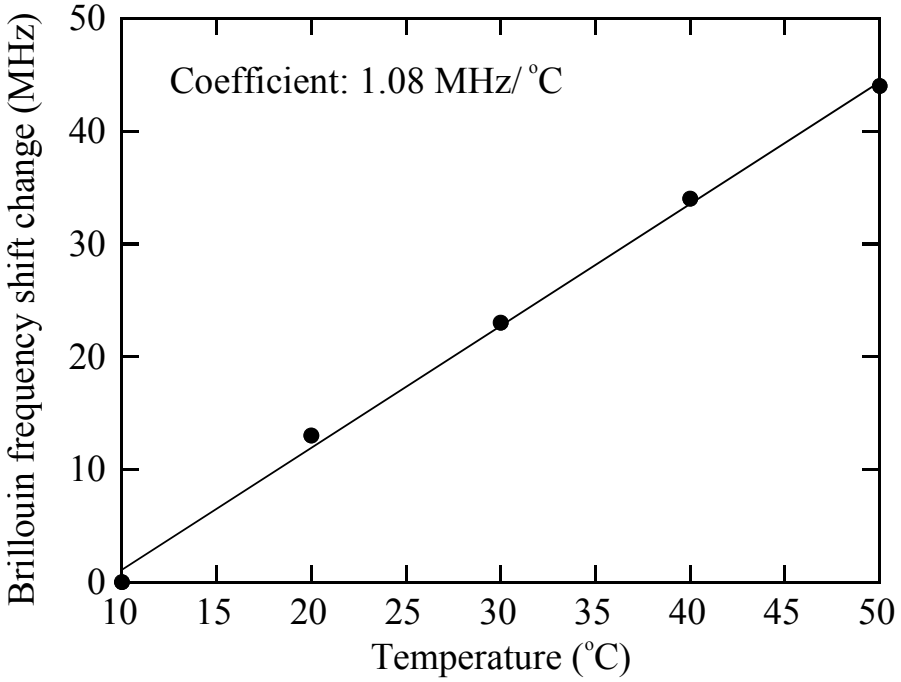

Figure 6.23 Brillouin frequency shift as a function of temperature

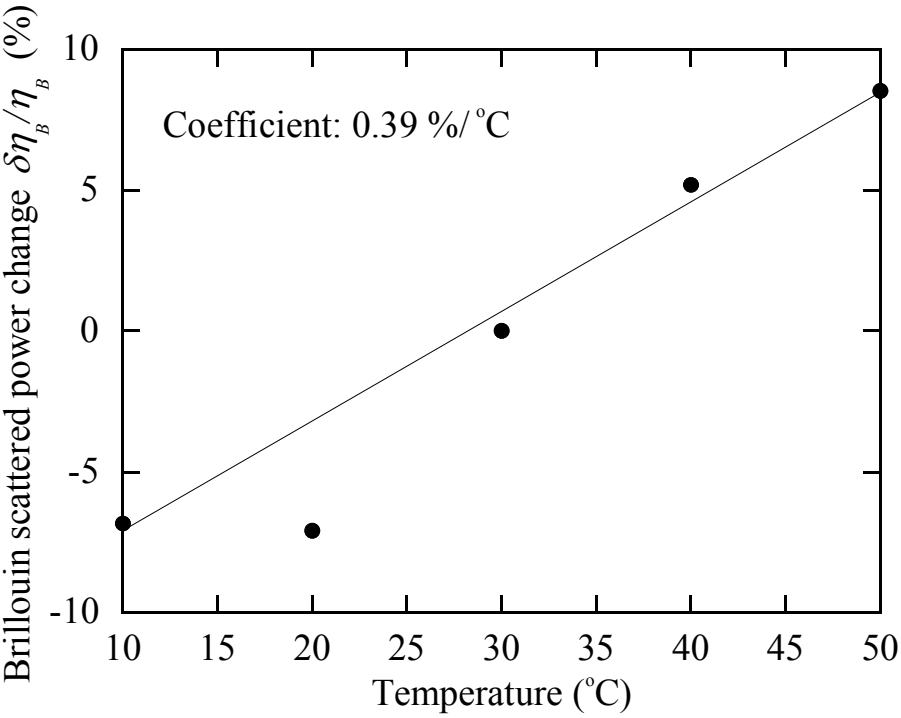

Figure 6.24 Brillouin backscattered power change as a function of temperature

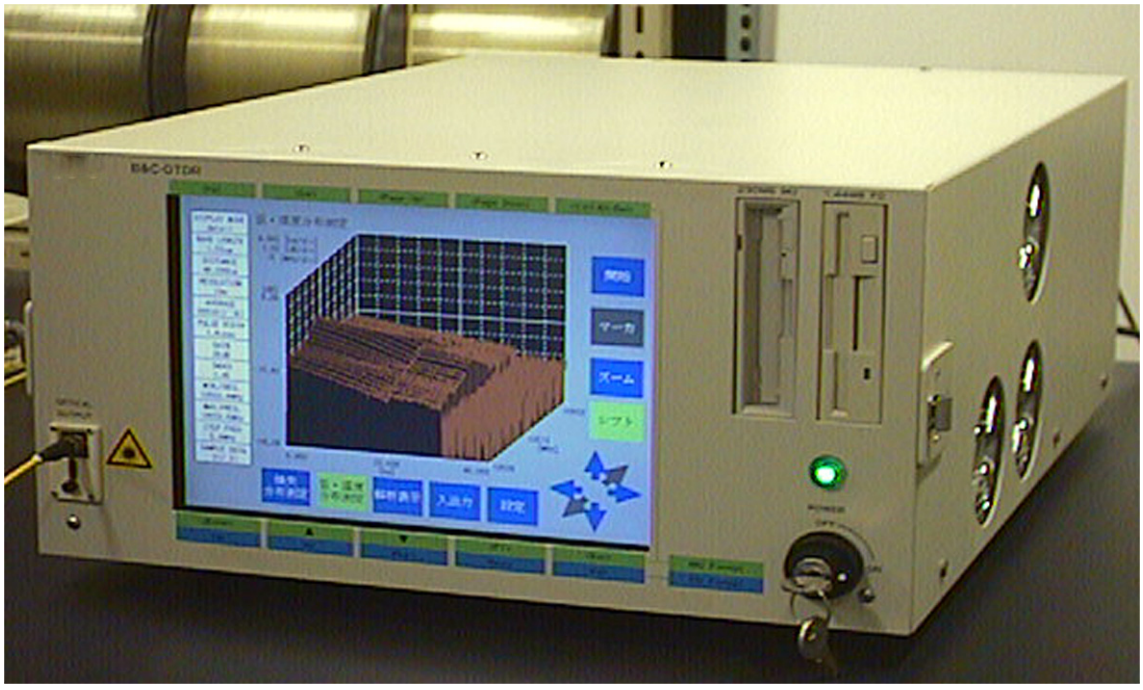

Figure 6.25 Photograph of the prototype 1.55-μm B-OTDR

6.7. Conclusions

This chapter described the applications of the highly developed C-OTDR for distributed strain measurement in an optical fiber, in order to evaluate the reliability of optical fiber networks. The following conclusions were obtained:

(1) The required SWDR for upgrading C-OTDR to B-OTDR was theoretically investigated, and it was found that an SWDR of over 20 dB was required to measure a 0.02% strain distribution in an optical fiber. By applying the highly developed C-OTDR discussed in chapters 2 and 3 through B-OTDR, the strain in a 90-km fiber could be measured from one end of the test fiber, with a spatial resolution of 100 m.

(2) The use of an optical frequency shifter for B-OTDR, with high frequency resolution and good stability achieved by using the sideband generation technique with a 14-GHz-bandwidth LN-PM, was proposed and demonstrated. This shifter has the potential to improve the frequency resolution in B-OTDR and enhance the dynamic range. The optical frequency shifter was thus applied in B-OTDR, and the distributed tensile strain in a 30-km DSF was measured with 100-m spatial resolution.

(3) The feasibility of B-OTDR using a 20-GHz wideband balanced receiver was also demonstrated, thus validating the basic approach used in current commercial B-OTDR.

(4) A 1.65-μm-band B-OTDR, capable of measuring both fiber-distributed strain and optical loss, was demonstrated for the first time. The feasibility of measuring the strain and optical fiber loss distributions in 30- and 100-km optical fibers in both the 1.55- and 1.65-μm bands was also confirmed.

(5) Through simultaneous measurement of ν_B and η_B to separate the strain and temperature, a temperature coefficient for η_B of 0.39%/ºC was found by 1.55-μm coherent B-OTDR. This result demonstrates a novel method for compensating the temperature dependence in B-OTDR measurement.

6.8. References

[6-1] I. Sankawa, Y. Koyamada, S. Furukawa, T. Horiguchi, N. Tomita, and Y. Wakui, "Optical fiber line surveillance system for preventive maintenance based on fiber strain and loss monitoring," IEICE Transactions on Communications, vol. E76-B, no. 4, pp. 402-409, 1993.

[6-2] Y. Mitsunaga, Y. Katsuyama, and Y. Ishida, "Reliability assurance for long length optical fibre based on proof testing," Electron. Lett., vol. 17, no. 16, pp. 567-568, 1981.

[6-3] Y. Mitsunaga, Y. Katsuyama, H. Kobayashi, and Y. Ishida, "Failure prediction for long length optical fibre based on proof testing," J. Appl. Phys., vol. 53, no. 7, pp. 4847-4853, 1982.

[6-4] T. Horiguchi, T. Kurashima, and M. Tateda, "Tensile strain dependence of Brillouin frequency shift in silica optical fibers," IEEE Photon. Technol. Lett., vol. 1, no. 5, pp. 107-108, 1989.

[6-5] D. Culverhouse, F. Farahi, C. N. Pannell, and D. A. Jackson, "Potential of stimulated Brillouin scattering as sensing mechanism for distributed temperature sensors," Electron. Lett., vol. 25, no. 14, pp. 913-915, 1989.

[6-6] T. Horiguchi, K. Shimizu, T. Kurashima, M. Tateda, and Y. Koyamada, "Development of a distributed sensing technique using Brillouin scattering," IEEE J. Lightwave Technol., vol. 13, no. 7, pp. 1296-1302, 1995.

[6-7] G. P. Agrawal, "Nonlinear Fiber Optics," San Diego, CA: Academic.

[6-8] D. Cotter, "Stimulated Brillouin scattering in monomode fiber," J. Opt. Commun., vol. 4, no. 1, pp. 10-19, 1983.

[6-9] T. Horiguchi, T. Kurashima, and M. Tateda, "Nondestructive measurement of optical-fiber tensile strain distribution based on Brillouin spectroscopy," Trans. IEICE Japan, vol. J73-B-I, no. 2, pp. 144152, 1990.

[6-10] T. Kurashima, T. Horiguchi, H. Izumita, S. Furukawa, and Y. Koyamada, "Brillouin optical-fiber time domain reflectometry," Trans. IEICE Jpn., vol. E76-B, no. 4, pp. 382-390, 1993.

[6-11] T. Horiguchi, T. Kurashima, and M. Tateda, "A technique to measure distributed strain in optical fibers," IEEE Photon. Technol. Lett., vol. 2, no. 5, pp. 352-354, 1990.

[6-12] T. Kurashima, T. Horiguchi, M. Tateda, and Y. Koyamada, "Large extension of dynamic range in distributed-fiber strain measurement using Brillouin spectroscopy," in the proc. of CLEO'91, CThN5, 1991.

[6-13] M. Niklès, L. ThBvenaz, and P. A. Robert, "Measurement of the distributed Brillouin-gain spectrum in optical fibers by using a single laser source," in tech. dig. of OFC'94, pp. 89-90, paper WFI, 1994.

[6-14] M. Niklès, L. ThBvenaz, and P. A. Robert, "Simple distributed temperature sensor based on Brillouin gain spectrum analysis," in the proc. of OFS'94, pp. 138-140, 1994.

[6-15] M. Niklès, L. ThBvenaz, and P. A. Robert, "Simple distributed fiber sensor based on Brillouin gain spectrum analysis," Opt. Lett., vol. 21. no. 10, pp. 758-760, 1996.

[6-16] K. Shimizu, T. Horiguchi, Y. Koyamada, and T. Kurashima, "Coherent self-heterodyne Brillouin OTDR for measurement of Brillouin frequency shift distribution in optical fibers," IEEE J. lightwave Technol., vol. 12, no. 5, pp. 730-736, 1994.

[6-17] N. Tomita, "Photonic sensing technologies for fiber networks," in the proc. of OFS-11, Tu2-S1, pp. 20-23, 1996.

[6-18] E. Cottino, P. G. Peret, and A. Zucchinali, "1625 nm OTDR monitoring in the optical links for telecommunications," in the proc. of OFS-11, 1996, pp. 38-41.

[6-19] N. Nakao, H. Izumita, T. Inoue, Y. Enomoto, N. Araki, and N. Tomita, "Maintenance method using 1650-nm wavelength band for optical fiber cable networks," IEEE J. Lightwave Technol., vol. 19, no. 10, pp. 1513-1520, 2001.

[6-20] T. Sato, T. Horiguchi, and Y. Koyamada, "1.6 μm band coherent optical time-domain reflectometry," in the proc. of 10th IMCT'94, pp. 102-105, 1994.

[6-21] P. C. Wait and T. P. Newson, "Reduction of coherent noise in the Landau Placzek ratio method for distributed fibre optic temperature sensing," Opt. Comm., vol. 131., pp. 285-289, 1996.

[6-22] T. Horiguchi, "Brillouin scattering for strain and temperature," Section 14.2, pp. 313-329, in J. Dakin and B. Culshaw eds., "Optical Fiber Sensors Volume Four Applications, Analysis, and Future Trends," Artech House, Inc., 1997.

[6-23] T. R. Parker, M. Farhadiroushan, V. A. Handerek, and A. J. Rogers, "Temperature and strain dependence of the power level and frequency of spontaneous Brillouin scattering in optical fibers," Opt. Lett., vol. 22, no. 11, pp. 787-789, 1997.

[6-24] T. Kurashima, T. Horiguchi, H. Ohno, and H. Izumita, "Strain and temperature characteristics of Brillouin spectra in optical fibers for distributed sensing techniques," in the proceeding of 24th European Conference on Optical Communication, vol. 1, pp. 149-150, 1998.

[6-25] T. C. Rich and D. A. Pinnow, "Evaluation of fiber optical waveguides using Brillouin spectroscopy," Appl. Opt., vol. 13, no. 6, pp. 1376-1378, 1974.

[6-26] K. Aoyama, K. Nakagawa, and T. Itoh, "Optical time-domain reflectometry in a single-mode fiber," IEEE J. Quantum Electron., vol. QE-17, no. 6, pp. 862-868, 1981.

[6-27] A. Yariv, "Introduction To Optical Electronics," New York: Holt, Rinehart and Winston, Inc.

[6-28] T. Okoshi, K. Kikuchi, and A. Nakayama, "Novel method for high resolution measurement of laser output spectrum," Electron. Lett., vol. 16, no. 16, pp. 630-631, 1980.

[6-29] J. Dhliwayo and D. J. Wedd, "Temperature error analysis for distributed temperature sensor based on stimulated Brillouin scattering," in the proc. of. OFS-11, pp. 554-557, 1996.

[6-30] T. Sato, T. Horiguchi, M. Tateda, Y. Koyamada, and H. Izumita, "Spectral-linewidth broadening in synchronous Raman fiber amplification caused by cross-phase modulation effects and its suppression," Optics Lett., vol. 22, no. 12, pp. 880-882, 1997.

[6-31] J. P. Dakin, D. J. Pratt, G. W. Bibby, and J. N. Ross, "Distributed optical fiber Raman temperature sensor using a semiconductor light source and detector," Electron. Lett., vol. 21, no. 13, pp. 569-570, 1985.

Chapter 7. Applications: optical fiber maintenance support, monitoring and testing system with advanced functions using highly developed OTDR technologies

This chapter clarifies the fundamental requirements, methods, and criteria for maintaining various types of access networks (i.e., PONs, and ring networks) and trunk networks carrying high-power signals. It also describes the recent development of an optical fiber maintenance support, monitoring, and testing system in accordance with these requirements. The future target technologies for this system, including optical time-domain reflectometry (OTDR) technologies described in chapters 5 and 6, provide advanced functions of this system.

7.1. Introduction

Broadband optical access services have been commercially available in Japan since 2000 [7-1], [7-2]. The number of broadband service users has increased rapidly [7-3]-[7-5], exceeding 28 million by the end of September, 2007, including over 10 million fiber to the home (FTTH) service users [7-6]. Broadband network provision currently requires a central office to accommodate thousands of optical fibers for access networks [7-7]. An optical fiber maintenance support, monitoring, and testing system is essential for reducing construction and maintenance costs and improving service reliability. The automatic optical fiber operations support system, called AURORA, has already been deployed in the optical fiber networks of NTT, Japan [7-8], [7-9]. This system must be further developed for application with wideband transmission systems and various network topologies, as shown in Figure 7.1.

Access networks with several topologies, including passive optical networks (PONs) [7-5] and ring networks using add-drop multiplexers (ADMs) [7-10], [7-11], have been installed in the field because of the diversification of optical communication services. The point-to-multipoint and ring network architectures are very important in terms of constructing optical fiber networks both effectively and inexpensively. The testing and maintenance method based on OTDR for conventional single-star networks [7-12], [7-13], however, cannot be adapted to these network architectures. To test and maintain optical fiber networks effectively, it is necessary to establish identical maintenance criteria for both point-to-multipoint and ring networks.

For trunk networks, trunk line communication traffic is growing quickly because of the expansion of FTTH services. To meet the demand for increased transmission

(a) Point-to-point (single star)

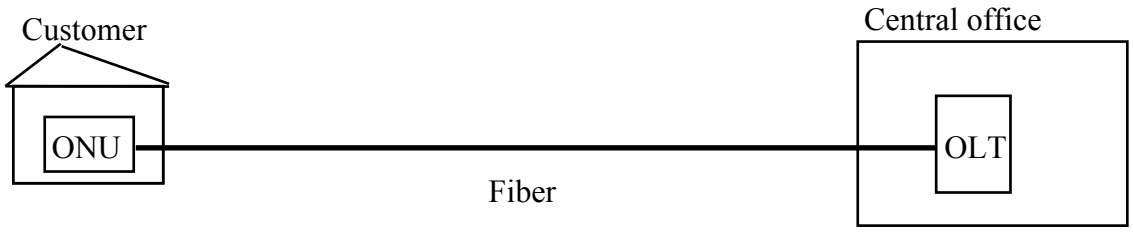

(b) Point-to-multipoint (PON)

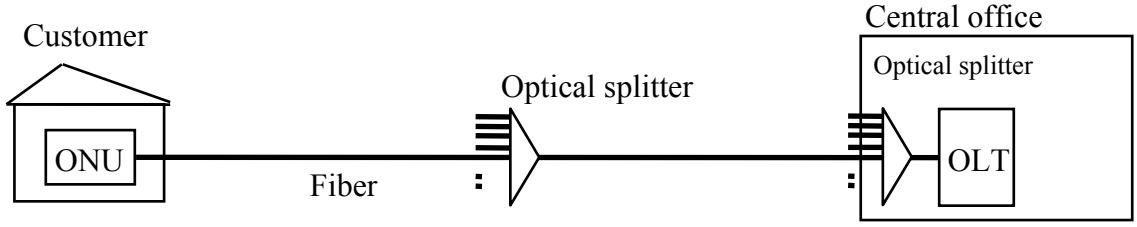

(c) Ring

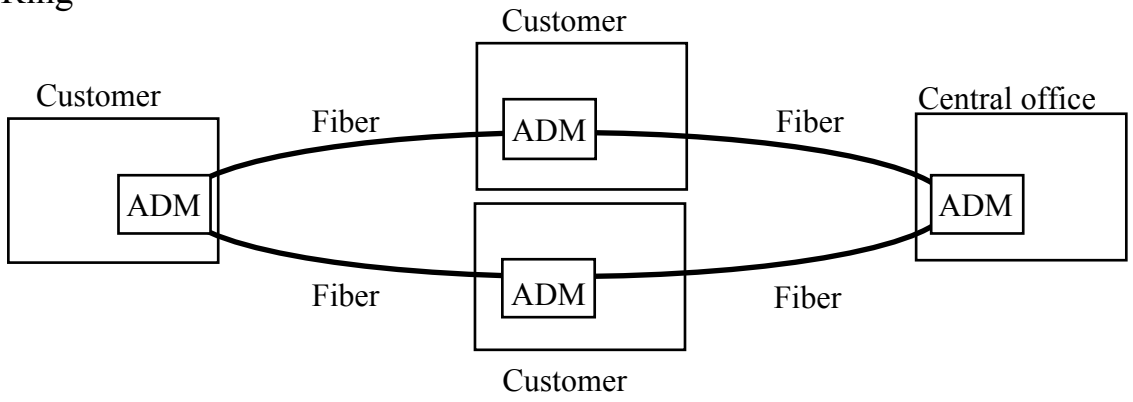

OLT: Optical line terminal
ONU: Optical network unit
ADM: Add /drop multiplexer NE (network element)

Figure 7.1 Various architectures for optical access networks

capacity, wavelength division multiplexing (WDM), remotely pumped erbium-doped fiber amplifiers (EDFAs), and distributed Raman amplifier technologies have been used in trunk line transmission systems [7-14]-[7-16]. Consequently, high-power communication signals and high-power pump light have been introduced into optical fibers. The resulting high-power light of several watts can induce damage in optical fibers or fiber-optic components. Furthermore, to prevent accidental eye or fire hazards during maintenance work, network operators must handle optical fibers or fiber-optic components carefully in central offices using high-power systems. To maintain such optical fiber networks reliably and safely, the requirements should be clarified for an optical fiber maintenance support, monitoring, and testing system that can be applied with optical fiber networks carrying a high total optical power.

Section 7.2 gives the fundamental requirements for an optical fiber maintenance support, monitoring, and testing system for application with PONs and ring networks. Then, section 7.3 discusses the criteria for in-service line testing for preventive maintenance. In particular, these criteria include the maintenance band and the requirements for maintenance test light filtering (such as the cutoff bandwidth, isolation, and other optical characteristics) for testing in-service fiber lines without interfering with optical communication signals in access networks. Section 7.4 gives the requirements for an optical fiber maintenance support, monitoring, and testing system for application with transmission systems using high-power signals. Safety procedures and maintenance guidelines for optical fiber networks using a high total optical power are also presented. Finally, section 7.5 describes the development of an optical fiber maintenance, support, and monitoring system (AURORA) using OTDR technologies, including the system's required functions. The future target technologies for AURORA are also presented.

7.2. Fundamental requirements of optical fiber maintenance support, monitoring, and testing systems for PONs and ring networks

Figure 7.1 shows the basic configurations of (a) point-to-point, (b) point-to-multipoint, and (c) ring networks. The required maintenance sections for an optical fiber maintenance support, monitoring, and testing system consist of all optical fibers between the optical line terminal (OLT) and the optical network unit (ONU) or network element (NE).

For (a) a point-to-point network, conventional OTDR technologies easily provide methods for the function of an optical fiber maintenance support, monitoring and testing system, when achieving surveillance and testing for both preventive and post-fault maintenance. For (b) a point-to-multipoint network, fiber sections between an optical splitter installed in an aerial closure or cabinet and ONUs cannot be monitored by OTDR from the central office. Since the backscattered signals from the individual branched fibers accumulate in the OTDR trace, an individual fault location in a branched fiber in a PON cannot be determined by conventional OTDR. For (c) a ring network, conventional OTDR can be applied from the central office to monitor fiber sections between the central office and a user building, but not to monitor fiber sections between customer buildings.

Table 7.1 lists the maintenance functions and suitable test methods for PON and ring networks. As an optional function, strain distribution measurement by B-OTDR, as described in chapter 6, can be included in an optical fiber maintenance support, monitoring, and testing system. In a PON, high-spatial-resolution OTDR (H-OTDR) is required in order to test branched fibers between an optical splitter and ONUs. In a ring network, a test light bypass module is required in order to test fiber regions between customer buildings.

Table 7.1 Maintenance functions and suitable test methods for PONs and ring networks

Category	Activity	Functions	Methods (typical)	Status (PON	Status (Ring)
Preventative maintenance	Surveillance	Detection of fiber loss increase	OTDR/loss testing	O	O*[4]
		Detection of signal power loss	Power monitoring	O	O
		Detection of water penetration	OTDR testing	O	O*[4]
	Testing	Measurement of fiber fault location	OTDR testing	O*[1]	O*[4]
		Measurement of fiber strain	B-OTDR testing	O	O*[4]
		Measurement of water location	OTDR testing	O*[1]	O*[4]
	Control	Fiber identification	OTDR testing/	O*[1]	-
			ID light detecting*2	O	O
		Fiber transfer	Switching*3	O	O
After installation before service or post-fault maintenance	Surveillance	Refer to alarm from path operation system	On-line/external medium	O	O
		Refer to alarm from customer service operation system	On-line/external medium	O	O
	Testing	Confirmation of fiber condition	OTDR/loss testing	R*[1]	R*[4]
		Fault identification between transmission equipment and fiber network	OTDR/loss testing	R*[1]	R*[4]
		Measurement of fiber fault location	OTDR testing	R*[1]	R*[4]
	Control	Fiber identification	OTDR testing/	R*[1]	-
			ID light detecting*2	R	R*[4]
		Fber transfer	Switching*3	O	O
		Storage in outside plant database	On-line/external medium	R	R
		Information on cable route	On-line/external medium	O	O

R: required; O: optional

*1) High spatial resolution OTDR (H-OTDR) is available for monitoring optical fibers to and beyond an outside splitter.

*[2]) ID light means identification light, e.g., 270-Hz, 1-kHz, or 2-kHz modulated light.

*[3]) Switching includes mechanical and manual switching.

*[4]) By using a test light bypass module.

7.3. Criteria for in-service line testing for preventive maintenance

7.3.1. Fundamental requirements

With a view to implementing a highly reliable optical fiber network transporting WDM signals with a wide spectral bandwidth, in-service fiber line monitoring techniques are important in terms of providing effective, efficient maintenance of optical fiber networks. The fundamental requirements of in-service fiber line testing are the following:

- It should be carried out without degrading communication signals in the optical fiber network.
- It must be capable of evaluating optical fiber characteristics even if there is interference with communication light.

7.3.2. Detailed requirements

Test light wavelength allocation

Table 7.2 categorizes the communication wavelength bands given in ITU-T Supplement.39. A long wavelength band (L-band) extending to 1625 nm has begun to be used for DWDM/CWDM transmission [7-17]-[7-19]. In addition, Rec. G.983.3 defines a new band of 1480-1580 nm (in the S-band) for a downstream Broadband PON (B-PON) to enable simultaneous distribution of Asynchronous Transfer Mode PON (ATM-PON) signals and additional service signals [7-20].

To achieve cost-effective in-service maintenance of optical fiber transmitting communication light with a wide spectral bandwidth, the assignment of maintenance wavelengths for fiber identification, fault location, and maintenance monitoring should meet the requirements of Rec. L.41 [7-21]. Table 7.3 lists the recommended maintenance wavelength assignments. In case 4, the maintenance wavelength of the 1650-nm band does not interfere with communication light between the O-band and the L-band. Figure 7.2 illustrates the categorized communication wavelength bands and the recommended wavelength allocation for PON and CWDM transmission. The U-band is now used solely as a maintenance band. Therefore, the 1650-nm maintenance wavelength is one of the best practical solutions for optical fiber maintenance support, monitoring, and testing systems deployed in an access network.

Table 7.2 Categorization of communication wavelength bands in ITU-T Supplement.39

O-band	E-band	S-band	C-band	L-band	U-band
1260–1360 nm	1360–1460 nm	1460–1530 nm	1530–1565 nm	1565–1625 nm	1625–1675 nm

Table 7.3 Maintenance wavelength assignment

	1310 nm-window	1550 nm-window	1625 nm-window	1650 nm-window
Case 1	Active	Vacant or maintenance	Vacant or maintenance	Vacant or maintenance
Case 2	Vacant or maintenance	Active	Vacant or maintenance	Vacant or maintenance
Case 3	Active	Active	Vacant or maintenance	Vacant or maintenance
Case 4	Active or vacant	Active	Active	Vacant or maintenance

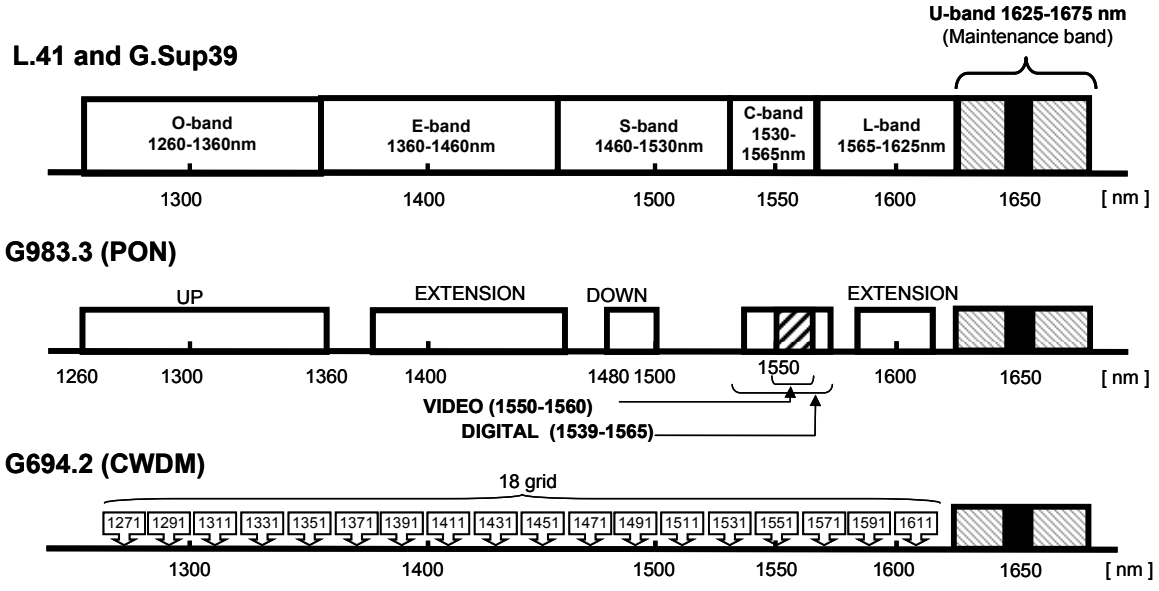

Figure 7.2 Maintenance wavelength allocation

Wavelength bandwidth of test light

The wavelength bandwidth of the test light source should be designed to account for the cutoff bandwidth of the optical filter. Figure 7.3 shows the wavelength spectra for a test light source and a test light cutoff filter, with the L-band used for the communication light. This diagram shows the wavelength allocations for the light source and the cutoff filter. The low edge of A and the high edge of C for the test light source and the low edge of B and the high edge of D for the cutoff filter should satisfy the following relationship:

$$B < A < \lambda_{test} < C < D \quad \text{[nm]}. \tag{7.1}$$

When we consider expanding the communication wavelength band, as described above, it is useful to specify the center wavelength of the test light, λ_{test}, at 1650 nm. This is because the U-band is not used for communication signals. Furthermore, to prevent any deterioration in the effective cutoff value of the optical filter, sideband noise from the test light source, which is not covered by the cutoff wavelength band of the optical filter, should also be sufficiently suppressed when compared with the cutoff characteristic of the optical filter, L_t (dB).

Requirements for test light cutoff filter

The test light should not affect the transmission quality of the optical transmission system, and each system has particular specifications, such as the minimum output power of a transmitter, the minimum sensitivity of a receiver, and the S/X ratio. Figure 7.4 shows a test setup for an in-service testing line. Here, a test light is launched into a transmission line by an optical coupler toward an optical network unit (ONU). Here, P_{cd} and P_t are the optical powers of the OLT and the test light just below the optical coupler, respectively. P_{cd} and P_t are obtained by subtracting the insertion loss of the optical coupler from the minimum output power of the OLT transmitter and the peak power of the test light source, P_p (dBm). The test light is attenuated by the test light cutoff filter, with cutoff value L_t (dB), at the end of the optical fiber line. Equation (7.2) gives the required optical filter cutoff to avoid any deterioration in the bit error rate (BER). This equation reflects the fact that the difference between the optical powers of the communication light and the test light adjacent to the ONU should be sufficiently smaller than the ratio of the signal power to the interference power (i.e., the S/X ratio), SX (dB):

$$\begin{aligned} &P_{cd} - (P_t - L_t) >> SX\ , \\ &L_t >> SX - P_{cd} + P_t \quad \text{(dB)}. \end{aligned} \tag{7.2}$$

Here, the fiber losses and connection losses in the optical fiber line are regarded as

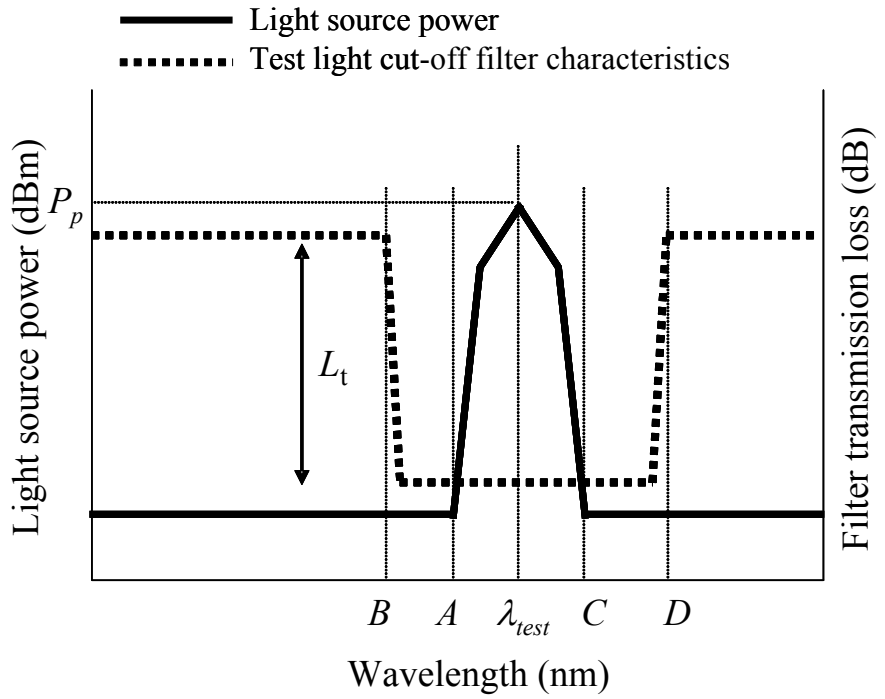

Figure 7.3 Light source and cut-off filter wavelength allocations

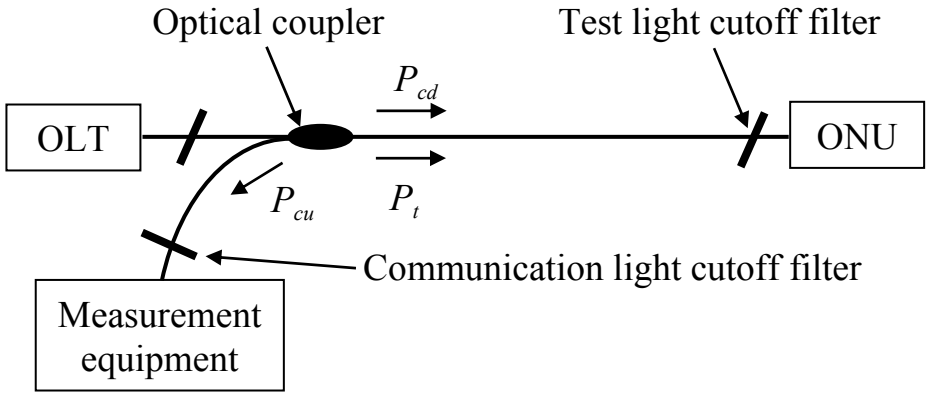

Figure 7.4 Test set-up for in-service line

independent of wavelength.

Test light cutoff filters should eliminate the maintenance test light without having any detrimental effect on transmission quality. Therefore, wavelength *B* should be longer than the transmission wavelength and shorter than wavelength *A*, and wavelength *D* should be longer than wavelength *C*, as shown in Figure 7.3.

The sideband suppression ratio (SBSR) of a conventional distributed feedback laser diode (DFB-LD) is about -40 to -50 dB. When monitoring an in-service line in an optical fiber network, the effective rejection ratio of the test light must be taken into account. Otherwise, the sideband noise of the test light is launched into the ONU and degrades the transmission quality. The effective rejection ratio of the test light depends on its spectrum, obtained by OTDR, and on the rejection band of the filter in front of the ONU. Therefore, in-service line monitoring requires designing a suitable test light spectrum and rejection band for the filter and spectral filtering criteria [7-22],[7-23].

The maximum crosstalk due to the test light to avoid any deterioration in the transmission quality is considered a requirement of the test light cutoff filter. To avoid any effects from other transmissions, PON and WDM transmission systems (defined in G.983.3 [7-20] and G.698.1 [7-24], respectively) have specified tolerances for the reflected optical power and the maximum optical crosstalk, respectively. The parameters of these tolerances correspond to the S/X ratio. By attenuating the test light power below the tolerance to other communication light in the transmission system, in-service testing can be carried out without affecting transmission quality.

Requirements for measurement equipment

The requirements for in-service testing measurement equipment should also be considered. In-service testing must be carried out on the premise that light with a wavelength other than that of the communication light is input into the detector of the measurement equipment. Therefore, to accurately measure the characteristics of an optical fiber line in such a situation, the measurement equipment, such as an OTDR or an optical power meter (OPM), should have a tolerance to the communication light power. In Figure 7.4, the communication light passes through the optical coupler for in-service testing and is launched into the measurement equipment. To suppress the effect of the communication light, it is useful to install an optical filter adjacent to the measurement equipment, allowing test light to pass but not communication light. In terms of OTDR measurement, the power of the introduced communication light, P_{cu} (dBm), must be much lower than that of the Rayleigh backscattered signal of the test light. The Rayleigh backscattering coefficient C_{rb} (dB) is expressed by the following

equation in terms of the Rayleigh backscattering parameter K and the OTDR pulse width T_p, as defined in IEC 61746 [7-25]:

$$C_{rb} = 10\log(K \cdot T_p) \quad \text{(dB)}. \tag{7.3}$$

Therefore, the optical filter requirement for suppressing fluctuation of the OTDR trace is given by the following inequality:

$$P_{cu} - L_c << (P_p - L_{dm}) + C_{rb},$$

$$L_c >> P_{cu} - \{(P_p - L_{dm}) + C_{rb}\}. \tag{7.4}$$

In Eq. (7.4), P_p (dBm) is the peak power of the test light source, L_{dm} (dB) is the optical loss corresponding to the OTDR single-way dynamic range, and L_c (dB) is the cutoff of the optical filter installed adjacent to the measurement equipment. Here, if the communication signal power is regarded as a sort of noise in the OTDR trace, then to reduce the resultant OTDR trace fluctuation to less than 0.2 dB, the attenuated communication signal power, $P_{cu} - L_c$ (dBm), must be 10 dB less than the Rayleigh backscattered signal power, $(P_p - L_{dm}) + C_{rb}$ (dBm).

7.4. Optical fiber maintenance support, monitoring, and testing system for optical fiber networks carrying high total optical power

7.4.1. Fundamental requirements

The concept of "high-power light" for an optical fiber maintenance support, monitoring, and testing system is defined as follows. When high-power light is launched into the optical fiber maintenance support, monitoring, and testing system, the fiber-optic components in the system can be damaged in such a way that they no longer meet their specifications (e.g., through optical loss). Generally, the term "high-power light" is used to refer to light with an optical power of several hundred milliwatts. The fundamental requirements for an optical fiber maintenance system for optical fibers carrying a high total optical power are the following:

- It must be safe for network operators to handle the optical fiber, cords, and fiber-optic components when they are carrying light with a high total optical power. Network operator safety must be maintained in accordance with the appropriate ITU-T or IEC documents [7-26],[7-27].
- The optical fiber maintenance support, monitoring, and testing system should provide the functions of surveillance, testing, and control listed in ITU-T Rec. L.40 [7-13] in order to meet the specifications for optical fibers or fiber-optic components, even if they carry high-power light.

7.4.2. System requirements

Two kinds of safety issues relate to optical fiber carrying a high total optical power. One is human safety, relating to exposure of eyes or skin to high-power light. The other is component safety with a high-power light input. When components have a larger optical loss than is usual, it can pose a fire hazard in the worst case.

It is important for optical fiber maintenance support, monitoring, and testing systems to be able to detect faults in optical fiber networks, because this enables network operators or physical plants to avoid dangerous situations. There are several ways to implement maintenance functions: OTDR testing, optical loss testing, and optical power monitoring of the optical signal or pump power by using an OPM. Therefore, optical fiber maintenance support, monitoring, and testing systems must have optical branching devices for test light insertion (e.g., optical couplers).

Table 7.4 lists the functions of optical fiber maintenance support, monitoring, and testing systems for optical fibers carrying high optical power. The list includes the system requirements for high-power light input and the methods used to meet these requirements.

Connections

To prevent formation of fiber fuses [7-28],[7-29], connectors should not be used to connect optical fibers, especially near the output of a high-power optical source. Instead, fusion splices should be used to connect optical fibers carrying a high total optical power. To avoid fire hazards, materials that do not easily induce a temperature increase should be selected as sleeve materials for fusion splices.

If connectors must be used to connect optical fiber carrying a high total optical power, the connector end faces must be carefully cleaned and polished [7-30].

Termination

・**Optical fiber cords for testing**

The minimum bending radius of optical fiber cords in an optical distribution frame (ODF) in a central office should be 30 mm, in accordance with ITU-T Rec. L.50 [7-31]. If a minimum bending radius of at least 30 mm is maintained for general single-mode fibers (e.g., like those defined in ITU-T Rec. G.652), they will not be damaged during operation of the optical fiber maintenance support, monitoring, and testing system for optical fibers carrying a high total optical power. The susceptibility to damage depends on the coating and jacket materials, the macro-bending loss, the energy conversion to local heating, the input power levels, and the wavelengths [7-32]. Fibers with improved bending capability, however, can be used under more severe conditions.

・**Optical fiber handling**

Because network operators have to handle optical fiber cords when installing or performing maintenance on an optical fiber maintenance support, monitoring, and testing system, they must carefully handle optical fiber or cord that carries a high total optical power. Of course, the handling work should be carried out without any tight bending of the optical fiber.

Test access modules

Components providing testing access have an optical connection point between optical fiber lines for test light insertion; a fusion splice should be used for this connection point. It is desirable that these components for test light insertion (e.g.,

Table 7.4 Functions in optical fiber maintenance support, monitoring, and testing system

Functions	System requirements for high-power light input	Methods
Connection	No fiber fuse or intense temperature increase	Use of fusion splices No need for optical connectors or polishing and cleaning of connector end faces
Termination	No tight bending of optical fiber	Minimum bending radius of 30 mm for testing optical fiber cords in ODF, but fibers with improved bending capability allow more severe conditions
Testing access for optical fiber line	No fiber fuse or intense temperature increase	Use of fusion splices Optical branching component with high tolerance to high-power light exposure
Optical switch with butt-joint splice connection mechanism (e. g., fiber selector)	No intense temperature increase or optical loss increase	Attenuation of high-power light or gap between fibers at butt-joint splice $d < 10\ \mu m$

optical couplers) have a high tolerance for exposure to high-power light.

Optical switches

An optical fiber maintenance support, monitoring, and testing system generally has optical switches for selecting a test fiber. An optical switch conventionally has a butt-joint splice connection mechanism with a large gap and a refractive-index-matching material, even if the optical fiber maintenance support, monitoring, and testing system can accommodate optical fibers carrying a high total optical power. Any high-power light launched into the optical switch should be attenuated to a safe level. The reason is that when light with a power of 200 mW or more is input, the optical loss in the butt-joint splice connection increases greatly, and the temperature also increases [7-33],[7-34]. Therefore, if the butt-joint splice connection mechanism is used in the optical fiber maintenance support, monitoring, and testing system, it is desirable for the gap d between fibers at a butt-joint splice to be less than 10 μm. If switches based on some other connection technology are used, however, higher light power might be allowable.

7.4.3. Testing and maintenance procedure

An auto-shutdown function is an effective way to prevent damage caused by accidents. Functions related to auto-shutdown should account for ITU-T Rec. G.664 [7-26]. Optical fiber maintenance support, monitoring, and testing systems carrying a high total optical power and optical fiber communication systems should have an auto-shutdown function for the sake of safety. Any time the auto-shutdown function is triggered, testing and maintenance with the optical fiber maintenance support, monitoring, and testing system should be undertaken afterward.

Specifically, the following fundamental testing and maintenance procedures should be carried out.

- First, power monitoring with low-power test light should be performed at central offices.
- Second, after confirming that there are no large loss points in the optical fiber network, low-power optical loss testing or OTDR testing should be carried out to detect fault locations.
- Finally, optical loss testing or OTDR testing with high-power light should be performed in optical fibers that carry a high total optical power.

7.5. Recent development of optical fiber maintenance support, monitoring, and testing system (AURORA), and future target technologies

Third generation of AURORA

The third generation of NTT's AURORA was developed in accordance with an upgrade scenario of "high fiber capacity and system cost reduction" [7-9] and has been deployed since 2002. The system cost was half that of the second generation of AURORA.

Figure 7.5 shows the basic configuration of this optical fiber maintenance support, monitoring, and testing system. AURORA consists of a server with a database (DB); a control terminal; an optical testing module (OTM), which contains an OTDR unit (OTU) and a test control unit (TC); optical fiber selectors (FSs) that select the fibers to be tested; test access modules (TAMs) to introduce test light into an optical fiber line; and termination cables with an optical filter allowing communication light but not test light to pass. In accordance with Rec. L. 41 [7-21], the OTDR test light wavelength is 1650 nm, which is different from the communication light wavelength. This means that the system can perform maintenance tests on in-service fibers without degrading the transmission quality [7-8]. The control terminal, located in a facility maintenance center for the outside plant, orders various optical fiber tests and administers fiber information. The compact OTM, TAMs, and FSs are accommodated in integrated distribution modules (IDMs) [7-7] in the central office. Termination cables with chirped fiber Bragg grating (FBG) filters are placed in front of the termination equipment (e.g., an ONU) in the customer building. The control terminal and server are linked to the OTMs by a data communication network (DCN) using TCP/IP.

Table 7.5 lists the main test functions of AURORA. The construction tests, which are carried out after cable installation, comprise an OTDR test and a loss test. These tests include automatic measurement and evaluation of splice losses, reflection values, and fiber losses. The maintenance tests comprise fault tests and periodic tests using OTDR. The fault test includes automatic identification of faults between a fiber line and the transmission equipment on the customer side. With periodic tests, the capability to detect any deterioration in a fiber line or water at a splice point facilitates preventive maintenance for optical fiber networks. For fiber identification, AURORA can remotely introduce identification light into in-service fibers without degrading the transmission quality.

Table 7.6 summarizes the specifications of the third generation of AURORA. The system capacity is about twice that of the second generation. The TAM consists of a

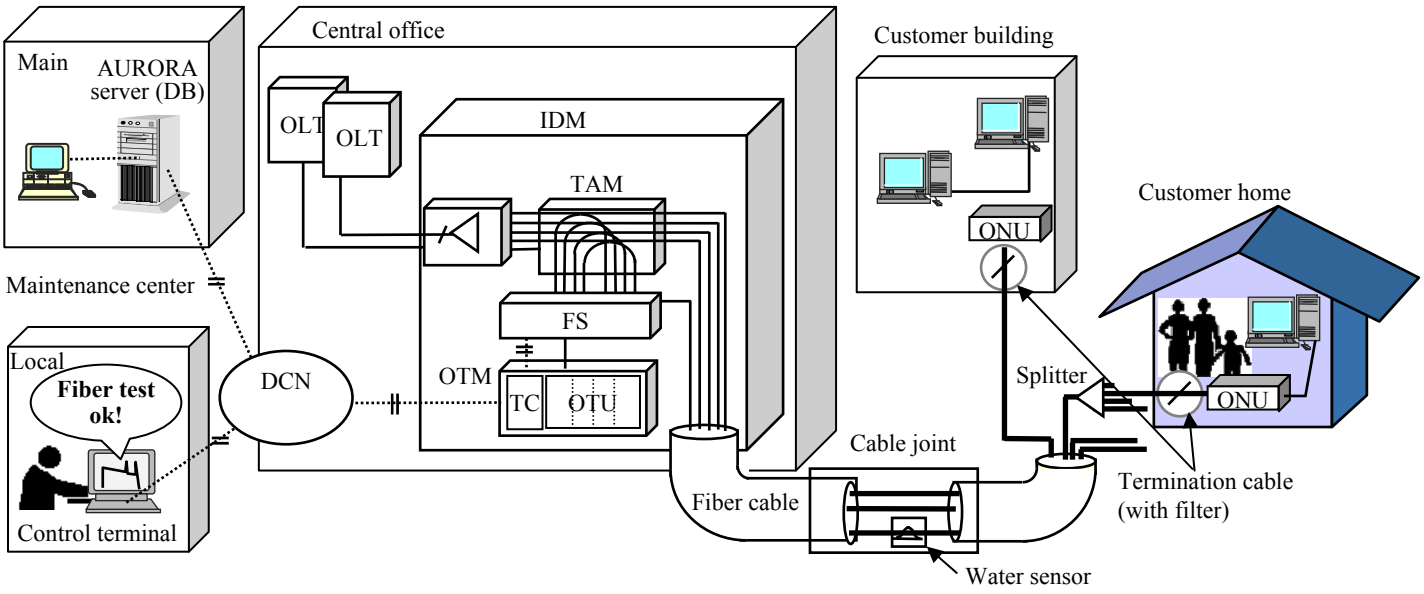

IDM: Integrated distribution module
TAM: Test access module
FS: Fiber selector
OTM: Optical testing module
DCN: Data communication network
OLT: Optical line terminal
ONU: Optical network unit

Figure 7.5 System configuration of optical fiber maintenance support, monitoring, and testing system (AURORA)

Table 7.5 Main test functions of AURORA

Category	Function
Construction	OTDR test: Splice losses and reflection values Loss test: Fiber losses
Maintenance	Fault test: Fault identification and location Periodic test: Detection of fiber line deterioration and water in cable joints
Fiber identification	Insertion of identification light

Table 7.6 Specifications of AURORA

Item	Second generation (TEM) 1996 ~2002	Third generation (OTM) 2002 ~	Additional requirements for advanced future system
System capacity	2,000 fibers / FTM 10,000 fibers / TEM 100,000 fibers / Server	4,000 fibers / IDM 12,000 fibers / OTM 200,000 fibers / Server	-
Maintenance band	1550 nm, 1650 nm	1650 nm	-
Control link	Original interface	Standard interface (TCP/IP)	High speed mobile IF of remote control terminal for field workers
TAM	8 ch WINC based on PLC SC/MT connectors	16 ch WINC based on PLC MU/MT connectors	L/U band optical coupler for wide band transmission Test light bypass module for ADM ring network
Termination cable	Dichroic reflective filter Polyimide thin film embedded in SC connector	Chirped fiber Bragg grating filter in SC connector Bandwidth: 1645 - 1655 nm Rejection ratio: >20 dB	FBG filter with a rejection ratio of more than 40 dB
Fiber selector (FS)	2x1600 Fiber alignment 250 μm pitch V-grooves Two movable master heads	1x2000 fiber alignment 127 μm pitch V-grooves One movable master head	Remotely installed FS to reduce cost of preventive maintenance
Test equipment	Multi-wavelength OTDR module Ring laser high dynamic range OTDR module	Standard OTU (1650 nm OTDR) LD based high dynamic range OTU	High spatial resolution < 2 m for PON High dynamic range C-OTDR Strain measurement for preventive maintenance

16ch wavelength independent coupler (WINC) with a fiber pitch of 127 μm, 8 MT connectors for outside cables, 16 MT connectors for FSs, and a simplified 16-port MU connector for indoor cables. The 1 x 2,000 FS consists of a fiber-moving head and a multi-fiber array composed of 250 sections. Each section consists of a stack of two 8-fiber ribbons. The 250 sections are arrayed side by side on one V-groove substrate with a pitch of 127 μm. The end of the multi-fiber array is cut to form a perfect mirror and aligned with a head fiber positioned in the same V-groove but without touching the array fibers. The IDM is composed of 4 jumper plate shelves with 63 TAMs and one FS per shelf, accommodating a maximum of 4,000 fibers [7-7]. The step-chirped FBG filter [7-35], with a center reflection wavelength of 1650 ± 5 nm, is used because it can be embedded in the SC connector of a termination cable more easily than can a conventional polyimide film filter [7-36]. When this system is applied with an L-band transmission system, the FBG filter must have a steep characteristic [7-37].

Future technology targets for AURORA

Applying the AURORA system with wideband transmission systems and various network topologies requires advanced specifications and technology for the system. Table 7.6 summarizes these additional requirements. The major technologies are the following:

(1) A fault isolation technique or fault location technique for a PON [7-38]-[7-49];
(2) A test light bypass module for an ADM ring network [7-50],[7-51];
(3) An L/U band optical coupler for coarse WDM (CWDM) and dense WDM (DWDM) systems [7-52]-[7-54];
(4) A remotely installed FS to reduce maintenance costs in rural areas [7-55];
(5) A high-dynamic-range system for trunk line monitoring, such as the advanced C-OTDR described in chapter 5;
(6) Fiber distributed strain measurement technique for evaluating optical fiber reliability by using 1.65 μm B-OTDR described in chapter 6; and
(7) High speed mobile interface (IF) of remote control terminal for field workers [7-40].

Figure 7.6 shows the fault isolation technique for branched optical fibers with an optical splitter. As the lengths of the branched optical fibers differ, the Fresnel reflections from optical filters #1 and #2 can be distinguished. The optical fiber with optical filter #1 can be determined as faulty because the reflection value of optical filter #1 changes from its initial level. The prototype system can isolate a fault in an optical fiber when the difference between the distances of the branched optical fibers is

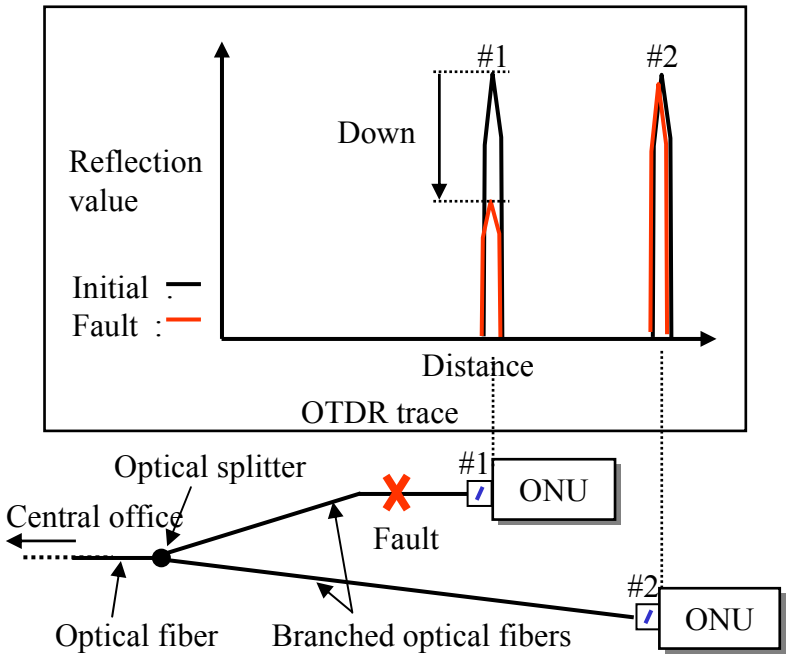

Figure 7.6 Branched optical fiber fault isolation technique

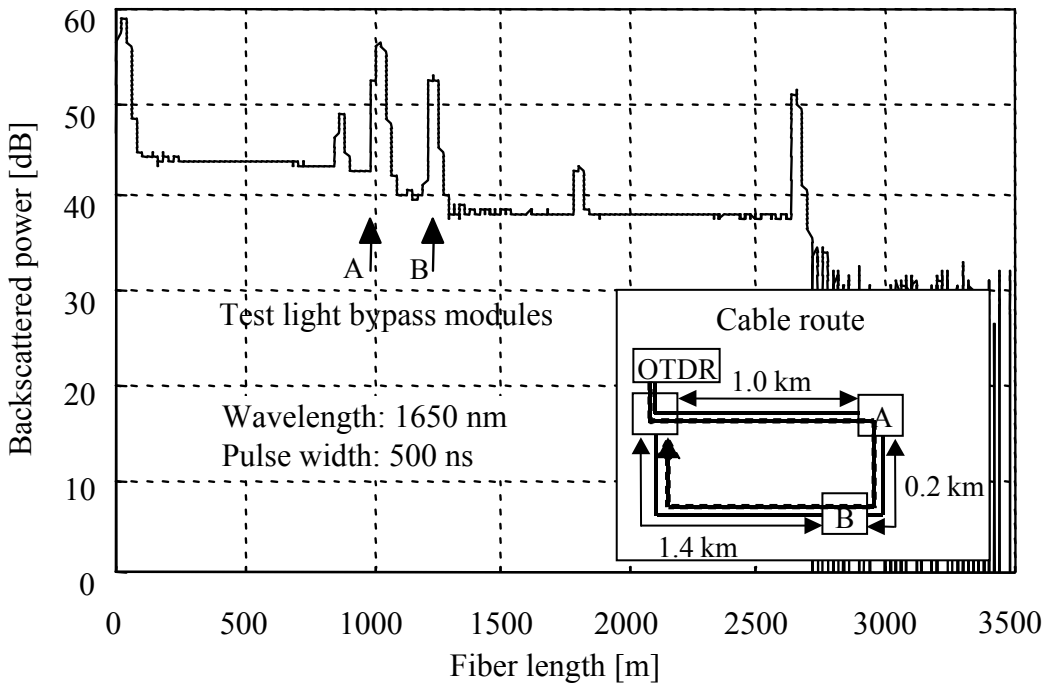

Figure 7.7 OTDR trace of field-installed optical fiber cables with test light bypass modules

more than 2.0 m [7-38]. This fault isolation technique is one of the practical solutions for maintaining the branched fibers in a PON [7-38]-[7-41].

A conventional OTDR is unstable because the Rayleigh backscattered signals from all the branched optical fibers accumulate in the OTDR trace. Sankawa et al. proposed a fault location technique for PONs [7-42]. This approach is difficult, however, for practical application, because the dynamic range is insufficient to monitor PON fibers. Measurement of individual branched fibers in a PON was also demonstrated by using an expensive arrayed waveguide grating (AWG) to assign an individual testing wavelength to each branched fiber [7-43]. Measurement of the Brillouin frequency shifts assigned to each PON branch was demonstrated by using a 1550-nm B-OTDR [7-44]. For in-service monitoring of PON fibers, a new function for an optical fiber line testing system was proposed [7-45]. This function uses a termination cable with individually assigned Brillouin frequency shifts and a 1650-nm-band Brillouin monitoring technique. The 1650-nm-band B-OTDR described in chapter 6, using a 1650-nm-band amplifier technique with a Thulium-doped fiber amplifier (TDFA) or a Raman fiber amplifier (RFA), enables measurement of the Brillouin frequency shift of 1650-nm test light from a PON termination cable [7-45]-[7-49]. The B-OTDR also provides an advanced function of AURORA to evaluate the reliability of optical fibers for the preventive maintenance.

Figure 7.7 shows the OTDR trace of a field-installed optical fiber cable with two 1650-nm test light bypass modules, located 1.0 and 1.2 km from a central office. This configuration means that AURORA with 1650-nm test light bypass modules can monitor the cables between buildings in the ADM ring network [7-50], [7-51].

Furthermore, my colleagues in NTT laboratories have been developing sophisticated methods to meet additional requirements for a future advanced system [7-38]-[7-55].

7.6. Conclusions

(1) This chapter has clarified the characteristics and requirements of optical fiber maintenance support, monitoring, and testing systems for access networks. It has described the fundamental requirements, maintenance sections, testing and maintenance items, and methods for maintaining point-to-multipoint and ring optical networks. Methods for PON and ring network maintenance were also described.

(2) The maintenance band and requirements for maintenance test light filtering (such as the cutoff bandwidth, isolation, and other optical characteristics) have been clarified, for the case of testing in-service fiber lines without interfering with optical communication signals.

(3) The chapter has also described the functional requirements of optical fiber maintenance support, monitoring, and testing systems for optical fiber networks carrying a high total optical power. These requirements apply to test equipment, optical switches for selecting a test fiber, test access modules for connecting test equipment to the communication line, optical fiber cords for testing, and optical connections in the maintenance system. The safety procedures and maintenance guidelines for an outside fiber plant carrying a high total optical power were also described.

(4) Finally, this chapter described the requirements of an advanced future system and demonstrated some methods for PON and ring network maintenance: a fault isolation method for PON using H-OTDR, and a ring network monitoring method using test light bypass modules and conventional OTDR.

(5) All of the above results contributed in a major way to make ITU-T Recommendations of L.53, L.66, and L.68 [7-55]-[7-58].

7.7. References

[7-1] H. Shinohara, "Fiber optic communication systems in Japan," in the proc. of LEOS2000, 13th Annual Meeting, IEEE, 2000.

[7-2] K. Okada, "The vision for HIKARI-soft services," NTT Rev., vol. 13, no. 4, pp. 4-8, 2001.

[7-3] Y. Maeda and K. Nakanishi, "Deployments of broadband optical access network systems in NTT, Japan," in the proc. of ECOC2003, vol. 5, pp. 16-19, 2003.

[7-4] Y. Maeda, "Overview of optical broadband in Japan," in the proc. of ECOC 2004, vol. 1, no. 1.1.2, pp. 4, 2004.

[7-5] H. Shinohara, "FTTH experiences in Japan," J. of Optical Networking, vol. 6, no. 5, pp. 616-623, 2007.

[7-6] "Number of Broadband Service Contracts, etc. (as of the end of September 2007)," MIC (Ministry International Affairs and Communications, Japan Government) Press release – Telecom, December 18, 2007.

[7-7] M. Tachikura, K. Mine, H. Izumita, S. Uruno, and M. Nakamura, "Newly developed optical fiber distribution system and cable management in central office," in the proc. of 50th IWCS, pp. 98-105, 2001.

[7-8] N. Tomita, H. Takasugi, N. Atobe, I. Nakamura, F. Takaesu, and S. Takashima, "Design and performance of a novel automatic fiber line testing system with OTDR for optical subscriber loops," IEEE J. Lightwave Technol., vol. 12, no. 5, pp. 717-726, 1994.

[7-9] N. Tomita, "Progress on automatic monitoring system for fiber-optic subscriber networks," in the proc. of OFS-13, WS1-3, pp. 9-14, 1999.

[7-10] H. Henning and F. Lars, "A novel, multi-service add-drop-multiplexer architecture for access and backhauling applications with 4.3 Gbit/s line rate," in the proc. of OFC/NFOEC2007, JWA91, Mar. 2007.

[7-11] S. Ikegawa, H. Sumi, and K. Karato, "Development of the new ADM ring system," NTT Technical Review, vol. 2, no. 4, pp. 70-74, April 2004.

[7-12] ITU-T Recommendation L.25, "Optical fibre cable network maintenance," 1996.

[7-13] ITU-T Recommendation L.40, "Optical fibre outside plant maintenance support, monitoring and testing system," 2000.

[7-14] H. Masuda, H. Kawakami, S. Kuwahara, A. Hirano, K. Sato, and Y. Miyamoto, "1.28 Tbit/s (32 x 43 Gbit/s) field trial over 528 km (6/spl times/88 km) DSF

using L-band remotely-pumped EDF/distributed Raman hybrid inline amplifiers," Electron. Lett., vol. 39, no. 23, pp. 1680-1670, 2003.

[7-15] P. B. Hansen, A. Stentz, T. N. Nielsen, R. Espindola, L. E. Nelson, and A. A. Abramov, "Dense wavelength-division multiplexed transmission in 'zero-dispersion' DSF by means of hybrid Raman/erbium-doped fiber amplifiers," in the proc. of OFC, PD8, 1999.

[7-16] K. Aida, S. Nishi, Y. Sato, K. Hagimoto, and K. Nakagawa, "1.8 Gb/s 310 km fiber transmission without outdoor repeater equipment using a remotely pumped in-line Er-doped fiber amplifier in an IM/DIRECT-DETECTION system," in the proc. of ECOC'89, PDA-7, pp. 29-32, 1989.

[7-17] K. Fukuchi, "Wideband and ultra-dense WDM transmission technologies toward over 10-Tb/s capacity," in the proc. of OFC2002, paper ThX5, pp. 558-559, 2002.

[7-18] K. Tsujikawa, Y. Nonoyama, H. Nakamura, T. Ogawa, H. Kawata, and T. Sugie, "Flexible and cost-effective metropolitan and access networks based on coarse-WDM technologies," in the proc. of International Conference on Optical Internet (COIN) 2002, pp. 28-30, 2002.

[7-19] Ehrhardt, N. Hanik, A. Gladisch, and F. Rumpf, "Field demonstration of a transparent optical 10 Gbit/s-WDM-network based on normalized transmission sections," in the proc. of OFC2002, paper TuH2, pp. 42-43, 2002.

[7-20] ITU-T Recommendation G.983.3, "A broadband optical access system with increased service capability by wavelength allocation," 2001.

[7-21] ITU-T Recommendation L.41, "Maintenance wavelength on fibers carrying signals," 2000.

[7-22] N. Honda, N. Araki, H. Izumita, and M. Nakamura, "New test light spectrum design for L/U-band extended optical fiber line testing system," in the proc. of OECC2003,15A4-5, pp. 57-58, 2003.

[7-23] N. Honda, H. Izumita, and M. Nakamura, "Spectral filtering criteria for U-band test light for in-service line monitoring in optical fiber networks," IEEE J. Lightwave Technol., vol. 24, no. 6, pp. 2328-2335, 2006.

[7-24] ITU-T Recommendation G.698.1, "Multichannel DWDM applications with single channel optical interfaces," 2005.

[7-25] IEC 61746, "Calibration of optical time-domain reflectometers (OTDRs)," 2005.

[7-26] ITU-T Recommendation G.664, "Optical safety procedures and requirements for optical transport systems," 2006.

[7-27] IEC 60825-2, "Safety of laser products - Part 2: Safety of optical fibre communication systems," 2007.

[7-28] R. Kashyap and K. J. Blow, "Observation of catastrophic self-propelled self-focusing in optical fibres," Electron. Lett., vol. 24, no. 1, pp. 47-49, 1988.

[7-29] Y. Shuto, S. Yanagi, S. Asakawa, M. Kobayashi, and R. Nagase, "Simulation of fibre fuse phenomenon in single-mode optical fibres," IEEE J. Lightwave Technol., vol. 21, no. 11, pp. 2511-2517, 2003.

[7-30] M. D. Rosa, J. Carrberry, V. Bhagavatula, K. Wagner, and T. Uenoya, "High-power performance of single-mode fibre-optic connectors," IEEE J. Lightwave Technol., vol. 20, no. 5, pp. 879-885, 2002.

[7-31] ITU-T Recommendation L.50, "Requirements for passive optical nodes: optical distribution frames for central office environments," 2003.

[7-32] I. Ogushi, H. Izumita, F. Ito, and M. Arii, "Catastrophic damage and destructive process induced in optical fiber cord by 33 dBm pump light at 1480 nm in WDM systems," in the proc. of OFC/NFOEC, OME6, 2005.

[7-33] I. Ogushi, H. Izumita, K. Tanaka, F. Ito, and M. Arii, "Observation of ignition induced by a high power light input at a butt-joint splice with refractive index matching material," in the proc. of OFC2006, OFK6, 2006.

[7-34] I. Ogushi, H. Izumita, K. Tanaka, F. Ito, and M. Arii, "Butt-joint splice with refractive index matching material for high power light in optical fiber communications," in the technical digest of SOFM 2006, pp. 33-36, 2006.

[7-35] K. Hogari, Y. Miyajima, S. Furukawa, N. Tomita, K. Tomiyama, and M. Ohashi, "Wideband and highly reflective step-chirped fibre grating filter embedded in an optical fibre connector," Electron. Lett., vol. 32, no. 13, pp. 1230 -1231, 1996.

[7-36] H. Takasugi, N. Tomita, H. Suzuki, and T. Akai, "A new fault-identification method using a dichroic reflective optical filter in optical subscriber loops," IEEE J. Lightwave. Technol., vol. 11, no. 2, pp. 351- 357, 1993.

[7-37] N. Nakao, H. Izumita, T. Inoue, Y. Enomoto, N. Araki, and N. Tomita, "Maintenance method using 1650-nm wavelength band for optical fiber cable networks," IEEE J. Lightwave. Technol., vol. 19, no. 10, pp. 1513-1520, 2001.

[7-38] Y. Enomoto, H. Izumita, and M. Nakamura, "Over 31.5 dB dynamic range optical fiber line testing system with optical fiber fault isolation function 32-branched PON," in the proc. of OFC2003, ThAA3 , pp. 608-610, 2003.

[7-39] Y. Enomoto, H. Izumita, and M. Nakamura, "Highly developed fiber fault isolation technique for branched optical fibers of PONs using high spatial

resolution OTDR and frequency domain analysis," The Laser Society of Japan, The Review of Laser Engineering, vol. 33, no. 9, pp. 609-614, 2005.

[7-40] Y. Enomoto, H. Izumita, and M. Arii, "Optical fiber management and testing system for PON enhanced with identification technologies using a mobile access terminal with a two-dimensional code scanner and fault isolation technologies using high spatial resolution OTDR," J. of Optical Networking, vol. 6, no. 5, pp. 408-414, 2007.

[7-41] Y. Koshikiya, N. Araki, H. Izumita, and F. Ito, "Newly developed optical fiber line testing system employing bi-directional OTDRs for PON and in-service line testing criteria," IEICE vol. E90-B, no. 10, pp. 2793-2802, 2007.

[7-42] I. Sankawa, S. Furukawa, Y. Koyamada, and H. Izumita, "Fault locating technique for in-service branched optical fiber networks," IEEE Photon. Technol. Lett., vol. 2, no. 10, pp. 766-768, 1990.

[7-43] K. Tanaka, H. Izumita, N. Tomita, and Y. Inoue, "In-service individual line monitoring and a method for compensating for the temperature-dependent channel drift of a WDM-PON containing an AWGR using a 1.6 μm tunable OTDR," in the proc. of ECOC'97, vol. 3, pp. 295-298, 1997.

[7-44] K. Shimizu, T. Horiguchi, and Y. Koyamada., "Measurement of distributed strain and temperature in a branched optical fiber network by use of Brillouin optical time-domain reflectometry," Optics. Lett. vol. 20, no. 5, pp. 507-509, 1995.

[7-45] N. Honda, D. Iida, H. Izumita, and F. Ito, "New function of optical fiber line testing system employing termination cable with individual Brillouin frequency shift and 1650 nm band in-service monitoring technique," in the proc. of OECC 2005, P364-365 7A-3, 2005.

[7-46] N. Honda, D. Iida, H. Izumita, and F. Ito, "Bending and connection loss measurement of PON branching fibers with individually assigned Brillouin frequency shifts," in the proc. of OFC2006, OThP6, 2006.

[7-47] D. Iida, N. Honda, H. Izumita, and F. Ito, "Identification fibers with individually assigned Brillouin frequency shifts for fault location in passive optical networks," in the proc. of OECC 2006, 4E1-2, 2006.

[7-48] N. Honda, D. Iida, H. Izumita, and F. Ito, "Optical fiber line testing system design considering outside environment for 8-branched PON fibers with individually assigned BFSs," in the proc. of OFS-18, ThE8, 2006.

[7-49] D. Iida, N. Honda, H. Izumita, and F. Ito, "Design of identification fibers with individually assigned Brillouin frequency shifts for monitoring passive optical

networks," IEEE J. Lightwave Technol., vol. 25, no. 5, pp. 1290-1297, 2007.

[7-50] Y. Enomoto, N. Honda, H. Izumita, and M. Nakamura, "Optical fiber line testing system using test light bypass module for ADM ring networks," in the proc. of ECOC 2001, vol. 3, We.B.1.6, 2001.

[7-51] Y. Enomoto, H. Izumita, and N. Tomita, "Optical fiber line testing system employing 1.65 μm test light bypass module for in-service monitoring of ADM ring networks," IEICE vol. E91-B, no. 8, pp. 2494-2500, 2008.

[7-52] N. Araki, H. Izumita, N. Honda, and M. Nakamura, "Extended optical fiber line testing system using L/U-band crossed optical waveguide coupler for L-band WDM transmission," in the proc. of OFC 2002, TuY2, 2002.

[7-53] N. Araki, H. Izumita, N. Honda, M. Nakamura, "Extended optical fiber line testing system using new eight-channel L/U-band crossed optical waveguide coupler for L-band WDM transmission," IEEE J. Lightwave Technol., vol. 21, no. 11, pp. 3316 - 3322, 200

[7-54] N. Honda, N. Araki, H. Izumita, and M. Nakamura, "Extended optical fiber line testing system using L/U-band optical coupler employing 4-port circulators and chirped fiber Bragg grating filters for L-band WDM transmission," IEICE vol. E86-B, no. 5, pp. 156-1566, 2003

[7-55] N. Araki, H. Izumita, and M. Nakamura, "Reduction in optical fiber maintenance cost by using automatic optical fiber operations support system with remote fiber selector," IEICE vol. E85-C, no. 4, pp. 915-920, 2002

[7-56] ITU-T Recommendation of L. 53, "Optical fibre maintenance criteria for access networks," (05/2003).

[7-57] ITU-T Recommendation of L. 66, "Optical fibre cable maintenance criteria for in-service fibre testing in access networks," (05/2007).

[7-58] ITU-T Recommendation of L. 68, "Optical fibre cable maintenance support, monitoring and testing system for optical fibre cable networks carrying high total optical power," (10/2007).

Chapter 8. Conclusions

This thesis has described the enhancement of optical time-domain reflectometry (OTDR) by using a coherent detection technique and optical fiber amplifiers, as well as its applications for optical fiber network monitoring. This final chapter summarizes the results obtained by developing and investigating coherent-detection OTDR (C-OTDR).

(1) The optimized configuration for OTDR with erbium-doped fiber amplifiers (EDFAs) was clarified by the results of theoretical and experimental studies. The performance of OTDR for maintaining optical fiber networks was enhanced by applying the EDFAs and the coherent detection technique. The resulting signal-to-noise ratio (SNR) improvement was investigated by numerical evaluation of the receiver sensitivity and noise, which originated from the amplified spontaneous emission (ASE) of the EDFAs. The EDFAs should be incorporated in the OTDR setup as post-amplifiers for the high-gain regime over 20 dB. Two concatenated EDFAs with a synchronously driven acousto-optic switch (AO-SW) could produce a 30-dBm high-power signal pulse light with low ASE. The feasibility of enhancing both direct-detection OTDR (D-OTDR) and C-OTDR with EDFAs as post-amplifiers was confirmed. By using the concatenated EDFAs with a synchronously driven AO-SW, D-OTDR and C-OTDR were demonstrated with SWDRs of 30.5 dB and 36 dB, respectively. This C-OTDR offers the possibility of an SWDR of over 40 dB. The nonlinear phenomena occurring in an optical fiber degrade the performance of C-OTDR. Although it has been theoretically predicted that the critical powers of stimulated Brillouin scattering (SBS) and stimulated Raman scattering (SRS) limit the incident pulse power in C-OTDR, the critical power at which such nonlinear phenomena occurred in a dispersion-shifted fiber (DSF) was found experimentally to be lower that these critical powers. This result provides new criteria for the SWDR limit of C-OTDR enhanced with EDFAs.

(2) The performance limit of C-OTDR enhanced with optical fiber amplifiers was theoretically and experimentally clarified. The critical pulse power, at which the C-OTDR performance is degraded by the effects of nonlinear optical phenomena in a single-mode optical fiber, depends on the amplified optical pulse waveform and the pulse width. For a pulse width of 1 μs or longer, the incident pulse power is limited by the effect of self-phase modulation (SPM). When an optical pulse having a power gradient within the pulse width is incident to a single-mode optical fiber, the optical frequency of the backscattered signal is shifted by SPM, and the center frequency of

the signal moves outside the receiver band, thus degrading the sensitivity of C-OTDR. For a pulse width of 100 ns, the incident optical pulse power is limited by four-wave mixing (FWM), which transfers the energy from the incident optical pulse to Stokes and anti-Stokes light, as a result of the interaction between the incident optical pulse and the ASE. In accordance with the above limits imposed by SPM and FWM, the high-performance C-OTDR enhanced with EDFAs obtained SWDRs of 48, 44, 39, and 29 dB for pulse widths of 10 μs, 4 μs, 1 μs, and 100 ns, respectively. These results are believed to be the best reported performance of a C-OTDR using EDFAs. The C-OTDR with a 48-dB SWDR and a pulse width of 10 μs could be applied for monitoring 160-km repeaterless optical transmission systems deployed in NTT trunk lines in Japan.

(3) The amplitude fluctuation in the C-OTDR trace, caused by fading noise, and the fluctuation of the coherent detection efficiency were both described using the probability density functions for each of the fluctuation factors. These fluctuations were also estimated theoretically for the case of applying reduction techniques. A new synchronous optical frequency-hopping technique was proposed. In this technique, an RF current pulse is induced in the drive current of a laser diode (LD) during the LD temperature changes. This technique stimulates optical frequency hopping, which is synchronized with the timing of launching the C-OTDR signal pulse, and increases the number of independent Rayleigh backscattered signals. This effectively reduces the amplitude fluctuation in comparison with a conventional technique that the author proposed previously. The amplitude fluctuation for a 1-μs pulse width was reduced experimentally to 1/7 of that with the LD temperature stabilized. For 100- and 30-ns pulse widths, the fluctuation was reduced to 1/11 of that with the LD temperature stabilized. These experimental results are in good agreement with calculated results. This reduction technique enables practical field use of the advanced C-OTDR.

(4) The high-performance C-OTDR, as mentioned above, can be applied to monitor optical fiber networks containing (a) in-line amplifiers as 1R repeaters and (b) distributed Raman amplifiers (DRAs).

In case (a), the optical transmission lines have 1R repeaters containing EDFAs optimized in continuous-wave (CW) gain mode. When applying conventional OTDR to measure optical lines, the leading edge intensity of the signal pulse from the OTDR system increases upon passing each 1R repeater. This optical surge, caused by the accumulated gain difference between the pulse gain and the CW gain of the EDFAs, breaks the feedback circuits in the repeaters. A technique was thus proposed for keeping the C-OTDR probe power as uniform as possible and avoiding any optical

surges. In this technique, dummy light with a wavelength of 1554 nm is multiplexed, via an acousto-optic (AO) switch, with the signal pulse having a wavelength of 1552 nm. The resulting enhanced C-OTDR had a 37-dB SWDR with a probe power of 6 dBm. This indicates the possibility of avoiding optical surges while testing optical fiber cable spans in optical transmission lines containing EDFAs.

In case (b), the optical transmission lines consist of several-hundred-kilometer lengths of single-mode fibers with DRAs and remotely pumped EDFAs. These optical fiber amplifiers are pumped with 1.48-μm light, which is incident from the counter end of the optical transmission line. By using a narrow-band filter to reduce the noise originating from the EDFAs, the highly developed C-OTDR described here can be applied to monitor such lines. A 340-km optical fiber line containing a DRA and a remotely pumped EDFA was successfully measured.

The two above applications commonly occur in maintaining the long-haul optical fiber cables of submarine optical transmission systems.

(5) Fiber-distributed tensile strain measurement is another important application of the advanced C-OTDR. The required SWDR for upgrading C-OTDR to Brillouin optical time-domain reflectometry (B-OTDR) was theoretically investigated, and it was found that an SWDR of over 20 dB was required to measure a 0.02% strain distribution in an optical fiber. The applications of C-OTDR upgraded to B-OTDR by enhancement with a sideband generation technique or a wideband coherent receiver were demonstrated; these applications include measuring the loss and strain distribution in an optical fiber. A proposed optical shifter using a high-speed $LiNbO_3$ phase modulator (LN-PM) had highly stable characteristics, with a 14-GHz bandwidth and a 20-kHz frequency resolution. The distributed tensile strain in a 30-km dispersion-shifted optical fiber was successfully measured with 100-m spatial resolution. The feasibility of B-OTDR using a 20-GHz wideband balanced receiver was also demonstrated. These B-OTDR implementations are highly simple and cost effective. A simultaneous measurement technique for separating strain and temperature was also discussed, and the dependence of the frequency shift and power of the Brillouin backscattered signals on the temperature was obtained experimentally.

B-OTDR is now commonly used for evaluating the reliability of optical fiber cables in fiber optic communication systems, and in structural monitoring applications.

(6) Finally, the fundamental requirements and methods for maintaining optical fiber networks were described. Specifically, the fundamental functions and methods were clarified for an optical fiber support, monitoring, and testing system for optical fiber networks carrying high-power signals, such as submarine optical transmission systems.

For access networks, advanced optical fiber monitoring systems were investigated for application with various network types, and the criteria for in-service line testing in an optical fiber were also presented. The above results were given in the context of the related standardizations of the International Telecommunication Union Telecommunication (ITU-T).

As summarized above, the highly developed C-OTDR described in this thesis is a basic technology for various applications, including optical fiber monitoring of long-haul optical transmission systems and fiber-distributed strain measurement for evaluating the reliability of optical fiber.

Furthermore, continued development of this C-OTDR technology can be expected to provide advanced functions for optical fiber maintenance support, monitoring, and testing systems that can be applied in future networks, such as WDM-PON, Super-PON for access networks, and so forth.

Acknowledgements

First of all, I thank Prof. Shinich Komatsu of the Department of Applied Physics, School of Advanced Science and Engineering, Waseda University, for his guidance, invaluable advice, and encouragement throughout this work. I would also like to thank Profs. S. Hashimoto, H. Nakajima, and K. Ukai of the Department of Applied Physics, School of Advanced Science and Engineering, Waseda University, for their fruitful advice on my thesis.

This thesis is based on research and development work done by the author at NIPPON TELEGRAPH and TELEPHONE Corporation (NTT). My sincere thanks go to Mr. H. Shinohara, Executive Director of the NTT Information Sharing Laboratory Group, Dr. M. Shimizu, Project Manager of the Access Media Project, and Mr. O. Yamauchi, Project Manager of the Second Promotion Project at NTT Access Network Service Systems Laboratories, for their continuous encouragement. I also thank Dr. T. Haibara, Mr. Kiminori Sato, Mr. A. Hirooka, Prof. T. Yabuta, and Dr. Koushi Ishihara for their kind encouragement and guidance. It was under their tenures as project managers of NTT laboratories that I had the opportunity to perform this research and development work. I also thank Dr. Nobuo Tomita, Mr. Minoru Nakamura, Mr. M. Arii, Dr. Fumihiko Ito, and Dr. H. Suda, who were Group Leaders at NTT Access Network Service Systems Laboratories, for their continuous support of this work and encouragement.

I thank Mr. M. Oka, Executive Director of Maintenance and Service Operations Department, NIPPON TELEGRAPH and TELEPHONE EAST Corporation (NTT EAST), for providing the opportunity for this work. I sincerely thank Dr. Nobuo Kuwaki, Executive Manager of Technical Assistance and the Support Center, NTT EAST, for strongly supporting this work and providing encouragement.

Very special thanks go to Dr. I. Sankawa, Dr. S. Furukawa, Prof. Y. Koyamada, Prof. T. Horiguchi, Prof. M. Tateda, Dr. T. Kurashima, and Mr. Toshiya Sato, who were colleagues of mine at NTT Access Network Service Systems Laboratories and co-authors of papers related to C-OTDR and B-OTDR technologies, for their technical discussions with me and advice on the work related to this thesis.

Furthermore, I thank Dr. Shigeru Tomita, Dr. K. Hogari, Dr. N. Nakao, Dr. Fumihoko Yamamoto, Mr. Noriyuki Araki, and Mr. Y. Koshikiya for their support of the ITU-T SG6 standardization activities.

Finally, very special thanks go to my colleagues, Mr. Kuniaki Tanaka, Mr. Y.

Enomoto, Ms. Nazuki Honda, Mr. Ikutaro Ogushi, and Mr. Daisuke Iida, for their great cooperation and fruitful discussions with me. Thanks are also due to many other colleagues at NTT.

List of publications

1. Published papers

1.1 Papers mainly contributed on this thesis

[1] H. Izumita, S. Furukawa, Y. Koyamada and I. Sankawa, "Fading Noise Reduction in Coherent OTDR," IEEE Photon. Technol. Lett. vol. 4, no. 2, pp. 201- 203, 1992.

[2] S. Furukawa, Y. Koyamada, I. Sankawa and H. Izumita, "Enhancement of OTDR performance using optical fiber amplifiers," The Institute of Electronics, Information and Communication Engineers (IEICE) Transactions on Communications, vol. J75B-1, No. 5, pp. 304 - 313, 1992. (in Japanese)

[3] H. Izumita, Y. Koyamada, S. Furukawa and I Sankawa, "Optical nonlinearities in coherent OTDR enhanced with optical fiber amplifiers," IEICE Trans., J76B-1, no. 2, pp. 171 - 181, 1993. (in Japanese)

[4] H. Izumita, Y. Koyamada, S. Furukawa and I. Sankawa, "Stochastic of amplitude fluctuation in coherent OTDR and its reduction technique," IEICE Trans., vol. J76B-1, no. 6, pp. 439 - 450, 1993. (in Japanese)

[5] H. Izumita, Y. Koyamada, S. Furukawa and I Sankawa, "The performance limit of coherent OTDR enhanced with optical fiber amplifiers due to optical nonlinear phenomena," IEEE J. Lightwave Technol. vol. 12, no. 7, pp. 1230 - 1238, 1994.

[6] H. Izumita, T. Sato, M. Tateda and Y. Koyamada, "Brillouin OTDR employing optical frequency shifter using sideband generation technique with high-speed phase modulator," IEEE Photon. Technol. Lett. vol. 8, no. 12, pp. 1674 - 1676, 1996.

[7] H. Izumita, Y. Koyamada, S. Furukawa and I. Sankawa, "Stochastic amplitude fluctuation in coherent OTDR and a new technique for its reduction by stimulating synchronous optical frequency hopping," IEEE J. Lightwave Technol., vol. 15, no. 2, pp. 267 - 278, 1997.

1.2 Related co-authored papers

[1] T. Kurashima, T. Horiguchi, H. Izumita and S. Furukawa, "Brillouin optical-fiber time domain reflectometry," IEICE Trans., vol. E76B, no. 4, pp. 382 - 390, 1993.

[2] T. Sato, T. Horiguchi, M. Tateda, Y. Koyamada, and H. Izumita, "Spectral-linewidth broadening in synchronous Raman fiber amplification caused by cross-phase modulation effects and its suppression," Optics Lett. vol. 22, no. 12, pp. 880 - 882, 1997.

[3] N. Nakao, H. Izumita, T. Inoue, Y. Enomoto, N. Araki, N. Tomita, "Maintenance method using 1650-nm wavelength band for optical fiber cable networks," IEEE J. Lightwave Technol., vol. 19, no. 10, pp. 1513 - 1520, 2001.

[4] N. Araki, H. Izumita, and M. Nakamura, "Reduction in optical fiber maintenance cost by using automatic optical fiber operations support system with remote fiber selector," IEICE Trans., vol.E85-C, no. 4, pp. 915- 920, 2002.

[5] N. Honda, N. Araki, H. Izumita, and M. Nakamura, "Extended optical fiber line testing system with L/U-band optical coupler employing 4-port circulators and chirped fiber Bragg grating filters for L-band WDM transmission," IEICE Trans., vol. E86-B, no.5, pp. 1562 - 1566, 2003.

[6] N. Araki, H. Izumita, N. Honda, M. Nakamura, "Extended optical fiber line testing system using new eight-channel L/U-band crossed optical waveguide coupler for L-band WDM transmission," IEEE J. Lightwave Technol., vol. 21, no. 11, pp. 3316 - 3322, 2003.

[7] Y. Enomoto, H. Izumita, and M. Nakamura, "Highly developed fiber fault isolation technique for branched optical fibers of PONs using high spatial resolution OTDR and frequency domain analysis," The LASER SOCIETY of JAPAN, The review of Laser Engineering, vol. 33, no. 9, pp. 609 - 614, 2005.

[8] N. Honda, H. Izumita, M. Nakamura, "Spectral filtering criteria for U-band test light for in-service line monitoring in optical fiber networks," IEEE J. Lightwave Technol., vol. 24, no. 6, pp. 2328 - 2335, 2006.

[9] Y. Enomoto, H. Izumita, and M. Arii, "Optical fiber management and testing system for PON enhanced with identification technologies using a mobile access terminal with a two-dimensional code scanner and fault isolation technologies using high spatial resolution OTDR," J. of Optical Networking,

vol. 6, no. 5, pp. 408 - 414, 2007.
[10] Y. Koshikiya, N. Araki, H. Izumita, and F. Ito, "Newly developed optical fiber line testing system employing bi-directional OTDRs for PON and in-service line testing criteria," IEICE vol. E90-B, no. 10, pp. 2793 - 2802, 2007.
[11] D. Iida, N. Honda, H. Izumita, F. Ito, "Design of identification fibers with individually assigned Brillouin frequency shifts for monitoring passive optical networks," IEEE J. Lightwave Technol., vol. 25, no. 5, pp. 1290 - 1297, 2007.

2. International conference

2.1 International conference mainly contributed on this thesis

[1] S. Furukawa, H. Izumita, I. Sankawa, and Y. Koyamada, "High dynamic range, low fading noise coherent OTDR using erbium fiber amplification and LD temperature changing techniques" in the proceeding of European Conference on Optical Communication / International Conference on Integrated Optics and Optical Fibre Communications (ECOC'91/IOOC'91), Mo.C1-3, pp. 81 - 84, 1991.
[2] H. Izumita, Y. Koyamada, I. Sankawa and S. Furukawa, "A Coherent optical time-domain reflectometer with a 40-dB dynamic range enhanced with erbium-doped fiber amplifiers," in the technical digest of Conference on Optical Fiber Communication (OFC'92), WK6. p.147, 1992.
[3] H. Izumita, Y. Koyamada, S. Furukawa and I. Sankawa, "Performance limits of coherent OTDR due to optical nonlinear effects," in the proceeding of Symposium on Optical Fiber Measurements (SOFM'94), pp.39-44, 1994 (Invited).
[4] H. Izumita, T. Sato, M. Tateda and Y. Koyamada, "Brillouin OTDR enhanced with an optical frequency shifter using a high-speed phase modulator," in the technical digest of Optoelectronics and Communication Conference (OECC'96), 17C1-3, pp. 138-139, 1996.
[5] H. Izumita, T. Sato, M. Tateda, T. Horiguchi and Y. Koyamada, "1.65 μm Brillouin optical time-domain reflectometry employing a Raman fiber amplifier and lithium-niobate phase modulator," in the technical digest of OFC'97, WJ7, pp. 159-160, 1997.
[6] H. Izumita, T. Horiguchi and T. Kurashima, "Distributed sensing techniques using Brillouin scattering," in the proceeding of the 12th - Conference on

Optical Fiber Sensors (OFS-12), OWD1, pp. 316 - 319, 1997 (Invited).
[7] H. Izumita, "Optical fibre cable network maintenance," ITU-T SG6 Workshop on Outside Plant for the Access Network, AM2- 3, Ha Noi, Vietnam, 24 November 2003.
[8] H. Izumita, "Recent development in fiber optic monitoring system for access networks," in the proceeding of OFS-16, We1-1, pp. 258-261, 2003 (Invited).

2.2 Related co-authored international conference

[1] Y. Enomoto, N. Honda, H. Izumita, M. Nakamura, "Optical fiber line testing system using test light bypass module for ADM ring networks," in the proceeding of ECOC '01, vol. 3, nol. 3, pp. 266-267, 2001.
[2] I. Ogushi, H. Izumita, K. Tanaka and M. Nakamura, "A highly developed coherent detection OTDR for measuring the distributed fiber loss and Raman gain of a 200 km single-mode fiber," in the proceeding of OFS-16, We1-2, pp. 262-265, 2003.
[3] N. Araki, N. Honda, H. Izumita, M. Nakamura, "Add-on filtering technology for L/U-band extended optical fiber line testing system using wideband and high cutoff chirped FBG," in the technical digest of OFC2004, ThW4, 2004.
[4] I. Ogushi, H. Izumita, K. Tanaka and M. Nakamura, "Measurement of a 340 km optical fiber line with a remotely pumped EDFA and DRA by using a highly developed coherent detection OTDR," in the proceeding of ECOC2004, Tu3.6.5, vol. 2, pp. 224-225, 2004.
[5] N. Honda, D. Iida, H. Izumita, and F. Ito, "New function of optical fiber line testing system employing termination cable with individual Brillouin frequency shift and 1650 nm band in-service monitoring technique," in the proceeding of OECC 2005, P364-365 7A-3, 2005.
[6] I. Ogushi, H. Izumita, F. Ito, M. Arii, "Catastrophic damage and destructive process induced in optical fiber cord by 33 dBm pump light at 1480 nm in WDM systems," in the technical digest of OFC2005, OME6, 2005.
[7] N. Honda, D. Iida, H. Izumita, F. Ito, "Bending and connection loss measurement of PON branching fibers with individually assigned Brillouin frequency shifts," in the technical digest of OFC2006, OThP6, 2006.
[8] I. Ogushi, H. Izumita, K. Tanaka, F. Ito, M. Arii, "Observation of ignition induced by a high power light input at a butt-joint splice with refractive index matching material," in the technical digest of OFC2006, OFK6, 2006.

[9] D. Iida, N. Honda, H. Izumita, and F. Ito, "Identification fibers with individually assigned Brillouin frequency shifts for fault location in passive optical networks," OECC 2006, 4E1-2, 2006.

[10] I. Ogushi, H. Izumita, K. Tanaka, F. Ito and M. Arii, "Butt-joint splice with refractive index matching material for high power light in optical fiber communications," in the technical Digest of SOFM 2006, pp. 33-36, 2006.

[11] N. Honda, D. Iida, H. Izumita, F. Ito, "Optical fiber line testing system design considering outside environment for 8-branched PON fibers with individually assigned BFSs," in the proceeding of OFS-18, ThE8, 2006.

3. Domestic conference

[1] H. Izumita, "Standardization trend of optical fiber maintenance technologies in optical access networks," IEICE Technical Report OCS2005-85, pp. 55 - 60, 2005 (Invited) (in Japanese).

[2] H. Izumita, "Recent developed monitoring technologies for optical access networks," IEICE Technical Report OFT2003-114, pp. 7 - 12, 2004 (in Japanese).

[3] H. Izumita, T. Sato, M. Tateda, Y. Koyamada and H. Suda, "Brillouin OTDR enhanced with wideband double-balanced receiver," in the proceeding of IEICE Communications Society Conference, B-981, p. 466, autumn, 1996 (in Japanese).

[4] K. Tanaka, H. Izumita, S. Furukawa, Y. Koyamada, M. Sumida and M. Murakami, "Coherent OTDR enhanced with optical fiber amplifiers for testing optical fiber transmission lines containing in-line Er-doped fiber amplifiers," IEICE Technical Report OCS93-23, pp. 21 - 26, 1993 (in Japanese).

4. International standards

The author has acted as a rapporteur of ITU-T SG6 since 2000 and developed the following recommendations:

[1] ITU-T Recommendation of L. 40, "Optical fibre outside plant maintenance support, monitoring and testing system," (10/2000), (The text of this Recommendation includes Appendices I to V approved on 09/03/2001).

[2] ITU-T Recommendation of L. 53, "Optical fibre maintenance criteria for access networks," (05/2003).

[3] ITU-T Recommendation of L. 66, "Optical fibre cable maintenance criteria for in-service fibre testing in access networks," (05/2007).
[4] ITU-T Recommendation of L. 68, "Optical fibre cable maintenance support, monitoring and testing system for optical fibre cable networks carrying high total optical power," (10/2007).

5. Patents in Japan

[1] 特願平 03-043864(特許第 00310709 号), “光パルス試験器”, 泉田, 他.
[2] 特願平 03-196491(特許第 00308803 号), “光パルス試験器”, 古川, 泉田, 他.
[3] 特願平 04-15887(特許第 00307863 号), “光パルス試験器”, 泉田, 他.
[4] 特願平 04-036577(特許 002901106 号), “光パルス試験器”, 小山田, 泉田, 他.
[5] 特願平 04-128852(特許第 00273132 号), “光パルス試験器”, 古川, 小山田, 泉田, 三川.
[6] 特願平 05-080934(特許第 00332741 号), “光パルス試験器”, 泉田, 他.
[7] 特願平 08-041177(特許第 003306819 号), “光パルス試験器”, 泉田, 立田.
[8] 特願平 08-201897(特許第 003237745 号), “歪・温度分布測定方法およびその測定装置”, 堀口, 倉嶋, 泉田.

6. Other publications in Japanese

[1] 泉田 史, “コヒーレント OTDR 技術”, O plus E 特集:光通信を支える測定評価技術, vol.24, no. 9, pp. 974-979, 2002, 新技術コミュニケーションズ編.
[2] 泉田 史, “光計測技術における IEC 国際標準化－IEC／TC86／WG4 の最新動向”, 光通信技術の最新資料集 6, pp. 215-217, 2002, オプトロニクス社編.
[3] 泉田 史, “光アクセス網の光測定”, 光測定器ガイド 全面改訂版 第 6 章, pp. 321-327, 2004, 松本弘一編 オプトロニクス社発行.
[4] 泉田 史, “アクセス系光ファイバー網のモニタリング技術の最新動向”, 光技術コンタクト, vol. 42, No. 2, pp. 3-11, 2004, 日本オプトメカトロニクス協会.